The University of Nottingham

UNITED KINGDOM · CHINA · MALAYSIA

Tailoring the Structure of Nanomaterials Formed by Light-Induced Synthesis

by Vladimir Astachov

Thesis submitted to the University of Nottingham
for the Degree of Doctor of Philosophy

Main Supervisor: Prof. Andrew Long

Second Supervisor: Prof. Derek Irvine

January 2018

Table of Contents

Abstract

A light is an energy portion that plays a very important role in nature. A light particle or photon can be absorbed, scattered or reflected. In some cases, light can greatly influence the formation of a crystal and guide its growth into hierarchical nano or microstructure.

This work explores the light-induced synthesis of nanomaterials (Au, Ag, CdS, ZnO) and light-induced polymer nanostructuration. This way of synthesizing nanomaterials is compared to other known routes. The main advantage of the synthesis method presented here is its ability to be used for water-based reactions at room temperature. This method can be applied to most water-based syntheses. In this work, results have been compared with template-assisted synthesis for Ag, CdS, and Au. The ZnO light-induced synthesis was used and compared to the hydrothermal ZnO synthesis method.

First, the effect of light over the synthesis of ZnO, Ag and semiconducting polymer P3HT and its mixture with $PC_{[70]}BM$ is demonstrated. The main results from this work include that computer-assisted light control systems might provide a shape-selective synthesis of nano/microstructures at room temperature. Also, light-assisted synthesis provides crystal growth without the use of a capping agent or polymer template.

Morphology control of polymer-monomer mixture is demonstrated which was achieved using Red and Blue LEDs. It was found that Red light increased the diameter of the voids in polymer films while on the contrary blue light decreased it. For ease of comparison, the mixed solvent study was carried out on the same polymers. The change of electrostatic interaction reflected on the change of the morphology of the polymer films. Templated Ag nanostructure synthesis was also performed showing different results when in the presence of light structures are more uniform and have

higher surface area. The work also demonstrates template-assisted synthesis of CdS quantum dots. The use of PPI type dendrimer showed that self-assembly of CdS quantum dots in a nanofiber is achievable at room temperature. Au nanostructures were synthesized using another organic template oleic acid. Synthesis results showed unusual Au nanoparticle morphologies.

Finally, low-power light was shown to influence the nanostructure synthesis and structuration at room temperature. The main effect was the change in the shape due to the vibration of water molecules. Water absorbs light mostly on the infrared region and very little in the visible range. Due to the low absorbance of visible light by water, it required longer time intervals in order to achieve the changes in morphology of the ZnO or Ag structures. Reaction time has been proven to be an important factor in light-matter interaction. In this work, AFM, SEM, UV-vis, PL, NMR and TEM were used for the characterisation of materials synthesized at room temperature.

Acknowledgements

I am deeply grateful to Professor Andrew Long for his support, supervision and guidance. Also thanks to Professor Derek Irvine for the useful suggestions in chemistry and supervision. I would also like to thank Professor Amir Fahmi for his supervision during my first year and for his help both in physics and chemistry. I would like to thank Professor Kwang Leong Choy for her supervision during my second year and for the support and guidance. I am very thankful to Professor Arūnas Jagminas for his advice in chemistry and support.

Special thanks to Professor Rimas Vaišnoras for his support and guidance during my work in the Nanomaterials laboratory. I am grateful to all my friends in England, Lithuania and in the rest of the World.

I am especially grateful to my special friends in Nottingham. ☺ ☺ ☺

And I am above all thankful to my parents and dedicate this work to them.

And of course...I am thankful to all the scientists in the World throughout history that never gave up on their science!!!

Abbreviations

AFM- Atomic Force Microscope

CB- Chlorobenzene

CHF- Chloroform

CTAC- Cetyltrimethylammonium chloride

DMF – Dimethylformamide

Dpm- particle density

EDX- Energy-dispersive X-ray Spectroscopy

EG-ethylene glycol

ESEM- Environmental Scanning Electron Microscope

FFT- Fast Fourier Transform

HRTEM- High-Resolution Transmission Electron Microscopy

HAADF- High Angle Annular Dark Field (imaging)

LED- Light Emmiting Diode

NMR- Nuclear Magnetic Resonance

NP- nanoparticle

PAMAM- polyamido amines (dendrimers)

PCE-Power Conversion Efficiency

PEG- polyethylene glycol

PPI-G4- polypropylene ymine dendrimer generation 4

$PC_{[70]}BM$ - Phenyl-Butyric-Acid-Methyl Ester with fullerene 60 or 70

P3HT – Poly-3 hexylthiophene 2.5 dyil regioregular.

PL – Photoluminescence

PTB7- Poly({4,8-bis[(2-ethylhexyl)oxy]benzo[1,2-b:4,5-b′]dithiophene-2,6-diyl}{3-fluoro-2-[(2-ethylhexyl)carbonyl]thieno[3,4-b]thiophenediyl})

PVP- Polyvinylpyrrolidone

STEM- Scanning Transmission Electron Microscopy

QD- quantum dots

THF- Tetrahydrofuran

TEM- Transmission Electron Microscopy

UV-vis – Utraviolet visible

Chapter 1 Introduction

The most problematic questions today are those related to energy [1] and pollution [2, 3] and are technology challenges which drive the whole science-community to create and promote solutions in order to address them. Nanoscience is providing goods and solutions for almost any problem starting from clean water [4] to medicine [5, 6]. Nanotechnology became very popular over the last few decades and offers a great future to humankind. Nanorobots in the future should be able to solve serious problems like starvation, diagnosis problems in medicine, space etc. [7, 8]. Recently nanostructurized silicon-based solar cell achieved 22% efficiency [9] and research increases in this area. Nanoscience brings novelties to society by improving devices and thus helping to improve our lives. However, the nanostructures synthesis procedure is specific for every material and morphology [10–14]. Tunnelling microscopes are able to build structures atom by atom which allows to build nanometer-sized objects but does enable mass production because it is time-consuming and expensive [15]. Nanomaterials depending on their size and shape possess different physical and chemical properties [16–20]. The synthesis of defined and/or complicated shapes was always a challenge [21–23]. The synthesis of nanomaterials usually requires toxic chemicals, also elevated temperatures are used in nanomaterial synthesis [24, 25]. Photochemical synthesis methods are limited in materials (Ag and photoreactive chemicals) and usually ultraviolet (UV) light is used which has a high energy in comparison to visible light [26–29]. The investigation of the formation of nanoparticles and other nano and microstructures was also poorly described by researchers [24–29]. Photochemical synthesis allows the use of less toxic materials and room temperature is usually enough for the reaction. On the other hand, control over the synthesis becomes difficult due to the limited variation ability during the synthesis. This is why existing experimental methods need to be upgraded which might be achieved if the hybrid method will be proposed (photochemical-sol-gel for instance). Improving nanochemical synthesis methods would upgrade the whole nanochemistry and other related disciplines as well. The main problem in synthesis of nanosized structures is that it is not possible to change the synthesis conditions at a certain point of synthesis time. If there is a template synthesis, then the chemicals dissolved in the solution sometimes cannot be suddenly removed if required. If there

is a synthesis at elevated temperature, then the solution cannot be cooled down immediately which sometimes could stop the reaction and leave the desired shape of metal nanoparticles. To overcome these problems a more flexible synthesis method is required. Photochemical or light-induced synthesis allows such changes during the synthesis. The light wavelength can be changed at any moment of the synthesis and the time of the irradiation can also be changed as desired. Also, elevated temperature is not necessary for the light-induced synthesis. The reaction can be stopped at any moment preventing the nanostructures from further growth. On the contrary, light-assisted synthesis also needs to be improved and upgraded.

1.1 Aims

The main aim of this work is to demonstrate the controlled synthesis and nano/micro structuration conception with Ag, Au, Ag-Au, ZnO, CdS, P3HT/ $PC_{[70]}BM$. This proposed method is different from the already existing methods since it it cheaper and more efficient. In the case of light-induced synthesis, it combines several wavelengths of light in one synthesis chamber. The method set-up allows the control of the time interval within irradiation period. The key project aim is to put light-induced conception along with other well know popular synthesis methods and use. And importantly to understand the light-matter interaction on the nanoscale in order to grow a variety of hierarchical nanostructures. This method solves the synthesis flexibility problems mentioned on the previous page (Ch.1 Introduction).

1.2 Major Work Conducted

To achieve the aims in 1.1 the main work steps have been proposed as follows:

- To synthesize ZnO and Ag hierarchical nanostructures under the Light Emitting Diode (LED) light, and to tailor the morphology of the polymer films using the same experimental set-up. Experiments in dark without the use of LED light will be conducted to study the influence of light irradiation. Conventional hydrothermal and template-assisted synthesis methods will also be carried out for comparison.
- To characterize ZnO, Au and Ag nanostructures using the scanning electron microscope. And to use the atomic force microscope for topographical characterization of polymer films.

- To assess the experimental results with existing theories that can explain the formation of the nanostructures and light-induced synthesis. And to evaluate the influence of light on the formation of the nanostructures.
- To study the mechanism on the light influence on the growth of the crystal structures. A nanostructure growth model will be established.
- The advantages and disadvantages of light-induced synthesis over known traditional synthesis methods will be highlighted, and research direction for future work will be proposed.

1.3 Outline of Thesis

The present work consists of seven chapters. Chapter 2 reviews popular nanomaterial synthesis methods and routes such as vapour-liquid-solid synthesis (VLS), Sol-gel, Hydrothermal, Photochemical, and Template-assisted. Also, the role of nanomorphology of most popular semiconducting polymer films used in nanoscience was reviewed and analysed.

Chapter 3 describes the experimental methodology in detail. Starting from the raw chemicals used and ending with the equipment used for the characterization. Specifics of each experiment are highlighted and sample preparations for every characterization are described in detail. Schematic depictions of most complicated experiments are included in the chapter with descriptions in order to make the experiments repeatable for the reader with minimum skills.

Chapter 4 focuses on polymer film morphology change and characterization using Atomic Force Microscope and Nuclear Magnetic Resonance. Polymer morphologies are analyzed and influence of solvents and light are discussed in detail.

Chapter 5 covers the template-assisted synthesis of Au and CdS. For the synthesis of Au oleic acid was chosen as a template to drive the Au growth into triangles and prisms. But CdS synthesis was performed using polymer- dendrimer which also serves as self-assembly agent.

Chapter 6 devoted to light-induced synthesis. The chapter also speaks about the light-induced synthesis of Ag, Ag-Au alloy nanoparticles. Light-induced synthesis and characterization of ZnO is described.

Chapter 7 describes the crystallization of nanostructures. An attempt to solve the most important questions by using crystal defect theories and explain the paths and ways of crystal growth. Also, light influence on materials discussed and analyzed.

Chapter 8 gives the suggestions for the future works. Light-induced synthesis with more materials and more complicated light-codes. Use of soundwaves and vibrations could give interesting results in the synthesis of nanoobjects.

Chapter 2 Literature Review

In this chapter, a detailed review is given on the nanomaterial synthesis methods. The most popular and efficient methods are described in detail. Special attention is given to the methods used in this work (photochemical, light-induced) and materials (silver and zinc oxide) that were synthesized in this work. Advantages and disadvantages of each technique are described. Current trends in nanosynthesis that are up to date are analyzed and discussed.

2.1 Introduction

Nanotechnology has greatly influenced science and the lives of most of us already. It includes almost all known disciplines: textiles [30–33], mathematics [34, 35], computer sciences [36], biology [37, 38], medicine [39, 40] etc. Synthesis methods are crucial for this type of science. Since the quality of the nanostructures depends also on the synthesis methods it is important to develop new methods and strategies and to continue upgrading the traditional methods. Depending on the size, shape, materials and quality of the nanostructures their properties can change significantly. In most cases it is desirable to have a monodispersive system with a particular size and/or shape of the material [41]. However, there are very few reports regarding chierarchical structures and the formation and growth mechanisms behind them [42, 43]. A range of synthesis techniques are used in nanochemistry: *vapor-liquid-solid* method (VLS), a *sol-gel* method, *hydrothermal* method, *template-assisted* and *photochemical* methods. In this work, we are going to review mentioned synthesis methods and highlight the advantages and disadvantages of each method.

2.2 Vapour-Liquid-Solid Synthesis

The vapor-liquid-solid (VLS) method has been widely studied and used to obtain one-dimensional structures like nanowires. The mechanism was developed 50 years ago and first used in the silicon industry by Wagner [44]. Then starting from the 1990's it was the beginning of the wide use of this method for nanostructure growth after the Lieber [45–47] group at Harvard University demonstrated the efficiency of this method. In the VLS process there are three main stages: (a to b) alloying, (b to c) precipitation, (c to d) axial growth (Fig. 2.1). This process runs only at high temperatures and involves vapor-liquid-solid phases of the material and thus is called the VLS process. With VLS it is possible to grow the structures from nanometer to

even centimeter scale. This mechanism requires one very important component: metal catalyst. The problem with this method is that not all the metals can work well. The main requirements for the catalyst materials are: (1) it must form a liquid solution with a component, (2) the catalyst must be more soluble in the liquid phase than in a solid phase, (3) the vapor pressure of the catalyst material over the liquid alloy must be small, (4) the catalyst material must be inert to chemical reactions, (5) the catalyst material must not make an intermediate solid. So the material catalyst must not evaporate during the process, must not react with the materials, must not spoil the reaction and basically guide the materials in the process in order to get the final formation of nanowires. This is the reason why gold works very well for growing Ge, Si, ZnO, nanostructures. The VLS method is popular for the growth of vertical nanowires with less than 100 nm diameter and a length ranging from a few hundred nanometers to a few centimeters. Nanowires found their application in optoelectronics [47, 48] and became very popular since the VLS method can provide both high quality and control over the growth process. Using the VLS process it was even possible to make branched structures [49, 50] which was usually difficult to achieve. It was found that not only gold can be used as a catalyst material thus expanding the borders of the synthesis tactics [51]. In the growth of Si nanowires via the VLS method and using Au as a catalyst leaves deep defects in nanowires.

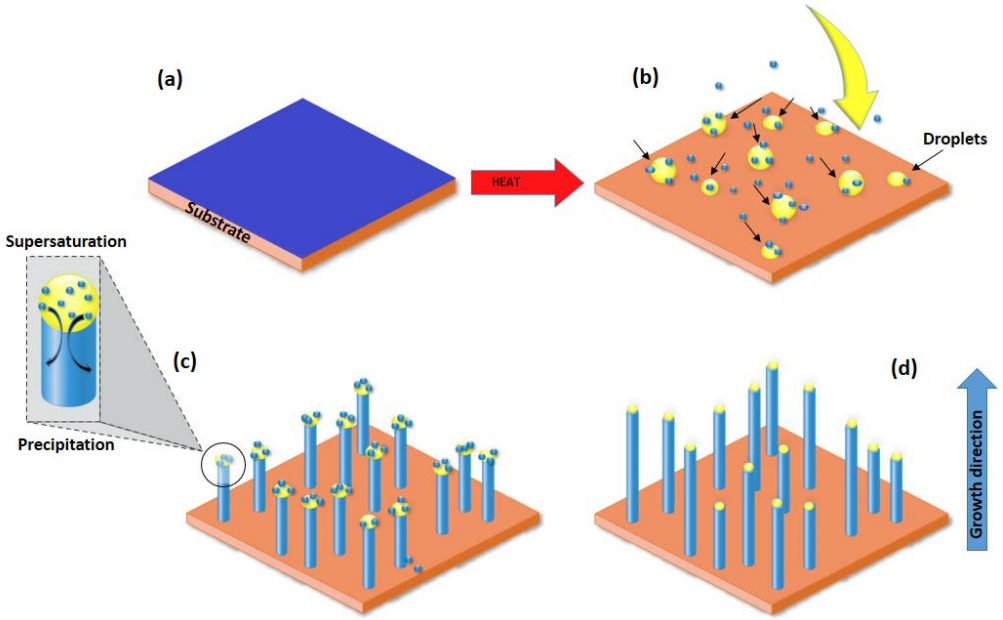

Figure.2.1 VLS method process in growing 1D nanowires. Step (a): substrate with the material on it. Step (b) heating up the substrate and dissolving-evaporating the material. Step (c): precipitation. Step (d): growth of 1D nanostructures (whiskers in the case depicted).

Also cleaning the final product and the equipment from gold is quite difficult [51]. Si wire synthesis was accomplished with other materials such as Ag [52], Al [53], Co [54], Cu [55], Fe [56], Ga [57]. The growth rate determining factor is the speed of incorporation of atoms into the nanowire and can be controlled via processing conditions. In this process (at high temperatures) van der Waals force and Ostwald ripening force are the driving particles to larger clusters and the formation of large droplets. Since every particle is trying to attain lowest possible energy and agglomerate, it requires precision in preparation, positioning them and heating the surface during nanowire growth. As it was mentioned before sometimes catalyst materials are not very efficient because they cause impurities (Au for instance) and thus permanent damage to the final product-nanowires. By increasing the amount of impurities of the catalyst material in the band gap causes degradation of optical properties of the nanowires which is so important for the industry. It was found that Au can be replaced by Pt [58–61] and causes even higher growth speed under the same conditions. Ke et al. synthesized Si nanowires using Al as a catalyst [62].

2.2.1 Issues with VLS Method

The same group faced specific problems related to the VLS synthesis method [62]. The basic issue was with Al oxidation and more airtight system design was required. Scientists used temperatures ranging from 500 ^{0} to 600 ^{0}C and H_2 and SIH_4 and it was found that these materials were reducing the oxidation but not completely eliminating it. Growing interest to the catalyst-free VLS method increased a number of works in this area. This useful method solves catalyst contamination problem and can be applied to a number of materials [63, 64]. Interestingly the self-catalytic process was reported in 2014 by Yu et al. [65]. The metal oxide nanostructures growth process was based on electron beam evaporation. The condensed electron beam was a decomposing metal oxide source and was performed with In(Sn), Ga, Al grown on Si. The control of the structures can be achieved by the variation of the synthesis time and becomes optimal after 150 seconds [65].

2.2.2 Advantage of VLS Method

A key role of the VLS synthesis in nanotechnology is the ability to grow vertical wires that have optoelectronic properties desired for photovoltaics, LEDs and electronics. Hochbaum et al. synthesized Si vertical nanowire arrays [66]. The nanowires were around 40 nm in diameter and Au colloid nanoparticles were used as a catalyst

material. The nanowires were uniform and to demonstrate the flexibility of the method researchers grew them directly into microchannels. However, deposition of nanoparticles onto any surface is always random and precise control of the nanoparticle deposition still remains a challenge. Other similar experiments were performed by different groups but they included work with dangerous chemicals such as hydrofluoric acid (HF) for cleaning purposes [66, 67]. Orlandi et al. [68] reports growth of SnO_2 nanobelts and dendrites by VLS method. The synthesis was performed at 1210^0 C in the carbothermal process in a sealed tube furnace at N_2 gas flow. Basically, researchers mixed SnO_2 and carbon powder and heated it up in the furnace for 2h. The resulting product was nanowires with branching out elements resembling branch-like structures. This experiment required small amounts of chemicals and high temperatures only. The major issue is the control of the size and width and achieving the diameter of less than 10 nm of the nanowire was a great challenge. The classic problems with this method are still the setup of the experimental equipment which is usually expensive and requires specific conditions such as fume hoods and inert gasses. Also as was mentioned before air-tight setup could be an issue which can lead to the imperfections of the nanowires and degradation of their optoelectronic properties. Use of high temperatures requires monitoring and control and also time and the properties of used materials are of great importance.

2.3 Sol-Gel Synthesis Method

The sol-gel process is the name for a group of synthesis used to synthesize usually metal oxide nano/micro structures. Normally in this process, sol and then the gel is formed in order to get the final product. The sol-gel process can be aqueous involving water as a main solvent or non-aqueous which involves organic solvents [69].

2.3.1 Aqueous Sol-Gel Process

This synthesis method is one of the most complicated due to the high number of chemical processes involved [70]. To control this process many parameters are involved: pH [71], temperature [72], hydrolysis and condensation rate [73], time [73], the concentration of anions, the rate of oxidation, metal oxide precursors [73] and even the method of mixing. In the aqueous sol-gel process to obtain sol – highly dispersive colloidal system condensational or dispersive methods are used. During this process, an “elastic solid” is formed. The network between the molecules is created and in the synthesis of metal oxides, it is like a polymer connection from metal to -oxo (M-O-H)

or -hydroxo (M-O-M) (M-metal) bridges [69]. Using this method, it is possible to synthesize various types of metal oxide nanostructures including: Si, Ti, Zn, Cr, Vn, Al, Sn, Ge etc. The initial solution usually contains either metal alkoxides (non-aqueous) or chlorides (aqueous) as precursors (Fig.2.2) then depending on the desired result the solution is either coated on a surface or it undergoes hydrolysis and polymerization states. The next step is wet gel and the removal of the solvent by evaporation either at room temperature or slightly heating up the material. The solvent can be water or any organic solvent but in most cases it is ethanol. The extraction of the material by centrifugation is also efficient or natural precipitation is used. In general, we can summarize these steps: 1) preparation of a solution, 2) conversion of prepared solution to sol, 3) aging, 4) shaping, 5) thermal treatment. At the final stage, we have an inorganic interconnected network- gel (sol-gel transition). The reason this method is one of the most popular in synthesis is the ability to shape the material into almost any desired form: fibers, films, powders, monoliths and convert it into the ceramic material by heat treatment.

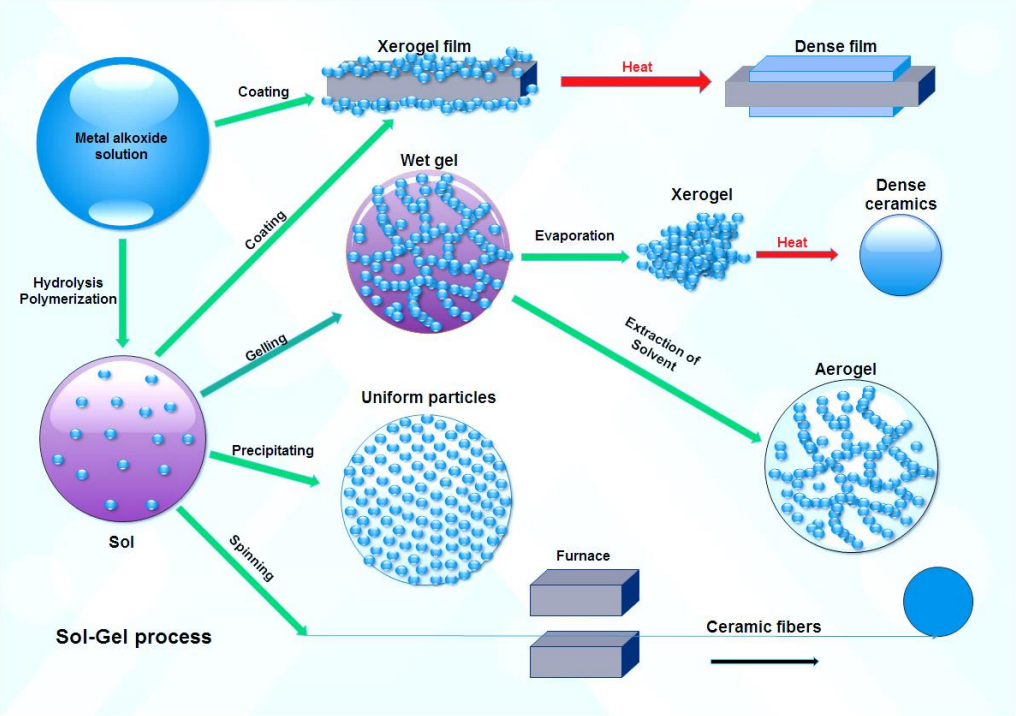

Figure. 2.2 depicts the process of sol-gel synthesis. First steps show the initial solution (metal alkoxide in our case). Other steps involve coating and obtaining xerogel film or directly using the hydrolysis process and polymerization leading to the formation of sol. After sol is obtained coating can be performed (depending on the result required). The last step processes involve evaporation and creation of xerogels or aerogels depending on evaporation techniques. The final product can be dense film, ceramic or fiber.

2.3.2 Issues with the Aqueous Sol-Gel Process

The major problem is the control of the reaction rate. The reactions in this process are simply too fast for most of the transition metal oxide precursors. Hence it results in the uncontrolled formation of shapes and sizes of metal oxide structures. It is also important to mention that every metal oxide precursor has its own reactivity thus making every synthesis process specific for every material. To overcome these problems and drive the reaction process in a more controlled way additives such as carboxylic acids are used. The role of these acids is to decrease or modify the reactivity of the metal oxide precursors and act as chelating agents. This method used in synthesis and coating of ceramics has proven to be very efficient because it gives the ability to coat almost any surface. However, post-treatment prevents precise control of the crystal size and shape. The fundamental issue with this process is the sensitivity to many factors which basically makes the process impossible to control and such parameters as the size distribution of shape of the material is barely controllable. Non-aqueous sol-gel synthesis can overcome some problems persistent in aqueous synthesis method by replacing water with organic solvents. Non-aqueous sol-gel synthesis. In this process, the transformation occurs also in liquid media but organic solvents are replacing water. The precursors for this process are "organic metals". Typically, it is a metal alkoxide or acetate. To define a typical formula of used precursor chemicals: R-O-M, H_3C-O-M, where R is the organic substituent. In the aqueous process normally metal gets oxygen from the water and in the non-aqueous process the oxygen comes either from solvent or is provided by the organic constituent of the precursor. In other words, the second possibility occurs when the metal oxide precursor molecule is giving part of its "body" to form a new molecule.

2.4 Hydrothermal Synthesis Method and ZnO

Hydrothermal synthesis is a widely used method usually to obtain nano/micro structured ZnO [74-76]. In most synthesis procedures the metal precursor is added into distilled water. The second process is usually the addition of either donor of oxygen (in the case of oxides synthesis) or the reducing agent (in Au or Ag synthesis). The last step is heating and stirring the solution for a couple of hours. The heating up is required to complete the synthesis process and sometimes even to speed up the growth of nanoparticles. Heating up spend also can affect the shape and size of the materials. Fig.2.3 depicts the chemical glass and the steel autoclave used in hydrothermal synthesis. A common issue with the autoclave is that the solution inside is heated up

in a furnace and without stirring. The temperature applied to autoclaves usually ranges from 80^0 to up to 250^0 C. Chemical glass or vial that can stand a few hundred degrees are also widely used in hydrothermal synthesis. They can be used to precisely control the concentration and even modify the growth during the process by simply adding the salt into the solution. Stirring can be precisely controlled as well and is usually a few hours in the synthesis process. Using this method nanostructures of ZnO [77], SnO_2 [78], TiO_2 [79], including sulfides [80] (ZnS, CdS, PbS, CuS, FeS, BiS) etc. were successfully synthesized with various shapes. This method provides good quality and size distributions of synthesized products also allowing to

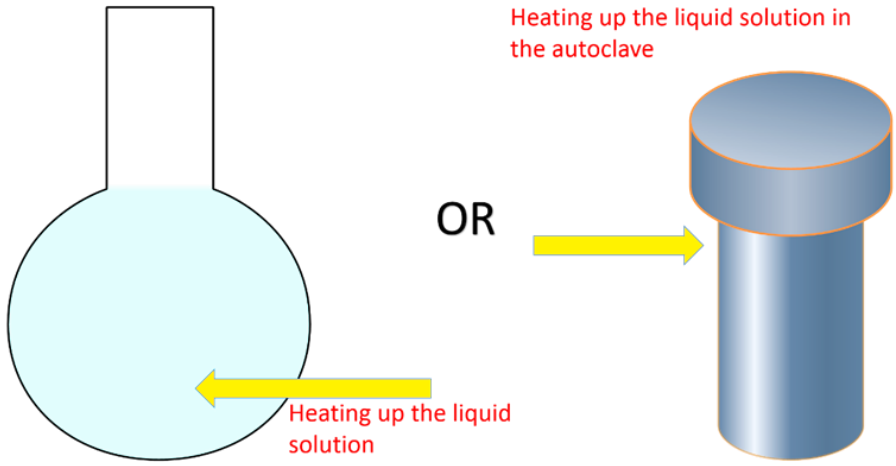

Figure.2.3 traditionally chemical glass and steel autoclave used in hydrothermal synthesis processes.

control the synthesis process by varying the synthesis time, pH, concentration and impurities of the solution. The first report on the hydrothermal method dates back to 1845 when German geologist Karl Emil von Schafhäutl [81] reported microscopic quartz crystals grown in a pressure cooker. The term Hydrothermal comes from ancient Greek (hydro- ύδωρ- water) and (thermos- θερμός- warm/hot) and is purely of geologic origin.The hydrothermal method can be used to synthesize many types of nanoparticles but became very popular for the synthesis of metal oxides [81–85]. SnO_2 was synthesized using this method in a variety of works [86–88] and proven to obtain high control over the sizes and shapes of the structures [76, 89]. Wang et al. synthesized tin oxide nanoflowers on the surface of indium tin oxide in the presence of PVP [90]. Structures were grown in autoclave at 200^0 C for 12h. The obtained product was around 300nm in width and resembles hedgehog-like structures. Along with PVP solution contained NaCl. The structure pathway is associated with the

synthesis time and the PVP polymer persistence. Patil et al. reported a hydrothermal route in the presence of hydrazine at 100^0 C for 12h [87]. The resulting product was spherical nanoparticles of 40 to 70nm width looking like clumps of rice and spherical particles together. The proposed reaction was basically the reduction of Sn precursor by hydrazine (few chemical reaction steps process). Lupan et al. report SnO_2 nanofibers with lengths of 10-100µm and width 50-100 nm [86]. In this synthesis, NH_4OH was used and the study suggests the chemical played a major role in the synthesis.

2.4.1 Synthesis Scheme and the Morphology

Scientists suggest the formation of amphoteric hydroxide $Sn(OH)_4$ and dissolution in NH_4OH followed by the formation of $Sn(OH)_6^{2-}$ ions and the formation of SnO_2 after the hydrothermal process. The study suggests that Sn ions play a key role in the formation of the thickness of nanowire and are found to be optimal at 1:20-25. All the mentioned experiments synthesizing SnO_2 suggest that the control over the morphology of the nanostructures can be achieved by changing either the chemicals or the processing conditions like temperature. Du et al. reported the formation of SnO_2 hollow microspheres in the autoclave at 160^0 C for 16 hours [91]. In this synthesis, researchers used methenamine($(CH_2)_6N_4$) and carbamide ($CO(NH_2)_2$) along with $SnCl_4$. They also controlled the pH by the addition of sodium hydroxide (NaOH) and having pH in the range of 9-11. The microspheres were of around 1µm in diameter and consisted of small nanospheres of 70 to 150nm in diameter.

2.4.2 Reaction Scheme and Morphology

The proposed reaction suggests that $CO(NH_2)_2$ was hydrolyzed into CO_2 and $NH_3 \cdot H_2O$ and only then the formation of nanosphere occurred. The process of the final microsphere formation remained unclear since it is structural and already consists of formed nanoproducts. However, researchers speculate that formation of the microsphere could be attributed to the microbubbles of CO_2 during the reaction. Basically, a microbubble was solving the agglomeration issue at that scale. The nanospheres were agglomerating around the microbubble thus creating the shell of SnO_2. This work shed some light on the synthesis of SnO_2 via the hydrothermal process. Changing the size and shape of the nano or microparticles and achieving high control over the synthesis process was always the main purpose of the nanochemistry as such. Chen et al. reported the hydrothermal synthesis of SnO_2 with different

morphologies [92]. Researchers obtained pine needle-like, nanospheres, nanosheets and grape-like nanostructures. Every structure had different preparation steps also varying in chemicals and processing parameters such as time and temperature. For the preparation of pine needle-like structure, $Na_2SnO_3 \cdot 3H_2O$ and NaOH were used. The later synthesis was followed by the addition of $(CH_2)_6N_4$ and in all four cases synthesis was performed in a Teflon-lined stainless steel autoclave. The synthesis temperature was 180^0 C for 24h. Fabrication of grape-like structures included the same procedure steps and the difference was the amount of chemicals and the tin precursor which was $SnCl_4 \cdot 5H_2O$. Other two cases of spherical and sheet-like structures had the same processing conditions: 180^0 C for 12h. Also, the same precursors were used $SnCl_2 \cdot 2H_2O$ along with NaOH and $Na_3C_6H_5O_7 \cdot 2H_2O$. The main difference was the amount of chemicals and in the sheet-like preparation procedure magnetic stirring was used.

2.4.3 Morphology Influencing Factors

It is not possible to answer the question whether the stirring could cause such changes in morphology since the solution with chemicals always has Brownian motion between the particles and molecules. In the hydrothermal synthesis of oxides usually, the acidity (pH) is one of the main factors determining the synthesis results [93]. But the authors did not focus on explaining the SnO_2 morphologies but rather on gas sensing properties such as H_2. As mentioned before the hydrothermal synthesis method is widely used to synthesize metal oxides with various shapes but probably the most popular material is zinc oxide (ZnO). This material has grown in popularity both for nano and microstructures and a hydrothermal method is a powerful tool in the synthesis of ZnO. In a typical hydrothermal synthesis of ZnO traditionally the zinc precursor and NaOH are involved. For the zinc precursor usually, it is zinc acetate or zinc nitrate and the NaOH serves as an oxygen donator.As mentioned previously pH and other factors like synthesis time and temperature play a key role. The properties of ZnO depend on the shape, size and surface structure of the material. Control of the synthesis process and also synthesis modelling are essential. Amin et al. reported work that focuses on the influence of pH, temperature, concentration and time in ZnO synthesis [94]. They synthesized different types of nanostructures like flowers, urchin-like, rods and tetrapod structures. The report mainly focussed on pH of the solutions. The chemicals used were zinc nitrate and $(CH_2)_6N_4$ for the pH control HNO_3 and $NH_3 \cdot H_2O$ or HCl

and NaOH were used. For the pH control depending on the materials approaches referred as procedure A and B. The pH values were set for 1.8, 2.5, 3.5, 4.6, 6.6, 8, 9.2, 10.7, 11.2 and 12.5 i.e. from strong acidic to strong basic solutions. It was found that the main controlling parameters were the pH and the temperature. By changing the temperature it is possible to change the morphology of the nanostructures. They obtained nanosized structures: tetrapods, flowers-like and urchin-like structures at high pH values pH=8 or more. While lowering the acidity led to the formation of the rods and even film-like structures. Also they found that by increasing the temperature the aspect ratio of nanorods increased [94].

2.4.4 The Time as Synthesis Influencing Factor

The time factor was also very important and by increasing the synthesis time the length of the nanostructures also increased. At the synthesis time of 1h the length of the nanorods were around 500nm and by increasing the time to 3h the length increased to 1μm. Further increasing the growth time to 10h the length of nanorods were 2.2 μm. It seems to be logical that at the constant concentrations and temperature the structures continue to grow. However, if we imagine the solution with ions and molecules of the chemicals inside it is also logical that the concentration should always decrease while the growth continues.

2.4.5 The Influence of Precursor

The influence of the precursor concentration is pointed out very clearly stating that the increase of the concentration of the precursor (zinc nitrate in this case) leads to the formation of polycrystalline films. While lower concentrations lead to the formation of nanowires. Researchers found that the length becomes constant at the concentration of 200 mM which basically suggests that there is a limit for ZnO growth [94]. Increasing the concentration led to the formation of film. This observation allowed to conclude that a linear relation can be drawn between the concentration and nanorod dimensions. This work actually showed the connection between the parameters such as time and concentration. However, the precursor and pH controlling chemicals seem to be the main parameter since the aspect ratio and the shape can be controlled by just adjusting the concentration. While the time and the temperature seems to be efficient only in affecting the aspect ratio of the structures. Other interesting works in ZnO hydrothermal synthesis were performed by various scientists using chemicals such as already mentioned before $(CH_2)_6N_4$ and other types including polymers and organic

molecules. Sugunan et al. investigated the influence of hexamine on the growth of the ZnO structures [95]. They used temperature 60-95^0 C for 24h to synthesize the few micrometer nanowires with around 30 nm thickness. The proposed model for this growth was the attachment of hexamine molecules attached to non-polar facets of the crystal thus leaving polar facets to grow and form the nanowires with high aspect ratios. It seems that for synthesis of particular shape of ZnO the extra-templating chemical was required.

2.4.6 pH as Morphology Influencing Factor

Some works report hydrothermal synthesis of ZnO without any template. Bhat et al. reports synthesis using zinc precursor, methanol and NaOH [96]. They maintained the solution in an oven for 8h at 160^0 C. The difference of every sample was the pH and they obtained spherical particles with a 100 nm diameter at pH=8, elongated cracker-like structures at pH=12 with a diameter of around 100 nm and 500 nm length. Varying the amount of chemicals but keeping pH=8 they also synthesized rods and spherical particles together ranging from 100 nm to 450 nm. At pH =9 the dominant structures became spherical nanoparticles with very few nanosized rods. While it is still possible to synthesize ZnO nanostructures without the aid of any other molecule obtained structures in such way usually have defects or size and shape distributions and might exhibit different properties. Hence this is not always desired and more precise approaches are required such as the use of hexamine.

2.4.7 Influence of Additives on ZnO Synthesis

Over the past fifteen years hydrothermal synthesis of ZnO using additives gained great popularity because of its effectiveness and the possibility to modify by simply changing the amount of additives. Chen et al. synthesized ZnO with various shapes and using different additives [97]. The temperature was chosen to be from 100^0 to 220^0 C and the time from 5h to 10h. The additive was chosen 1,6-Hexadianol and it resulted in the formation of rod-like structures with various sizes and lengths basically ranging from 300 nm to 700 nm. The thickness of the rods also differs from 30 nm to 70 nm. When additive was previously mentioned hexamine ($(CH_2)_6N_4$) the result was snowflake-like and the size was around 200-300 nm. Using ethanolamine as an additive polyhedrons were synthesized with sizes from around 150 nm to 220 nm. Also they observed the change in shape from rod to polyhedral after increasing the temperature. The researchers observed and described the synthesis however they did

not explain the shape formation behind the process. Zhang and Mu have grown ZnO homocentric bundles using zinc acetate and NaOH with the addition of polyether [98]. The synthesis was performed at 160^0 C for 16h in an autoclave. The shape of the ZnO crystals were attributed to the growth habits of ZnO and the influence of polyether. The role of polyether is proposed to be templating the zinc-containing molecules and due to the process when $Zn(OH)_2^{4-}$ is surrounded with PEO-PPO the resulting growth makes the homocentric bundles. These structures are made of hexagonal and pyramid-like ZnO crystals that grow due to ZnO growth habit.

2.4.8 Different Morphologies of ZnO

Lu and Yeh synthesized ZnO powder with temperature at 200^0 C and used ammonia which also served as a pH controlling chemical [99]. The heating time was ranging from 30mins to 2h. The obtained powder after SEM characterization revealed microsized rice-like ZnO structures. Also they observed that increasing the pH from 9 to 12 the aspect ratio of the structures increased forming 3µm rods. Another simple method was proposed which led to the formation of ZnO various nanoparticles by Music et al. [100]. The nanoparticles were mostly spherical and the synthesis procedure included the use of tetramethylammonium hydroxide (TMAH) which led to 10-20nm nanoparticles along with dendron looking like structures of 200 nm and larger in size. Synthesis methods that are most simple and do not require high temperatures or complicated polymer mixtures make the hydrothermal method one of the most attractive both for science and industry. Cunha et al. demonstrated synthesis of urchin-like structures which are referred as nanoflowers in the article [101]. They used zinc chloride and ammonium hydroxide and the synthesis was performed at 90^0 C pH=10.5 for different amounts of time. All the structures were urchin-like with slight differences: thickness, density of the nanorods that come out of the center, sharpness of the nanorods and packing of the structures which also could be accidental. The experiments were performed for different amounts of time ranging from 15 minutes to up to 72 hours. The results revealed that at a synthesis time of 72h the nanorods were the sharpest in comparison to other samples and the 30mins, 2h and 6h synthesis showed nanorods of urchin-like structures having the smallest aspect ratio. Synthesis in supercritical water was performed by Viswanathan and Gupta [102]. Basically they oxidized zinc acetate in supercritical water in less than a minute. The obtained nanoparticles were with sizes ranging from 120 nm-320 nm in diameter. Li et al.

synthesized different shapes of ZnO ranging from nano to micro size [103]. Two different precursors were used: ammonia referred to as A and ammonia and zinc nitrate referred to as B. The synthesis temperature was 80^0 C for 12 or 24 hours. In the case of A precursor nanowires were obtained with different diameters and lengths and using the B approach thicker nanowires and hexagonal shaped nanowires were obtained. It is important to mention that all the nanowires were synthesized on a large scale on zinc foil and all of them were vertically aligned. They report that sharp wires were obtained at alkaline solutions while more flat within less alkaline medium.

2.4.9 Synthesis of Complicated ZnO Structures

Synthesis of more difficult structures has always been a challenge because of the different properties that those structures exhibit. One of the most attractive ZnO nanostructures is a flower-like structure which has a center and branching out leaves or Dendron-like shapes. One of the very unusual works was performed by Shao et al [104]. Flower-like structures were synthesized using zinc chloride and ammonia. Copper plate was immersed into the reaction solution before the heating up. The synthesis temperature was 95^0 C for 2h. The obtained structures had plates branching out from the center and resembled roses 30 microns in diameter and 150 to 250 nm thickness of the leave (fragment of that rose). Important to notice that rose-like structures were in ordered manner and distributed over the sample very uniformly as indicated by SEM. While the addition of polymers could be explained by the template-like role the use of ammonia raised the question of the chemical reaction within the solution. According to ref [84] this reaction could be written as:

$$NH_3 + H_2O \longleftrightarrow NH_3 \cdot H_2O \longleftrightarrow NH_4^+ + OH^-$$

$$Zn^{2+} + NH_3 \longrightarrow Zn(NH_3)_4^{2+}$$

$$Zn(NH_3)_4^{2+} + OH^- \longrightarrow ZnO$$

Or

$$Zn^{2+} + OH^- \longrightarrow Zn(OH)_4^{2-}$$

$$Zn(OH)_4^{2+} \longrightarrow ZnO \qquad (2.1)$$

As we can see ammonia is creating intermediate products which later form ZnO structures. In the case when hexamine is used it is known that during thermal decomposition of HMT it releases the hydroxyl ions that are very important in the

formation of ZnO. So the reaction with hexamine can be written in the following way [84]:

$$(CH_2)_6N_4 + 6H_2O \longleftrightarrow 6HCHO + 4NH_3$$

$$NH_3 + H_2O \longleftrightarrow NH_4^+ + OH^- \qquad (2.2)$$

$$2OH^- + Zn^{2+} \longrightarrow ZnO + H_2O$$

Synthesis of microsized urchin-like structures (nano-flowers referred in the article) were synthesized using zinc acetate and NaOH at 90^0 C for 30 minutes by Wahab et al [105]. The structures were basically sharp few μm length rods with sharp tip and around 300nm in diameter. Structures were uniformly dispersed over the sample and the size and shape distribution was very uniform. Another interesting work that showed flower-like, urchin-like and various other shapes ZnO structures was performed by Zhang et al [106]. Researchers found that such factors as the polarity and the saturated vapor pressure of the solvent are the key factors in shape and size formation of the final product. Also influence of already mentioned factors such as pH, temperature and time were confirmed in this work. Still the growth reasons and the directions are not clear. And the growth habits of the crystals should be well investigated.

2.4.10 Growth Mechanisms of ZnO

One of such works towards investigation of the growth habits of the crystals was made by Li et al [103]. Researchers used zinc acetate and ammonia hydroxide. The autoclave was a stainless steel silver lined tube type with a valve for gas relief at the upper part. The temperatures applied ranged from 200^0 to 350^0 C. The obtained structures were hexagonal prism-like wires with micron sizes. The growth habit of the ZnO structures are related to the growth of crystal faces and they are related to the elements of the coordination polyhedron at the interface. The article suggests that ZnO can grow either faster or slower in some directions. Depending on the solution concentration and pH ZnO crystals can take different shapes. For instance, the fastest growth direction for ZnO is [0001] thus providing nanowire growth in most of the synthesis. The growth processes and the growth habits will be discussed in detail in the Results and Discussion chapter. The hydrothermal method is not limited and can be used not only for oxides.

2.5 Hydrothermal Growth of Ag Structures

Another material that is widely synthesized using the hydrothermal method is silver. Zou et al. synthesized different shapes of silver nanoparticles using the hydrothermal method [107]. The synthesis was performed in the autoclave using $AgNO_3$ and ammonia. Scientists synthesized various shapes of silver nanoparticles: spherical, triangles, rods, hexagons. It is important to mention that along with the chemicals PVP was used as well. Authors believe that it was PVP that caused both the templating and the reduction. Also they found that the variation in concentration for both PVP and $AgNO_3$ can change the shape and size of the nanoparticles. Another hydrothermal work on silver nanoparticles was performed by Aksomaityte et al [108]. For this synthesis a counter-current pipe reactor was used. Silver acetate and PVP were used with different concentrations and at different reactor temperatures. The synthesized particles were 30-40 nm in size as reported. Most of them were spherical in shape. Yang and Pan used the hydrothermal method to synthesize silver and chosen sodium alginate both as a template and the reducing agent [109]. They used different temperatures for 6h and 12h of synthesis. The obtained particles were spherical when the synthesis temperature was 100^0 C for 12h and in the case of 120^0 and 180^0 C mixture of triangles and hexagonal nanoparticles with various size distributions. Kometani and Teranishi demonstrated Ag nanoparticle synthesis in a flow-type reactor system [110]. The reactor allowed the rapid mixing of two solutions: one containing silver precursor and another one a reducing agent. The second solution contained PVP and the nanoparticles were triangles, rods and sphericals with sizes of around 200 nm and 500 nm for the rods.

2.5.1 Hydrothermal Growth of Au and CdS Nanostructures

Along with silver, synthesis of gold also has been reported. Liu et al. used the hydrothermal method to synthesize gold nanoparticles with narrow size distributions [111]. For this synthesis chloroauric acid $HAuCl_4$ and l-histidine $C_6H_9N_3O_2$ were used. The temperature used was from 65 ^{0}C to 150 ^{0}C and the size distribution of the particles were 11.5 nm which is not easy to synthesize using other methods. Some particles were triangle-like with rounded corners (around d=10 nm). Another hydrothermal method for Au synthesis was performed by Liu et al [112]. The pH was controlled and the dendrimer of PAMAM type was chosen as the stabilizing agent. The particle sizes were around 5.6 nm which was a high achievement considering the agglomeration and other factors at that scale. Cadmium sulfide nanostructures and nanoparticle can also

be synthesized via the hydrothermal approach. Xiang et al. synthesized CdS flower-like, leave-like and branched structures [113]. The reaction time, temperature found to be most influential and found to be optimal was 180 ^{0}C at a particular concentration. The study showed that increasing the synthesis time the structures were more and more complicated. The role of pH on CdS hydrothermal synthesis has also been reported [114].

2.5.2 Microwave-Assisted Synthesis

One of the processes that can be associated with the hydrothermal process is Microwave-assisted synthesis. Instead of producing heat by conventionally heating up the solution it is heated up by microwaves in an oven. Using this method, it is possible to synthesize the variety of materials. Some of them we are going to review briefly. One of the main advantages of this approach is that the solution is heated up immediately since the microwaves transport the energy through the materials. CdS microwave assisted synthesis was performed by Caponetti et al [115]. The synthesis was performed in an oil-water microemulsion at 2.45GHz frequency and 22-30W power of the oven. The results obtained were rather outstanding since they obtained very small 2.7nm CdS crystals. They maintained 35 ^{0}C temperature during the synthesis process and concluded that due to the interaction between the electromagnetic field and the dipoles of the water eventually initial faster growth occurred. Synthesizing CdS with such small sizes was always challenging and usually required either a very well controlled synthesis processes or a very good templating since nanoobjects at that size tend to aggregate or due to Van der Waals forces agglomerate rapidly [116, 117]. Esmaili and Habibi-Yangjeh synthesized CdS in 4-6minutes [118]. They used 1-ethyl-3-methylimidazolium ethyl sulfate (RTIL) and water mixture. ESEM micrographs reveal that the sizes were ranging from 50nm to up to few hundreds of nm. Various nano and micro ZnO structures were synthesized using zinc nitrate and pyridine via microwave hydrothermal synthesis [119]. The synthesis time was 10mins and the temperature 900 C. Changing the concentration of pyridine it was found that shape and size can also be controlled. Motshekga et al. demonstrated microwave synthesis of metal oxides supported on carbon nanotubes [120]. Zhu et al. demonstrated the synthesis of tellurium nanorods and nanowires [121]. As we can see the hydrothermal microwave-assisted syntheses basically do not have limits in terms of the materials that can be used and the high quality of the product that can be

achieved. To understand the internal processes we must first ask: what are microwaves? Microwaves are electromagnetic waves with frequencies of 300MHz to 300GHz. When a portion of the microwaves hits a polar molecule, such as water for instance, the water molecule is trying to orientate with the electric field of the wave Fig. 2.4. After the orientation process has occurred and the dipolar (H_2O) molecules orientate they have already lost the energy portion due to the molecular friction and this energy is then transferred in the form of heat [122, 123].

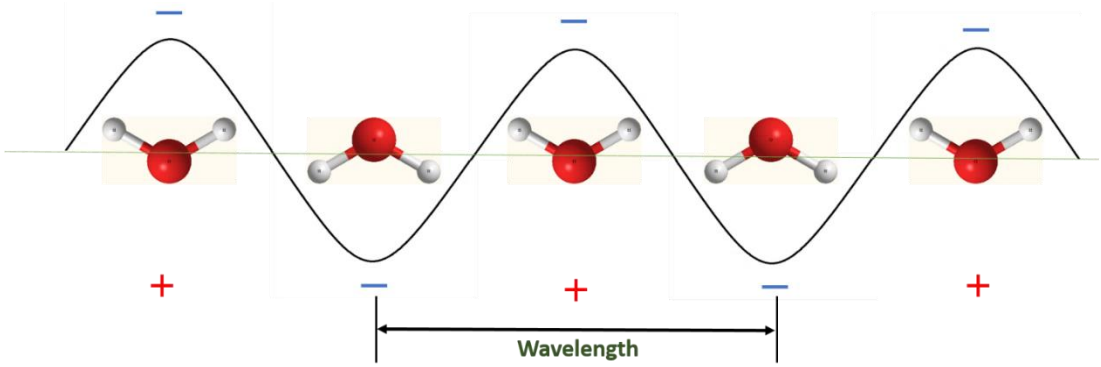

Figure. 2.4 orientation of water molecules in an electric field after the microwave hits the water.

Water is a good microwave absorber with a relaxation time of 9×10-12 s at 200 C and a relaxation frequency of around 18GHz [123]. Microwave-assisted hydrothermal synthesis provides uniform and rapid heating of the solution causing the synthesis of a uniform nanosized object with small size distributions.

2.6 Photochemical Synthesis of Nanoparticles

Another important method that is used in nanosynthesis is the photochemical method. It is believed that light can cause reduction reactions with the nanoparticle precursors. Also, it is important to mention the fact that photochemistry cannot be used on all materials. Traditional photochemical synthesis is the synthesizing of silver nanostructures. Basically, this method is a liquid chemistry method and involves traditional (nitrates, chlorides etc.) chemicals dissolved in a liquid medium with or without the addition of the reducing agent. The silver nanoparticles were triangular shaped after exposing the solution containing silver nitrate and sodium citrate to the green light. The synthesis was done with Light emitting Diodes (LEDs) and with a laser as a source of light.

2.6.1 Wavelength of Light Influence on the Synthesis

J., Zhang et al. found that depending on the wavelength of light it is possible to control the aspect ratio of the nanorods [124]. Their photosynthesis is based on a seed-mediated approach. To synthesize seeds $AgNO_3$ and BSPP solution was used and irradiation with UV light of 254 nm. Then the solution was added to the mixture of $AgNO_3$ and sodium citrate. The irradiation was performed for 24 hours using a 150W light source and filters with filtering from 600 nm to 750 nm +-20 nm. The result yielded in very uniform nanorods with pentagonal cross-sections. The work showed that increasing the excitation wavelength from 600 to 750 nm the aspect ratio of nanorods tends to increase. Maretti et al., made another photochemical synthesis method that was performed in THF and in toluene, results showed high fluorescence of Ag nanoparticles [125]. The synthesis was done in the nitrogen atmosphere and in the air. The precursors were silver acetate with cyclohexylamine and a UVA was used as the light source. According to the report, the solution showed the formation of nanostructures in around 3 minutes (by changing the color of the solution). TEM images indicated only spherical shape of the nanostructures and the difference in size with each solvent. Nanoparticles synthesized using THF were twice smaller as that with toluene. In the case of the reaction with THF particles size 5 +-2nm and with toluene around 10+-2nm. The presence of cyclohexamine proved to have an influence in synthesis as another solution containing toluene and hexadecylamine was proven to increase the size distribution of the NP's from 5nm to up to 20nm. This approach could be useful if fluorescent NP's desired. Park et al., used the synthesis method in which a UV lamp was used as well [27]. The main difference with previous methods is that citrate-capped seeds were used. Authors hypothesized that the synthesis occurred due to photoelectron transfer from citrate to Pt nanoparticle seed. The resulting Ag morphologies were nanorods and nanoparticles. Exposure to UV light with variation in time for every sample showed a significant difference in the resulting product. Exposing for 45 minutes to UV formed nanoparticles and clump-like structures and increasing the exposure time to 60 minutes gained nanorods with great aspect ratio. Nanorods were of around 100 nm thick and 5-6 micrometer in length. Further based on the work done by Redmond et al [126] the reaction was explained in the following way:

$$\text{Citrate} \xrightarrow{hv} \text{acetone-1,3-dicarboxylate} + CO_2 + 2e^- \qquad (2.3)$$

This process according to the authors leads to the formation of Ag nanostructures with extra electrons and the reducing source for Ag^+. This experiment suggests an interesting reaction pathway since the citrate is proposed to be an electron "donor" and other photochemical processes basically should be coming out from this perspective as well.

2.6.2 Shape of the Nanoparticles

However, there is no explanation on the dependence of excitation on the shape of the nanostructure. Pietrobon and Kitaev synthesized decahedral silver NP's by using $AgNO_3$, sodium citrate, PVP, L-arginine and $NaBH_4$ [127]. The nanoparticles were first grown using a chemical reduction of $NaBH_4$ and afterward the solution was exposed to a metal halide lamp (white) of 400-watt power. An experiment was also done with a blue filter which led to the formation of smaller decahedra NP's. The reaction was monitored using an UV-vis spectroscopy. The results showed that increasing the time of exposure to the light from 2 to 15 hours the size of decahedral NP's was ranging from 35 nm to 45nm respectively. The role of the chemicals is described to be essential. PVP makes stable nanoparticles and the arginine accelerates the photochemical transformation process. While $NaBH_4$ is a well known strong reducing agent widely used in nanochemistry. In thermal synthesis decahedra nanoparticles do not form so the conclusion is that the light is essential for this synthesis. Another very similar photosynthesis was performed by Zhang et al [128]. they used 150 W halogen lamp the filters were 500 +- 20nm, 550+-20 nm and 600+-20nm and 650+-20nm. The solution also contained $AgNO_3$, sodium citrate but the difference was in the use of BSPP and NaOH. The results were nanoparticles with different shapes: triangular bipyramids, triangles and spherical NP's. Triangles and spherical NP's were observed after stopping the synthesis after 1hour and 8hours respectively. These results basically suggest that the light is playing only the role of force to make a chemical reduction. R., Jin et al. Reports synthesis of nanoprisms also using silver nitrate, sodium borohydride and trisodium citrate then the addition of BSPP helps to form the nanoprisms [129].

2.6.3 Influence of Time and Light on the Nanoparticle Growth

Light and time also has an influence over all growth process. For the irradiation a 40W fluorescent lamp was used in [129]. They found that increasing the irradiation time from 55 to 70hours the triangles grow more uniform and basically no spherical particles were observed. Most of the photochemical synthesis of silver nanoprisms, nanoparticles, nanorods includes the use of $AgNO_3$ and $NaBH_4$ for the formation of seeds at the initial stage. Since atoms and small clusters attach to the bigger objects inside the colloid the seeds are required. During the growth process the role of light was being introduced. The light can transform spherical nanoparticles into triangles and it is also believed that the growth is mainly influenced by light.

Possible interpretation. Later R., Jin again reports a very similar synthesis procedure that their group used before (regarding the chemicals) [130]. The main difference is that they used a dual-beam illumination this time to grow the nanoparticles. They state that all the process is driven by surface plasmon excitations and the whole process can be controlled by simply changing the wavelength. The plasmon excitation leads to the fusion of the NP's or the termination of the growth after they reach final size controlled by light. They used a 150W xenon lamp with a 12W output and optical filters for 50 h. The TEM analysis showed that nanoparticles had two distributions of nanoprisms: the smaller particles with an edge of 70+-12nm (type 1) and the larger ones 150+-16nm (type 2). The thickness was observed to be the same for both types of nanoprisms. The process explained with dipole resonance of Ag nanoparticles. The control of the secondary wavelength allows the control of the size of the nanoparticles due to bimodal growth. Bastys et al. used light emitting diodes to grow silver nanoprisms [131]. The nanoprisms exhibited strong absorption in the IR region. The wavelengths of LEDs were: 518 nm, 641 nm, 653 nm. This work also confirmed the influence of longer wavelengths enabling the formation of the side length of the nanoprism. The size of the structures was about 150 to 200 nm (edge length). To grow NP's as in previous methods first seeds were prepared by reducing the $AgNO_3$ with $NaBH_4$ and the addition of sodium citrate. The only difference from previously mentioned methods is that PVP was used as a template. In photochemical synthesis, most of the works are mainly done on silver nanostructures with some modifications usually the addition of chemicals or the varying of the light source. In any photochemical synthesis usually, silver is somehow involved in one way or another.

2.6.4 Influence of Chemicals on Growth of the Structures

Dong and Zhou used the photochemical method to synthesize gold nanostructures [132]. The experiment was done under UV (300 nm) light and using a PEG-acetone mixture as a template also pre-synthesizing seeds of Au. The work reports that the speed of the reaction can be controlled via increasing the concentration of citric acid (increasing the concentration of the citric acid the reaction speed increases). The reaction resulted in near uniform spherical nanoparticles with sizes from 10 nm to 12 nm. They also report that by increasing polymerization degree the size of the nanoparticles decreases and the size of the nanoparticles increases by increasing the wavelength or irradiation.

The role of the pre-formed seeds. The addition of pre-formed gold seeds was added to the silver nitrate containing solution and then irradiated with UV light [132]. The result was the formation of an Au nanoparticle with an Ag shell. It is suggested that Au (seed) particles catalyze the reduction of Ag ions under the UV light leading to the formation of an Ag shell. Also synthesis of gold nanowires was modified by this group. First synthesis of Au nanowires was proposed by Esumi et al. [133] using UV light form a xenon lamp (200W) of 253.7nm and using $HAuCl_4$ and HTAC as a template. They report that only spherical particles obtained at low concentrations (1mmol dm-3) and only increasing the concentration up to 5 times the nanorods were obtained. The obtained nanorods of this group contained also nanoparticles and were varying in thickness and length. This method was improved by the previous group of Dong and Zhou [132]. They grew nanorods with more uniform size and length distributions. The novelty was the use of different solvents and mixtures of solvents. The mixture of DMF and water ratio can actually control and optimize the growth and the aspect ratio of gold nanorods. As a template in this synthesis CTAC was used. The solution contained DMF-CTAC-acetone mixture and the result of the synthesis highly depended on CTAC micelle. The explanation was that due to the change of solution polarity the CTAC micelle transforms from a spherical to a rod-like shape and thus leading to higher number of micelle aggregation. In this way molecules form almost perfect template for rod-like nanostructures. This statement was confirmed by changing the concentration of CTAC. It was found that at higher concentrations of CTAC the growth of nanorods is poor. This result could be explained by CTAC molecules blocking the pathway for the growth of nanorods. At optimal conditions the

aspect ratios from 50 to 150 were obtained. It was also found that longer exposure to the light time was favorable for the formation of the nanorods. The photochemical method is efficient and exciting since it can be controlled and always modified. Room temperature is always enough for the photochemical synthesis. Synthesis can be stopped at any moment of the synthesis process i.e light can be switched off. It is cheap and portable (depending on the size of the set-up) which is easy to install. On the other hand to run photochemical synthesis photo-sensitive chemicals are required which also limits the spectrum of materials that can be synthesized photochemically. The only problem is that the method is not very popular and very few articles are available in this topic.

2.7 Template-Assisted Synthesis of Nanoparticles

This method is widely used in nanosynthesis. Templates are usually used in order to achieve uniform structures and to avoid using high temperatures (in the liquid phase). In template-assisted synthesis the pre-synthesized template is usually in liquid phase and the molecules of the desired material are allowed to either settle down or make a chemical bond with the template (inside the template) thus usually it creates one dimensional nanostructures [134-136]. In most cases the templates are organic (like polymers) and the materials that are being synthesized are metallic or semiconducting [137]. In the case of template assisted synthesis in liquid phase the template could be: (a) dissolved in the liquid (water, acid or any organic liquid depending on the material) or (b) a solid prepared template (could be made from any material that is possible to nanostructurize or make desired voids or shapes). In the (a) procedure usually polymers are used. The desired structures are Ag, Au or alloy nanoparticles and in (a) usually polymers are dissolved and the metal precursor is added afterwards (for example $AgNO_3$). After stirring for some time in order to get the maximum interaction between the molecules the reducing agent is added for the formation of the nanostructures. The shape of the nanostructures is usually spherical but it also depends on the template. For instance, in the synthesis of silver nanowires only ethyleneglycol (EG) and silver nitrate are used [138]. The EG serves as both the reducing agent and the template. Also such polymers as dendrimers could be used as well, since they have a spherical shape and dendritic structure also most of them are soluble in water. The structure of the dendrimer is shown in Fig.2.5. As we can see the diameter of the dendrimer increases with the increase of the generation [139]. Dendrimers are

attractive because of the different functional groups that they have which can also be used in synthesis of hybrid materials dendrimer-nanoparticles for instance [140-142]. Linear polymers have an elongated structure and by using them as

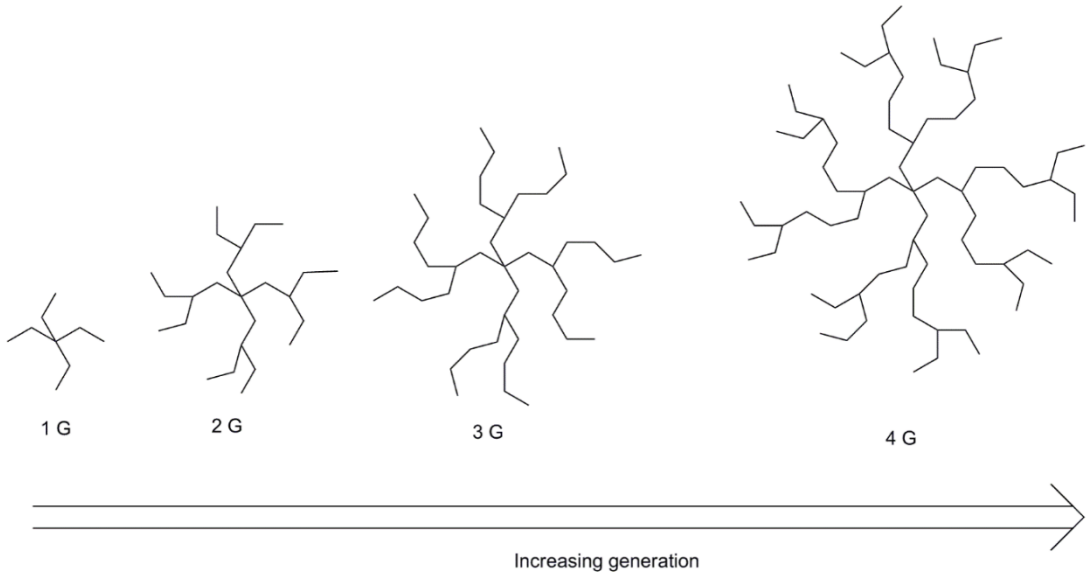

Figure.2.5 depicts structure of dendrimers: dendrimers have branched structure and different generations. With increasing generation dendrimers become more branched and their diameter also increases.

templates can limit the size and shape of metallic crystals by forming large nanoparticles. However, dendrimers have branches as depicted in Fig. 2.5 and nanoparticles can be synthesized either in between the branches Fig.2.6 or between the molecules of the dendrimers (if the concentration is high enough). Before the synthesis process using dendrimers we should pay attention to their unusual non-linear structure that can be easily chemically modified [143] this fact makes them attractive candidates for the template synthesis of nanoparticles. The only disadvantage is the high price. Important experiments were done using polymers in synthesis of gold, silver, platinum and palladium nanoparticles. Dendrimers have a branched structure thus they allow synthesis of very small nanoparticles (few nm) since the nanoparticle precursor (single molecule) can be incorporated between the branches of the dendrimer Fig. 2.6. After the reduction nanoparticles are limited in size because they are “trapped” inside the molecule and

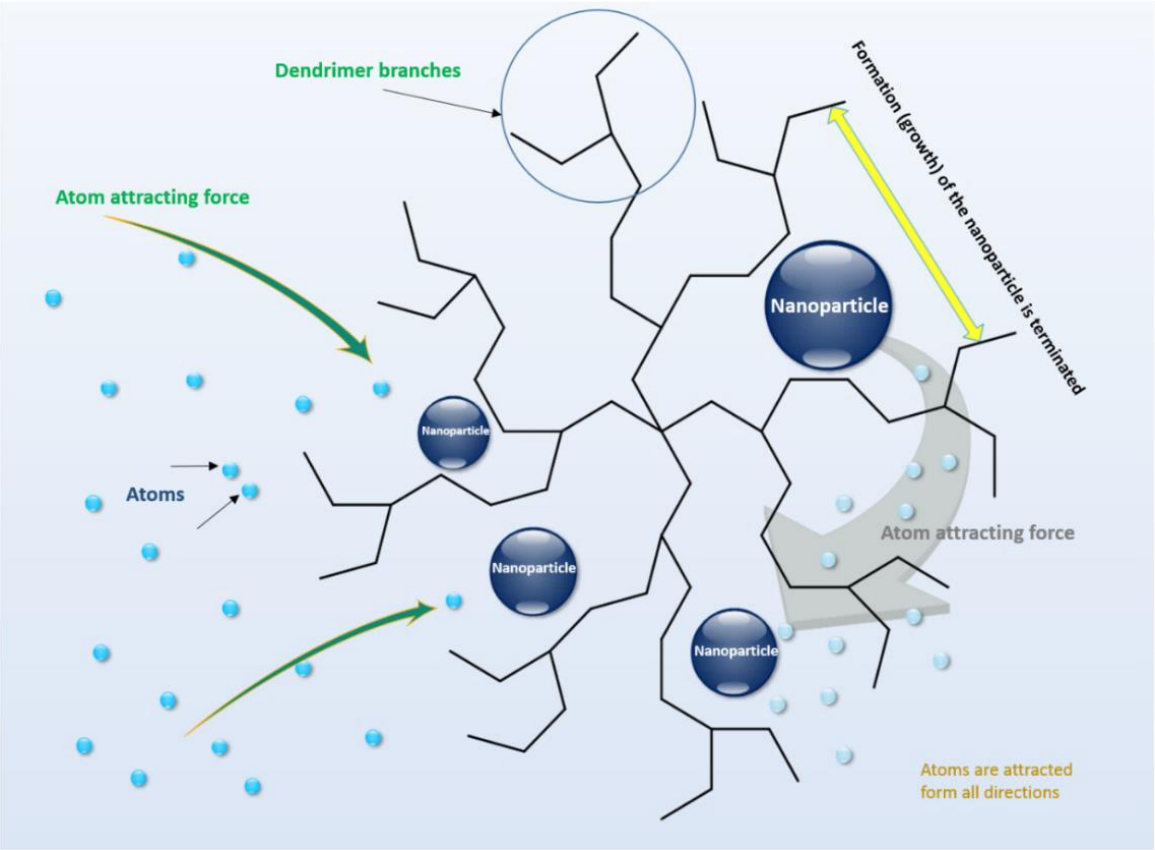

Figure. 2.6 one of the possible synthesis scenarios using dendrimers. The formation of the nanoparticles occurs between the dendrimer branches. When the growth occurs it is terminated by the dendrimer and this effect helps to template the nanoparticles and get the particular size depending on the concentration.

further growth is prevented. There are different types of dendrimers and they have different parameters and also can have various chemical groups attached. After the formation of the nanoparticles (in case of Ag and Au) the change of the solution color indicates the formation of the nanoparticles) the solution is centrifuged, washed and the structures are removed or if the template is attached to the material other chemical processes like etching might be involved. Thus some works in nanoparticle synthesis were performed using dendrimers that should be brought for consideration. One such works in synthesis of 1-2 nm gold nanoparticles using PAMAM type dendrimer was done by Kim et al [144]. The Au nanoparticles were spherical in shape and researchers proved that using a 4th generation dendrimer and higher it is possible to synthesize nanoparticles of less than 2 nm. And increasing the dendrimer generation basically no significant changes in size were observed. In such way also Pt and Ag nanoparticles were successfully synthesized with sizes ranging from 2.2 nm to 5.5 nm [145].

Reduction of $AgNO_3$ or $HAuCl_4$ with $NaBH_4$ is usually instant and can be expressed as:

$$AgNO_3 + NaBH_4 \longrightarrow Ag + 1/2H_2 + 1/2B_2H_6 + NaNO_3 \quad (2.4)$$

$$4HAuCl_4 + 3NaBH_4 + 9H_2O \longrightarrow Au^0 + 3NaCl + 3H_3BO_3 + 13HCl + 6H_2 \quad (2.5)$$

These reactions occur in liquid reducing metal precursors with strong reducing agents such as sodium borohydride. Adapted from ref [146]. Another process that exists in dendrimer encapsulated nanoparticle synthesis is the galvanic redox process. This process is the electron transfer between two metals in different oxidation states and refers to the electrochemical process. This process was used in Pd and Cu nanoparticle synthesis [147]. Using dendrimers usually small spherical particles can be obtained. This is a very powerful template since it can produce nanoparticles of sizes with less than 2 nm. One of the previously mentioned organic molecules is ethylene glycol and is also used in templated synthesis. EG with $AgNO_3$ produces Ag nanowires with different aspect ratios acting both as a template and a reducing agent. When $AgNO_3$ is dissolved in water it creates ions Fig.2.7. The ions float freely in a solvent and the molecules of EG hits them and mix. This is why usually such processes include stirring before the reaction starts. But in the case of EG and Ag it starts immediately and is not rapid like in the case of $NaBH_4$.

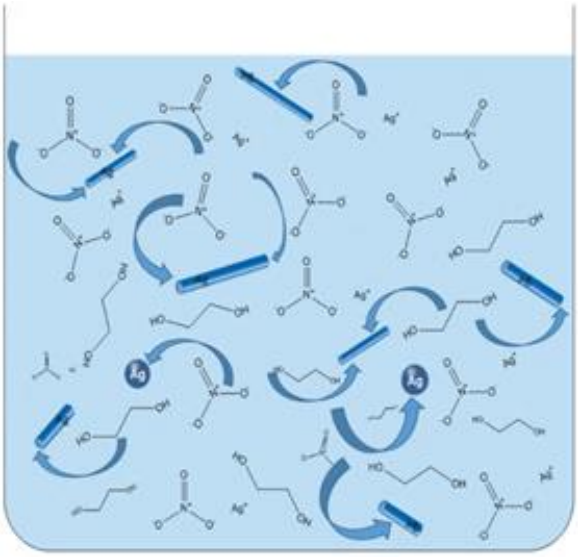

Figure.2.7 depicting the synthesis process of Ag in a liquid solution with the presence of ethylene glycol (EG) used both as a template and a reducing agent. As we can see after $AgNO_3$ was dissolved in the water (and then mixed with EG) it 'collapses' into ions and then the reduction occurs.

After silver dissolved due to the reduction silver atoms start to attract each other thus forming subnanometer clusters. Later steps are the growth of the nanostructures but since they are in EG matrix they form linear structures such as nanowires Fig. 2.7. Also using a solid template is very popular in template assisted synthesis. The solid template is usually made of aluminum and called anodized aluminum oxide or AAO. AAO is usually a film with mutually parallel voids. AAO after its use as a template is dissolved and the nanowires collected by washing and centrifuging the supernatant Fig. 2.8. Using AAO template it is possible to grow a variety of vertically aligned materials including Si [148]. There are different types of AAO anodization and template preparation techniques and methods which can be found elsewhere [149].

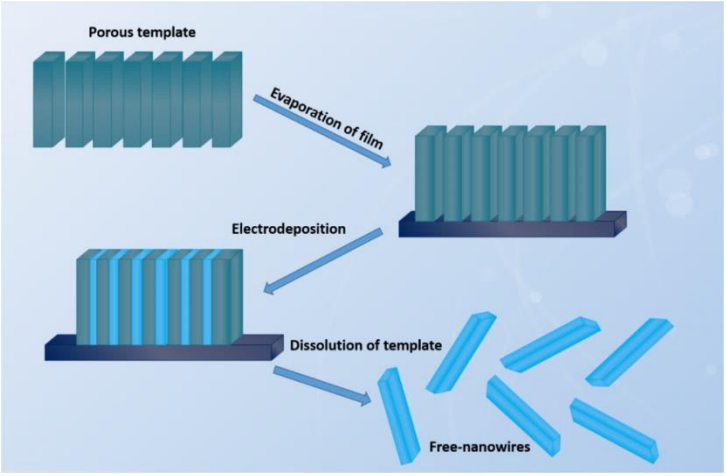

Figure. 2.8 porous Al template. First step includes evaporation of the film onto the template. Then electrodeposition and removal of the template leaving free nanowires.

Yang et al. used AAO in combination with the calcination process to synthesize Ag nanowires [150]. As indicated by SEM nanowires were vertically aligned with small defects that were Ag microparticles. Kim et al. synthesized Pd nanowires by pulsed electrodeposition [151]. Nanowires were of 500-700 nm in length and around 50 nm in thickness. The Pd nanowires were grown on $5cm^2$ area which can be considered as large. AAO can be used in synthesis of TiO_2 [152], Ni [153], carbon nanotubes [154], Au/Ni [155] however the products obtained by this template are usually in the shape of nanowires. The template-assisted synthesis method is efficient but only limited sizes and shapes like spherical particles or nanowires can be obtained in most cases. Also removal of the template and selection of the template creates extra complications for the process as such. The advantages of this method are that the structures obtained are very monodispersive, uniform in size and shape. This is a much desired quality for

industry and science. Template-assisted synthesis is also another very popular method for the nanostructure synthesis. The template if it is organic can drive the crystal growth in a particular way creating one or another shape of the crystal. This method has one disadvantage because it is not easy to remove the template after the synthesis. If the template is organic it also might interact with the synthesis product. If the template is not organic then another step of removing the template is required.

2.8 Control of End-Functionality of P3HT

Synthesis of conducting polymer has been a great interest for chemists for many years [156]. Electroconductive polymer or semiconducting polymer can be used in a variety of applications [157] since it has flexibility, solubility and a physical properties of a solid conductive material [158]. The properties of P3HT depend mostly on its end-functionality groups. In this work we are not going to synthesize or functionalize polymers. However, it is reasonable to briefly review the end-functionalization strategies of P3HT. There are two simple strategies for end-functionalization of P3HT: (1) Functionalization via Grignard metathesis polymerization and (2) use of functional Ni-based initiators.

2.8.1 Functionalization via Grignard Metathesis Polymerization (GRIM)

This strategy was reported first time in 2000 [159]. In this process using thiophene group Grignard McCullough-type polymerizations were successfully quenched. But this strategy was limited since it was applicable to only trimethylsilyl groups. McCullough suggested more efficient *in situ* functionalization strategy that involves GRIM polymerization quenching with different Grignard reagents [160, 161]. In this synthesis the end-functionalization is determined by Grignard reagent. Incorporation of additives like styrene and 1-pentene proven to control the end group composition [162]. Also Thelakkat and Lohwasser optimized the procedure and identified that excess of Grignard species and LiCl influence GRIM kinetics [163]. This improvement led into low polydispersity and perfect control of the end group of the polymer.

2.8.2 Functional Ni-Based Initiators

Ni-based initiators polymer synthesis strategy can provide almost perfect product with low polydispersity and controlled molecular weight [164, 165]. Specially designed Ni-based initiators can give a variety of P3HT polymers with different end groups like: amino, ethynyl, carboxylic acid or phosphonate [163, 166-168]. Also a concept for Ni-based external initiators led to a synthesis of P3HTs with different end-functional

groups like: pyridines, thiols, and phenols [169]. This approach also allows synthesizing complicated polymeric architecture. The disadvantage is that traces of Ni impurity can “disturb” the polymer chain ends eliminating the desired group.

2.8.3 Organic Molecules and the Morphologies of Thin Films

Synthesizing the polymer or adding specific functional groups to its end is still half way to the application. The main question is: what will we do after the desired polymer is synthesized? We will answer this question in the next subchapters. The synthesis or structuration methods sometimes limit the morphology of the nano or microstructures [170]. Organic molecules like polymers play an important part in the synthesis of nanomaterials [171]. Polymers can be synthesized for a variety of purposes like photovoltaics[172] or sensors [173]. The synthesis of polymers is beyond the scope of this work. However, a brief introduction on polymer synthesis will be reviewed and discussed. Special attention is given to morphological variations of the structure of polymers on the nanoscale.

2.8.4 The Importance of Polymer Morphology

The present work focuses on a few types of polymers which are semiconductive. Semiconductive polymers have a very wide range of applications as mentioned above from solar cells to light emmiting diodes or LEDs. The most popular are thiophene type polymer and the PCBM monomer mixture. They are relatively cheap and used as a "Playground" for researchers in order to develop concepts about processes happening on a nanoscale. Thiophene type polymers can be dissolved in a variety of solvents at room temperature which gives the flexibility required for the research.

2.9 Morphology of Polymers and Influence on Organic Solar Cells

Progress in organic solar cells led to the development of novel nanostructuration methods of the polymer layers [174-177]. As has been demonstrated the efficiency of the polymer solar cell strongly depends on the materials and nanomorphology of the polymer layers [178]. For a better understanding of the topic first donor acceptor materials should be introduced. The most efficient proven to be P3HT/PCBM and PTB7/PCBM mixture layers [179]. The first layer P3HT/PCBM where P3HT-RR corresponds to Poly(3-hexylthiophene-2,5-diyl) regioregular (RR) which is a donor and PCBM stands for [6,6]-Phenyl C butyric acid methyl ester where C- is a fullerene which can be usually C61 or C71 and this derivative is an acceptor in an organic solar cell film. PTB7 is poly[4,8-bis[(2-ethylhexyl)oxy]benzo[1,2-b:4,5-b′]dithiophene-2,6-

diyl][3-fluoro-2-[(2-ethylhexyl)carbonyl]thieno[3,4-b]thiophenediyl] and is one of the most efficient low bandbap polymers for the photovoltaics. PCBM acceptor contains benzene ring and fullerene Fig.2.9. atoms in the fullerene.

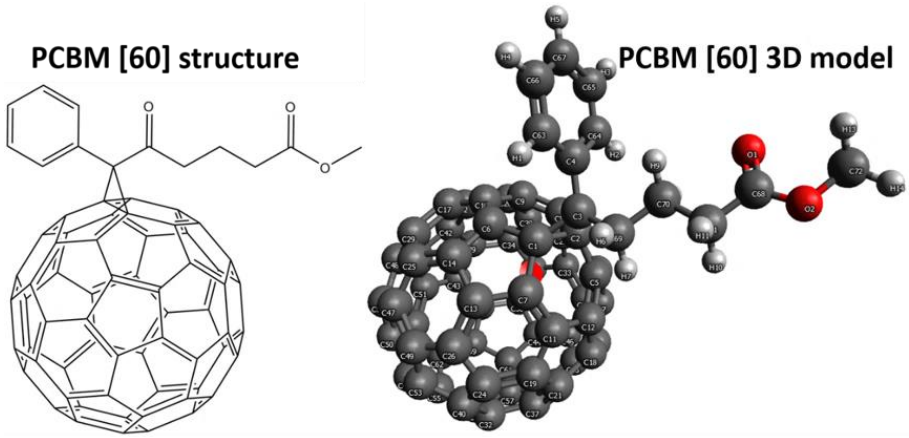

Figure 2.9 structural formula of PC61BM and 3D model.

The most popular type of PCBM is $PC_{61}BM$ and $PC_{[70]}BM$. The difference between these two molecules is the amount of carbon atoms $PC_{60}BM$ contains 60 carbon and $PC_{[70]}BM$ contains 70 carbon atoms Fig. 2.10. The second molecule reported to be more efficient in organic solar cells (C70). PCBM makes one of the best acceptor materials due to its solubility in organic solvents. This is very important feature in order to achieve printable and thin film solar cells.

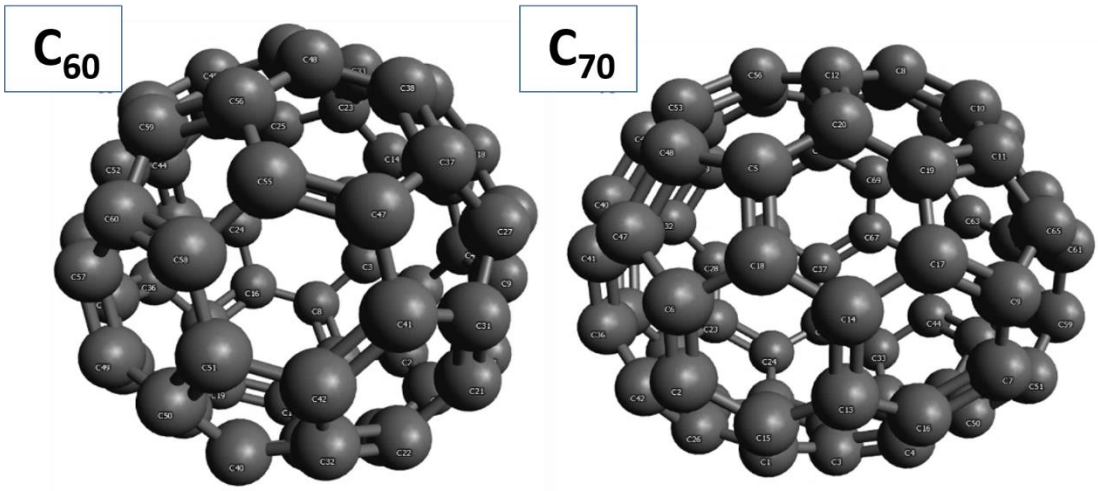

Figure. 2.10 depicts 3D models of fullerenes of two different kinds: C60 in the left and C70 in the right. These molecules define the number on PCBM molecule.

PCBM and its derivatives are usually a necessary ingredient for the organic photovoltaic devices which show very high power conversion efficiencies [180-182].

2.9.1 P3HT/PCBM -Based Solar Cells

Another very important and probably most popular semiconducting polymer used in flexible solar cell fabrication is the P3HT [177]. This polymer has good donor properties and is widely used for solar cell fabrication. The structural formula of P3HT and the 3D model are depicted in Fig. 2.11. It is reported that P3HT in organic solar cells makes a p-type bonding thus creating a particular nanomorphology of the film [172, 183]. This type of nanomorphology usually characterized by AFM. Nanomorphology has a great influence on the performance of the solar cells [184, 185]. Such AFM investigations were performed by Villers et al [186]. The work included nanomorphology control in P3HT/PCBM films. They show that PCBM creates domains in the film thus greatly influencing the morphology of the film. Keawprajak et al. studied the influence of solvent on thin P3HT/PCBM film [187].

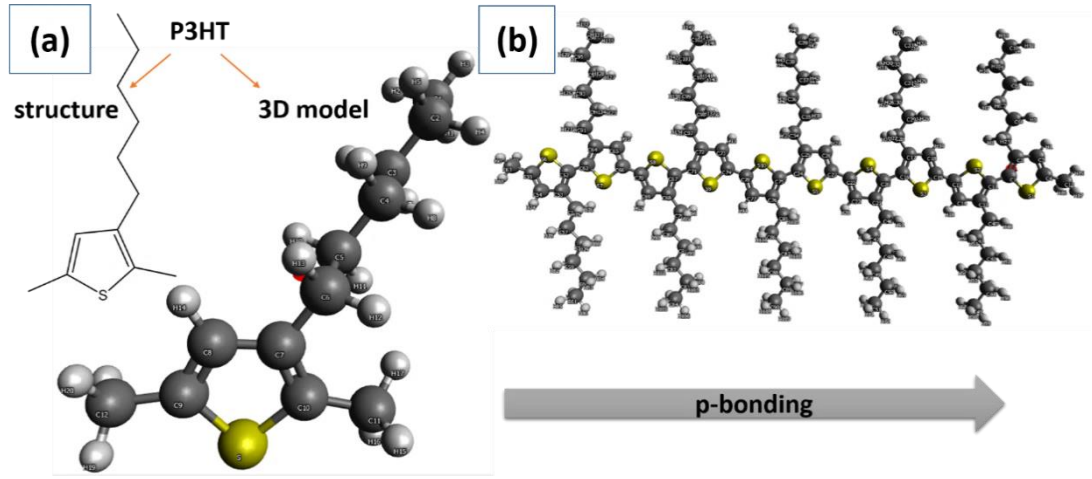

Figure. 2.11 depicts the P3HT semiconducting polymer. (a) the structural molecule and the 3D model of the P3HT and (b) the stacking of the P3HT molecules by p-bonding within the films reported by some works.

They improved solar cell PCE by 20% using TCB and temperature treatment. The roughness of the films was influenced both by solvent and temperature treatment. Lowest roughness was achieved by applying 180^0 C temperature and lowest TCB concentration of 12mg/ml. It is important to mention that the AFM scan area was 25µm which is relatively high for this type of scan. Another report by Chirvase et al. has also shown the influence of nanomorphology upon the performance of the photovoltaic device [188]. Different amounts of PCBM were added to the P3HT/PCBM mixture. An AFM scan was performed at different amounts of PCBM and revealed the formation of nanohills when the concentration was 50%. Also the device showed best characteristics at 50% of PCBM.

2.9.2 Influence of Temperature on Polymer Morphology

The influence of temperature on polymer films showed also morphological changes which led to the structural changes inside that could either increase or decrease the device performance [189]. Shi et al. incorporated nematic liquid crystal into the P3HT/PCBM matrix and improved the PCE [175]. Increasing the amount of liquid crystal AFM images showed changes in nanomorphology. At weight amount 3% the textures could be barely seen but increasing it to 6% it was more obvious. When the amount of liquid crystal was increased to up to 10% the textures were clearly seen and the upper and lower parts of the film were obvious. “Paths” and “hills” could be observed which indicated specific orientation of the P3HT/PCBM and liquid crystal. However, it was difficult to analyze the micrographs since they were not analyzed in detail. It was difficult to answer the question whether it was the P3HT or the PCBM or the temperature that was influencing the morphological changes.

2.9.3 Structural Changes of the P3HT

Grigorian et al. made an investigation on the structural properties of the P3HT [176]. The work revealed that drop-cast P3HT films were highly crystalline and underwent minor changes during temperature treatment. On the contrary films deposited by spin-coating exhibited less crystallinity and changed much more under temperature treatment. It is important to mention that for the investigation Gazing Incidence X-ray diffraction was used (GID). They concluded that P3HT underwent structural changes under temperature treatment and that those changes were reversible. Also they concluded that at higher temperatures π-π distance decreases and interplanar lamellae distances interstacking spacings, crystalline packings are influenced as well. Nicho et al. studied P3HT and different organic molecules [177]. The AFM was used for the morphological charactersations. Researchers showed that by varying the amount of organic molecules it is possible to control the nanomorphology of the P3HT films.

2.9.4 P3HT Mixture with other Polymers

Mixing P3HT with other polymers can give a different morphology. Thus using polystyrene (PS) and P3HT mixture in toluene to make thin films by spin-coating revealed morphology changes upon the variation of the amount of PS. 80:20 ratio led to the formation of spots with diameter ranging from a few hundreds of nm to up to a few microns [177]. 60:40 led to the wider spots with similar sizes as that of 80:20 ratios. The most interesting was 0.5:95 by weight which led to a complete

nanostructurisation of the features on the film (nano-island formation). The same experiment was done using polymethylmetacrilate (PMMA). Changing the amount of the secondary organic molecule researchers demonstrated a relatively high control of the nanomorphology of the P3HT film using toluene as a solvent. Saini et al. demonstrated that the influence on the P3HT could be done by using carbon nanotubes [190]. It was found that multi-walled carbon nanotubes can be dispersed uniformly within the P3HT and as a matter of fact polymer wrapped around the tubes. NMR analysis indicated a chemical interaction between the polymer and the tubes. Lu et al. investigated P3HT/PCBM [60 and 70] morphologies via optical techniques [180]. They fabricated solar cells with efficiencies of around 5%. The finding of this work was that annealing helped to improve the PCE of the device. Increasing the annealing temperature PCBM was forming clusters which were removed by addition of Al. The temperature range was from 100 C to 280 C. By increasing the temperature PCBM clusters were increasing in numbers at 180 C. The investigation of the morphology was conducted mainly via an optical microscope which did not show the nanomorphology. However, microfeatures greatly depend on the nanofeatures.

2.9.5 Solvent Influence on Morphology

Chang et al. also studied the effects on the solvent residues in the P3HT/PCBM films also using optical microscopy [181]. They showed that casting the solvent has an influence on the morphology of the films. They also showed that regardless of the solvent PCBM agglomerates when heated up have an influence on the solar cell parameters. Liao et al. used different solvent annealing and investigated the effects on the morphology of the P3HT/PCBM films [182]. Researchers used non-solvent, bad and good solvents to show the influence on the morphology. PCBM and P3HT molecules were arranging differently within the film after the vapor treatment which was affecting the device parameters.

2.9.6 Annealing Under Solvent Vapours

Another similar work was performed by Verploegen et al. [183]. This work included an investigation of solvent vapors on the P3HT/PC_{60}BM morphology. They found that THF can induce crystallinity in PCBM. THF and chloroform vapor annealing resulted in the swelling of the P3HT layers and importantly decrease in a π-π stacking distance which leads to morphological changes and can improve device performance. Chen et al. used the annealing method to investigate the performance on the devices based on

P3HT/PCBM [172]. All of the methods of polymer morphology control mentioned above are either solvent and solvent mixture based or temperature based. The P3HT/PCBM system is usually the most investigated however another increasingly popular system is the PTB7/PCBM Fig.2.12. This donor-acceptor system can give higher efficiencies of the devices and has a bright future in the area of flexible photovoltaics. However, the control of this type of polymer seems to be the same as controlling any polymer morphology since the same conditions can be applied to the PTB7 and the morphology change can improve the device efficiency.

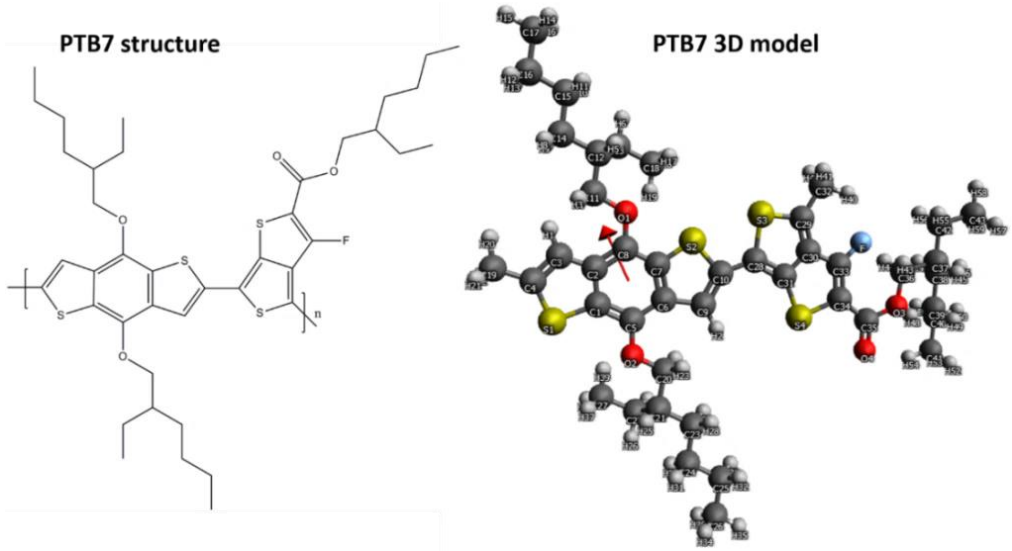

Figure. 2.12 PTB7 structural formula and 3D model in the right.

Guo et al. demonstrated such PTB7 property by preparing films and the influence of the solvents such as chlorobenzene, 1,2-dichlorobenzene, and 1,2,4-trichlorobenzene were investigated [191]. The used polymer had 40% of fluorinated monomers and 1,8-diiodooctane can improve the performance and influence the morphology which are correlated. The films that were made using chlorobenzene had the smallest domains while the DIO influences the PCBM and not the PTB7 which also influences the whole PCE of the device. He et al. fabricated PTB7/$PC_{[70]}BM$ inverted solar cell with an efficiency of 9.2% which is greatly higher than most polymer based solar cells [192]. This article proposes the trend towards 10% which actually can be commercialized. However, currently there are not many works reporting PTB7 morphology manipulation since most of the works are aiming at creating solar cell and increasing the efficiency. Another work by Yanagidate et al. was also creating the PTB7/ $PC_{[70]}BM$ device that had a LiF buffer layer which helped to improve the PCE [193]. The morphologies characterized by the AFM showed that the device with greater

efficiency had smaller nanofeatures however the roughness measurements were not provided. The P3HT/ $PC_{[70]}BM$ and PTB7/ $PC_{[70]}BM$ systems are the most popular and used for the organic solar cell prototype in the laboratory. Depending on the conditions applied polymers can arrange in a particular way which will cause the solar cell efficiency. The main problem is the control of the arrangement of the polymers which still remains a challenge.

2.10 Summary

This chapter gave the introduction to the existing synthesis methods of the nanomaterials. Most important techniques and strategies were reviewed and analyzed. Existing techniques require expensive equipment (VLS or CVD) or high temperatures and/or dagerous chemicals (hydrothermal method). Special attention is given to the photochemical synthesis. In most cases photochemical synthesis can be performed with light-responsive materials or chemicals. Unfortunately not many works has been done in this direction and clear gap can be filled with the light-induced synthesis proposed in this work. Photochemical method is limited to the Ag or Au. Or can be with plasmon-related mnaterials. If the light is not absorbed by the material then the material cannot be affected by the light. Other synthesis methods are well investigated and high precision is achieved over the years using them by a variety of scientists over the World. This fact puts light-related synthesis method in a shadow as less efficient and undeveloped. Photochemical synthesis is the smallest subchapter in the literature review and the method requires an improvement. Also existing nanostructuration methods for the polymers was reviewed and analyzed. Surface morphology can influence overall efficiency of the solar cell and is very important for the future organic photovoltaics. Most popular semiconductive polymers were considered and the strategies of improving their morphology was reviewed. The most common strategies of changing the polymer film morphology is the treatment of the polymer film with solvent vapours or heating it up called annealing. Polymer surface morphology variation is really limited due to the polymer chemistry and is time consuming.

Chapter 3 Experimental Methods

In this chapter experimental methods such as the experiment set-up preparation, synthesis procedure, sample preparation and characterization will be described. Characterization methods and techniques are introduced and described.

3.1 Raw Chemicals

For the synthesis of nanoparticles and nanostructures the raw materials were used: oleic acid ($C_{18}H_{34}O_2$), nitric acid 70% (HNO_3), chloroauric ($HAuCl_4$), P3HT Poly(3-hexylthiophene-2,5-diyl) regioregular 1g, $PC_{[70]}BM$ [6,6]-Phenyl C71 butyric acid methyl ester mixture of isomers 99% 500mg, chloroform 2l, dimethylformamide 500ml, tetrahydrofuran 2l, dimethylsulfoxide 1l, xylene 1l, ethanol, ethanol anhydrous. Silver nitrate, sodium hydroxide, cadmium acetate dihydrate, sodium borohydride (powder), tri-sodium citrate dihydrate, cadmium acetate dihydrate. All chemicals were purchased from Sigma-Aldrich UK. Substrates: silicon wafers 7X5 and mica (for AFM) were purchased from Agar Scientific. For the TEM investigation copper grids formware were also purchased form Agar Scientific. PPI-G4-32 dendrimer from SyMO-Chem.

3.2 Procedure for Synthesis

3.2.1 Synthesis of Gold Nanoparticles

For the gold nanotriangle synthesis oleic acid, nitric acid and chloroauric acids were used. Step1: Chloroauric acid was weighted to have 1mmol and added to the 50ml vial. Step2: 0.1ml of concentrated (70%) nitric acid was added to the vial with chloroauric acid. Step3: Oleic acid was added to the vial(50ml) and shook manually. The solution was left for 24 hours without further stirring. After 24 hours the bright yellow precipitate removed and deposited via drop-coating on the silicon wafer for the ESEM without further procedures. Schematic depiction of the experiment is depicted in Fig.3.1.

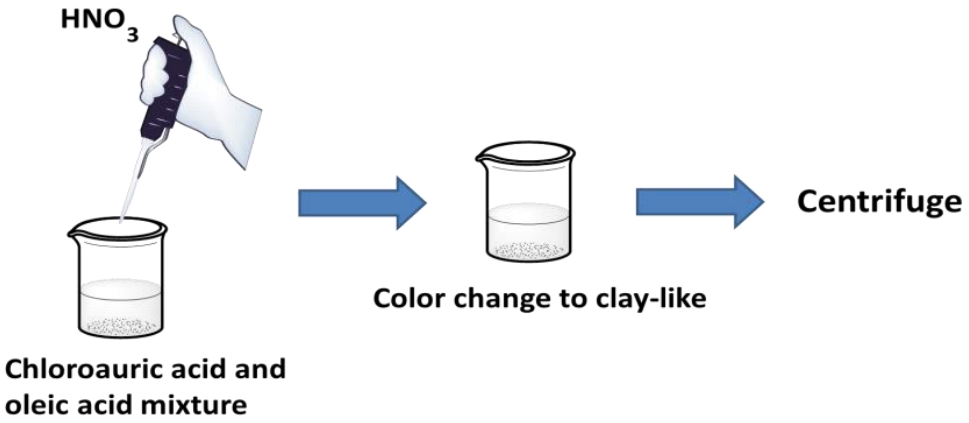

Figure 3.1 shows the experimental set-up scheme. In the mixture of chloroauric and oleic acids concentrated nitric acid is injected using a micropitette. Then after some time when the color of the liquid changes to bright clay-like the nanoparticles are formed. The last step is centrifuge and the extraction of gold nanoparticles for the characterization.

The extraction of nanoparticles was performed using ethanol and distilled water. The solution turned to be clay-colored and was not liquid anymore. It looked like a solid soap. First ethanol was used to dissolve the particles. After dissolving the particles the solution was centrifuged two times in ethanol and then 3 times in water. For easier sample preparation ethanol can be used as a solvent.

3.2.2 Synthesis of CdS Quantum Dots

Cadmium acetate dihydrate ($Cd(CH_3CO_2)_2$) 1mmol was added to the 20ml vial along with 15ml of distilled water and 1mmol of PPI(SyMo-Chem) type 4th generation dendrimer (poly(propylene imine))) containing NH_2 groups. The mixture was stirred overnight at 200 rpm stirring speed using a magnetic 1cm bar. The next step was the addition of sodium sulfide (Na_2S). For the AFM characterization, the solution was spin-coated at 2500 rpm for 60s on a silicon wafer (AgarScientific).

3.2.2.1 Preparation Procedure of CdS Quantum Dots

The synthesis of CdS was performed under nitrogen atmosphere and at room temperature. Two three neck chemical glasses were used to prepare the components for the synthesis. Rubber caps were used to cover all the 3 necks first. Then in two of the rubber caps sterile syringe needles were inserted to ensure the nitrogen circulation. The middle neck was connected to the nitrogen bottle fig.3.2 After the chemicals were dissolved the Na_2S solution was injected from step1 to step2 using a syringe and

elongated needle. After the solution turned from transparent to yellowish it indicates that CdS quantum dots were formed.

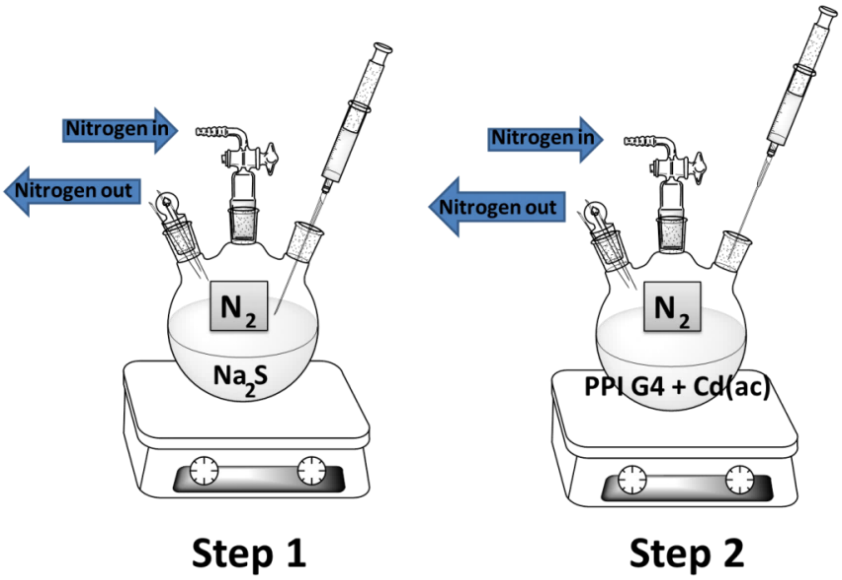

Figure 3.2 depicts synthesis of ordered CdS quantum dots using a PPI type dendrimer. At first all the chemicals are dissolved separately in a solvent. And the nitrogen flow is provided to both mixtures. The mixture containing sodium sulfide is taken from the solution step 1 and injected into the solution containing cadmium precusrsor and the dendrimer step 2.

3.3 Experiment Set-up for Synthesis of ZnO, Ag, Ag-Au Nanostructures

In this subchaper we will describe the light-induced synthesis set-up preparation and procedure used. Light-induced synthesis was performed at room temperature for ZnO, Ag, Ag-Au and nanostructuration of the polymer films P3HT/ $PC_{[70]}BM$ and PTB7/ $PC_{[70]}BM$.

3.3.1 Experimental Set-up for Light-Induced Synthesis

For all these materials (ZnO, Ag and Ag-Au) the same experimental set-up was used. This consisted of a laptop, a microcontroller, LEDs, prepared solutions and a synthesis chamber. The detailed experiment set up is shown in Fig.3.3.

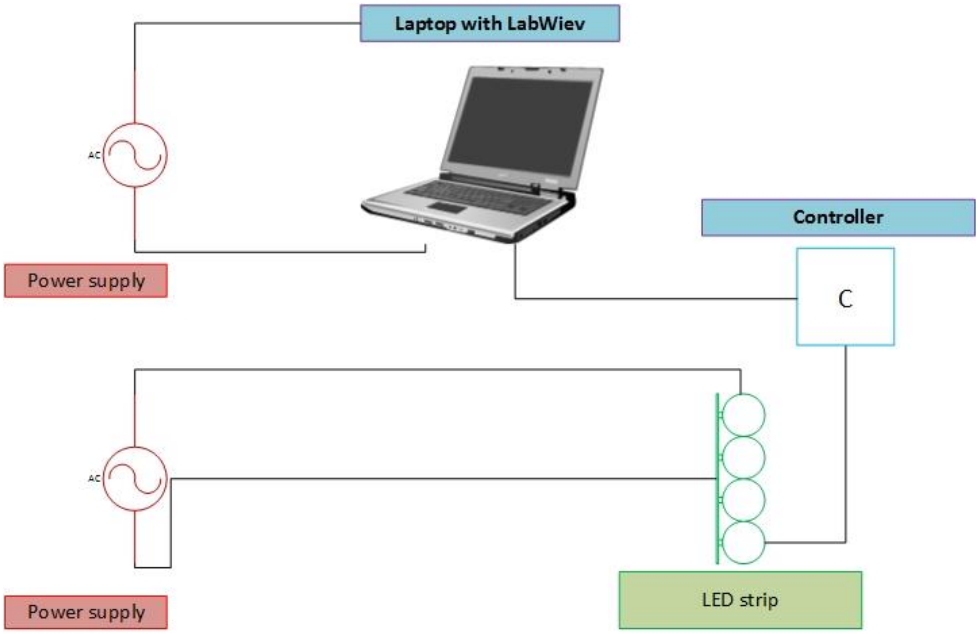

Figure.3.3 depicts the setup of the experiment. The main components are the LED strip and the controller with a laptop. The controller was programmed from the laptop and then the LED strip was placed into the synthesis chamber with the chemical solution.

The control of the LED sequences was programmed using LabWiev Software and transmitted from a laptop to the controller and then to the LED. The controller was a National Instruments USB 6008 driving the LEDs via solid state relays. The key point of this experiment was to control the energy (light) portions to the samples. This set-up allowed great light-induced synthesis control and time-dependent energy portions from different parts of the optical spectrum. Also it was possible to control the cycle number which precisely controlled the synthesis time. The synthesis chamber was simply black box with aluminum foil inside to reflect the visible light. The distance between the light source (LED) and the sample was always 15cm.

3.3.2 Procedure for Light-Induced Synthesis of ZnO

Zinc acetate dihydrate ($Zn(O_2CCH_3)_2(H_2O)_2$) was dissolved with different molar ratios (1mmol, 2mmol, 3.2mmol) in distilled water (20ml vial 15ml of water) with the addition of of 1ml of ethanol. Then from the stock solution 1ml of sodium hydroxide (NaOH) was added (2mmol/ml). The vial was immediaty placed into the light chamber. The light sequence was chosen to be as shown in Tab.3.1. All the chemicals were purchased from sigma Aldrich. For Ag and Ag-Au synthesis these sequences were slightly modified (RGB and green-red) and for the polymers only red and blue lights were used. Photoinduced synthesis and nanostructuring were carried out for

12hours in the synthesis chamber. RGB-code was 1s red, 1s green and then 1s blue. Then the cycle was repeated.

Table.3.1 the light sequence code for the ZnO synthesis experiment.

Title	Wavelength (nm)	Wavelength (nm)	Wavelength (nm)	Wavelength (nm)	Wavelength (nm)	Wavelength (nm)	Time
Code1	634 (red)	518 (green)	634 (red)	518 (green)	634 (red)	Off	12h
Code2	634 (red)	461 (blue)	634 (red)	461 (blue)	634 (red)	Off	12h
Code3	518 (green)	461 (blue)	518 (green)	461 (blue)	518 (green)	Off	12h
Code4	518 and 461	461 (blue)	Off	518 (green)	634 and 518	518	12h
Time	10 seconds	30 seconds	25 seconds	10 seconds	25 seconds	10 seconds	Repeating

3.3.3 Specifics of the Light-Induced Synthesis

The light-induced synthesis set-up and conditions were the same for all the materials ZnO, Ag, Ag-Au and nanostructuration of the polymers. The specifics of the synthesis revealed the importance of every small and non-significant move and condition. Such as importance whether the experimentalist will inject or pour sodium hydroxide into zinc acetate or the other way around. The results can change dramatically leading to results with a great bias. Also if the vials or chemicals used are not pure enough this would lead to a change in shape and or size of the final product.

LED light.During the synthesis a LED light must be switched on all the time. Before the chemicals are mixed a LED light must be on and also during the mixture of the chemicals. It is also recomended to do the synthesis in the dark area where the daylight cannot reach the samples (because of UV). For the synthesis in dark it is also recommended to wrap the vials or beakers in aluminium foil to avoid any light reaching the chemicals. Also when light is shinning through the bottom of the vial it does not influence results Fig.3.4. The influencial factor is stirring or shaking. No magnetic stirrers or shakers should be used. This helps to assemble the hierarchical nanostructure. For better analysis the light wavelenght should be measured and the spectrum obtained. Since every light wave (color) has a different energy it is very important to know which energy portion (higher or lower) influences the growth. The LED wavelength of light was characterized using an OceanOptics USB4000 optical bench spectrometer calibrated from 300nm to 800nm and used with SpectraSuite software.

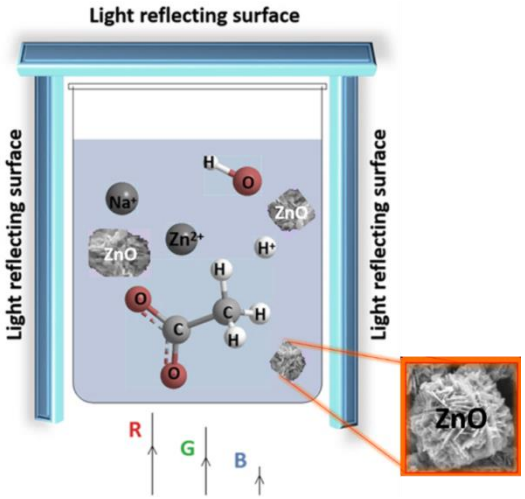

Figure.3.4 shows schematic set up of the ZnO light induced synthesis at room temperature. The vial or glass beaker is surrounded with light reflecting surfaces and the light is shining from the bottom.

3.4 Procedure of the Synthesis of Ag and Ag-Au Nanostructures

Silver nitrate ($AgNO_3$) was prepared with a concentration of 1mmol/ml in a 20ml vial (15ml of the solution) in distilled water. The second step was the addition of trisodium citrate ($Na_3C_6H_5O_7$) with the same concentration (1mmol/ml) of 1ml and placing the solution into the light chamber without stirring. To produce Ag-Au nanoalloy the addition of chloroauric acid with the molar ratio to make 50:50 (50% of Ag ($AgNO_3$)and 50% of Au ($HauCl_4$)) was prepared into a 20ml vial and placed into the light chamber for 12 hours. The samples were prepared for the SEM investigation without further washing or centrifuging by drop-casting and drying then at 40^0 C temperature for 4-5hours.

3.5 Polymer Morphologies

A morphological structure change experiment was performed using semiconductive polymers and a LED light. The experimental set-up described in subchapers 3.4 – 3.6. The morphological change was performed with polymers in the chloroform at room temperature and using a LED lights of two wavelengths red (633nm) and blue (461nm).

3.5.1 Light-Induced Morphology Manipulation of PTB7/ $PC_{[70]}BM$ and P3HT/ $PC_{[70]}BM$

The P3HT, PTB7 and $PC_{[70]}BM$ were purchased from Sigma-Aldrich and used without further purification. For the experiment two types of solutions were prepared: P3HT/ $PC_{[70]}BM$ and PTB7/ $PC_{[70]}BM$. The molar ratio was chosen to be 1:1. For the solvent-

based experiment only the P3HT/$PC_{[70]}BM$ system was used. For the light-induced nanostructuration experiment two systems were used: P3HT/$PC_{[70]}BM$ and PTB7/$PC_{[70]}BM$. All the solutions were in chloroform ($CHCl_3$). After dissolving the polymers the samples were placed into the light chamber without stirring and left for 12 hours. After the light chamber the solutions were spin coated on a silicon wafer and characterized using AFM.

3.5.2 Specifics of Polymer Morphology Light-Induced Approach

This experiment that proven light can influence the morphology of the polymer films has few important details that are worth mentioning. First of all chloroform was chosen since it is the best solvent for these polymers. Secondly the concentration plays an important role. The concentration as it was mentioned in 3.10 was 1:1 molar ratio of both polymers. If the ratio will be 1:10 then the solution turns too dark (it is dark brown in color) and the light cannot penetrate through the sample. Also chloroform evaporizes very fast and vials should be closed immediately after adding a polymer. In this experiment it is not important whether the chloroform is added first into the vial or the polymer. Also a polymer mixture should not be stirred while under a LED light. Stirring can greatly influence the overall result.

3.6 Characterisation Equipment

In this subchapter the equipment used for the characterisation of the materials will be described. The parameters of the equipment and the working principle will be analyzed. Important features like the advantages of each method will be emphasized.

3.6.1 High Resolution Transmission Electron Microscopy (HRTEM) and High-Angle Annular Dark-Field Imaging (HAADF)

Transmission electron microscopy (TEM) measurements were carried out on a (high resolution) TEM (TECNAI Biotwin, FEI Ltd. and JEM-2110F, JEOL) operated at 100 kV and 200 kV, respectively. Prior to the TEM measurements, a solution with nanoparticles was drop-coated on carbon coated copper grids (400 mesh, AGAR Scientific) using a solid substrate support. The HAADF was intergrated and conducted for the duration with the HRTEM scan in STEM mode.

3.6.2 HRTEM Working Principle

The Transmission Electron Microscope can provide a better resolution than any optical microscope in existence and zoom into the lattice of the crystal. In Fig.3.3 The TEM working principle is depicted. First the source of the electrons called the electron gun „shoots“ the electrons to the sample. The electrons then scatter and fly in many directions and this is where the magnetic lense comes to the aid. Magnetic lense can focus the electrons via the magnetic field. The magnetic lense is basically an electromagnet.

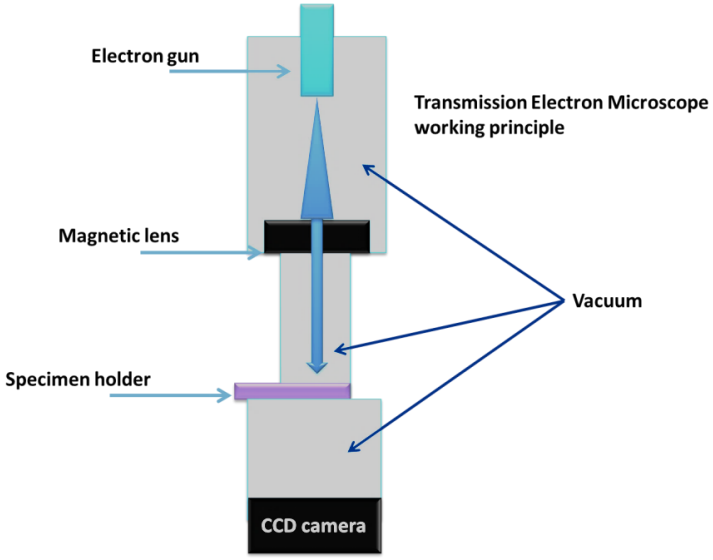

Figure 3.3 depicts schematics of the TEM working principle. The electron gun shoots the electrons through the magnetic lense which focuses the beam. Then the beam goes through the sample. Normally the electron beam falls on the fluorescent screen showing the result. But today electron microscopes are equipped with CCD cameras which helps to improve the characterization.

The TEM itself has a chamber or camera (made of steel) and it contains a high vacuum. When electrons pass through the sample they cannot get through thick areas of the sample. For instance metal nanoparticles would stop some electrons creating a shadow which would be visible on the CCD camera (which is connected to the PC).

3.6.3 HAADF Mode

The dark field mode of the HAADF can show the areas which are reflecting the electrons. It is a HRTEM mode and the image of an object (a nanoparticle for example) appears bright while on a dark background. The bright areas shows the reflected electrons and can help determine whether it is an organic soft material (if the operator is not sure). In the HAADF mode the sample can be titled to collect back-diffracted electrons called Bragg reflections. This method is also used in studying lattice defects.

3.7 Characterization using Environmental Scanning Electron Microscope

The ESEM characterization has been carried out using a JEOL WINSEM JSM-6400 at a 20kV accelerating voltage as well as a Phillips FEI XL30 FEG-ESEM with various accelerating voltages. Incorporated into the ESEM is an EDX analyzer supplied by Oxford Instruments. EDX scans have been carried out on different parts of the sample in order to confirm the elemental analysis of the structures.

3.7.1 Scanning Electron Microscope (SEM) Working Principle

The SEM is an elecron microscope which uses electrons to hit the sample and then the reflected electrons hitting the detector create an image Fig. 3.4. The electron microscope is used to study both the metallic and polymeric structures. It does not go through the sample like in the TEM scan. The SEM can be compared to an optical microscope apart from the fact that it uses electrons instead of light. Electrons behave like waves (due to the particle-wave duality) and at high energies have low wavelengths. The SEM image is produced due to low energy secondary electrons. The more electrons that are reflected the brighter the image is. Electrons that go into the depth of the sample (for example into the void or pit of the structure) are usually absorbed and not reflected into the detector. The best modern SEM can achieve a resolution of less than a 1nm.

3.7.2 Environmental Scanning Electron Microscopy (ESEM)

The Environmental Scanning Electron microscope is a Scanning Electrone Microscope that is designed for wet or biological samples. The specimen for the ESEM does not have to necessarily be coated. The ESEM allows a more detailed investigation on biofilms and is mostly widely used in biosciences

.

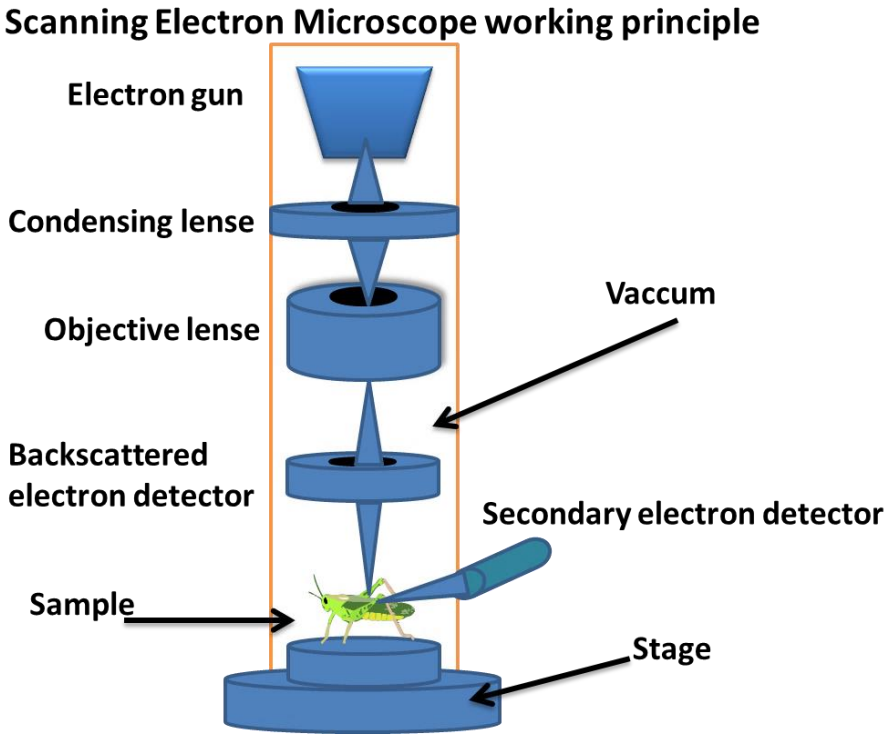

Figure 3.4 depicts the working principle of SEM. The first electron gun creates a beam of electrons which are focused by magnetic lenses. Then after being focused they hit the sample and get reflected from it into the detector which then creates an image. The whole process happens in a high vaccum.

3.7.3 Dispersive X-ray Spectroscopy (EDX)

The EDX is usually an option in SEM and can be used to determine elements in the material. It shows which chemical elements are on the sample or the composition of the sample. When the electron is released from the material it creates a hole and another electron with the higher energy fills the hole releasing energy in the form of an x-ray. Secondary electrons make every element emit a characteristic x-ray (a specific x-ray with different energy portions). The x-ray signal can be separated by a silicon-lithium detector then the signal is amplified and analyzed.

3.8 Atomic Force Microscope (AFM)

An Atomic force microscope (Dimension 3100a Nanoscope, Veeco Instruments Inc.) was used to image the fabricated nanofibers and polymer thin films. The imaging of the samples was conducted in tapping mode using silicon nitride cantilevers (Bruker AFM Probes) with a resonance frequency of about 330 kHz, a spring constant of 45 N/m and a tip radius of less than 10 nm.

3.8.1 AFM Working Principle (contact mode)

The Atomic Force Microscope (AFM) was used in the present work to determine the surface morphology or texture of the samples. The AFM is actually a Nanoscope which can go from micron scale to nanometers depending on the model and the operator (user). The AFM actually has contact with the sample by touching it. It is not an optical technique and the images are computer generated. Fig.3.5 depicts the schematics of the AFM working principle. The most simple description of the AFM is that the triangular needle scans all over the sample while the laser (usually red) shines on top of it. The needle tip is attached to the microsized spring that is called a cantilever.

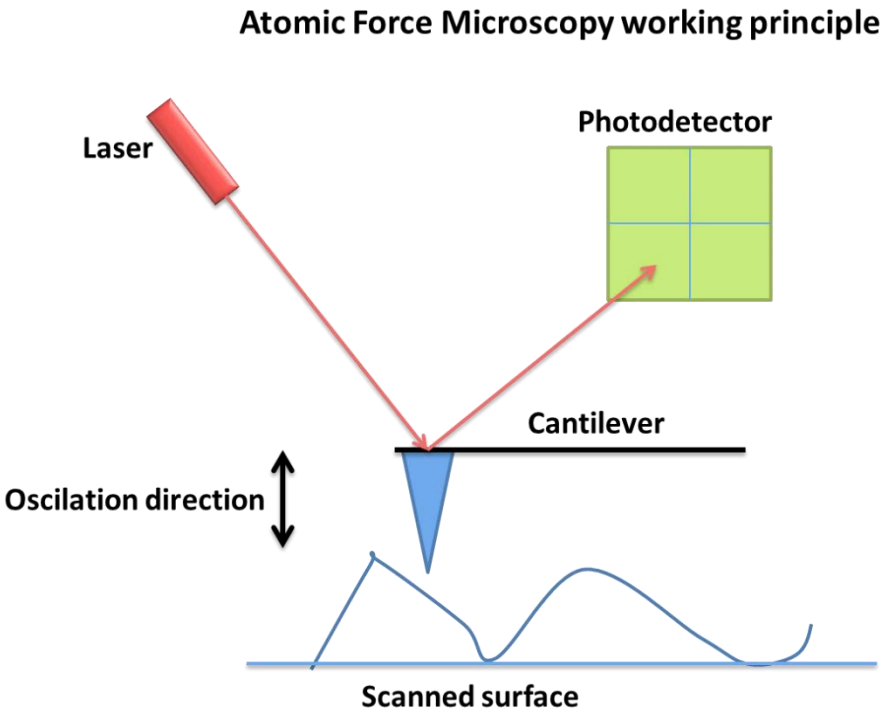

Figure.3.5 shows the schematics of the AFM microscope. The main part of the AFM is the head which is scanning the specimen. The tip (blue triangular in the image) is touching the surface of the specimen and the holding spring called a cantilever is bending. The laser is shining on the tip and the reflection angle of the laser is changing. The reflected laser is going to the photodetector which is connected to the analyzing computer.

When the tip is scanning the surface the cantilever is bending and the tip is moving upwards and downwards changing its height. The height changes in a few nanometers and the laser that falls on the tip is reflected to the detector. Everytime the height is changes the reflection of the laser spot changes the position on the photodetector. So during one scan we have only one line of pixels. To scan the whole area usually the AFM table is moving to x and y axis. To scan the area of 10X10 micrometers of a sample with the AFM model D3100 we typically need around 30mins. This would also

depend on the parameters adjusted. The scanning speed should be 0.4Hz. The surface of the sample can be almost anything from soft materials like polymers to nanodiamonds. The rougher the surface is the easier it is to brake the tip. Typically mica or silicon wafer surfaces are suitable for the AFM samples. The samples can be prepared by drop-casting the material on top of the substrate which leads to the rough surface in most of the cases. Or it can be spin-coated which leads to thin and smoots films.

3.8.2 AFM Tapping Mode

The AFM has two main modes. The contact mode and the tapping mode. It is very important to mention the difference between these two modes. In the contact mode described in the previous subchapter we have a contact between the tip and the surface of the sample. In the contact mode the tip is dragged all over the sample. But it also has some disadvantages. In the contact mode the tip can „catch“ dust and drag it over the sample thus preventing accurate results. Also the probability of breaking the tip in the contact mode is higher. This is where the tapping mode comes to an aid. In the tapping mode everything happens the same as in the contact mode but with one difference. In the tapping mode or as it is sometimes called the intermittent-contact mode the tip oscilates. The spring jumps up and down fig.3.5 It constantly oscilates and touches the surface of the sample at the lowest point of oscilation.

3.8.3 Scanning with Tapping Mode

In the tapping mode the tip would do exactly the same as in the contact mode it will touch the surface (only once) the cantilever will bend according to the sample surface roughness. But the probability of catching dust or any other molecule is much decreased and also breaking it is not very probable anymore. Therefore extending the life of the probe (cantilever and the tip).

3.9 UV-vis and Photoluminescence Spectroscopy

The UV-Vis and photoluminescence spectra of the CdS nanoparticles in the PPI[G4] solution were recorded at room temperature using a Cary 50 UV-Vis spectrophotometer and a Cary Eclipse fluorescence spectrometer (both Varian Inc.), respectively. The monochromator slit width was 10 nm.

3.9.1 UV-vis Working Principle

The UV-vis spectroscopy is the ultraviolet-visible range spectroscopy. It is considered as the most simple spectroscopic optical technique. The UV-vis spectrometer schematics are shown in Fig.3.6. The UV-vis has a light source (usually two lamps: UV and the visible range). The light source is a powerful lamp that shines trough the slit (called the entrance slit) then it goes to the diffraction grating or prism. Then the visible light is dispersed into different wavelengths and enters the second slit called the exit slit. From the exit slit it hits the sample which can be from a solution to a thin film. After it hits the sample a portion of light is absorbed by the sample material. After the absorption it reaches the detector which then tells us what energy portion was absorbed and the intensity of the light beam. From that it calculates the intensity of absorbed light by a sample. After the light dispersion from the prism we see a light dispersion or a rainbow. To avoid all the colors hitting the sample we need the exit slit which is a small hole designed to let only one wavelength to pass. In the UV-vis spectrum graph there are x and y axes. The axis y stands for intensity which depends on the photons passed through the sample. And the x axis represents the wavelengths of light. To achieve different wavelenghts of light during the scan the prism in the spectrometer slowly moves and allows different wavelengths of light to passs through the exit slit.

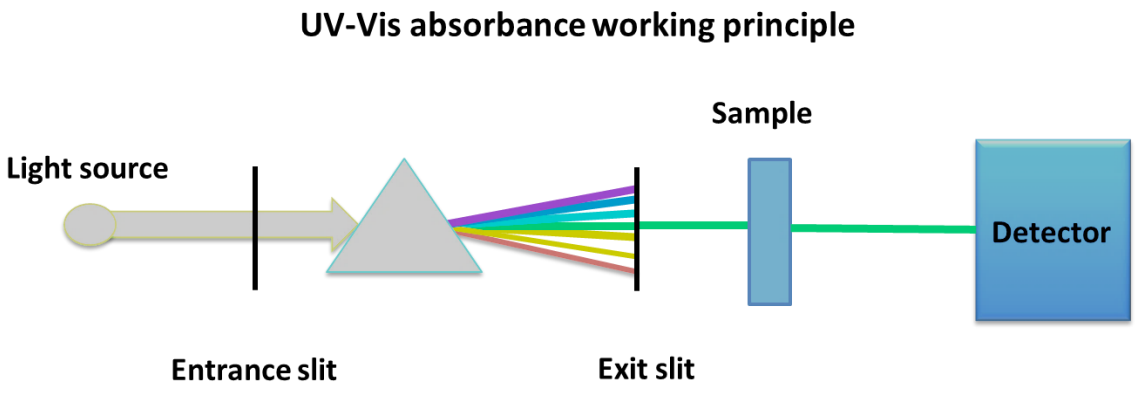

Figure.3.6 shows the UV-vis chematics. The light source goes throught the slit and then through the prism which breaks the light into many wavelengths. Then the exit slit allows one wavelength to pass which goes through the sample and then to the detector.

3.9.2 Photoluminescence Working Principle

The Photoluminescence spectroscopy is one of the most widely used spectroscopies in optics for semiconductors and a variety of materials including organics. The schematic depiction of PL spectroscope is in Fig.3.7. PL consists of a light source which is exciting the sample. The sample emmits back another photon of a lower wavelength and hits the detector. The role of the monochromators here is to eliminate ‚noise' which are re-diffraction and spherical aberrations. Monochromators basically increase the resolution making it more precise and easier to analyse.

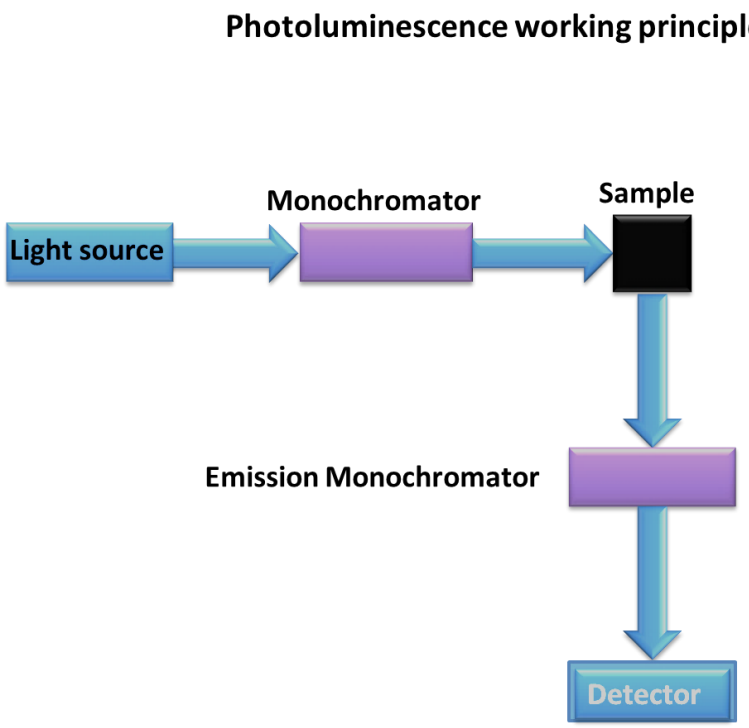

Figure 3.7 depics the working principle of the photoluminescence spectrometer. First the light source shines on the monochromator which then gives one wavelength to excite the sample. After the light hits the sample another wavelength is emitted already by a sample. After it is emmited by a sample it reaches the emission monochromator and then the detector.

3.9.3 PL Signal from the Material

When the photon hits the target it gets absorbed by an electron. Then the electron gets excited and goes to the higher energetical state. However, the excited electron does not stay long in the excited state and jumps to the lower energetical state emmiting the photon. The emitted photon is the photon that is absorbed by a detector in the PL spectroscope which makes the PL spectra.

3.10 Nuclear Magnetic Resonance

The Proton NMR analysis was performed in deuterated chloroform at 300MHz. NMR is a powerful and common technique in organic chemistry [194] and physics [195]. The NMR consists of a magnet that is capable of producing a uniform magnetic field and sources of radiofrequency. Magnets are usually superconducting and are cooled to very low temperatures like 4K (Kelvin). To achieve this temperature liquid helium is used. Modern instruments are capable of producing magnetic fields of 10T (Tesla) Fig.3.8. The NMR is for magnetic field interaction with the nuclei and not with electrons. A nucleus has magnetic moments that interact with the applied magnetic field. The magnetic moment of a nucleus may differ from the applied magnetic field and the electronic orbital angular momentum may be induced (circulation of electronic currents) and gives a rise to a small additional magnetic field at the nuclei. So when the external magnetic field 'hits' the nuclei it affects the nuclei local magnetic field and every nuclei has a different electronic structure near it. So every nuclei has a specific signal response (which also depends on the environment of the nuclei).

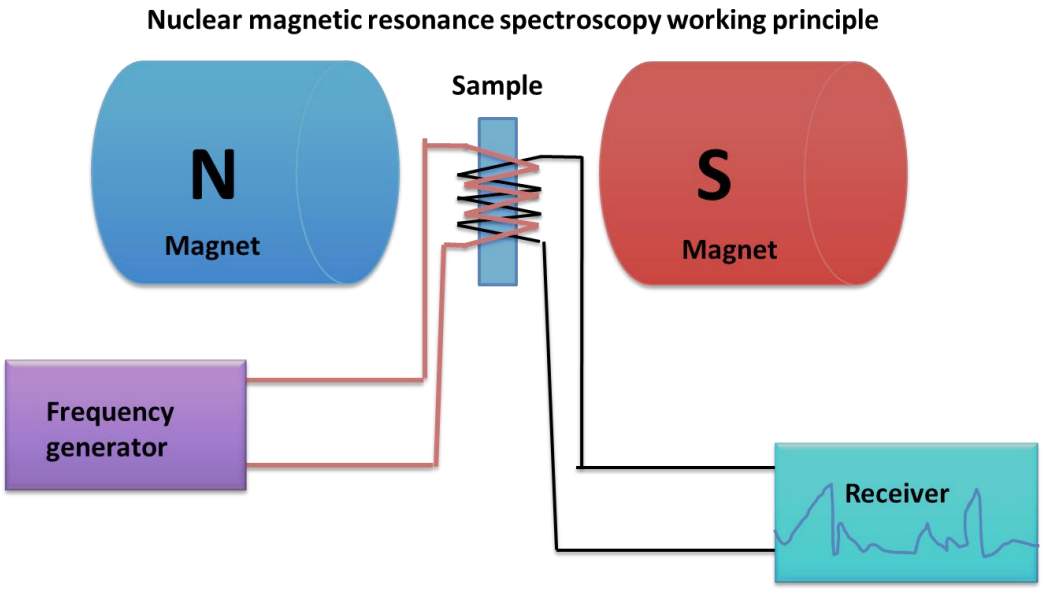

Figure 3.8 depicts a schematic diagram of the NMR spectrometer. The magnets create a large field of up to 10T. The sample is in the magnetic field. Radio frequency is generated by a frequency generator and the wires coil the sample. The second coil is receiving the signal which is then received by a receiver and analysed.

3.11 Data Analysis

The data from the spectrometers was analyzed using Origin pro. software. And the files from the AFM were analyzed using Gwyddion software. The size distribution of the nanoparticles was made using Gwyddion first. The desired TEM or SEM image was chosen first. Then objects were marked on the image and the data collected from the Gwyddion. Then it was imported to Origin pro and the graphs of size distribution were drawn.

3.11.1 RGB Light Coding

The coding of light was one of the most important parts in the light-induced synthesis. The RGB light code is the automatic sequence which includes 1 second for every wavelength (Red, Green, Blue and white then repeating the sequence again). To better explain the coding we need to see the graphs depicting the constant wavelengths and the interrupting wavelengths of light Fig.3.9.

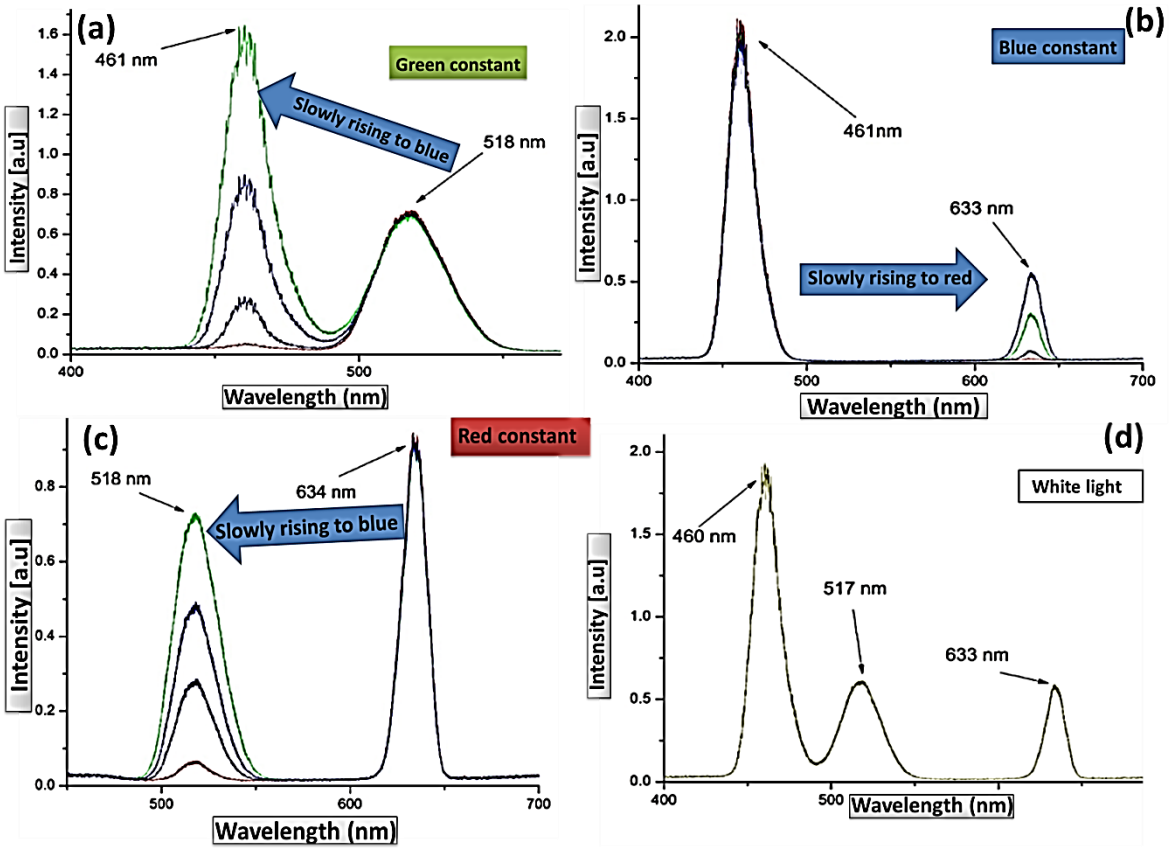

Figure 3.9 shows the LED spectra during the RGB code. (a) Green constant then rising to Blue constant (b) and then to Red constant (c) after rising to blue but then switches all the wavelengths and we have a white light (d).

Fig.3.9 requires special explanation. When the RGB code starts we have a Green LED on (called constant) after that slowly overlapped by the blue LED Fig.3.9 (a). The overlapping is relatively slow (1sec) by increasing the intensity of the particular wavelength. If we have a Green LED as a constant then the blue LED increases its intensity which overlaps with the green LED and at a certain time interval we actually have 2 wavelengths shining on the sample. After the blue LED reaches its intensity peak the green LED is off and another LED starts overlapping the blue LED. Fig.3.9 (b) the blue LED is constant (not changing) and the red LED is on the rise. The Red LED increases in intensity and after some moments we have the blue and red LED shining at the same time. When the Red LED reaches its intensity peak the blue LED is off.

3.11.2 Reaching White LED Peak

After reaching red the LED light is a constant and the blue LED increases in intensity Fig.3.9 (c). However, this time the blue LED will not reach its peak alone and the red LED will not get off. At one point all the wavelengths of light switch on with their highest intensities overlapping each other and we will have the white light LED Fig.3.9 (d). After a second the whole process will repeat itself over and over again.

Chapter 4 Study of Polymer Film Morphology Tailored by Solvents and LED

In this chapter the results of the experiments conducted with polymers will be analysed in detail. Polymer morphology change was induced in the polymer films using two methods: one using solvent mixtures and the other involving light.

4.1 P3HT-PCBM Solvent Effects on Nanostructuration

This experiment was conducted using P3HT and $PC_{[70]}BM$. These two materials were mixed and dissolved in various solvents. Also the materials were dissolved separately in order to better investigate the effects on the nanomorphology of every solvent. The solvents were non-polar such as hexane, cyclohexane, toluene, chloroform (CF) and four polar aprotic solvents as chlorobenzene (CB), tetrahydrofuran (THF), dimethylformamide (DMF). For a proper investigation of the influence on the polymer morphology a step by step designed experiment with at least one polymer type is required. Since one the most popular semiconducting polymers is P3HT as a donor and $PC_{[70]}BM$ as an acceptor the further experimental investigation was conducted using only them. The light induced nanostructuration showed unexpected results and the P3HT/$PC_{[70]}BM$ system was not enough for a proper analysis. The observed effect was also checked with another polymer PTB7 in the PTB7/$PC_{[70]}BM$ system with the same conditions as P3HT/$PC_{[70]}BM$. The set of the same experiments was carried out in order to make a comparison and draw optimal conclusions. The colour set in every AFM analysis was chosen to best highlight the features of the polymer film and the most important image details. Fig.4.1 AFM image of P3HT/$PC_{[70]}BM$ in chloroform. The Fig.4.1 will serve as a reference since it has only one solvent and was not affected by external fields. As some works suggest the P3HT morphology depends on packing [196] and also on temperature [197]. This is why the polymer nanostructuration experiments were conducted at room temperature.

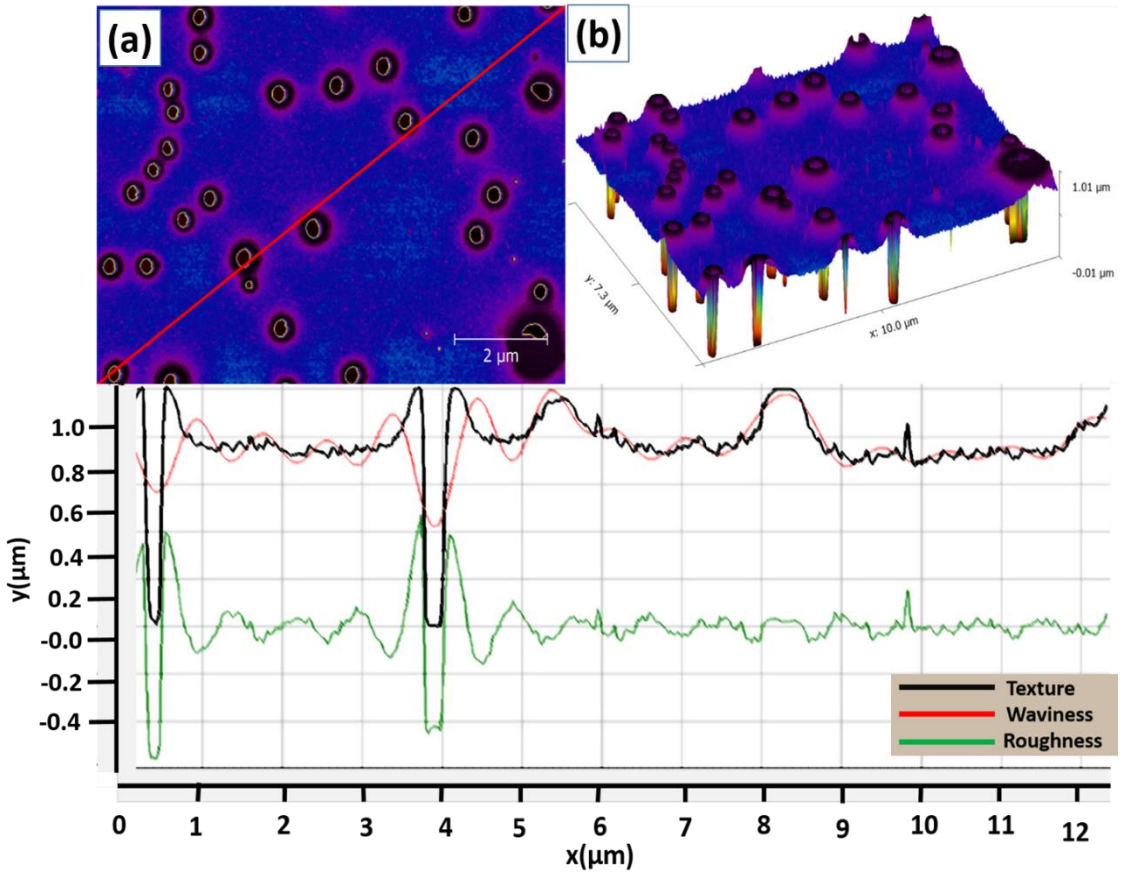

Figure.4.1 The AFM image of the P3HT/PC$_{[70]}$BM in chloroform. (a) shows volcano-like structures with few hundred nm in diameter. The "volcanos" are distributed over the sample in a particular manner as if they attract each other. Most of them form two to three "volcanos" family. (b) shows a 3D model of the (a). As it can be seen in (b) "volcanos" are narrower at the top and expand at the bottom. The graph below is the roughness of the film from (a) red line. The black line in the graph corresponds to texture; the red corresponds to waviness and the green to roughness.

As it is shown in Fig.4.1 the morphology of the P3HT/PC$_{[70]}$BM looks "volcano" like and the 3D image confirms the similarity of these structures to actual volcanos. However, the most surprising feature is the distribution of the holes over the sample. The AFM scans showed that the "volcanos" have a "clever" distribution. This statement means that there is a reason why we get nanofeatures in a particular arrangement. The distance between the holes can either be interpreted as an arrangement that occurs in either rows, or that they are distributed in "family groups" of two or three". This distribution can be related to any of the system components i.e. to P3HT or PC$_{[70]}$BM or/and due to the solvent which is chloroform in this case. As we will see later the final morphology is influenced by all components (P3TH, PCBM and the solvent). The next AFM scan was PCBM in chloroform alone Fig. 4.2.

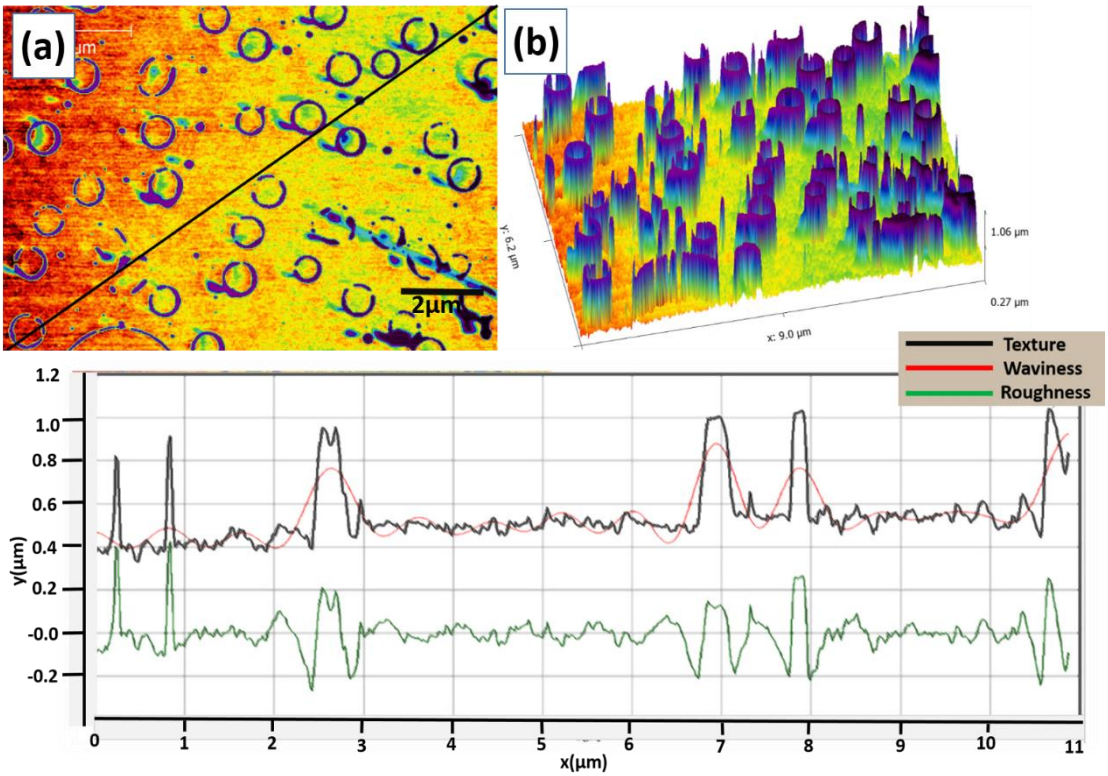

Figure. 4.2 The AFM image of the $PC_{[70]}BM$ in chloroform. (a) shows AFM top view. As it can be seen the circles are not complete (most of them). (b) shows the 3D model which suggests "tube" look but not "volcano" anymore. The graph below in the roughness of the film from (a) red line. The black line in the graph corresponds to texture, the red corresponds to waviness and the green for roughness.

Fig.4.2 depicts the $PC_{[70]}BM$ in chloroform. This micrograph confirms the appearance of "volcanos" is due to the PCBM and not the P3HT. However, the structures in Fig.4.2 are not exactly the same as in Fig.4.1. This is due to the P3HT as well. The P3HT has also an influence in morphological formations. For better understanding of the influence of PCBM we need to understand the influence of solvents over the PCBM alone. Another sample was prepared with the $PC_{[70]}BM$ alone in hexane. Dissolving in hexane was difficult and required an ultrasonic bath for 10-15minutes. The morphology was more micro-sized rather than nanosized Fig.4.3.

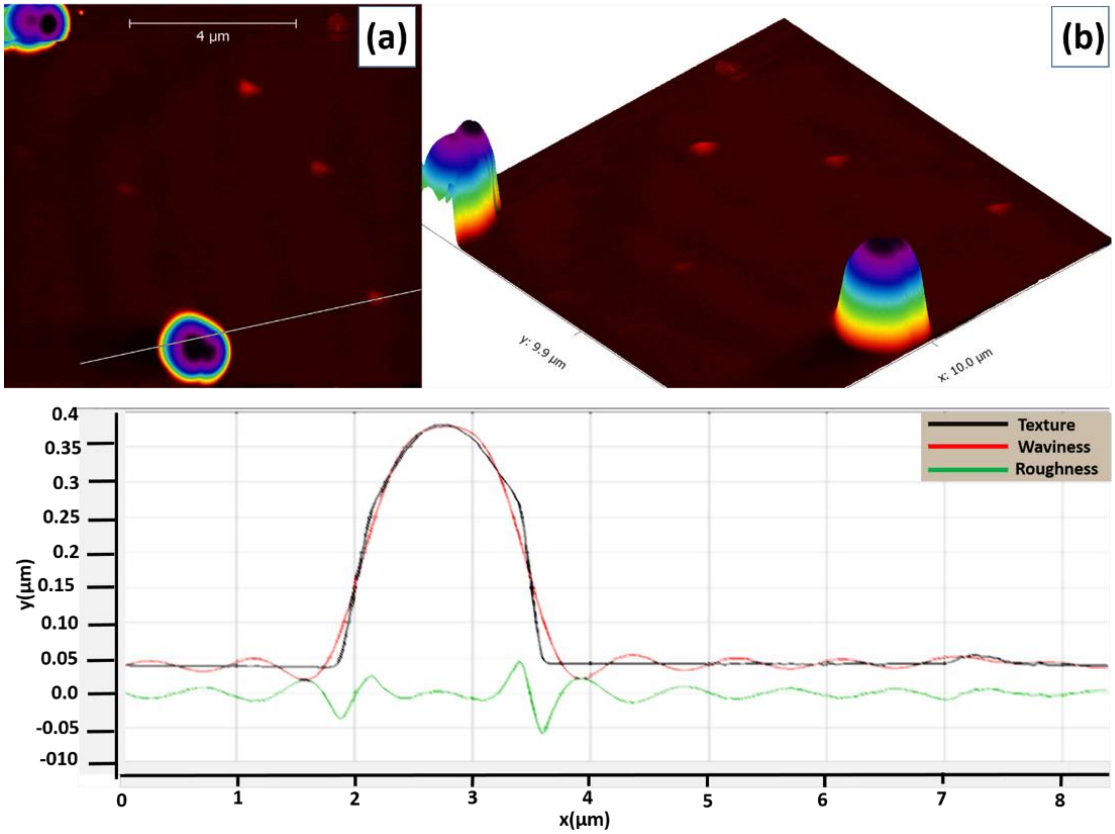

Figure.4.3 The AFM images of the $PC_{[70]}BM$ in hexane. (a) the PCBM "clump" with a few micrometers in width and distributed over the sample with great distances of tens of microns. (b) the 3D model showing no "volcano" formations. The black line in the graph corresponds to texture; the red corresponds to waviness and the green to roughness.

The PCBM clumps were distributed over the sample but with huge inter feature distances of 20 and more micrometres. Additionally, the structures were not "volcano" or "tube" shaped as in Fig.4.2 and Fig.4.1. The structures in Fig.4.3 look more like "balls" or "eggs" and are almost perfectly round-shaped and do not contain any voids or holes. Fig.4.3 suggests a significant influence of the solvent since we do not observe "volcanos" anymore. But one scan with a different solvent does not provide sufficient information or proof. To prove the influence of the solvent another AFM scan was performed using the $PC_{[70]}BM$ in THF. This AFM scan shown in Fig.4.4 indicates structures that visually look similar to the Fig.4.3 with some important differences.

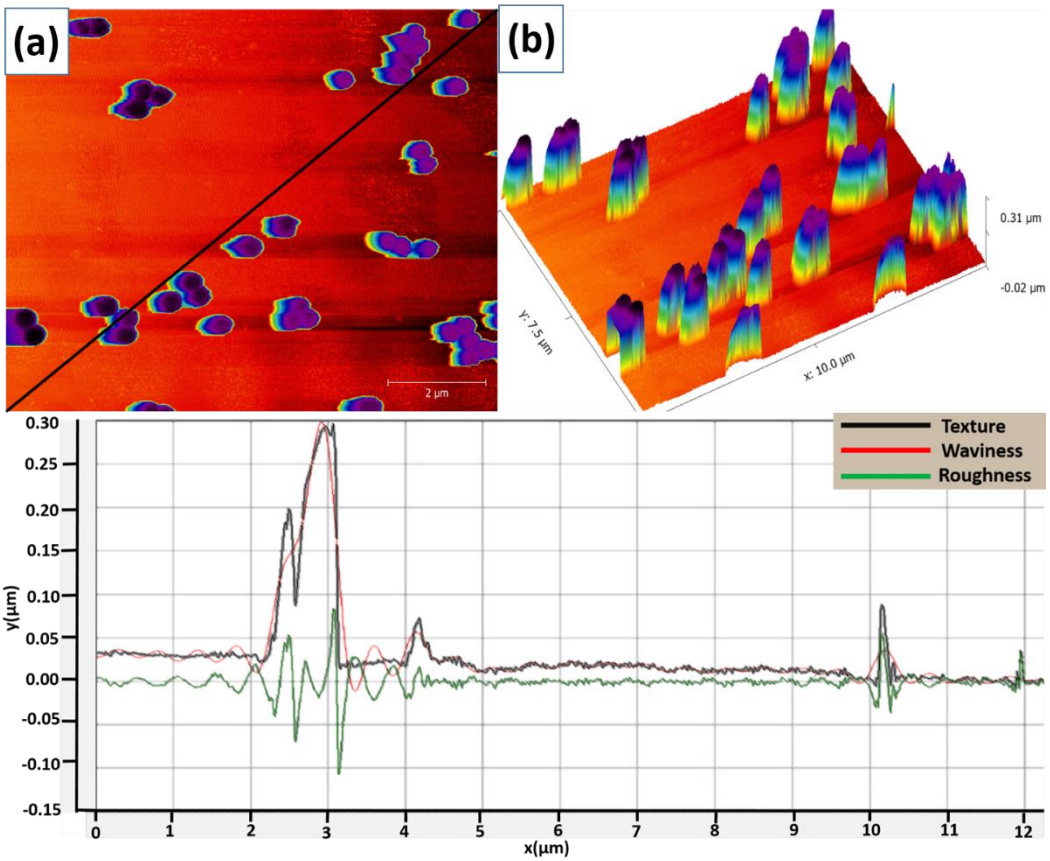

Figure.4.4 The AFM images of the $PC_{[70]}BM$ in THF. In (a) we can see round "clumps" formed in a particular manner usually two to three and more. Also some of the particles are "alone". (b) shows 3D model in which we can see the formation of the PCBM "hills" that are very uniform and similar. The black line in the graph corresponds to texture, the red corresponds to waviness and the green for roughness.

The main difference is the size of the structures and importantly the deposition over the sample. In the case of the THF as a solvent the PCBM structures behave very similar to the one used with the chloroform. However, in the case with the THF they do not form "volcanos" or "tubes" and have no voids or roughness on the surface that could be compared to the "volcanos". In Fig.4.3 it seems that the THF "forces to assemble" those PCBM "clumps" closer and form a more "colony-like" distribution. These "colonies" were distributed over the whole sample with almost the same manner. Which was later shown to be due to the distribution changes when combined with some other solvent and mixing the P3HT with the $PC_{[70]}BM$. The scan with the DMF was performed and no "colony" or "volcano" or even clump like structures were observed Fig.4.5.

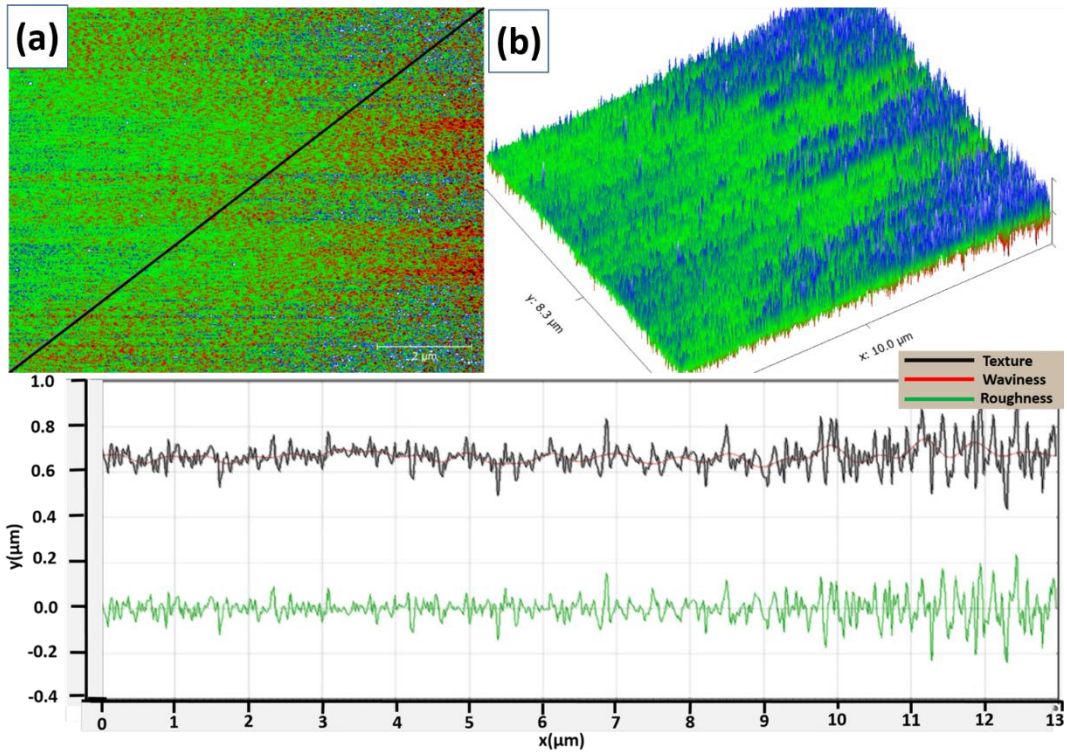

Figure.4.5 depicts the AFM images of the $PC_{[70]}BM$ in the DMF. (a) difficult to define the features. However, the color was chosen for a maximum highlight of the features. (b) the 3D model shows the roughness which is almost dotted and distributed without a "colony" manner over the sample. The black line in the graph corresponds to texture, the red corresponds to waviness and the green for roughness.

This scan in Fig.4.5 confirms the influence of a solvent over the PCBM molecule distribution. The AFM image in Fig.4.5 looks more like vertical needles and the scan was performed a couple of times changing the AFM tips in order to eliminate any scan errors. For now, it is too early to make conclusions and try to link the morphology with the solvent parameters such as dielectric constant or dipole moment. The objects in Fig.4.5 are very small and have no particle like similarities like those observed in previous scans (Fig.4.1 to Fig.4.3). In Fig.4.5 (b) the 3D image shows blue lines that are vertical and are highest and the green lines that are diminishing. Another sample of PCBM in chlorobenzene was prepared and characterized using the same technique and method (same speed spin-coating) Fig.4.6. This time the film surface is different from the previous scans and it is similar to the one in Fig.4.5. The PCBM do not form large clumps neither "volcanos" nor "tubes". But the needle-like formations spread over the whole sample. This investigation shows the influence of different solvents over the same material which is PCBM in this case.

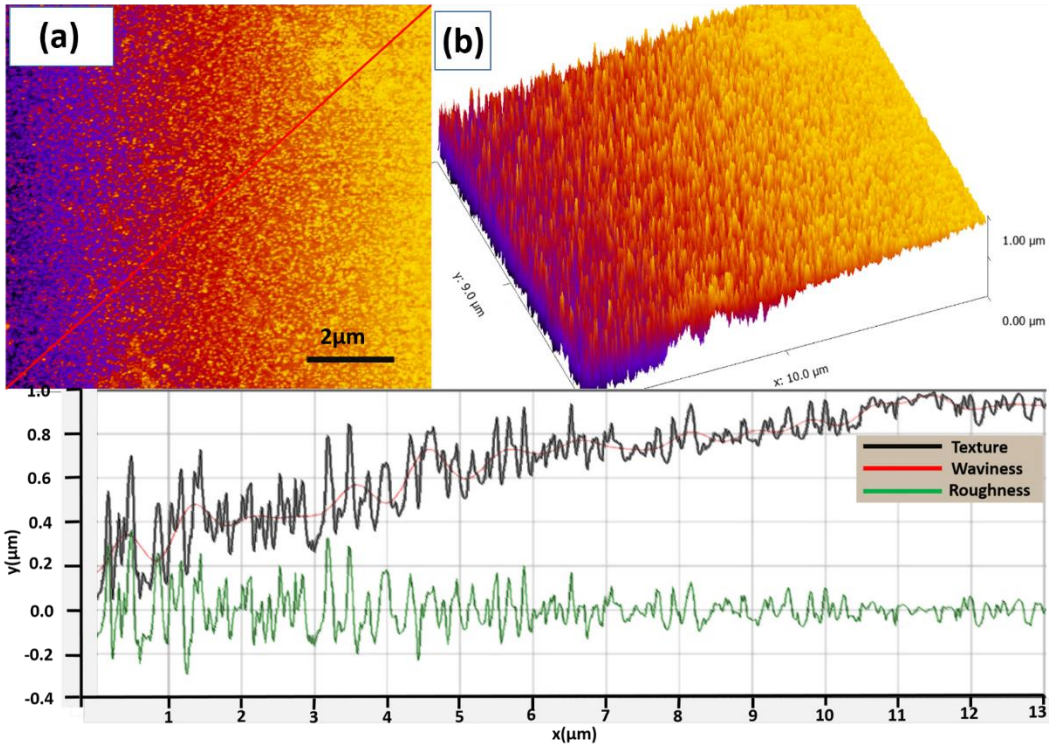

Figure.4.6 The AFM image of the PCBM in Chlorobenzene. (a) has very small features but they have a higher distribution level and are deposited uniformly without leaving empty space on the sample. (b) the 3D image confirming the vertical PCBM distribution over the sample with decreasing roughness as confirmed by the graph below. The black line in the graph corresponds to texture, the red corresponds to waviness and the green to roughness.

The present AFM topography of the $PC_{[70]}BM$ in chlorobenzene might be attributed to the crystallization degree as was reported using the P3HT/PCBM [198]. Also it was reported that the morphology of the films depends on the concentration [198]. DMF and chlorobenzene are polar solvents and they have huge differences in dielectric constant values. However, the morphology does not look very different which means that the dielectric constant does not have an influence in the process of the morphology formation. Another parameter such as the dipole moment is 3.82 for DMF and 1.54 for chlorobenzene. The difference between these constants is 2.28. On the other hand, it is best to neglect these parameters and check the morphology using other solvents such as cyclohexane which has dipole moment equal to 0.0. Fig.4.7 Shows AFM image of PCBM in cyclohexane. Cyclohexane is non-polar solvent and has dipolar moment of 0.0. Dielectric constant is 2.02. The observed morphology in Fig.4.7 shows the formations that also do not look like “volcanos” or “tubes” however they form “hills”. This AFM micrograph (Fig.4.7) shows uniformly distributed “hills” with relatively uniform heights Fig.4.7 (b) and a graph roughness analysis. This result gives hints to what may be the most important parameters in morphology formation.

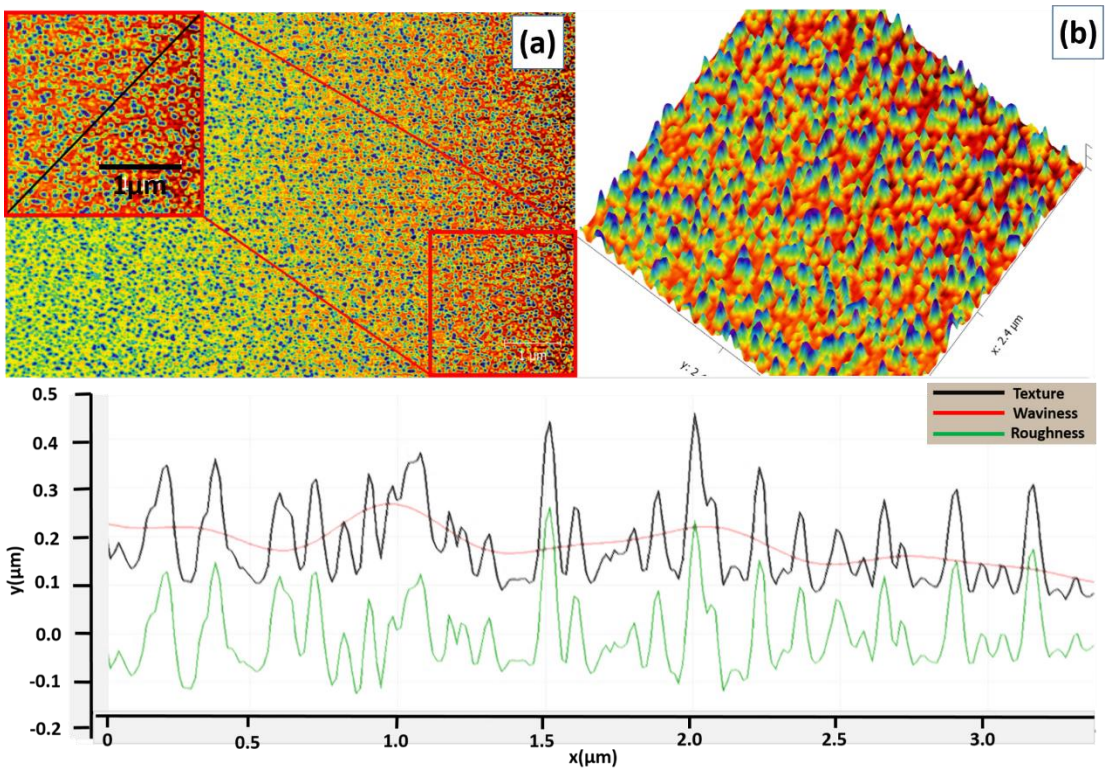

Figure.4.7 The AFM image of the $PC_{[70]}BM$ dissolved in cyclohexane. (a) shows that structures are formed uniformly over the whole sample. The red square was analyzed in detail in order to make a more precise analysis of the morphology. (b) the 3D model of the scan confirming relatively high width and height uniformity. The black line in the graph corresponds to texture, the red corresponds to waviness and the green to roughness.

It is clear that the greatest influence is due to the solvent (we are using the same concentration in all the samples 1mg/ml). On the other hand, the PCBM alone repeats very similar morphologies alone Fig.4.2. These effects could be due to the ranging solubility in different solvents. As it was demonstrated the morphological changes are caused by both the P3HT and the PCBM. However, the PCBM was investigated alone and with different solvents. The solvent influence over the PCBM morphology was demonstrated. While the P3HT/PCBM in chloroform and the PCBM alone in chloroform film morphologies look similar PCBM alone in chlorobenzene morphology is far from the reference Fig.4.1. This could be due to the solvent parameters such as the dipole moment.

4.2 Influence of Solvents and Solvent Mixtures on the P3HT/PCBM Morphology

For a proper investigation of the polymer morphology and to achieve optimal results it is necessary to use a small polymer system composed of a maximum of two components. This is why the P3HT/PCBM system was chosen for the investigation. The P3HT/PCBM is the actual active material for the organic solar cell and it is most studied [184]. This is a valuable reason for choosing the P3HT/PCBM. Fig.4.8 depicts the AFM image of the P3HT/PCBM system dissolved in cyclohexane. As compared to Fig. 4.7 where PCBM alone was in cyclohexane we can observe the similarities in the morphology.

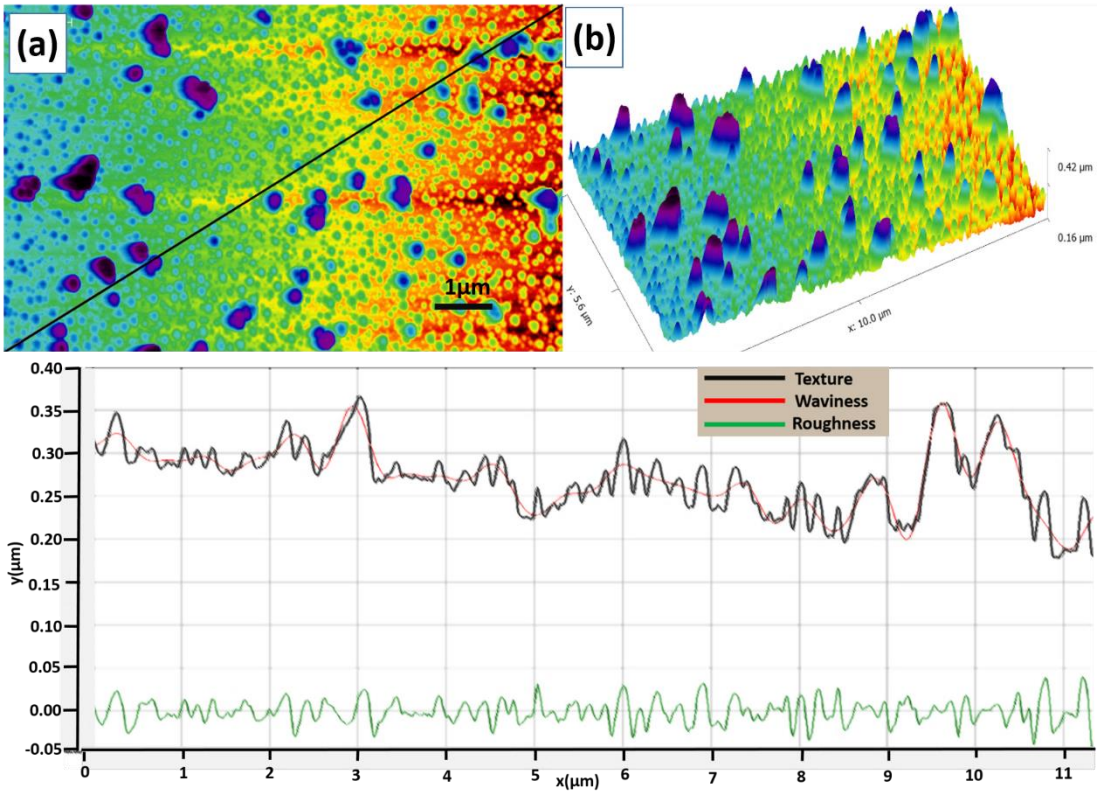

Figure.4.8 The AFM image of the P3HT/PC$_{[70]}$BM in cyclohexane. (a) shows large and small clumps over the sample. (b) wider formations are also higher and the smaller "hills" are also lower in diameter. The black line in the graph corresponds to texture, the red corresponds to waviness and the green to roughness.

These observations suggest that the PCBM is dominant in the formation of nanomorphologies with the P3HT. To prove the idea of the PCBM dominance we need to use another solvent which would not be as good as chloroform and not as bad

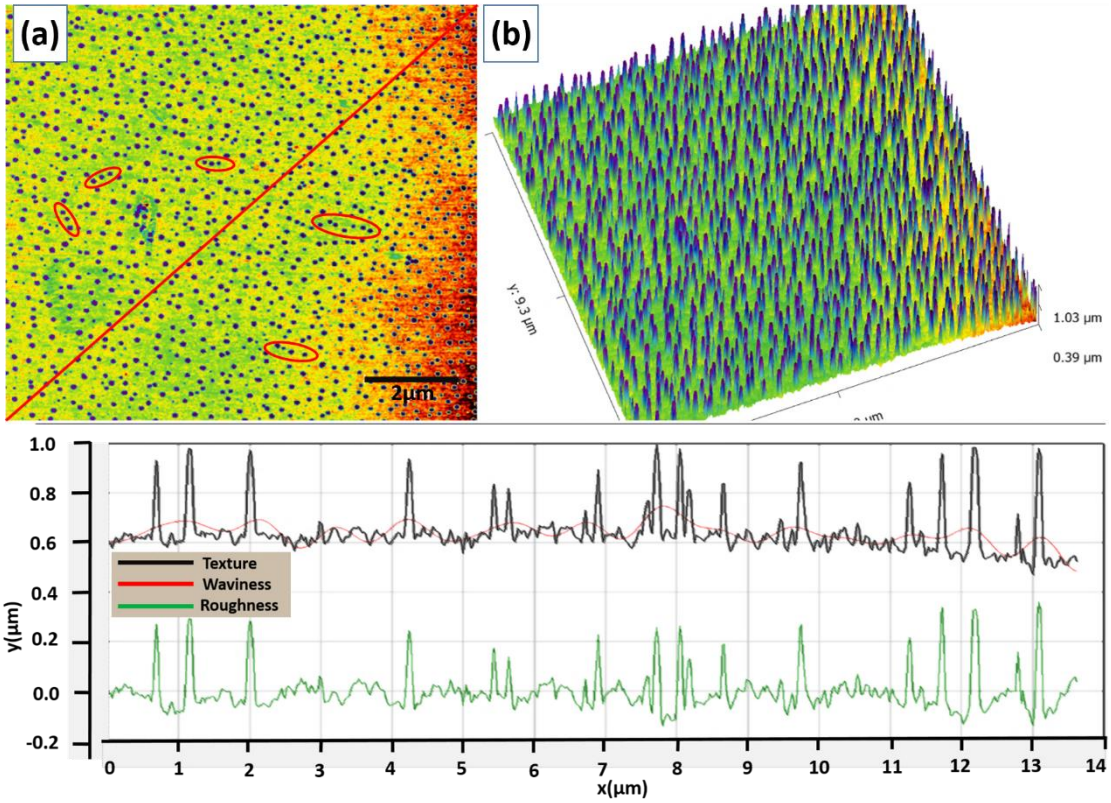

Figure.4.9 AFM image of the PC[70]BM in toluene. (a) Top view showing very uniform dots formed without "family" like behaviour. (b) the 3D model showing "vertical sticks" or "rods" with very uniform height. The black line in the graph corresponds to texture, the red corresponds to waviness and the green for roughness.

as hexane or cyclohexane. Toluene is the perfect candidate. Fig.4.9 is the AFM image of the PCBM alone in toluene. As we can see the formations are vertical "islands" and are distributed in groups Fig.4.1 (a) red circled. Toluene is a non-polar solvent that can dissolve both the P3HT and the PCBM. The dipole moment of toluene is 0.36 and the dielectric constant is 2.38 which is close to the values of cyclohexane and hexane (2.02 and 1.9 accordingly). However, hexane is a poor solvent for both the P3HT and the PCBM. Fig.4.10 shows the AFM micrograph the P3HT/PCBM in toluene. Fig.4.10 is comparable to that in Fig.4.9 where the PCBM in toluene alone. Fig.4.10 also has "familes" or "islands" (Fig.4.10 (a) white circled) comparable to that in Fig.4.9 (a) red circled. This result sheds light on the role of the PCBM in the P3HT/PCBM morphology formation. And while some solvents do not cause the formation of "islands" (chlorobenzene or DMF) toluene "keeps" similar morphologies for both the P3HT/PCBM and the PCBM systems.

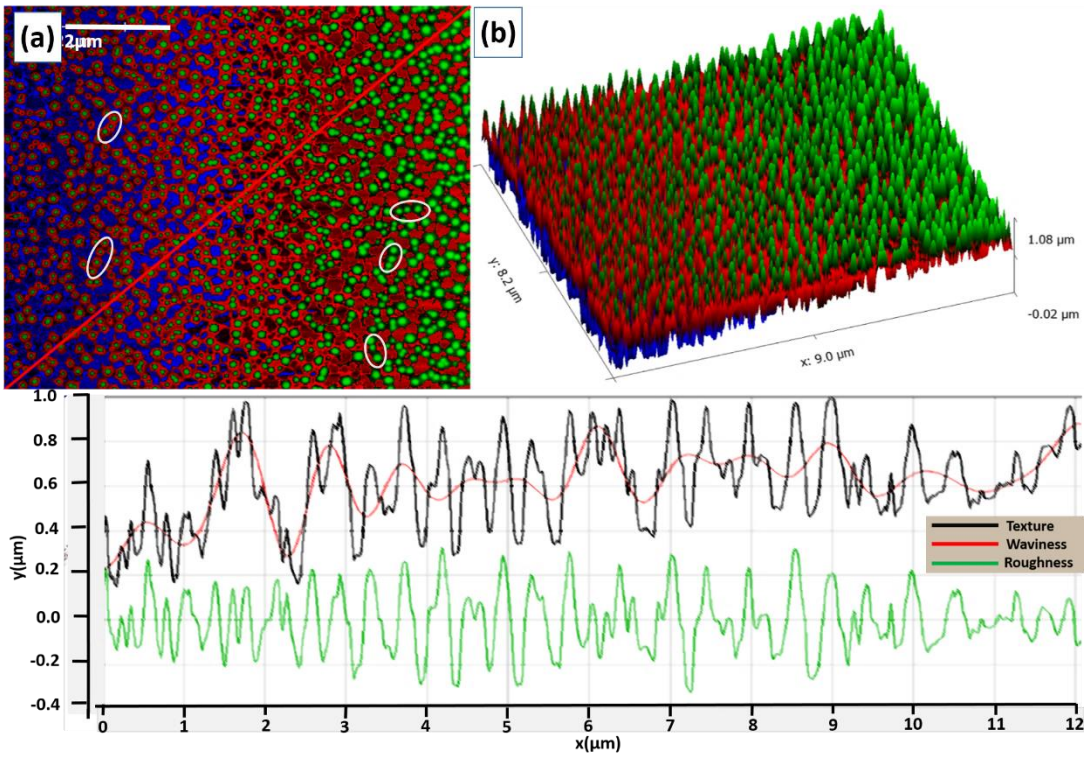

Figure.4.10 The AFM image of the P3HT/PC$_{[70]}$BM in toluene. (a) shows round shaped "hills" that do not contain holes and are uniformly distributed over the sample. (b) the 3D model of the image. The black line in the graph corresponds to texture, the red corresponds to waviness and the green to roughness.

As demonstrated in the subsection 4.4 of the present work the nanomorphologies or morphologies of the P3HT/PCBM and the PCBM alone in different solvents vary. However, we can conclude that the PCBM itself has the main influence on the final morphology in the P3HT/PCBM system. For a better understanding of the possible control over the nanomorphology a more profound investigation is required. The next subsection 4.6 deals with the P3HT and the PCBM dissolved in different solvent mixtures.

4.3 Mixed Solvent Approach

This part deals with polymers used in previous sections (4.4 and 4.2) the P3HT and the PCBM dissolved in a mixture of solvents and also in varying amounts of solvents. The purpose of the present subsection is to demonstrate that morphological control can be achieved by mixing solvents together varying amounts of solvents. Fig.4.11 is the AFM image of the P3HT dissolved in the THF and mixed with the PCBM which was dissolved in the DMF. As we can see the morphology is similar to that in Fig.4.4.

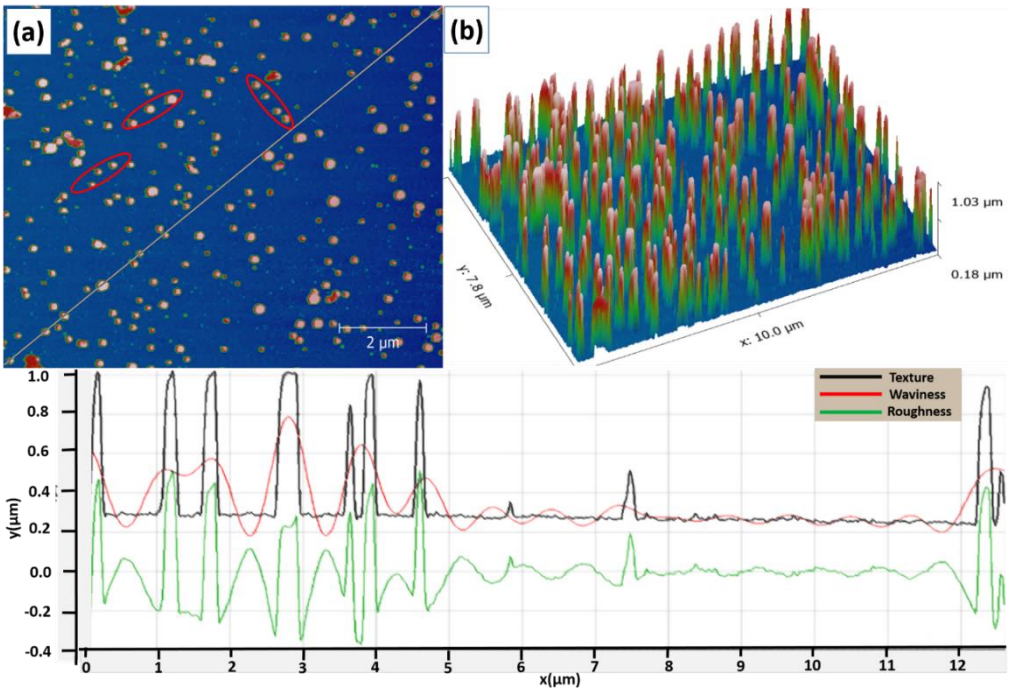

Figure.4.11 The AFM image of the P3HT 0.5mg/ml of THF and PC[$_{70}$]BM 1mg/ml of DMF. (a) the "islands" are still present. Also the formations of "groups" or "families" red circled. (b) 3D image showing vertical "islands". The graph is the texture (black), waviness (red) and roughness (green).

In Fig.4.4 the PCBM alone was dissolved in the THF. The observed morphology is very similar to that in Fig.4.11 containing "groups" of formations (red circled). The main difference is the diameter of the structures. In Fig.4.11 the diameter is smaller suggesting the influence of the P3HT. On the other hand, it is not enough to conclude the influence of the PCBM from Fig.4.11 without a comparison of the same system with an increased amount of PCBM. Fig.4.12 is the AFM image of the P3HT/PCBM dissolved in the THF and the DMF as in Fig.4.11 but with the PCBM amount increased two times. As we can see from Fig.4.12 the morphology obtained is basically the same as in Fig.4.11. However, the amount of vertical "islands" changed and the distribution is different. In Fig.4.12 the "islands" are more agglomerated and form clumps of "islands". This result suggests a significant role of the PCBM in the formation of "islands". If this statement is true, then decreasing the amount of PCBM should decrease the amount of islands or completely ruin the formation of "islands". Fig.4.13 is the AFM image of the P3HT/PCBM in the THF and the DMF but with decreased amount of the PCBM two times. The image clearly shows the "collapse" of the previously observed "islands" (Fig.4.11 and 4.12). The formations look more like randomly distributed nanoparticles rather than polymer formations. Fig.4.13 also shows formations which look more like agglomerated "islands" (black circled).

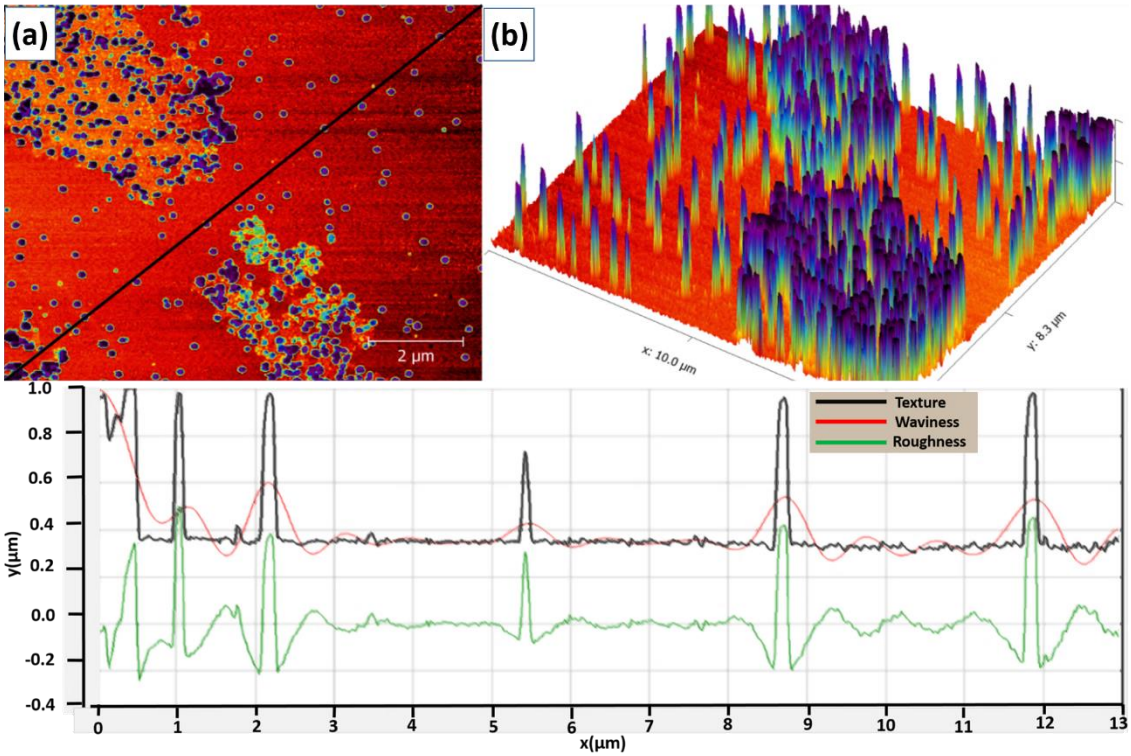

Figure.4.12 The AFM image of the P3HT 0.5mg/ml of the THF and the PC[$_{70}$]BM 2mg/ml dissolved in DMF. (a) higher amount of "islands" randomly distributed. (b) the 3D structure shows increase in vertical islands. The graph is the texture (black), waviness (red) and roughness (green).

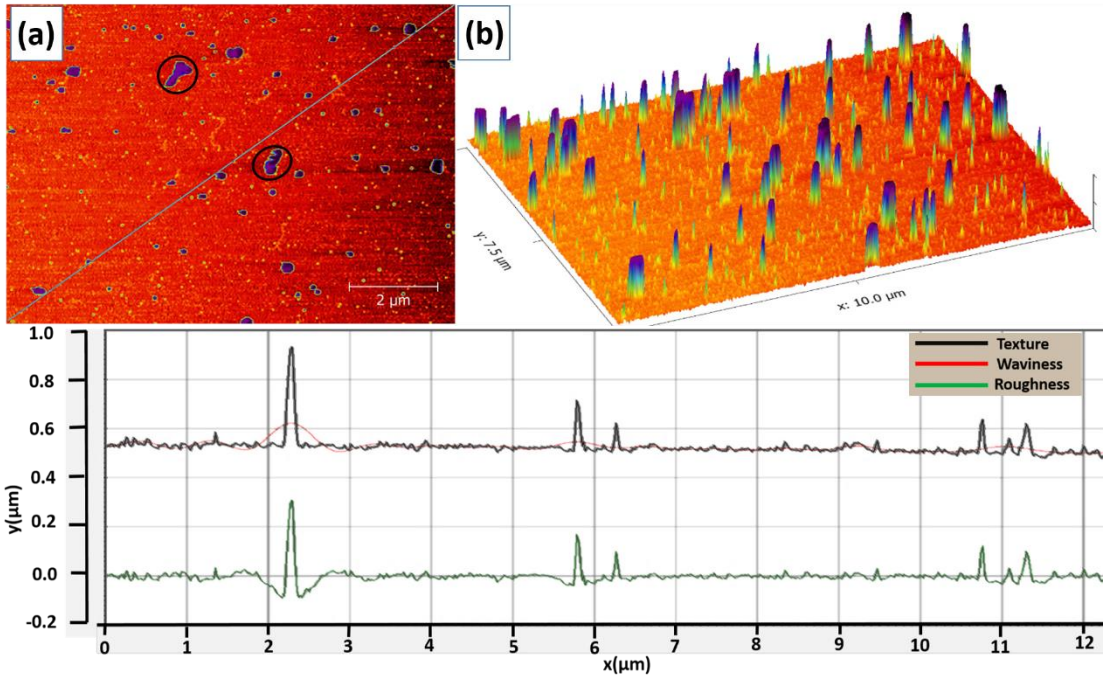

Figure.4.13 The AFM image of the P3HT 0.5mg/ml of the THF and the PC$_{[70]}$BM 0.5mg/ml of DMF. (a) indicates clumps and ruins of the "islands" confirming the role of PCBM in nanomorphology formation (black circled). (b) the 3D showing the height distribution of the vertical formations. The graph is the texture (black), waviness (red) and roughness (green).

This result undoubtedly confirms the influence of the PCBM in the formation of the nanomorphology. For the final confirmation the amount of PCBM was decreased to 0.29mg/ml and the amount of P3HT was left at 0.5mg/ml. Fig.4.14 AFM image which finally confirms that the PCBM plays a major role in the formation of "hills" thus providing the control possibility by varying the amount of PCBM. Fig.4.14 do not show any observable formations at all. In fact, the image looks like "noise" without any distinguishable features.

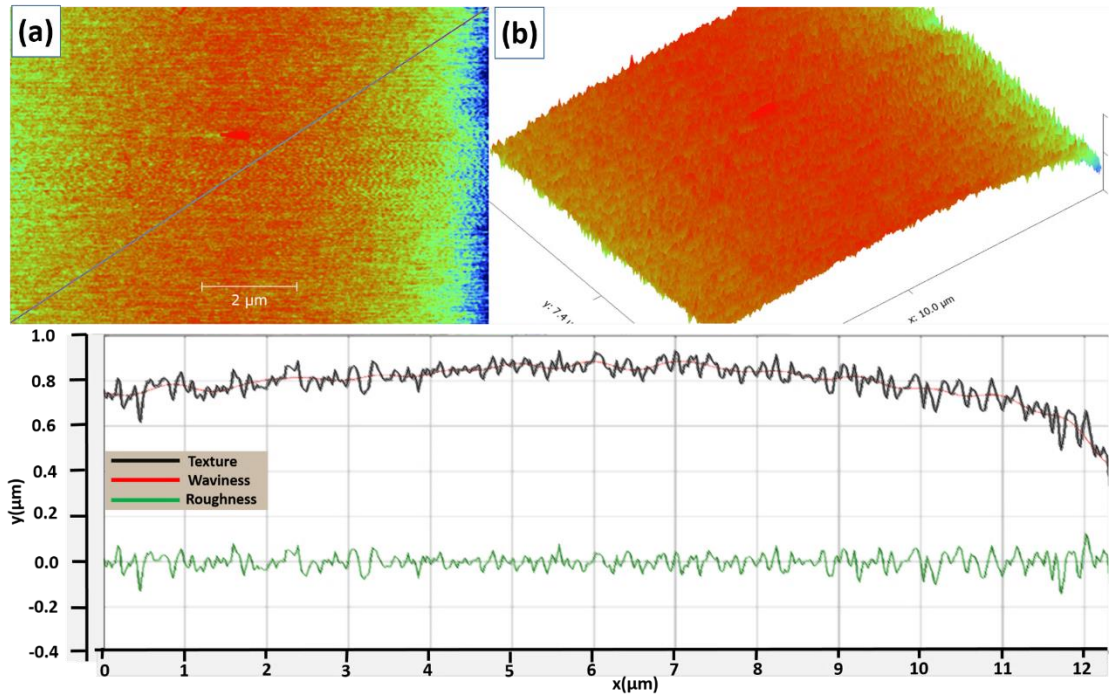

Figure.4.14 The AFM image of the P3HT 0.5mg/ml of the THF and the $PC_{[70]}BM$ 0.29mg/ml of the DMF. (a) completely ruined "island" formations. (b) 3D does not even detect vertical "islands" or "hills". The graph is the texture (black), waviness (red) and roughness (green).

The P3HT/$PC_{[70]}BM$ system morphology can be influenced by varying the amount of the $PC_{[70]}BM$. While the amount of the P3HT does not show significant morphological changes $PC_{[70]}BM$ was proven to play a major role. These findings provide basic ideas on the control of nanomorphology in P3HT/$PC_{[70]}BM$ systems. Every solvent has a different molar mass and parameters such as capability to dissolve one or another polymer. Every solvent makes polymer molecules to be on a different distance from one another and also change the conformation. When the film from the polymer solution is cast onto the surface of the silicon or mica surface the polymer molecules

settle down in a particular manner which at the end forms the morphology. During the film formation the polymer chains might be arranged in various ways creating complex morphologies. The reason for different colours in every vial is the distance between the molecules which vary depending on the solvent Fig.4.15.

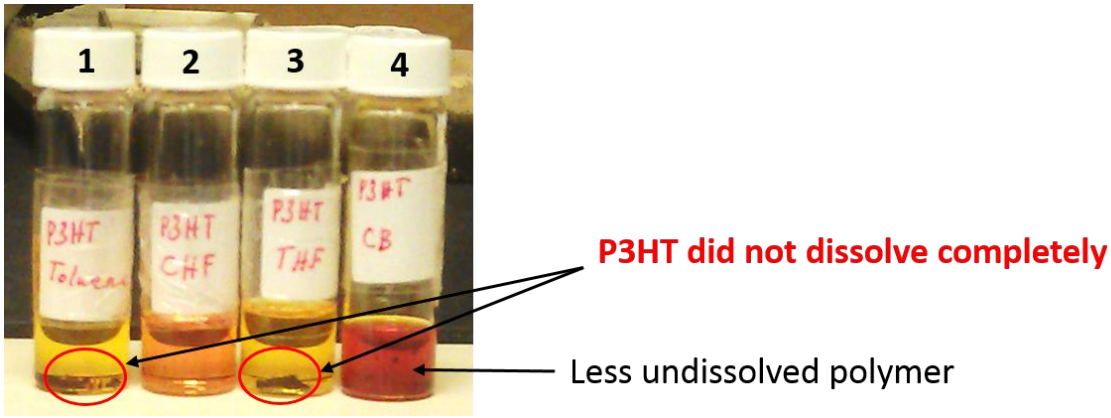

Figure.4.15 P3HT polymer dissolved in different solvents: 1 toluene, 2 chloroform, 3 tetrahydrofuran and 4 chlorobenzene. The concentration is 1mg/ml in all 4 vials.

4.4 PTB7/ $PC_{[70]}BM$ Light-Induced Morphology Control

In this subchapter the PTB7/PCBM nanomorphologies affected by light are discussed and analysed. The samples were exposed to blue and red LED light. Since shorter wavelengths have higher energy (blue light) and longer wavelengths lower energy (red light) it was the most logical choice for the sample irradiation. A mixture of PTB7/$PC_{[70]}BM$ was prepared in chloroform with concentrations 1mmol/ml under exposure of blue (461nm) and separately red (634nm) LED light. The LED exposure time was 12 hours. Non exposed sample was prepared in order to make a comparison. All the samples were deposited on a silicon wafer via spin-coating at 2500 rpm for 1 minute and characterized using the AFM D3100 in tapping mode. The difference in nanomorphology showed tendency depending on the wavelength of the light. Fig.4.16 AFM image of PTB7/$PC_{[70]}BM$ in the dark.

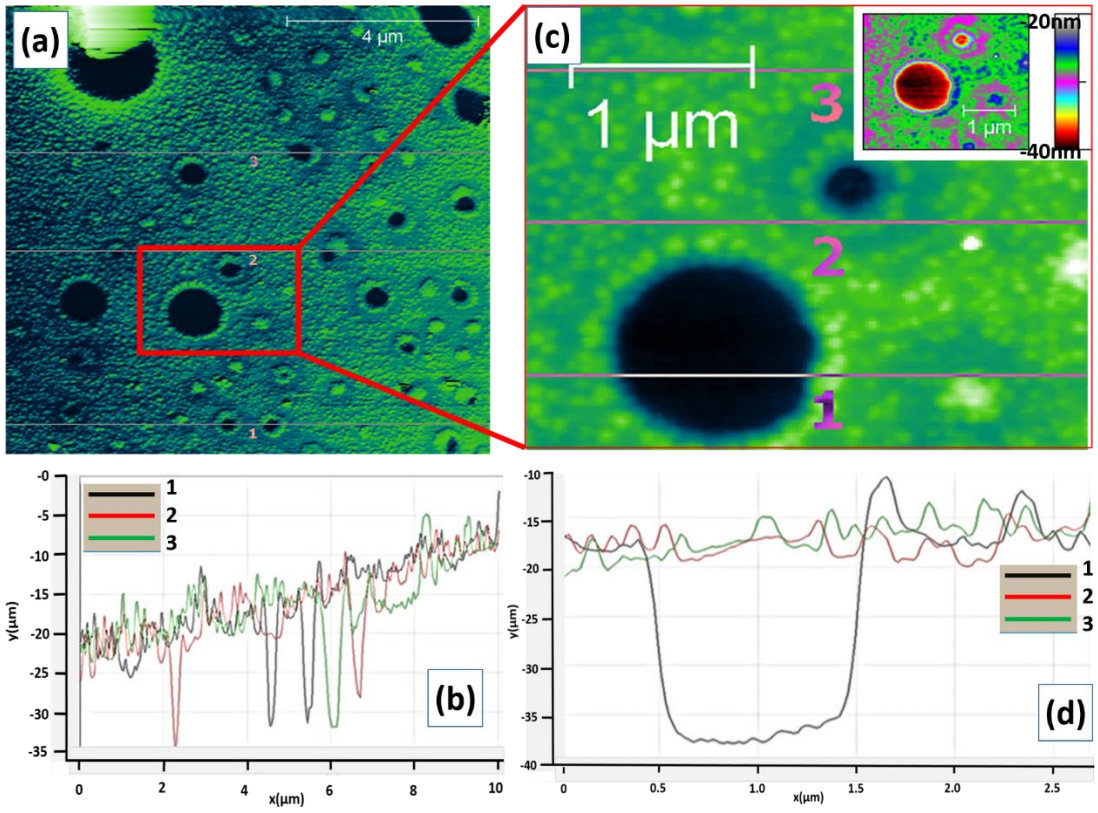

Figure 4.16 The AFM image of the PTB7/PC$_{[70]}$BM 1:1 in chloroform reference sample: (a) Reference sample without the treatment of light. The voids are randomly deposited on the surface and the roughness is characterized on three lines and represented in (b). In the image (c) is zoomed red square from the image (a) and analysed in detail. The insert in the right corner shows height with specially chosen colour panel. (c) Shows roughness profile from (c).

The sample in Fig.4.16 was not exposed to any source of light and the vial was wrapped in aluminium foil to avoid daylight. As we can see in Fig.4.16 the AFM micrographs reveal the formation of voids or holes which range in diameter and are randomly distributed over the sample. The holes do not form any "groups" or lines. For more precise evaluation Fig.4.16 was analysed in detail. In Fig.4.17 the AFM image of PTB7/PCBM in chloroform (in dark) with a more detailed analysis of voids and 3D image. As it can be seen from Fig.4.17 the voids are ranging from 350 nm (void No.9) to 1.79 µm (void No.15) in diameter. The structures resemble volcanic structures rather than just nanoholes. The colours in the inset in Fig.4.16 (c) are made to better highlight the details. The same system showed an obvious change in void distribution and shape when exposed to the light. Fig.4.18 is the AFM image of the PTB7/PCBM exposed to the blue light for 12 hours. The structures change the shape to elongated distorted ellipse-like formations. Also a few round shaped voids were observed. The more detailed analysis in Fig.4.19 defined the roughness and void diameter (length).

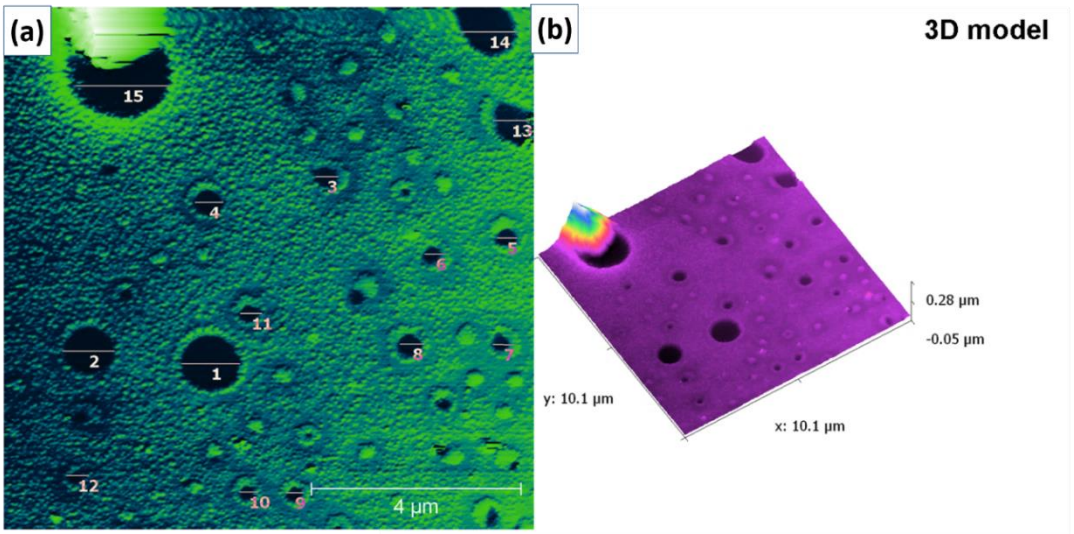

Void No	1	2	3	4	5	6	7	8	9	10	11	12	13	14	15
Δx [µm]	1.12	1.00	0.43	0.55	0.39	0.41	0.41	0.49	0.35	0.37	0.41	0.43	0.71	1.08	1.79

Figure 4.17 The AFM image of the PTB7/$PC_{[70]}BM$ 1:1 in chloroform reference. (a) The AFM micrograph void size analysis. Voids 1, 2, 13, 14, 15 are the largest ones which exceed 700 nm diameter. (b) Shows 3D image of (a). The colours are chosen to represent the height in the best way showing small details of the micrograph.

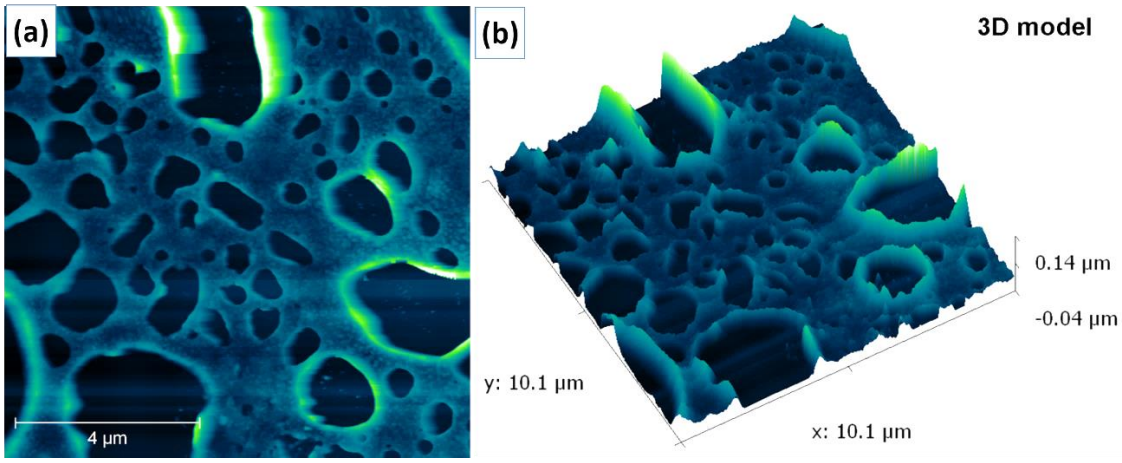

Figure 4.18 The AFM image of the PTB7/ $PC_{[70]}BM$ 1:1 in chloroform exposed to the blue light for 12h. (a) the voids are ranging from round-shaped to elongated distorted ellipse-like. (b) 3D model showing the features similar to a volcano. Colours are chosen to maximize the highlight of the features.

The holes after exposure to the blue light seem to be more chaotic and varying in sizes more than in the reference sample (Fig.4.17). Some of the voids in Fig.4.19 changed diameter by increasing a few times. The voids after the exposure to the red light became wider containing some nano-features inside Fig.4.20(a). The Fig.4.20 (b) shows the 3D model of the polymer film which indicates that crater-like morphology has been broken. The voids increased to the limits which made them almost "in-touch" with each other. Fig.4.21 more detailed analysis of voids of Fig.4.20.

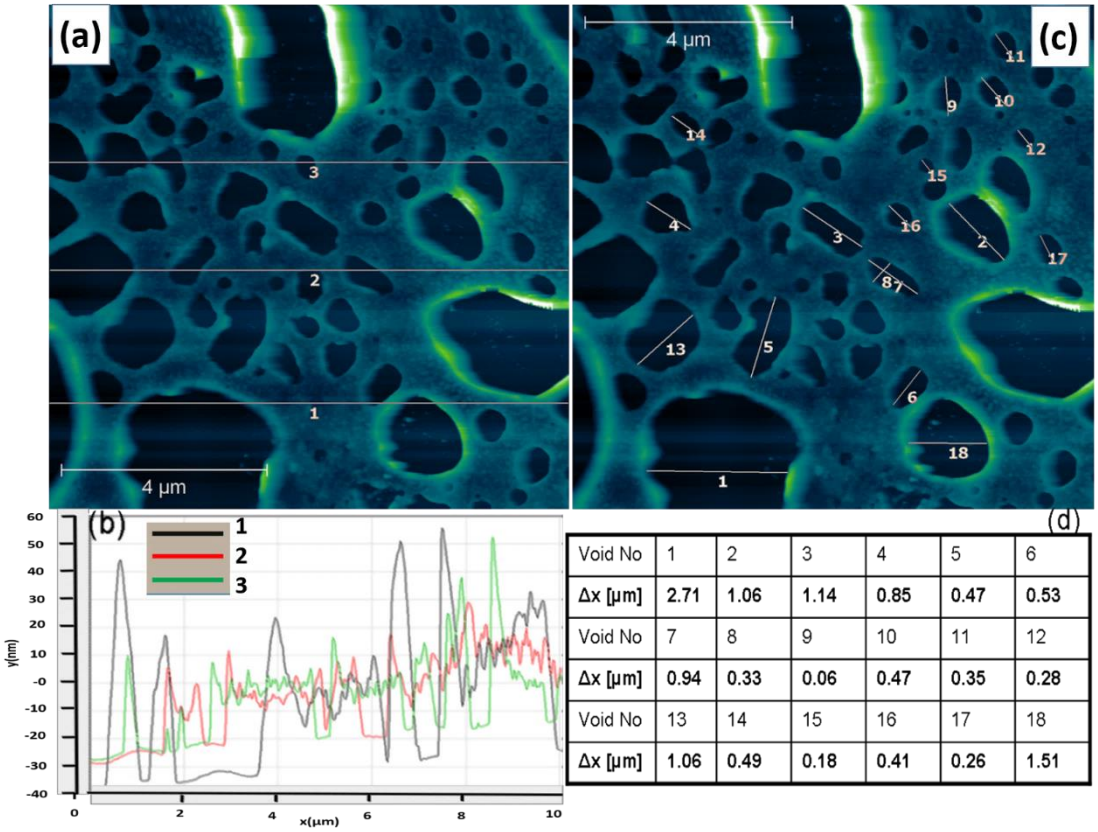

Void No	1	2	3	4	5	6
Δx [µm]	2.71	1.06	1.14	0.85	0.47	0.53
Void No	7	8	9	10	11	12
Δx [µm]	0.94	0.33	0.06	0.47	0.35	0.28
Void No	13	14	15	16	17	18
Δx [µm]	1.06	0.49	0.18	0.41	0.26	1.51

Figure 4.19 The AFM image of the PTB7/PC$_{[70]}$BM 1:1 in chloroform exposed to the blue light for 12h. (a) is the roughness analysis on 3 different places marked 1, 2 and 3. (b) is the graph that shows the roughness from (a). (c) detailed void length analysis and (d) values of void analysis from (c).

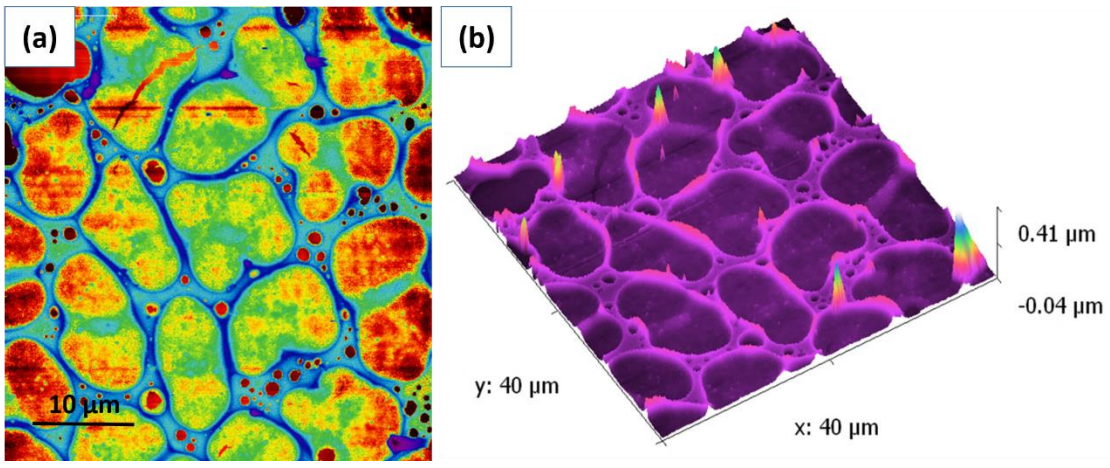

Figure 4.20 The AFM image of the PTB7/PC$_{[70]}$BM 1:1 in chloroform exposed to red light for 12h. (a) voids became vider with smaller voids in between. (b) the 3D view of a film showing that volcano-like structures completely vanished. Colours are chosen to maximize the highlight of the features.

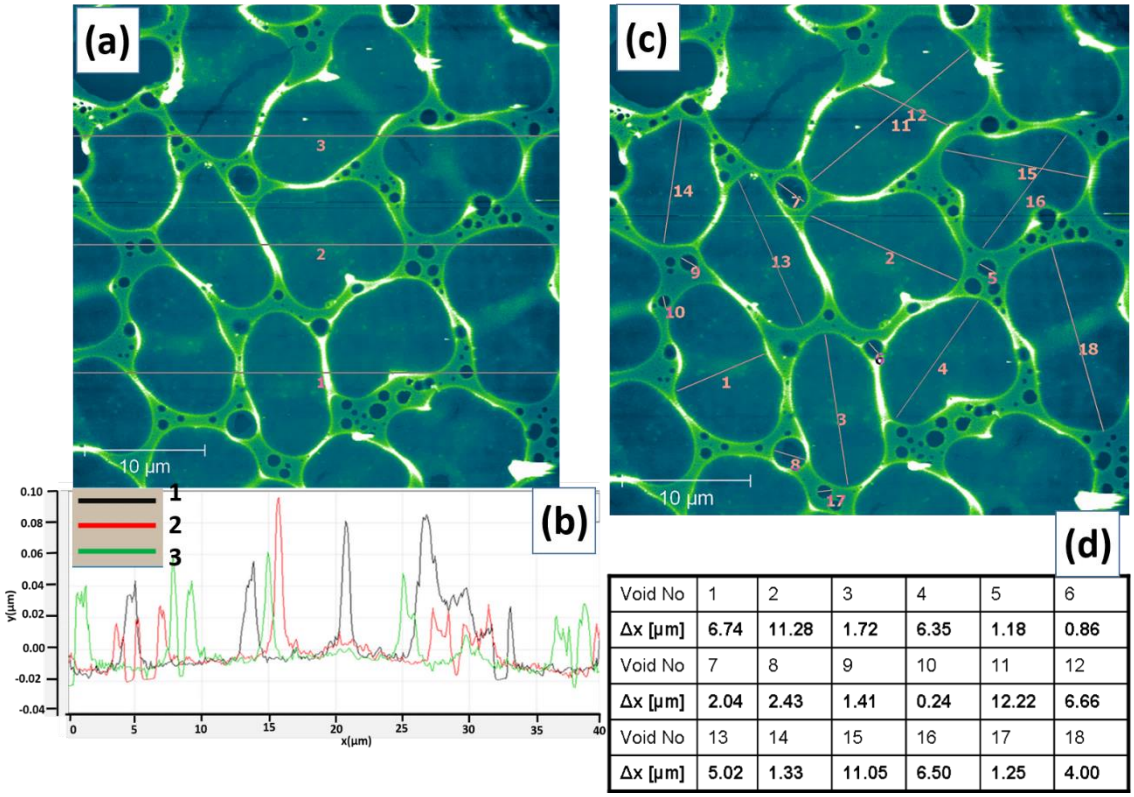

Void No	1	2	3	4	5	6
Δx [µm]	6.74	11.28	1.72	6.35	1.18	0.86
Void No	7	8	9	10	11	12
Δx [µm]	2.04	2.43	1.41	0.24	12.22	6.66
Void No	13	14	15	16	17	18
Δx [µm]	5.02	1.33	11.05	6.50	1.25	4.00

Figure 4.21 The AFM image of the PTB7/PC$_{[70]}$BM 1:1 in chloroform red light for 12h. (a) roughness measurement 1, 2 and 3 lines represented in (b) graph. (c) diameter of voids measurement results in table (d).

The nanostructuration of the PTB7/PC$_{[70]}$BM films via light was proven to be very efficient. Room temperature was also sufficient which excluded any thermal effects. In order to simplify the polymer-solvent system good solvent such as chloroform was used. Energy portions with different frequencies gave significant changes on the nanomorphology of the PTB7/PC$_{[70]}$BM system. If the effect is true and does not depend on a specific polymer like P3HT then replacing it with another polymer would allow control of the polymer morphology.

4.5 P3HT/PC$_{[70]}$BM Light-Induced Nanostructuration

In this subchapter we will investigate the effect of light on the P3HT/PC$_{[70]}$BM dissolved in chloroform. The conditions were the same as in subchapter 4.8. The concentration 1:1 and the exposition time were 12 hours. First of all, the reference sample was prepared. The sample that was not exposed to any light at all (wrapped in Al foil). If the effect is true then it should work with more than one polymer i.e it should work with more than the PTB7/PC$_{[70]}$BM system. Fig.4.22 AFM image showing the P3HT/PC$_{[70]}$BM reference sample. The features look very similar to Fig.4.2.

The voids form “groups” (red circled) and resemble volcano-like structures Fig.4.22 (b). Further AFM image analysis of the P3HT/$PC_{[70]}$BM reference sample reveals the roughness and the crater depths Fig.4.23 (a) and (b). The shapes of most of the voids are not perfectly round and are slightly elongated. Surface roughness is ranges from -50nm to up to 40nm narrowing at the bottom. Void diameter analysis in Fig.4.24 (a) shows that the diameter also ranges from nanosizes to microsized dimensions. However, the nanosized voids dominate on this sample ranging from 60nm to around 90nm in width. The nanomorphology of the film changes after exposure to the blue light Fig.4.25. The surface of the film looks more like the Moon surface and the holes become more spherical compared to the reference sample. The void distribution looks less chaotic and the shape is changed as indicated by the 3D model in Fig.4.25 (b) and (d). The hole diameters range from 30nm to 90nm and remain on the nanoscale. The shape of the volcanos become sharper and starts looking like actual “nano-volcanos”. After the material was exposed to blue light the sizes of the holes decreased but the distribution looked the same as in the reference sample Fig.4.26 (red circled). In Fig.4.26 the roughness analysis indicated that the depth of the craters was mostly on the micro scale with the holes narrowing at the bottom. This behaviour of the polymer could be explained by the specific arrangement of the molecules which can be caused by molar ratio, solvent or a mixture of the solvents influence a connection of the molecules with each other. In this case the first two possibilities have been excluded since we used the same solvent with molar ratios 1:1. This means that portions of light created new chemical bonds that crosslinked or partially destroyed the polymer thus causing new reorientations.

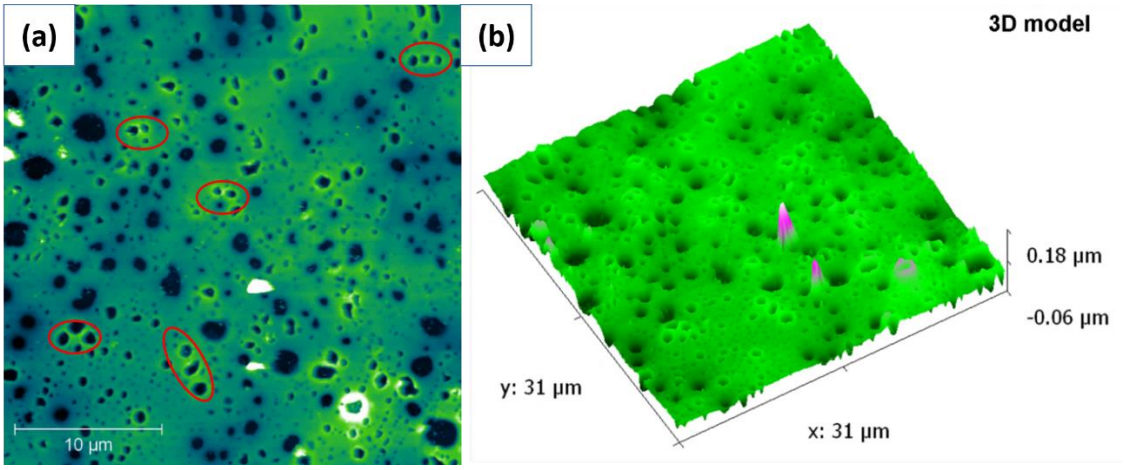

Figure 4.22 The AFM micrographs of the P3HT/PC$_{[70]}$BM 1:1 in chloroform reference. (a) the general AFM image showing the nano and micro features. In (a) formations of "groups" are observed red circled. (b) image shows the 3D of the (a) image. The colours are chosen to represent the height in the best way showing small details of the micrograph.

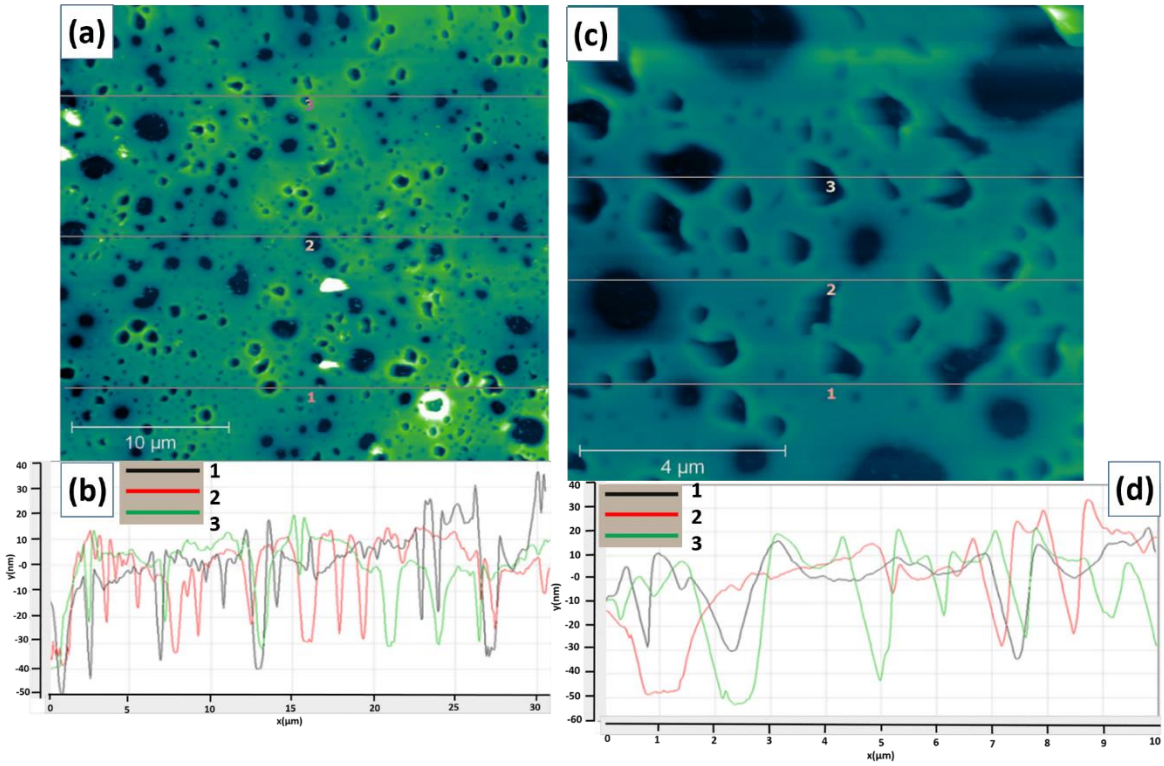

Figure 4.23 The AFM images of the P3HT/PC$_{[70]}$BM 1:1 in chloroform reference samples. (a) the image shows 30X30 micrometres in the AFM sample. The roughness measurement was done and it corresponds to the 1, 2 and a 3 lines in (b). In the image (c) another area of the same film was scanned in order to make a more detailed analysis. Roughness measurement 1, 2, and 3 lines corresponds to the graph in (d) image.

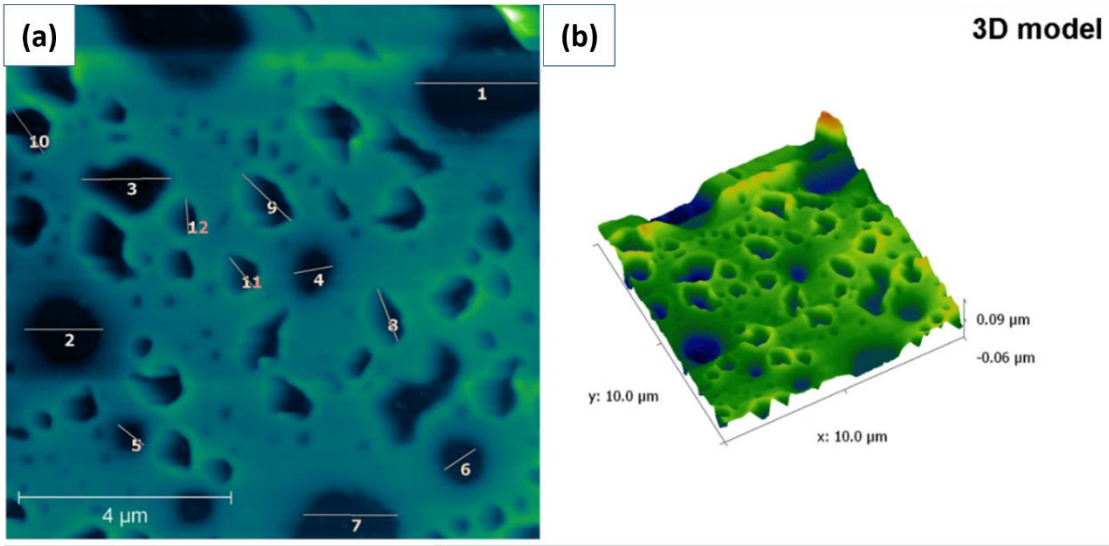

Void No	1	2	3	4	5	6	7	8	9	10	11	12
Δx [µm]	2.30	1.48	1.68	0.72	0.49	0.59	1.78	0.37	0.92	0.59	0.43	0.06

Figure 4.24 P3HT/PC$_{[70]}$BM 1:1 in chloroform reference sample. (a) The AFM void size analysis shows that the hole size is pretty similar to the one in Fig.4.8.4 The shape has some insignificant difference and structures look more elongated. (b) The 3D model shows domination of the volcano-like structures.

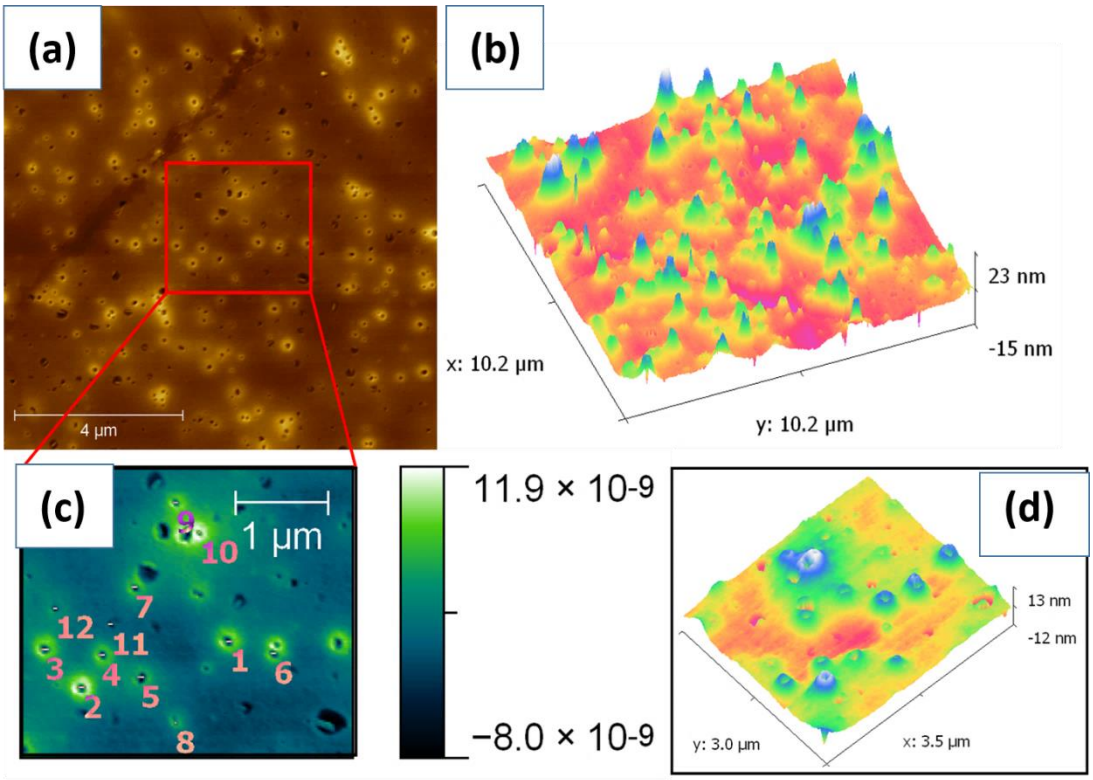

Void No	1	2	3	4	5	6	7	8	9	10	11	12
Δx [µm]	0.07	0.09	0.09	0.07	0.07	0.06	0.06	0.03	0.06	0.04	0.05	0.05

Figure 4.25 the AFM images of the P3HT/PC$_{[70]}$BM 1:1 in chloroform exposed to the blue light for 12h. (a) 2D AFM image 10X10 micrometres clearly shows the decrease of the hole size of up to 10 times (see the (c) and detailed analysis table on the bottom of the image). The holes are of nanometre scale size. Image (b) shows the 3D model of the film. The volcano-like structures look sharper in their shape. And (d) image shows the 3D image of (c) inset. The colours are chosen to represent the height in the best way showing small details of the micrograph.

Also, the repeated experiment with the thermometer (which was very well attached to the vial overnight) has shown that the overall temperature of the sample increases to up to a maximum of 1.5 ^{0}C that makes around 25^{0}C of the solution. Also if it was the thermal effect it would only go in one direction i.e. the holes would be either increasing or decreasing. However, the last experiment with the P3HT/$PC_{[70]}$BM in chloroform and the red light confirms the formation of polymer nanostructures, as shown in Fig.4.27. The size of the elongated craters and holes ranged from around 120nm to 300nm Fig.4.27 (b).

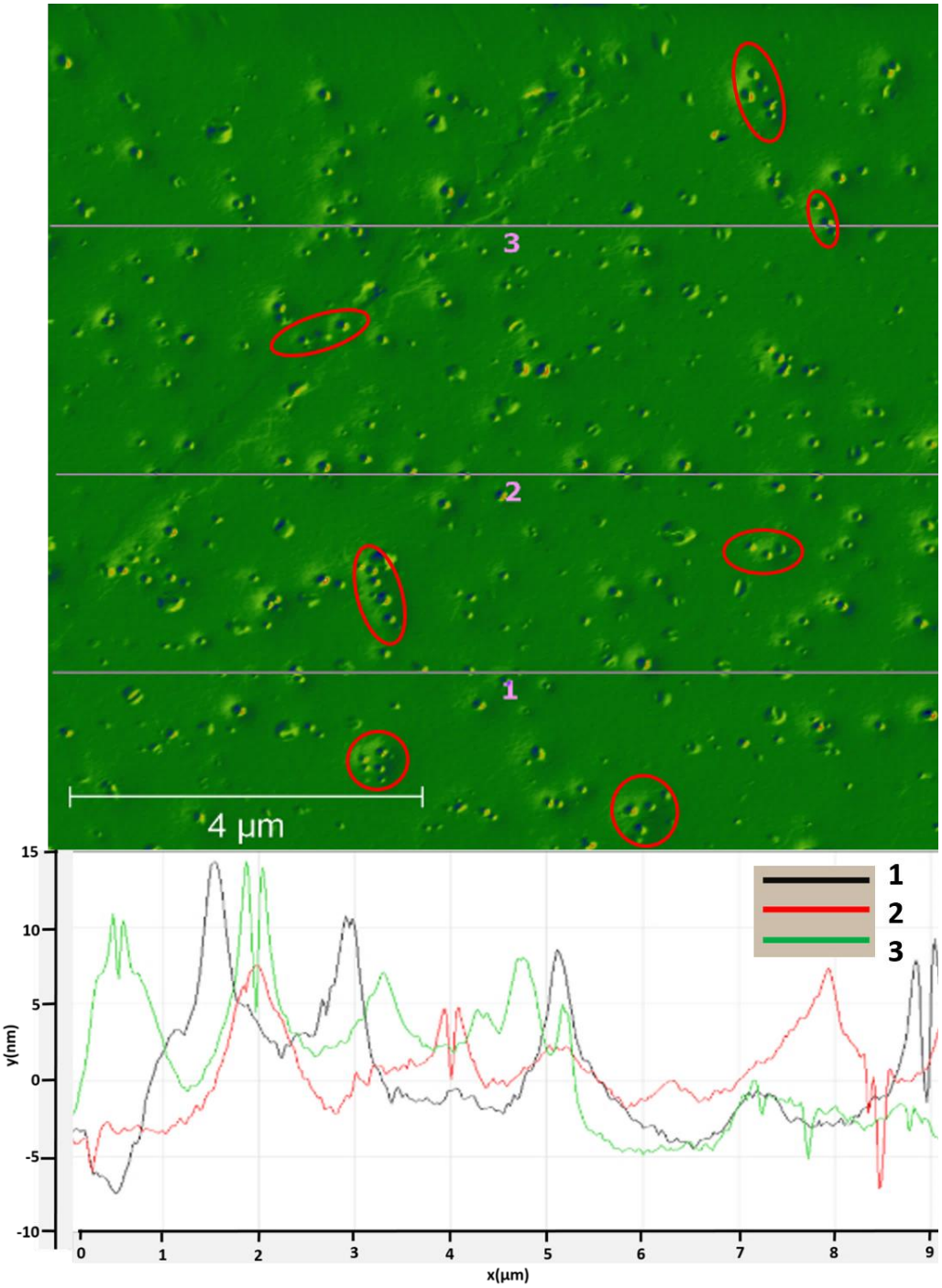

Figure 4.26 The AFM image with a surface analysis of the P3HT/$PC_{[70]}$BM exposed to the blue light for 12h. Red circled are the volcano-like structures with more than one void forming "groups".

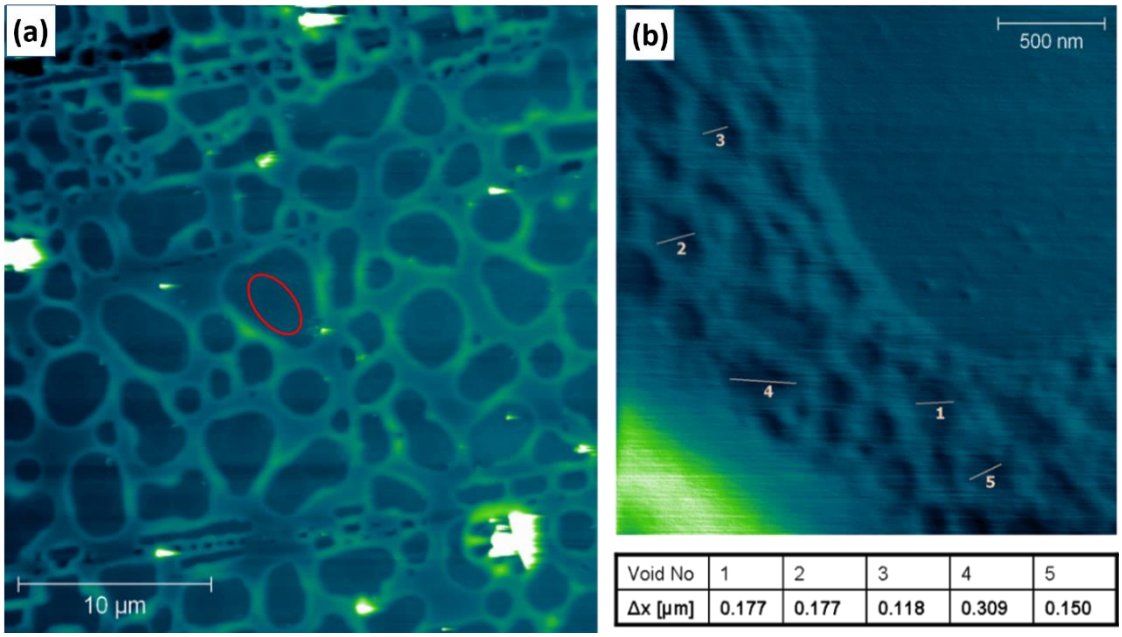

Void No	1	2	3	4	5
Δx [µm]	0.177	0.177	0.118	0.309	0.150

Figure 4.27 The AFM micrographs of the P3HT/$PC_{[70]}$BM 1:1 in chloroform exposed to red light for 12h. (a) Shows the 30X30microns size image. (b) detailed analysis of the nanofeatures and their sizes (bottom table).

In Fig.4.28 we can see the AFM image scanned at the particular place highlighting features on the walls and providing more information about the volcano or crater like formations on the nanoscale. These features a very similar to the PTB7/$PC_{[70]}$BM irradiated with red light Fig.4.21. A detailed analysis of the nanofeatures inside the voids was performed and presented in Fig.4.29. The roughness analysis demonstrates 4-10nm and the crater sizes are within a few hundreds of nanometres. This measurement provides important information that allows us to see that microformations are made of nanoformations. Importantly microfeatures repeat nanofeatures which possibly repeat molecular arrangements inside the film. As can be seen in Fig.4.29 (a) and (c) and the inset the bigger microsized crater is surrounded with smaller nanosized craters. Fig.4.29 (a), (b) shows the detailed roughness analysis, (c) and (d) the void diameter analysis. The diameter of voids ranges from 90nm (void No.13, 17) to 370nm (void No.1). To have better understanding on what is happening we need to look into the molecules. NMR is a widely used technique for the polymer characterization and can provide information about polymer conformations inside the film.

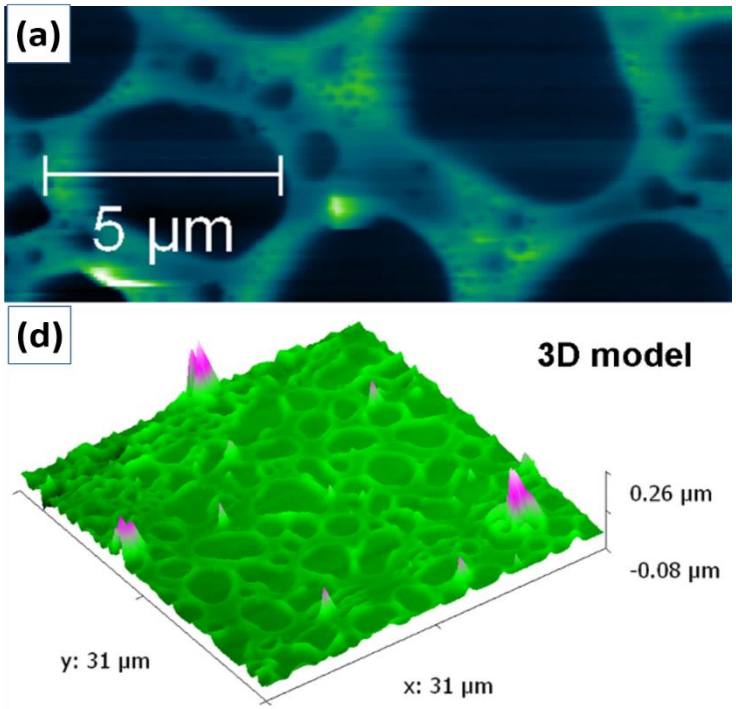

Figure 4.28 The AFM image of the P3HT/PC$_{[70]}$BM 1:1 in chloroform exposed to the red light for 12h. (a) AFM showing nanofeatures on the "walls". (b) the 3D model showing hole distribution over the 31X31µm area.

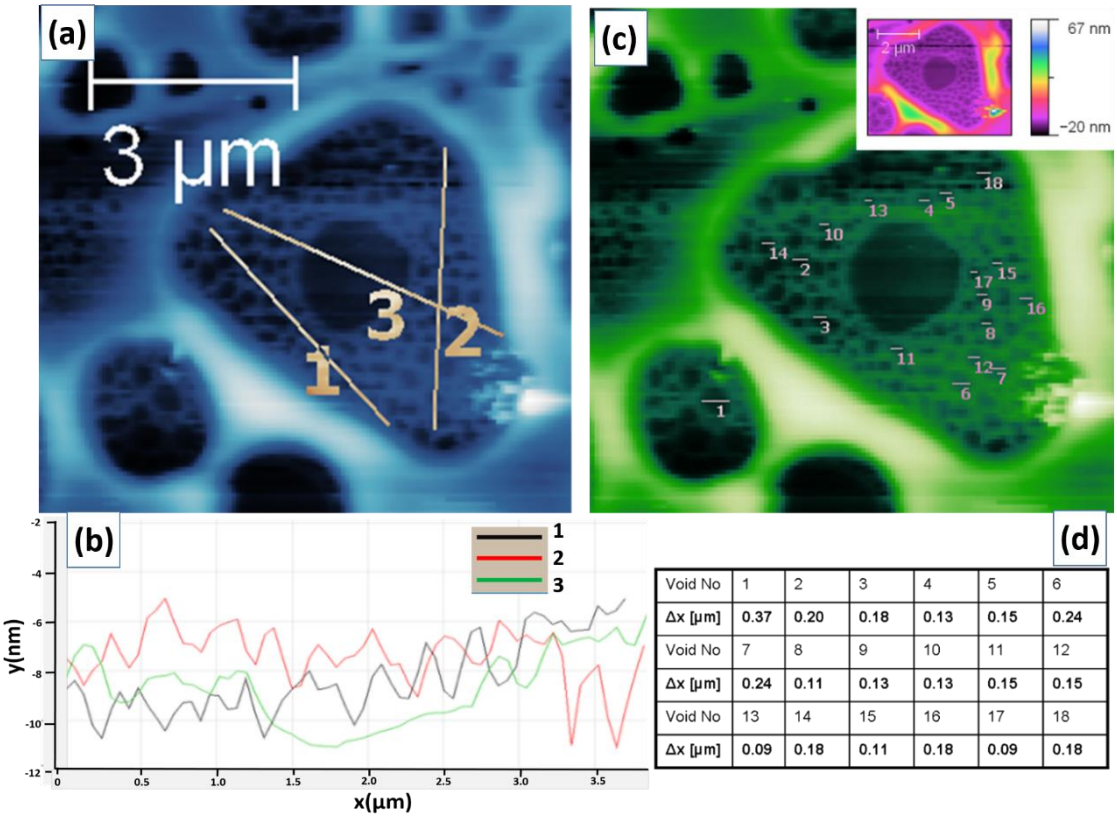

Void No	1	2	3	4	5	6
Δx [µm]	0.37	0.20	0.18	0.13	0.15	0.24
Void No	7	8	9	10	11	12
Δx [µm]	0.24	0.11	0.13	0.13	0.15	0.15
Void No	13	14	15	16	17	18
Δx [µm]	0.09	0.18	0.11	0.18	0.09	0.18

Figure 4.29 The AFM image of the P3HT/PC$_{[70]}$BM 1:1 in chloroform exposed to the red light for 12h. (a) and (b) roughness analysis of the nanofeatures inside the crater or hole. (c) and (d) hole size analysis inside the microcrater. The table (d) shows hole diameters. The inset highlights the hole distribution in more contrast colours.

4.6 ^{1}H NMR Spectrum and ^{1}H NMR Prediction

Proton NMR analysis was performed in deuterated chloroform at 300MHz. Fig.4.30 shows the ^{1}H NMR spectrum of the PTB7/$PC_{[70]}$BM and the structural formula of the polymers. The chemical shift peaks in Fig.4.30 are very similar for most of the spectrum and the difference is related to slight variations in intensity most probably related to sample concentration. The line broadening of the NMR spectrum can be explained due to (a) rapid exchange with solvent and the protons are regained from other molecules. When these processes happen faster than once per millisecond it lead to the broadening of the lines as we see in Fig.4.30. Slower processes lead to narrow peaks and no spin-spin coupling in the molecules and (b) slight changes in the environment of groups due to the restrictions of being fixed into a polymer chain. The modeled NMR prediction of the PTB7/$PC_{[70]}$BM is shown in Fig.4.31 As we can see the molecules in Fig.4.31 have no chemical bond and serve as a reference prediction of NMR in $CDCl_3$ at 300MHz.

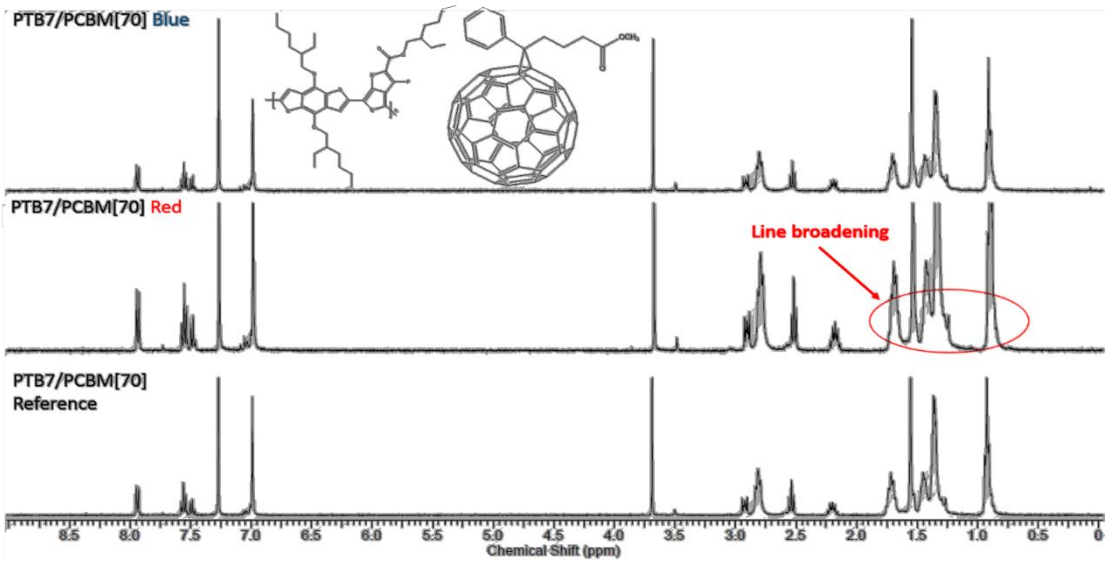

Figure.4.30 Experimental 1H NMR of PTB7/$PC_{[70]}$BM exposed to different wavelengths: marked as a reference (without exposure), red and blue. The peaks are varying only on the intensity (y) scale. Chemical shifts are in the same positions.

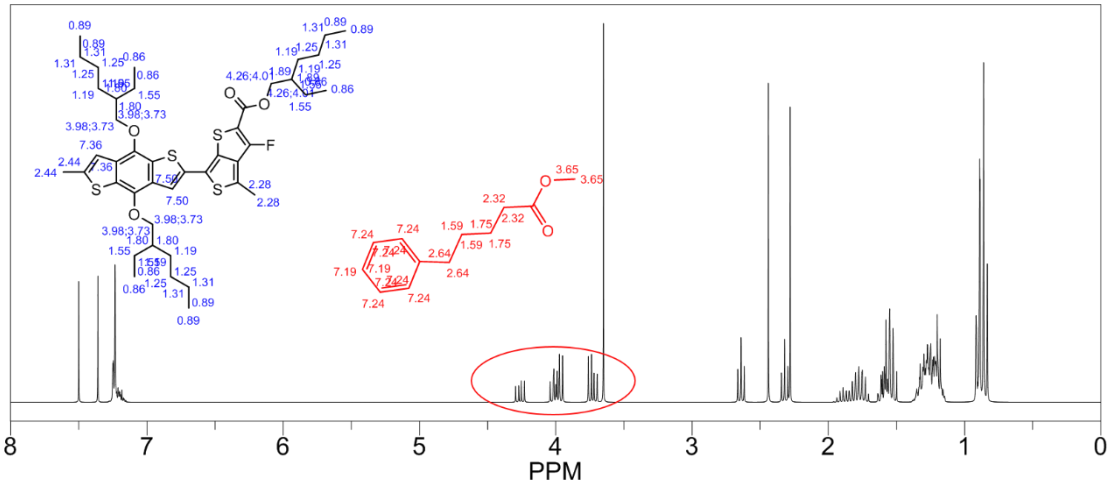

Figure.4.31 The proton NMR spectra prediction for the PTB7/PC$_{[70]}$BM. If the spectra is calculated without making any bonds between the molecules we have four peaks at the center at around 4ppm (red circled) which does not persist in experimental NMR Fig.4.30. Fullerene removed to ease the simulation process.

In Fig.4.32 experimental NMR of the P3HT/ PC$_{[70]}$BM is depicted. Importantly NMR indicates a small peak that appears at around 5.1 (middle spectra) and grows after the red light irradiation and then almost disappears completely irradiating with blue light. The peak is at around 6.6 and appears to be significant after the red light irradiation and grows after exposing to the blue light. It appears that higher energy photons can influence the polymer bonding by breaking or creating the bond. One of the key observations is that the line broadening is far more reduced after exposure to the light. This would tend to indicate that the level of restrictions in the molecular structures has been reduced. Thus this was postulated to indicate degradation of the polymeric structure upon irradiation. The new peak present in the spectrum discussed above may, therefore, be new low molecular weight species that are fragments that have been cleaved from the polymer/polymer blend. The change appears to be related to the expansion or contraction of the voids observed in the materials surface upon irradiation. Surprisingly most of the peaks in both samples (the P3HT/PCBM and the PTB7/PCBM) are at the same positions except in the P3HT/PC$_{[70]}$BM that has peaks at around 5.0 and 6.6. This, of course, can give another speculation that nanomorphology is greatly influenced by PC$_{[70]}$BM and could indicate that this material are more stable when irradiated. However how exactly the molecules are distributed inside the film remains unclear.

Further the NMR prediction gave preliminary results that are presented in Fig.4.34, Fig.4.35, Fig.4.36 and Fig.4.37 which have been conducted to look at various elements of the structure to determine if these fit any of the patterns defined in the NMR and thus may help rationalize the degradation chemical transformations that it are proposed to result from the irradiation on the sample.

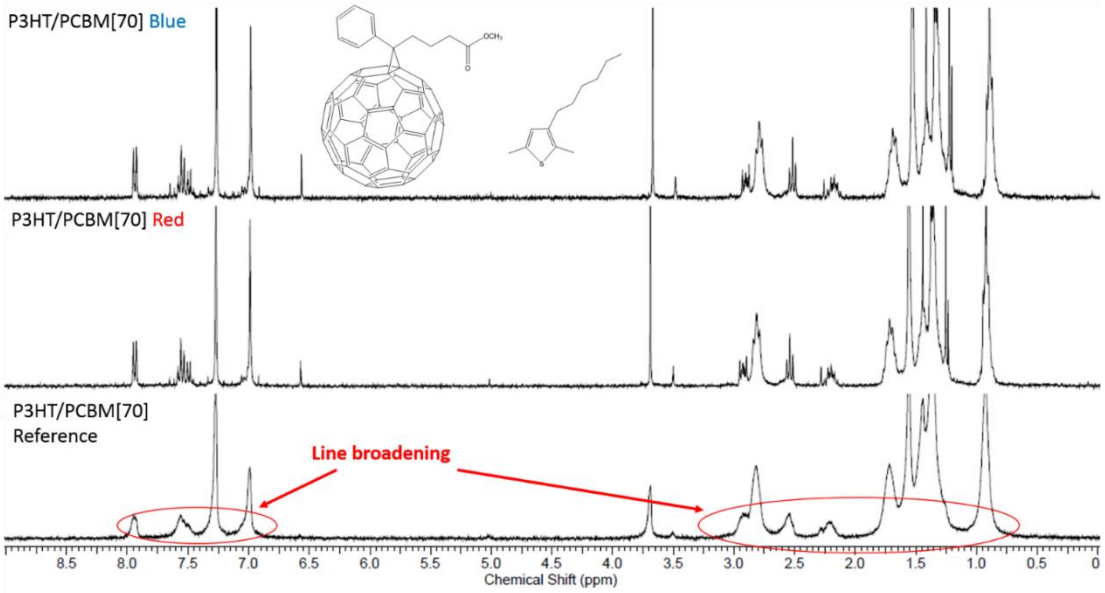

Figure.4.32 The experimental ^{1}HNMR of the P3HT/PC$_{[70]}$BM exposed to different wavelengths: marked as a reference (without exposure), red and blue. The difference in chemical shift peaks is at 6.5 at around 5, and 3.5 shows mainly a change in intensity. Other chemical shift peaks also show a difference in intensity. Line broadening due to the rapid exchange with solvent and regaining lost protons from other molecules.

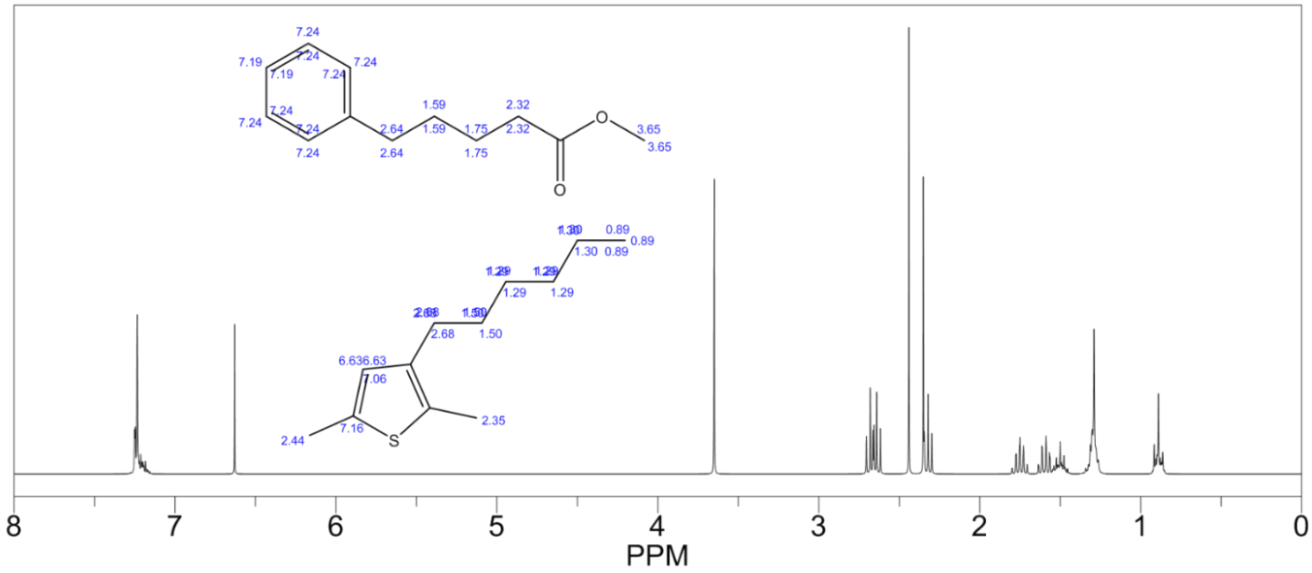

Figure.4.33 the predicted ^{1}HNMR of the P3HT/PC$_{[70]}$BM. The molecules do not contain chemical bonds between each other. The spectrum does not match the experimental results completely. The prediction spectrum implying that the molecules actually interact and make chemical bonds.

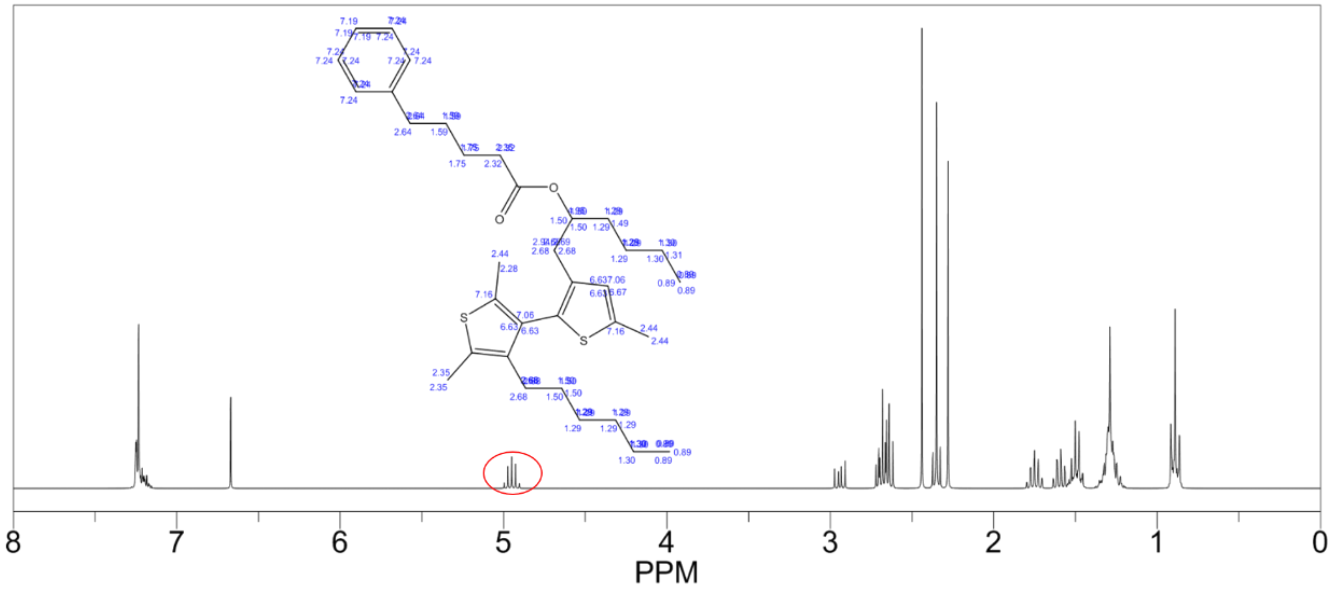

Figure. 4.34 the predicted NMR spectrum for the P3HT/PC$_{[70]}$BM. Red marked peaks at around 5.0 corresponds to the red marked bond on the structural formula.

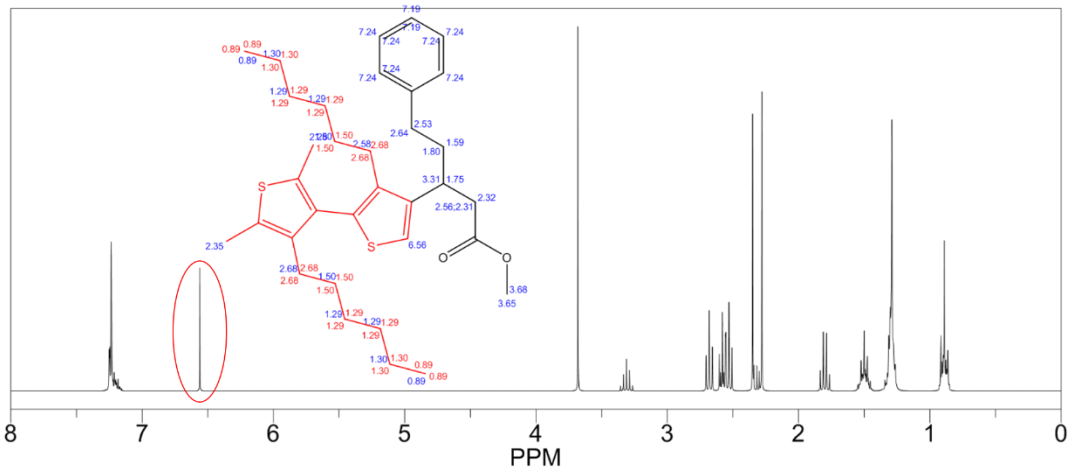

Figure.4.35 the predicted NMR spectrum for the P3HT/PC$_{[70]}$BM. Marked in red gives peak at 6.56. This peak appears higher in intensity after irradiating the sample with higher energy photons (blue).

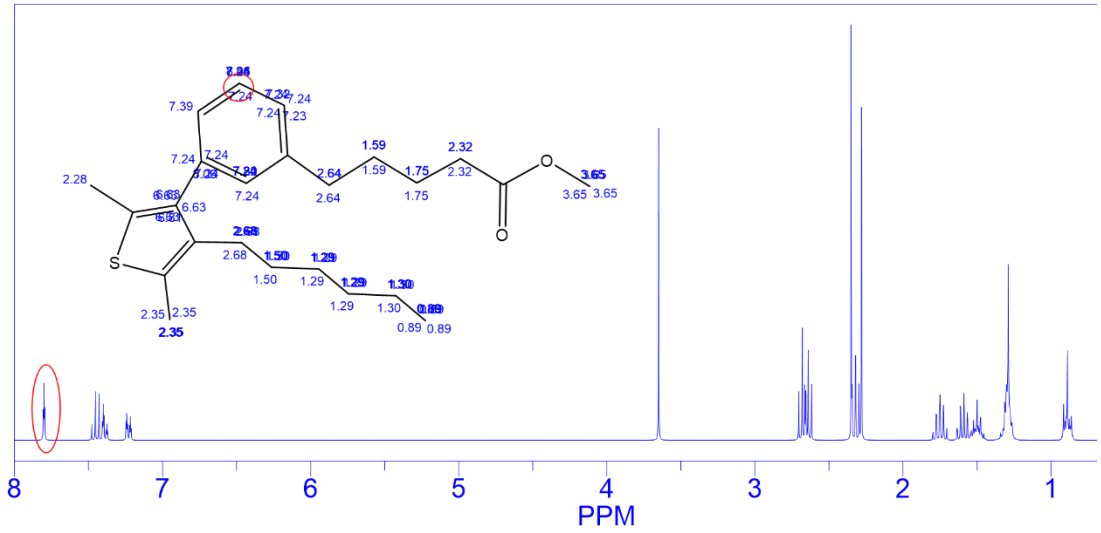

Figure.4.36 the NMR prediction for the P3HT/PC$_{[70]}$BM. Red marked peak corresponds to the red marked position in the structural formula of PCBM.

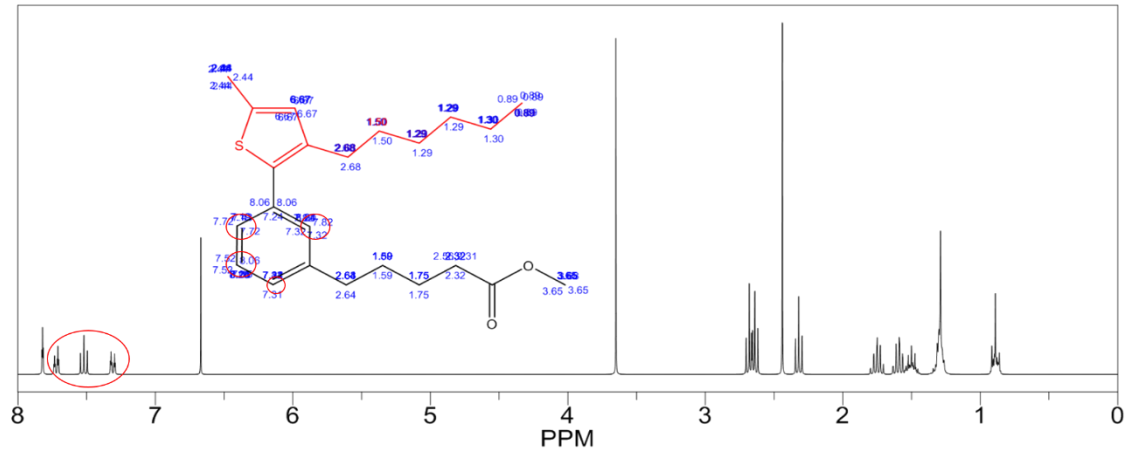

Figure.4.37 predicted NMR spectra for P3HT/PC$_{[70]}$BM. Red marked peaks correspond to red marked parts on PCBM structural formula. These peaks give a rough idea on what molecular conformations might be.

The NMR results did not show any vivid difference between the polymers exposed to the light and those unexposed. However, minor changes were observed and can be associated with the degradation of the polymer and decompose it into the smaller chemical compounds which could cause minor peaks in NMR spectra and also morphological changes observed by the AFM. Blue light has a higher energy than that of the red light and could be the reason for the higher polymer degradation.

4.7 Summary

It was demonstrated that the semiconductive polymer film morphology can be changed at room temperature. Change of the arrangement of polymer molecules can be achieved in the solution using only solvent or solvent mixtures. Using different solvents for the P3HT gives different morphologies of the film. The advantage of the method is that the polymer does not have to be deposited first and all change is done while polymer in the solution. Polymer monomer mixture the P3HT/PCBM morphology can be influenced in two cases: using one solvent like chloroform and mixture of different solvents. A varying amount of the solvents in the mixture also plays a great role in polymer film morphology. Most efficient polymer film morphology influence was demonstrated using the light-induced method. Light-induced method did not require mixing more solvents or use of one particular type of solvent. Changing wavelengths of light it was shown to influence polymer film morphology in one direction. Film morphology changed mainly one parameter: diameter of the voids. This method never used before demonstrates a very comfortable way of selective morphology change with more than one polymer. Light-induced morphology change was never used before and has promising future.

Chapter 5 Template-Assisted Synthesis of Ag, Au and CdS Nanoparticles

In this chapter, the template-assisted synthesis is described for Ag, Au and CdS nanoparticles. As a template the PPI type dendrimer with generation 4 was chosen. The concentration was 1:1 metal salt and dendrimer. For characterization a High-Resolution Electron microscopy (HRTEM) and Energy-dispersive X-ray spectroscopy (EDX) was used. Template-assisted synthesis is a widely used method in nanoscience (see subchapter 2.7). It allows the synthesizing at room temperature of nanostructures with a few nanometers in size. The method uses organic templates soluble in a solvent (which can be water) and molecules then interact with the crystals by shaping them into a certain structure. It has always been a challenge to synthesize nanometer range particles. Nanometers sized particles usually aggregate or agglomerate and are not stable. Stabilising particles has been a great challenge in nanosynthesis. Self-assembly of the particles of a few nanometers in size is even a greater challenge. These problems will be solved in the following subchapters.

5.1 Template Choice

The template-assisted synthesis result depends on a template and the metal precursor. The interaction of a metal precursor with the template molecules can define the entire synthesis process and the final result. In our case the PPI type dendrimer was chosen. This type of dendrimer has a dendritic structure and has NH_2 groups which are negatively charged. Silver Ag^+ and cadmium Cd^{+2} both ions are charged positively. Negatively charged dendrimer groups and positive metal ion will attract each other and the growth of metal crystal will be blocked. In the case with the Cd^{+2} it needs 2 electrons which means that two NH_2^+ groups will be able to attach. This process should presumably cause some kind of self-assembly of the CdS quantum dots.

5.2 Template Choice in the Synthesis of Au

Oleic acid can have isomers without affecting it with high power lasers or other light sources. Oleic acid has two isomers cis and trans and is expected to use them as a template when the reduction of the gold precursor occurs. Since the cis isomer has an angle (Fig.5.18) the formation of Au structures can be shaped via the molecules with an angle (cis isomer) and the molecules without an angle (trans isomer). The growth will be finally terminated by the packing of oleic acid molecules.

5.3 Ag and Au Synthesis Using PPIG4 Polymer

The HRTEM investigation revealed spherical structures Fig.5.1. The sizes were 2-3nm in diameter. PPI dendrimer worked perfectly as a template to achieve nanoparticles with the diameters smaller than 5 nanometres. Most of the nanoparticles are around 3nm in diameter. Fig.5.2 shows TEM images of the silver nanoparticles in a different area of the grid. Size distribution Fig.5.3 is quite narrow which is good for the synthesis of nanoparticles using the dendrimers. Similar size distribution Fig.5.5 of the gold nanoparticles is around 4nm however some parts of the grid are quite different Fig.5.4 and contains nanoparticles with a diameter of around 5-7nm. It is reasonable to make comparison between gold and silver NP's because the syntheses were carried out by using the same concentrations and the same PPI G4 polymer.

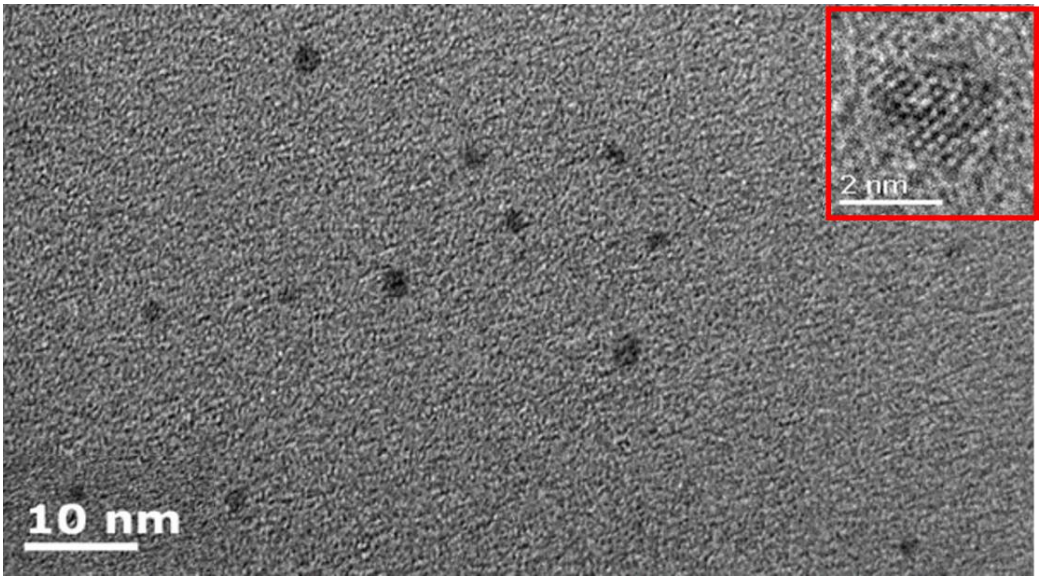

Figure. 5.1 The HRTEM image of the silver nanoparticles synthesized with the PPI-G4 inset shows "artefact" nanocluster with a diameter of around 8 atoms. The resolution is not perfect because of the copper grids used in this measurement.

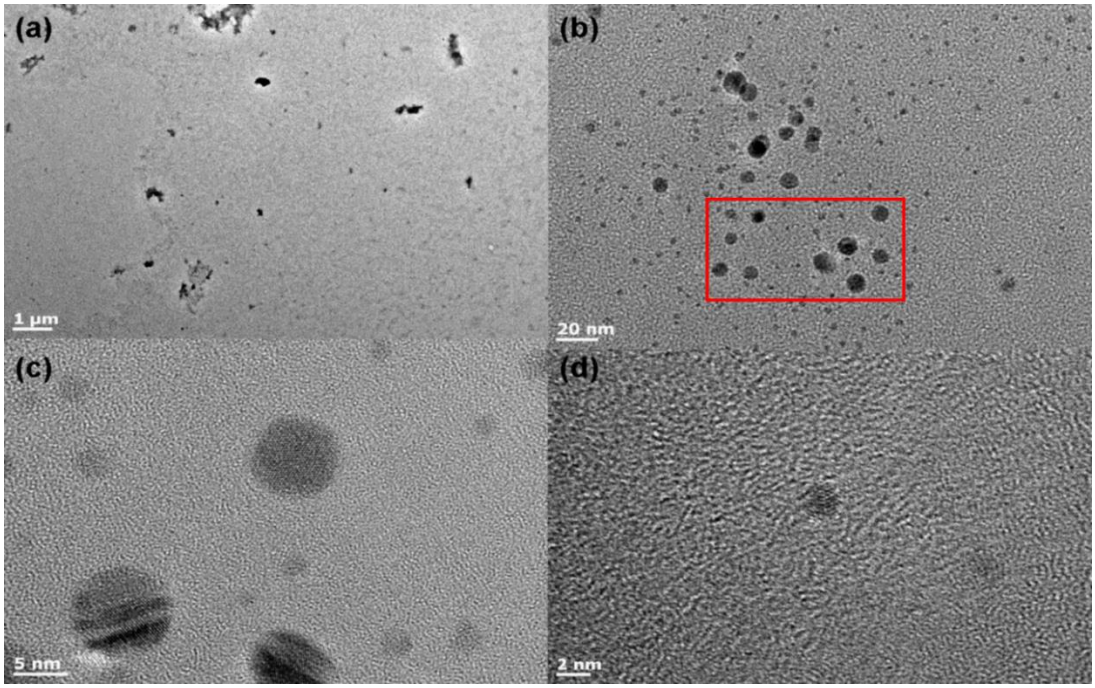

Figure.5.2 The HRTEM images of silver nanoparticles synthesized using the PPI-G4 dendrimer. (a) 1 micrometer scale shows the distribution of NP's on the grid, (b) zoomed to 20 nm we can clearly see bigger NP's surrounded with smaller ones (c) shows actual diameter of the NP's which is 5-7nm. (d) nanoparticle with diameter around 2nm.

The growth of the Ag nanoparticles was terminated by the PPI dendrimer and the shapes of the nanoparticles are spherical. Nanoparticles with sizes of 3nm and more formed because of the reduction of the $AgNO_3$ at different places in the PPI dendrimer. Since the PPI G4 has a diameter of around 4 nm [139] the formation of all nanoparticles cannot be attributed to the formation between the branches of the dendrimer.

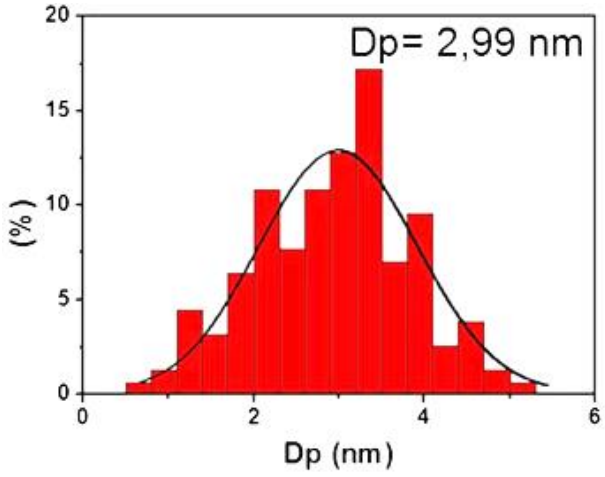

Figure.5.3 The size distribution of the silver nanoparticles. From this analysis it is obvious that the highest number of the nanoparticles had about 3 nanometers in diameter. Dp- particle density.

As shown in Fig.5.8 dendrimers have 4 stages of being in solution depending on the concentration [139, 199] Fig.5.8. First is *diluted* when concentration is small and the molecules are far away from each other. They basically meet very rarely and almost never interact. The second stage is when the concentration is higher and is called *contact*. The contact stage allows dendrimers to meet and even bounce of each other. The third stage is *collapse*. This stage allows the molecules to meet, to be in touch but without interpenetration. And the final stage is *interpenetrate*. In this stage the concentration of the dendrimers is high enough for them to be constantly in touch and most importantly overlap and sometimes 'stick' to each other making chains or other organic formations. In Fig.5.7 and Fig.5.8 shows the proposed nanoparticle growth mechanism. As shown in Fig.5.4 Au nanoparticles were bigger so it was possible to make an EDX scan which will be shown below. Also theoretical simulation was carried out using 300nm and electric field intensity on the surface of the nanoparticles was investigated. The size distribution analysis from Fig.5.4 is shown in Fig.5.5. As we can see the Au NP's are bigger in comparison to that of Ag with size limit less than 20nm.

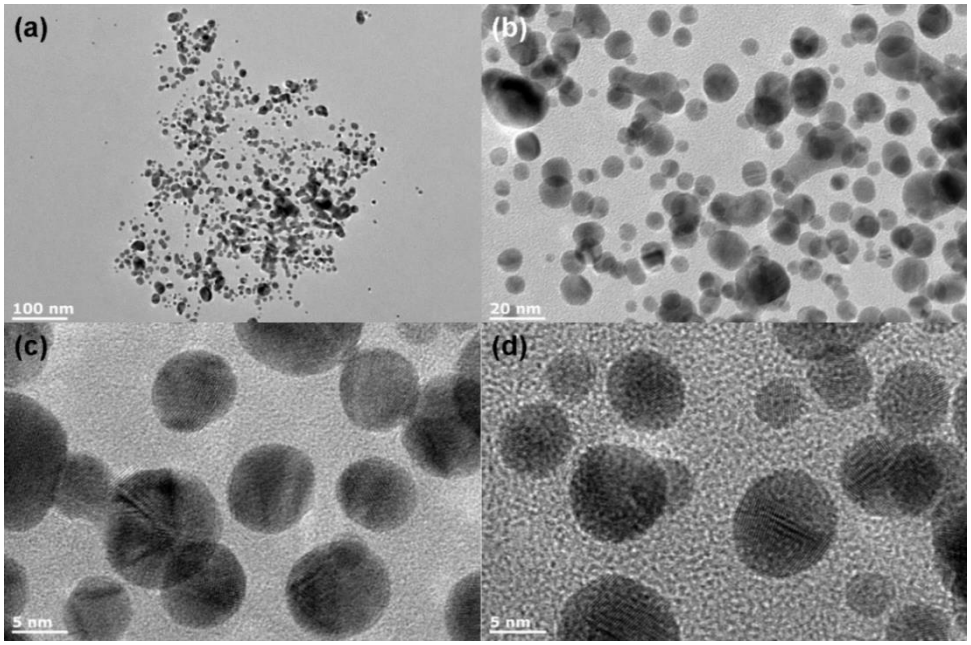

Figure.5.4 gold nanoparticles (a), (b) confirms the metal (non-transparent for electron beam), (c) and (d) spherical shape nanoparticles with crystal structure.

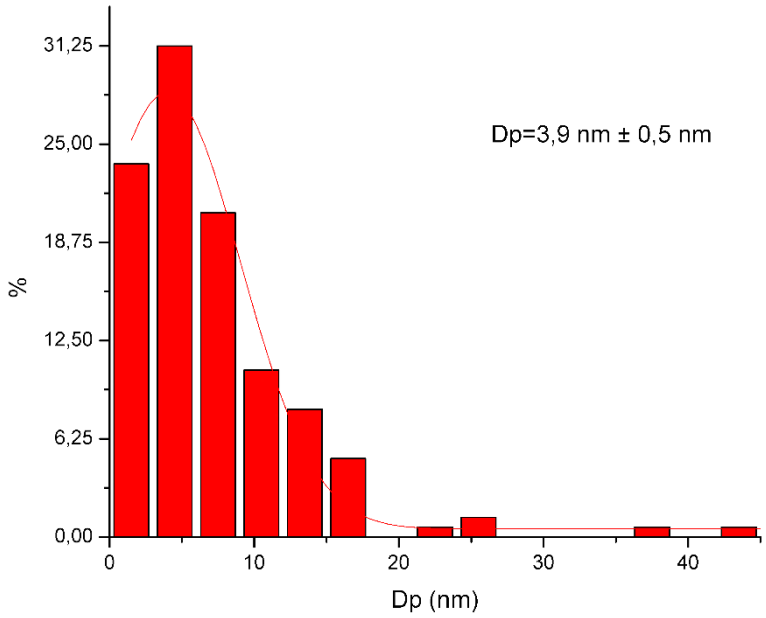

Figure.5.5 size distribution of the gold nanoparticles. From this analysis it is obvious that the highest number of the nanoparticles had about 4 nm in diameter. Dp-particle density.

NP's can be grown inside the dendrimer or in between the molecules as in Fig.5.8. Using the same dendrimer nanoparticles of Au and Ag, with similar size distributions, these were synthesized. Confirmation of the elements was performed using EDX integrated in HRTEM. Fig.5.6 shows the EDX of the Au NP's with dendrimer. Other elements like Fe, Al, Cr and Na were found as well. Copper lines appeared because of the TEM grid. While there are impurities in the experiment with gold, insufficiently strong signals could be observed in the case of the silver.

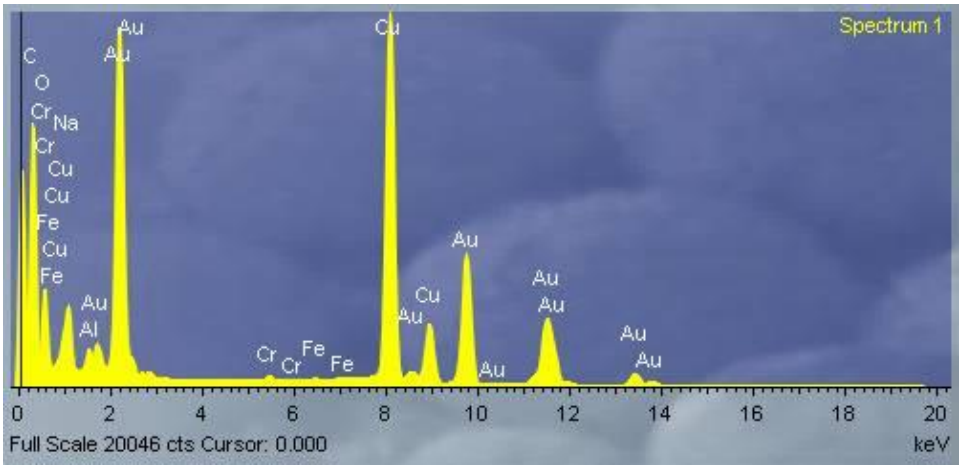

Figure.5.6 EDX of the Au NP's synthesized with PPI-G4 dendrimer.

This basically states that there is certainly something wrong with the conditions or the equipment. Thus the synthesis method requires review. The growth rate of the nanoparticles during the modelling process is very important. In this case there could only be two main ways that the NP's grow Fig.5.7 and Fig.5.9. In Fig.5.7 the silver nitrate molecules could "go" inside the dendrimer and then once the reducing agent is added the NP's grow inside the dendrimer.

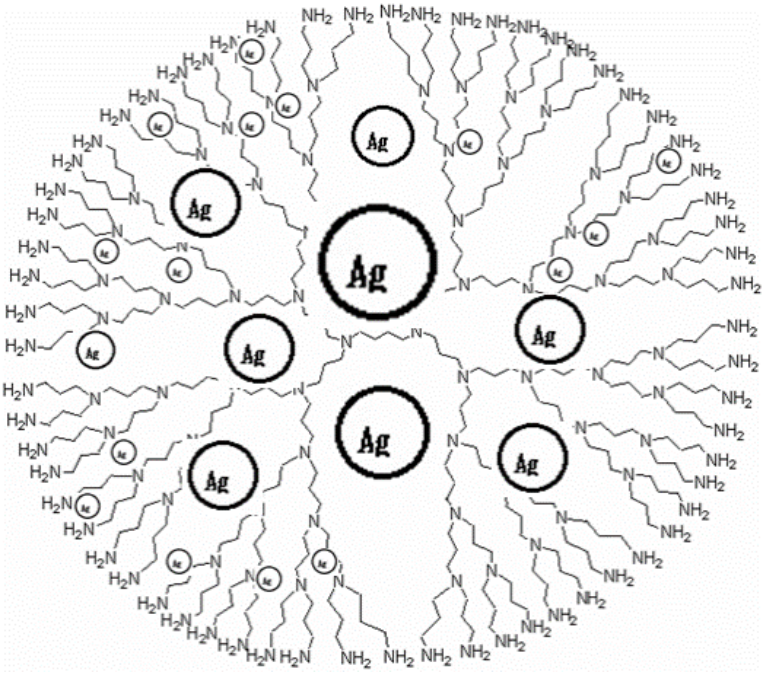

Figure.5.7 The possible formation of the nanoparticles inside the dendrimer system. The nanoparticles could form inside the dendrimer or as it is shown below.

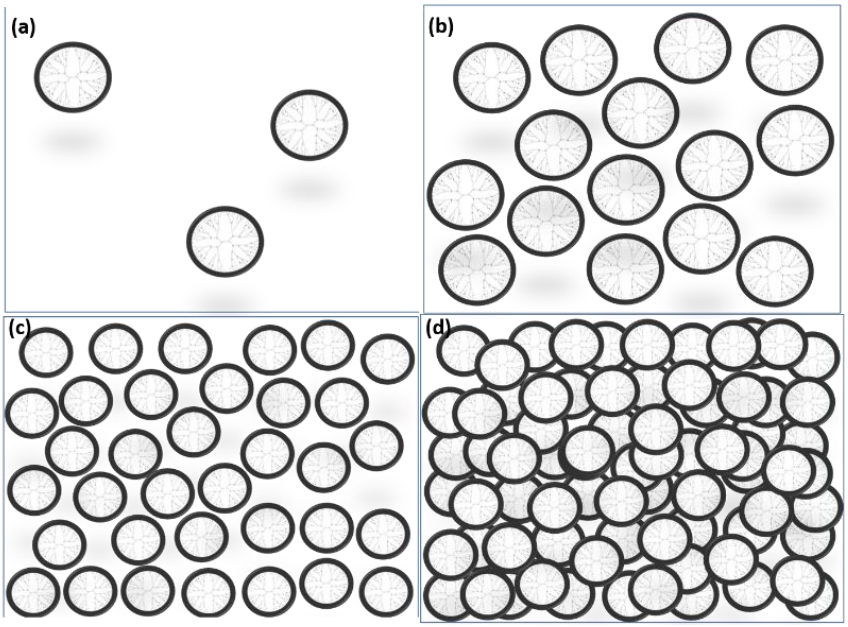

Figure.5.8 dendrimers at different concentrations. (a) diluted, (b) contact, (c) collapse, (d) interpenertrate.

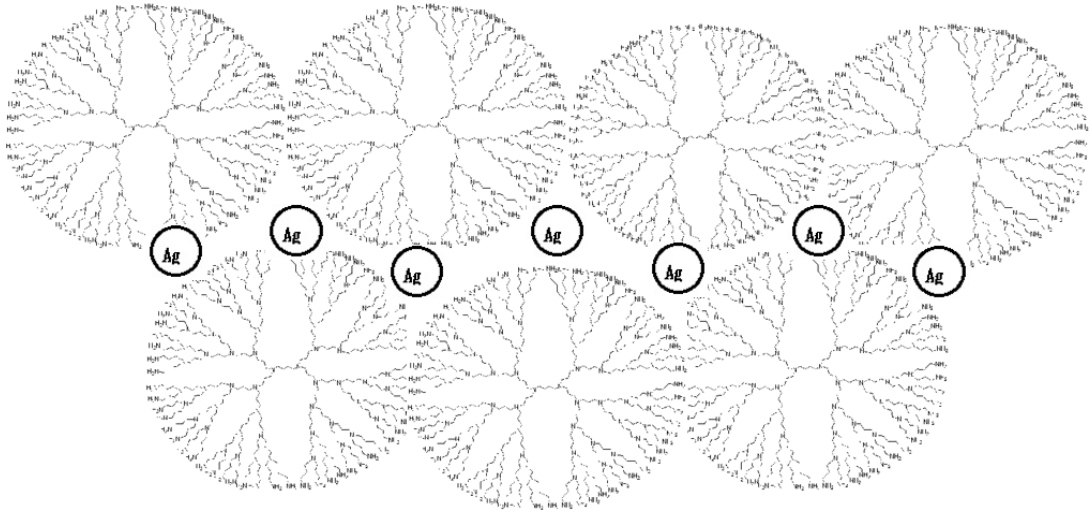

Figure.5.9 The possible formation of the nanoparticles within the dendrimer matrix. In both cases we have the formation of nanoparticles. The function of the PPI-G4 is to be used as a template to prevent growth and agglomeration processes.

Template-assisted synthesis was performed with a PPIG4 dendrimer in synthesis of Au and Ag. The nanoparticles have a narrow size distribution. Also models of nanoparticle formation are suggested. The conditions were the same for both Ag and Au. However, the Au particle average diameter was proven to be higher (Dp=3.9nm).

5.4 Synthesis and Self-Assembly of CdS Quantum Dots

In this subsection the synthesis of CdS nanoparticles or quantum dots will be described and analyzed. Since it was difficult to confirm the self-assembly and positions of the CdS UV-visible spectroscopy (UV-vis), Photoluminescence spectroscopy (PL), High Resolution Transmission Electron Microscopy (HRTEM) and Atomic Force Microscopy (AFM) were used. As has been described in the Literature review the dendrimer size (diameter) grows by increasing the generations, as well as the number of surface groups. The presence of ions in the solution can also have important effects on the properties of the dendrimers. It was demonstrated that presence in aqueous solution of determined ions – i.e., Cd^{2+} and AcO^{-} from dissolved cadmium acetate salt ($Cd(CH_3COO)_2$) – can transform the configuration and the shape assumed by the cationic G4 poly(propylene imine) PPI dendrimers (4th generation with NH_2 functional groups) in the solvent [200]. In turn, this controls the directional self-assembly of the dendrimers into supramolecular fibers [201]. The obtained 1D assembly are of great technological interest. Since CdS fibers are created by ions, they can also be also easily disassembled by the addition of NaCl salt in solution due to

ionic competition [201]. This wet chemistry based method allows the production of nanofibers with tens of micrometres in length and approximately 2 nm of thickness. Fibers PPI[G4] (with NH_2 terminal groups) were first generated in the presence of Cd(CH3COO)$_2$ (1:10 PPI[G4]:Cd($CH_3COO)_2$ ratio). In water, Cd($CH_3COO)_2$ dissociates into Cd^{2+} and acetate (AcO^-) ions. While the metal ions coordinate to the surface amino groups of the dendrimers, the anisotropic AcO^- ions accumulate in proximity of Cd^{2+}, triggering the formation of ionic clusters at the dendrimer's surface. These also generate hydrophobic patches on the dendrimer's surface (due to the methyl tail of AcO^-), which lead, together with ionic bridging, to the directional assembly of dendrimers in the water solution. As a second step, CdS quantum dots were synthesized in situ along the self-assembled fibers following the addition in solution of Na_2S in the experimental Na_2S:Cd($CH_3COO)_2$ ratio of 1:2 under nitrogen atmosphere. Following drop-casting the solution onto solid substrates and spin-coating, the formation of PPI-G4 nanofibers was confirmed by AFM and TEM. As illustrated in Fig.5.10 and Fig.5.11, micrometer-long fibers with a diameter of 2 nm were randomly distributed on the top of the entire silicon wafer.

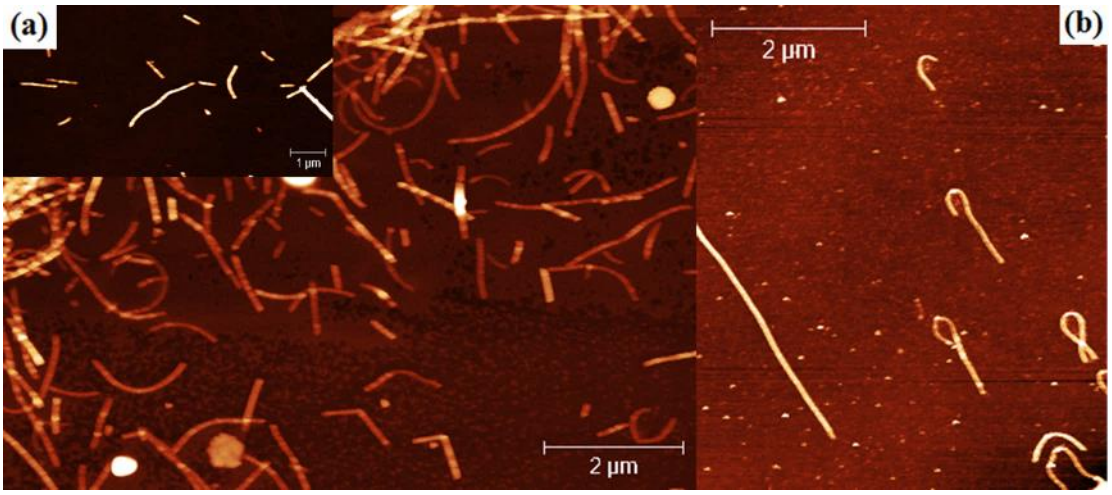

Figure 5.10 The AFM micrographs of nanofibers fabricated using PPI[G4] and cadmium acetate with a molar ratio of 1:10 after 48 hours of stirring (a). Nanofibers functionalized with CdS quantum dots formed in situ through dissolution of Na_2S in a molar ratio of 1:2 with PPI[G4]:Cd($CH_3COO)_2$ (b). The inset in the micrograph (a) shows a different area of the sample proving that nanofiber formation occurs in the entire solution; not accidentally in some spots of the sample.

HRTEM indicate the CdS crystal structure within the nanofiber matrix. CdS nanoparticles grow along (inside) the dendrimer nanofibers. In addition, the micrographs suggest close packing between dendrimer and cadmium sulfide in the nanofiber, confirming that the in situ formed CdS domains act as a "bridge" between the dendrimers along the nanofiber. Consistent with previous evidences on the native PPI[G4]-Cd($CH_3COO)_2$ nanofibers [201] also in this case as soon as sodium chloride (NaCl) is introduced into the hybrid system the nanofibers functionalized with CdS quantum dots start to disassemble rapidly (Figure 5.12). This disassembly is due to ion-competition – i.e., chloride ions replace acetate ions that act as "ionic glue" between the dendrimers in the fibers triggering disassembly [201].

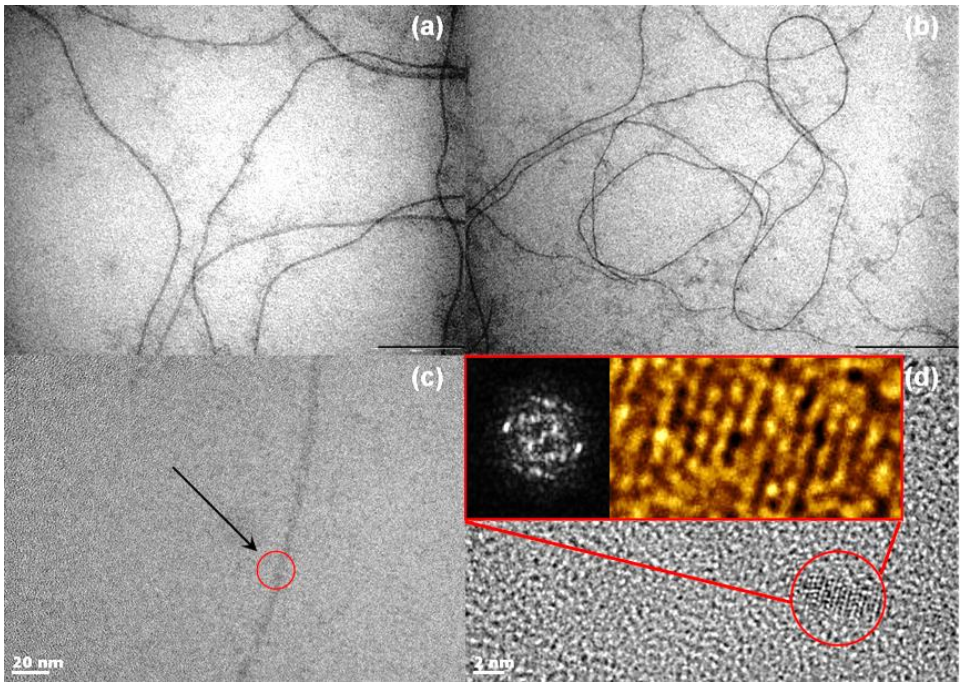

Figure 5.11 TEM (a) and HRTEM (b) and (c) micrographs of the obtained nanofibers functionalized with CdS quantum dots. HRTEM micrographs confirm that nanoparticles formed within the dendrimer nanofibers. Inset in (d): FFT calculation image and zoom of the CdS nanocrystal with diameter of around 2nm.

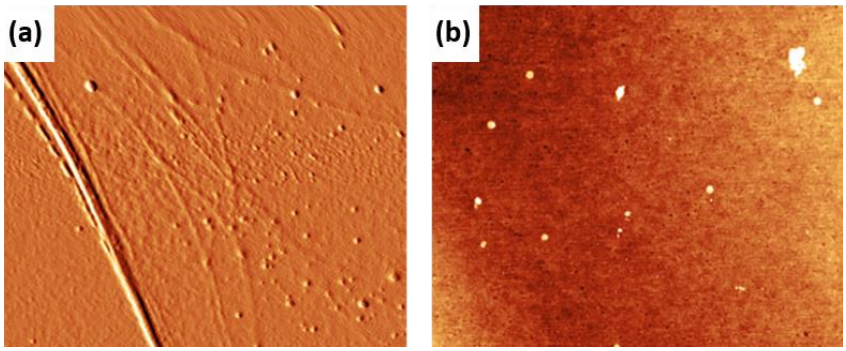

Figure 5.12 Atomic force micrographs of CdS functionalized nanofibers before adding NaCl (a) and after adding 0.1 mmol NaCl (b) into the solution.

CdS quantum dots into the fibers were characterized using both UV-Vis and fluorescence spectroscopy Fig.5.13.

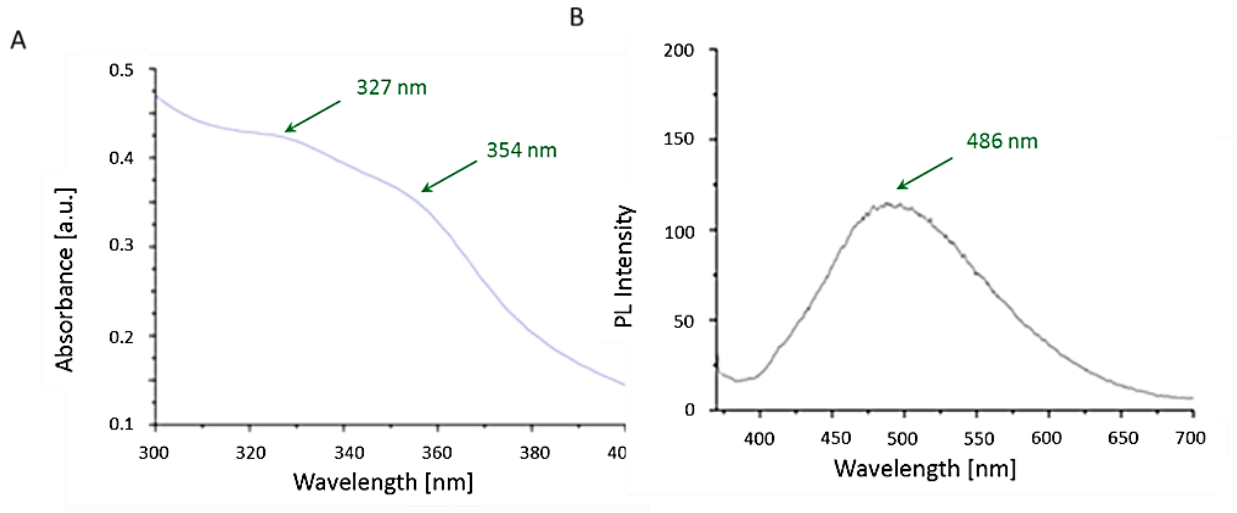

Figure 5.13 the Absorption (a) and photoluminescence (b) spectrum of the CdS QDs in the PPI-G4 solution.

The absorption of the CdS QDs and other optical properties such as photoluminescence mostly depends on the particle size. For example, cadmium phosphide, a material with a band gap of 0.5 eV, can be made in all colours of visible light by decreasing the nanoparticle size in the range of 2-10 nm [202]. In general, particles larger than the size of an exciton in the monocrystalline material start to absorb close to 515 nm (in the case of CdS). With decreasing particle size, the absorption shifts to shorter wavelengths [203]. In comparison with the CdSe NPs, sulfur has a lighter mass and lower electron density, and therefore the CdS absorption peaks are usually blueshifted compared to CdSe. However, the exclusive absorbance peak of the CdS nanoparticles is not completely distinguishable in our studies, due to dendrimers' and the CdS's absorbance peak positions are attributed to the CdS crystals approaching molecular sizes [204]. This demonstrates particular behaviour of the CdS that can be confirmed by photoluminescence spectra [204]. The photoluminescence peak at 486 nm is called green emission band of the CdS [205]. The broad photoluminescence peak can be explained due to the persistence of defects on the surface of the CdS crystals. It was reported that the smaller CdS crystals will increase the intensity of the PL spectra due to the defects related emission [205]. The green emission of the CdS can be explained by recombination of e^- (free e^- or trapped e^-) from the conduction band or different

levels (donor or acceptor) with free holes or holes that are either trapped or captured on different levels of the CdS crystal [206-208].

5.5 The Synthesis of Au Nano and Micro Structures Using Oleci Acid as a Template

In this subsection the synthesis of Au triangles and pyramids is demonstrated and analyzed. The most important synthesis scenarios are described. $HAuCl_4$ was used as a precursor first dissolved in 0.1ml of HNO_3 and then mixed with oleic acid. The mixture was left for 24 hours. As indicated by the SEM Fig.5.14, the resulting product contained mainly three types of structures: uniform microsized triangles of ~55 nm in thickness, pentagonal pyramids and nanopyramids around 500 nm in width.

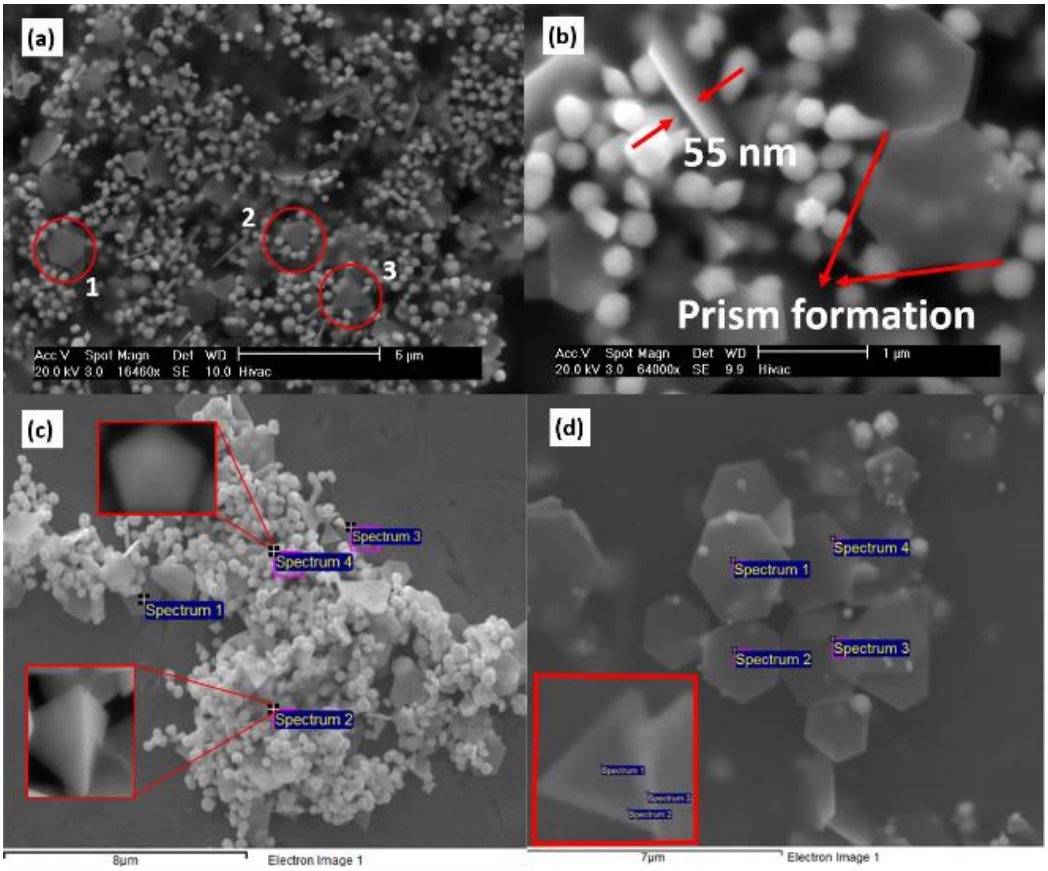

Figure. 5.14 The SEM images depicts Au triangles, hexagons and pyramids. (a) indicates 1- hexagonal, 2- non complete-triangle and 3- completely formed triangle, scale bar 5µm (b) shows the thickness of ~55nm of the structures, scale bar 1µm (c) Scale bar 8µm and (d) Scale bar 7µm show the EDX analysis targeting for all the types of the structures. The EDX results are presented in Tab.5.1 and Tab.5.2 (inset of the triangle in red square).

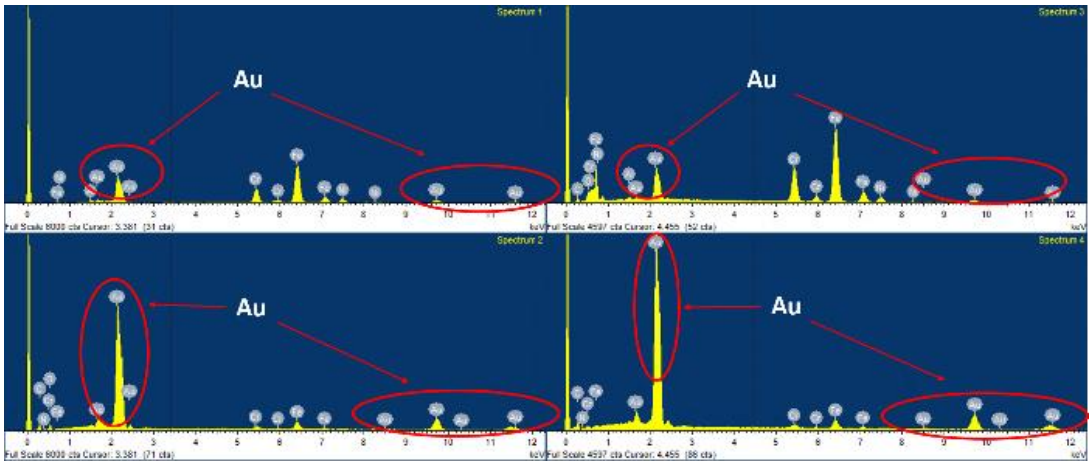

Figure.5.15 The EDX confirming that structures from Fig.5.14 (c) consists of gold. The particles in Fig.5.14 (c) are of around 500nm in length and the intensity of the signal is different for every EDX Spectrum. Other elements like Fe, Cr and Ni coming from the substrate. C, O and N peaks are from the organic chemicals used in the synthesis process.

Table.5.1 The EDX scanning results from Fig.5.14d of the hexagonal shaped structures. The presence of elements other than Au is attributed to the substrate and the chemicals used in synthesis.

No.	C	N	O	Cr	Mn	Fe	Ni	Au
Spectrum1	32.18	3.55	1.63	1.42	-	4.61	0.41	56.19
Spectrum2	45.50	-	2.35	6.52	0.53	22.22	2.68	20.21
Spectrum3	40.19	2.34	2.29	4.28	0.32	14.03	1.67	34.88
Spectrum4	43.79	2.33	3.12	3.36	-	11.12	1.35	34.92

Table.5.2 The EDX scanning results from Fig.5.14d inset of the triangle in red square.

No.	C	O	Cr	Fe	Ni	Au
Spectrum1	44.98	3.38	8.23	28.28	3.05	12.08
Spectrum2	42.12	2.92	7.41	25.25	2.86	19.43
Spectrum3	40.66	2.85	3.42	10.76	1.22	41.09

Energy Dispersive X-ray spectroscopy (EDX) confirmed the presence of gold and carbon Fig.5.15. The presence of other materials like Ni and Fe is attributed to the beam penetrating into the steel substrate and most of the pyramids were transparent even to the electron beam Fig.5.14b and Fig.5.14d. As seen in the EDX spectra in Fig.5.15 the Au peaks are quite intense confirming that all the structures are made of Au. Since micro sized triangles are transparent even for the electron beam, and EDX also detects the substrate as well, the situation with nanostructures is quite different. The intensity of the EDX lines (percentage in Tab.5.1 and Tab.5.2) of the nanoparticles (width 500 nm) are very important since they help to show whether the nanostructure is actually made of Au inside. The samples from Fig.5.14d have lines that are not detected in other scans (like the Mn line). This could be explained by the electrons penetrating through the 50 nm thickness gold particles much more easily and reaching the steel substrate. For the objects of 500 nm, the electron beam cannot penetrate through completely and the Au signal is more intense. The model of the formation of these structures is unclear however the formation will be speculated below and the possible scenarios suggested and explained. The particles have a clear size and shape distribution ranging from micro to nano scales. The smallest are the regular triangular pyramids, which are very uniform and distributed around the microtriangles. The hexagonal structures appear to be pre-formed and form triangles later if the growth continues Fig.5.16. It is hypothesized that the first step for the micro- triangle growth is the formation of the hexagonal structure. SEM scanning shows the presence of such structures Fig.5.15. It is also possible that the first angular structure in the synthesis process was formed due to the combination of the bent oleic acid cis and trans isomers (see Fig.5.19) but the resulting product did not have the same angle as the oleic acid.

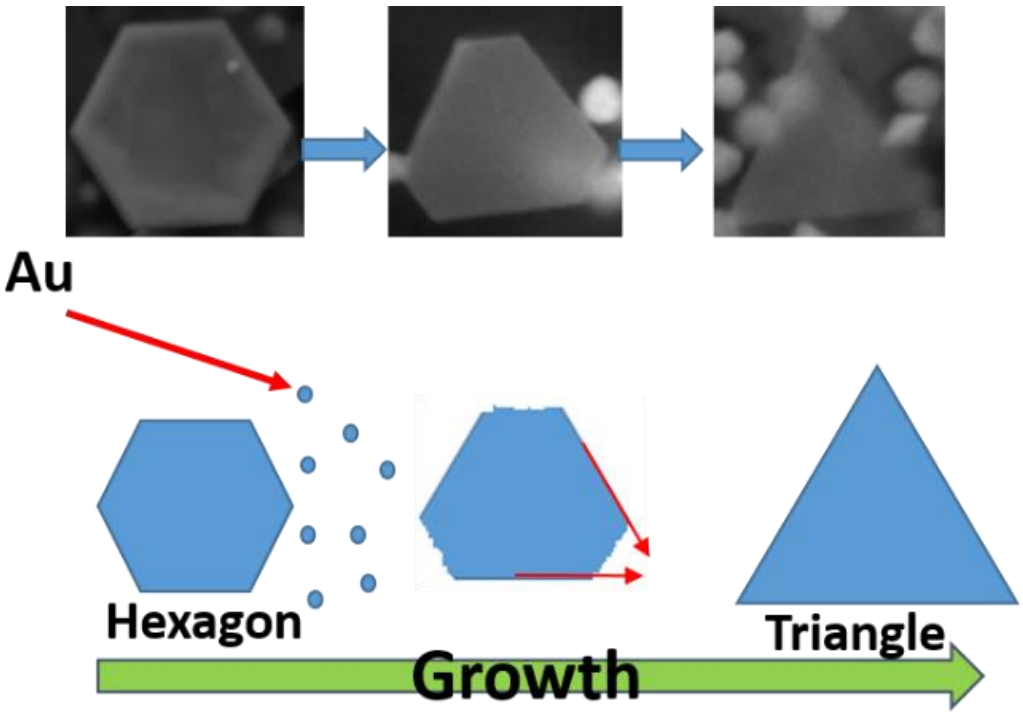

Figure 5.16 a model of the micro sized triangle formation. Hexagonal particles form first then grow until the final triangle is formed.

The first formations were hexagonal and those with smaller aspect ratios remained the same without further growth Fig.5.17. One of the main structures confirming the multi angle formation hypothesis is the pentagonal pyramid. The structure has the angles all over the surface. This type of formation could occur if the template has more than one angle. Let's presume that organic molecules with one angle assemble randomly with other angle molecules and the final formed template allows metal structures to grow forming multi angle structures. Depending on the distribution of the organic molecules, pentagonal, triangular and hexagonal structures were grown. The distribution of the triangle prisms also helped to analyze the growth and the formation process of the angle shapes and it is believed that small structures were created first. Oleic acid has two isomers: cis and trans differing in structure Fig. 5.18. It was reported that HNO_3 causes the isomerization of oleic acid from the cis to the trans state [209, 210]. Oleic acid (OA) in the cis state has an angle at the area of the double bond Fig.5.18. At the initial stages of the synthesis the formation of the nanoparticles believed to be caused by the OA and at the same time OA was shaping the structures not allowing them to form spherical particles.

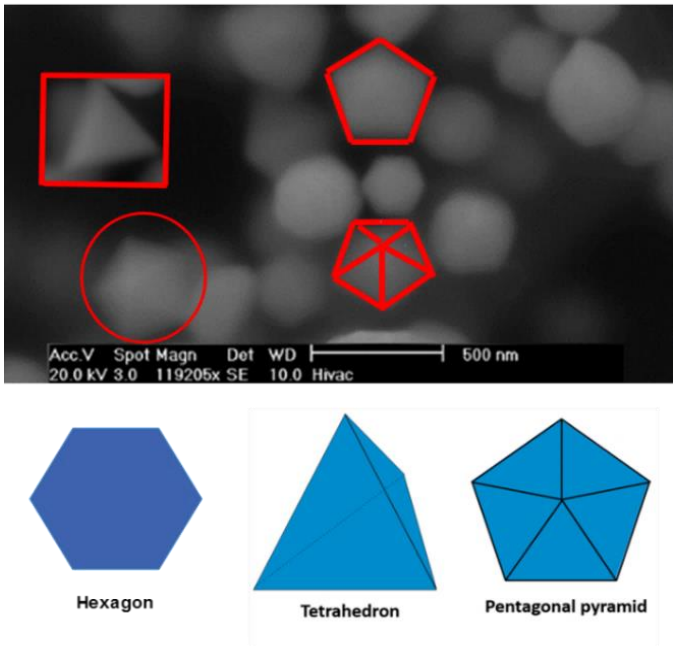

Figure 5.17 depicts the main types of gold nanostructures: hexagonal, tetrahedron and pentagonal pyramids. Hexagons transformed into microtriangles, while tetrahedrons and pentagonal pyramids remained the same.

So at the initial stages Au atoms were driven to form structures with angles because of the cis isomer of the OA. Hence small triangular and pentagonal prisms were formed. Larger, micro-sized triangles were created later in the process - the process of reduction was not rapid and the small amount of HNO_3 did not create trans isomers instantly. While it was cis isomer dominant in the OA matrix, the $HAuCl_4$ was reduced and angles created leading to the growth of 3D pentagonal pyramids. After the HNO_3 converted a proportion of the cis OA to its trans isomer the angles started to evolve into longer Au structures because a 'free' pathway opened. The presence of only the trans isomer (elaidic acid) would be expected to cause the formation of either nanorods or nanoplates but without any driver to create an angular structure because of the linear state of the elaidic acid molecule [210-212]. The distribution of nanopyramids around the prisms suggests that small structures were dominant at the initial stages of the synthesis and after 'opening' the pathway (trans isomer) for the growth their aspect ratio started to increase, thus pushing out the small structures and causing them to cluster around the bigger ones.

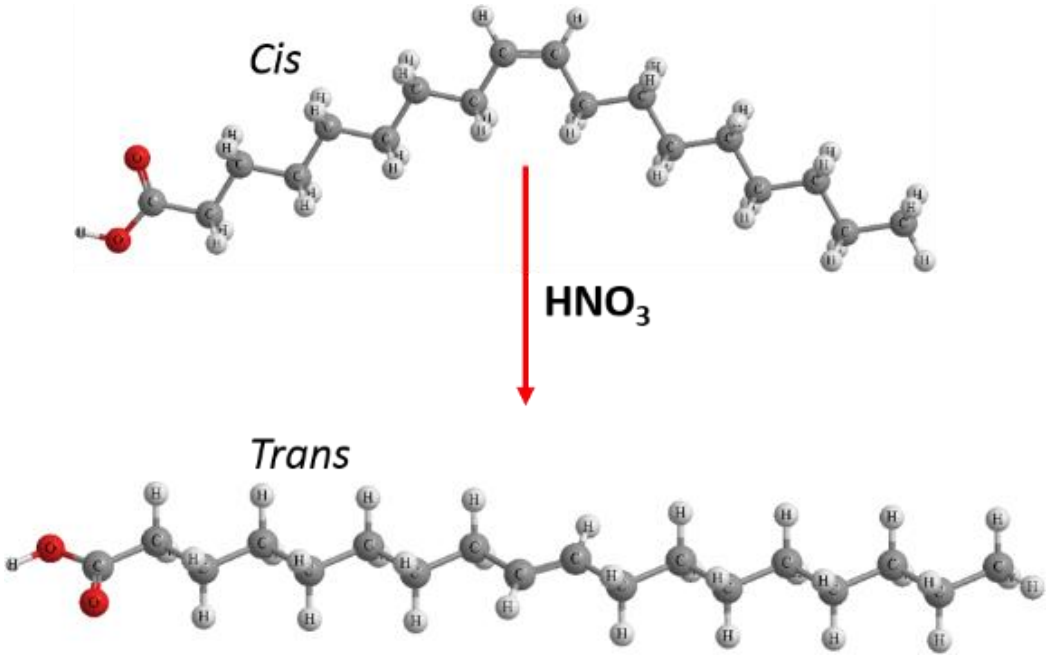

Figure.5.18 cis and trans isomers of oleic acid.

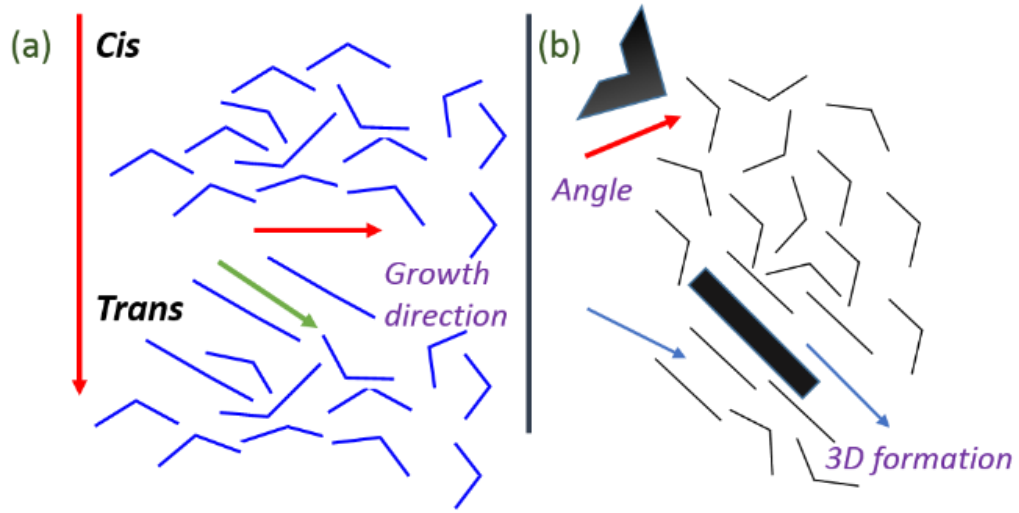

Figure.5.19 The proposed growth mechanism: (a) the matrix of molecules in state cis and trans allows formation of triangles with high aspect ratios (b) explains the formation of angles (red arrow) and 3D growth pathway (blue arrows) formed by trans isomers.

Also it is hypothesized that after the isomerization process molecules could 'stick' together again but in a different way, forming new templates for the hexagonal particles (2D growth) and straight edges for the microstructures. When the mixture of cis and trans isomers varies more complex 3D structures could have a 'chance' to appear. The investigation of isomerization speed could be a key factor for the precise growth control of gold nanomaterials in the future.

5.6 Summary

Template-assisted synthesis demonstrated Ag and Au nanoparticle spherical shapes. Au and Ag ion are charged positively and it is logical to assume that they would make a bond with NH negative group. A small cluster can be surrounded by dendrimer molecules and stop growing when a critical space is filled (crystal is start "touching" dendrimer molecules). Although it is speculated that the main reason for the gold pyramids and triangle nanoparticles was the isomerization of oleic acid it is not the fact that we have 100% of isomers within the solution. The most likely scenario that it was a combination of cis and trans isomers 50/50 which led to the formation of the angular nanostructures. But also the whole process can be attributed to the growth habits of Au. In the case of the CdS it was demonstrated that the synthesis method of the CdS quantum dots arranged in a nanofiber is possible at room temperature. This experiment also showed one step self-assembly on the nanoscale which is usually difficult to achieve. The experiment demonstrated the great importance and role of dendrimers. They not only assemble but also work as a templating agent which expands the borders of the PPI type dendrimer use in the synthesis of quantum dots.

Chapter 6 Light-Induced Synthesis of Ag, Ag-Au and ZnO structures

In this chapter light induced synthesis and the results of ZnO will be described and analyzed. The photochemical synthesis of Ag and Ag-Au was performed using light-responsive chemicals (sodium tricitrate).

6.1 Synthesis of Ag and Au-Ag Nanostructures

As mentioned in the literature review of this work silver nanostructures can be synthesized using organic molecules and the photochemical or light-induced method. The challenge in the synthesis of the Ag is to change the synthesis direction in real time. Light-induced synthesis allows real-time morphology change of Ag structures during the synthesis. This part describes the light induced experiments with Ag and Ag-Au alloys. In the different light sequence, the same materials acted differently and formed different structures Fig.6.1.

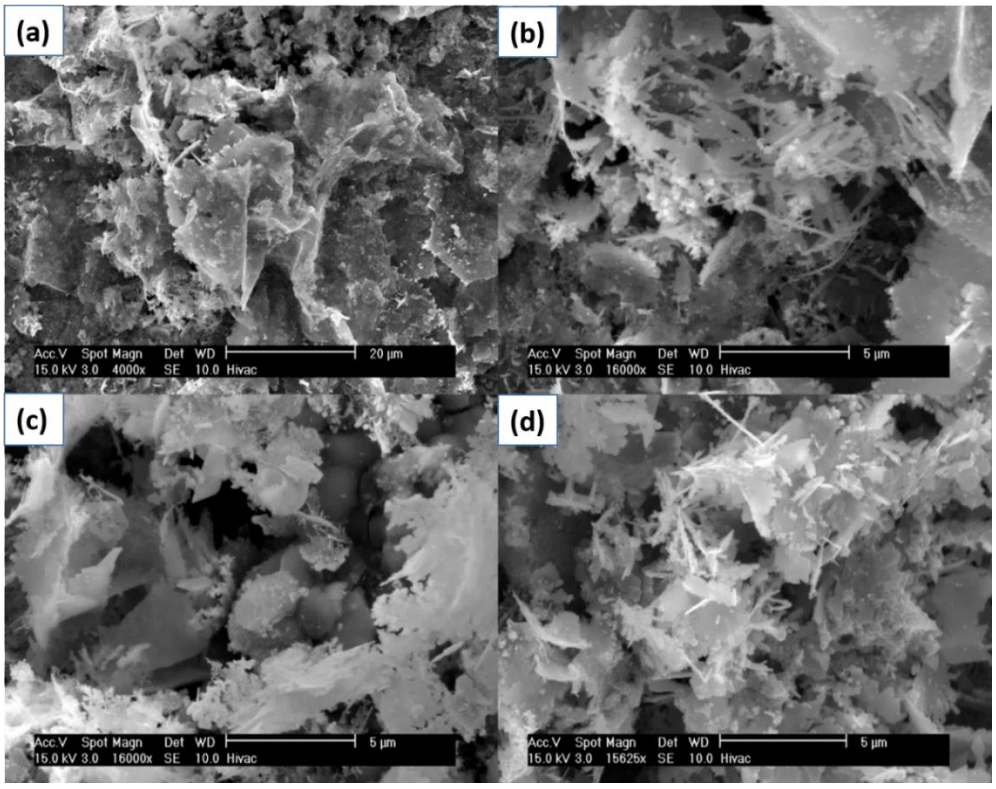

Figure.6.1 the ESEM images of Ag structures grew at RGB LED light for 12h. (a) view of Ag structures with 4000X magnification. (b) and (c) zoomed areas that highlights some "dendritic" structures which also looks like film. (d) dendrite-like structures that are deposited under various angles.

Fig.6.1 shows ESEM images of the Ag structures synthesized under an RGB light sequence. The structures look similar to the dendritic formations. However, it is difficult to precisely define these structures since they have distorted shapes and orientations. Fig.6.1 suggests that every light wave has a different "formation force". Every light wave has a different portion of energy which can influence the growth of the nanoparticles in a particular way. Various growth methods of the silver nanoparticles have been studied in a variety of works [213]. However, regarding photochemical or light-induced synthesis the precise model or the explanations were not proposed. Fig.6.1 shows "wrecked" Ag formations it seems that Ag "wanted" to form a one type of structure for example a structure with an angle. However, another portion of energy interrupted the formation and started another formation already attached to the existing one and then a third portion of energy interrupted the process which led to the distortion of the formations. Fig.6.2 shows ESEM of the Ag structures grown using the RGB code from another area of the sample. These images show us other shapes of Ag structures. Image in Fig.6.2 (a) shows tree-like structures. Red circled is the saw-like structure resembling "triangle with teeth".

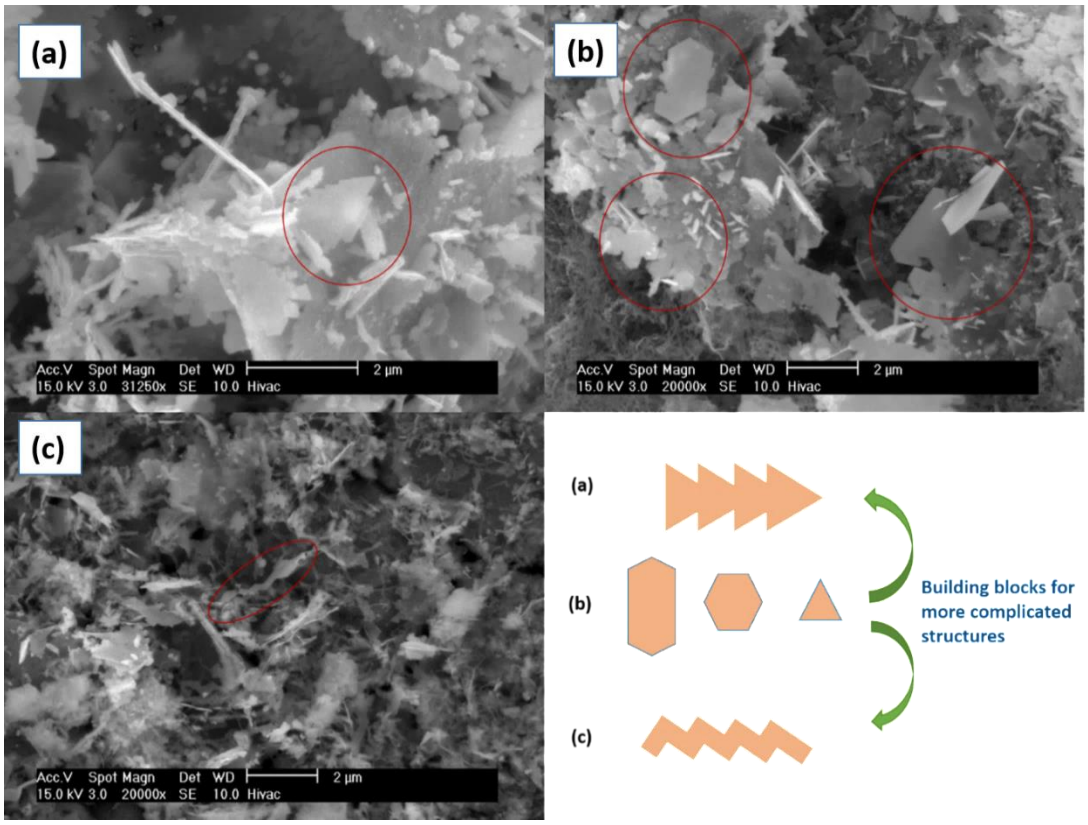

Figure.6.2 the ESEM images of Ag grown using an RGB light sequence for 12h. (a) red circled dendritic structure on the sample. (b) shows variety of angle-containing structures: hexagons, triangles and other elongated squares. (c) red squared area of "nanosaw". Zig-zag structure. And proposed growth mechanism for every structure.

Fig.6.2 (b) shows other types of structures like triangles and polygons that did not evolve into the formation of more complicated structures. Fig.6.2 (c) red circled "nanosaw" formed probably out of triangles which look like a "zig-zag". And the last image is proposing the formation models for the structures. These structures were formed photochemically changing the energy in time (1second period) and strictly depended on the light frequency. If the last statement is true, then with the same concentration and a different wavelength the results will not be repeatable. This was confirmed by Fig.6.3 when UV light (365nm) was used for the synthesis for 12h. Fig.6.3 shows spherical particles

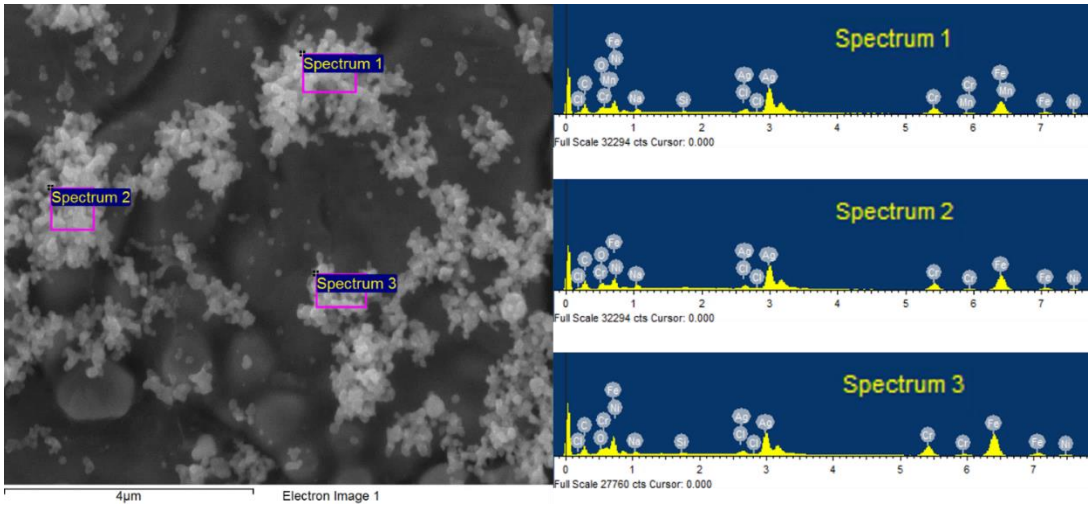

Figure.6.3 the ESEM image and EDX of Ag grown under weak UV light for 12h. EDX confirms the Ag persistence. The background lines such as Ni, Cr and Fe are due to the used steel substrate. Cl line is very close energetically to Ag. These lines could be attributed to the software error. Na is a residue of the sodium tricitrate which was used as slow reducing agent.

Notice the formation of the nanoparticles without any template or the addition of the polymer. This result suggests the great role of the light in the formation of the silver nano and micro structures. EDX also confirmed the Ag in different areas of the sample. In order to get more information about the method and the growth behavior it is reasonable to synthesize alloy nanoparticles such as Ag-Au. Adding to the same solutions small amounts of Au containing chemical (4% of chloroauric acid). Photochemical synthesis of Ag-Au using the RGB light code could reveal if the photochemical method is universal for the synthesis of Au containing alloys. Fig.6.4 depicts the ESEM images of Ag-Au alloy nanostructures with EDX (d) spectrum of the wire. Fig.6.4 shows a variety of different structures including wires and cubes with different sizes. The synthesis code in Fig.6.4 was RGB as in Fig.6.1 experiment.

However, the shapes of the structures in Fig.6.1 and Fig.6.4 greatly differ which leads to the conclusion that the Au ions tend to lead the formation of wires and cubes. However, no “saws” were observed in the sample with the RGB code for the Ag-Au synthesis. Another photochemical combination of Red, Green and Blue wavelengths led to the formation of microsized “saws” with a thickness of around 40 nm Fig.6.5.

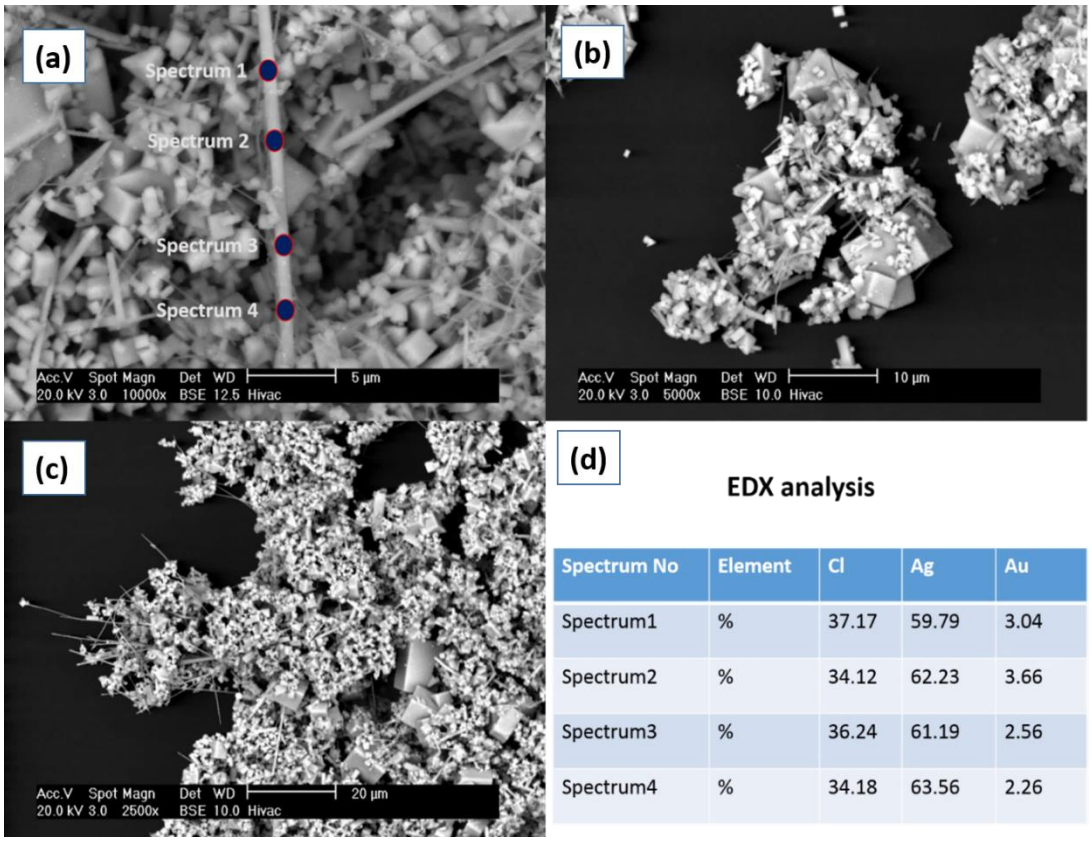

Spectrum No	Element	Cl	Ag	Au
Spectrum1	%	37.17	59.79	3.04
Spectrum2	%	34.12	62.23	3.66
Spectrum3	%	36.24	61.19	2.56
Spectrum4	%	34.18	63.56	2.26

Figure 6.4 the ESEM images of the Ag-Au alloy grown photochemically under the RGB code for 12h. (a) wires and cubes. The EDX spectrum (d) is taken on the wire to confirm the presence of the Au. (b) and (c) shows different areas of the sample. The structures are mostly cubes and wires.

In Fig.6.5 the red circled area show the most vivid “saws” with sizes of up to 100 of micrometers. The interesting feature is that the structures do not grow larger “teeth” and only are increase in length. It seems that the structures are terminated for some reason. The reasons are the energy portions i.e. the light wavelengths. The green light forms triangles and the red light increases the aspect ratio since the red light is responsible for the elongation of the structures as was described in the literature review.The blue light probably serves as a disturbing wavelength in this case. The formation process in this synthesis could start from the wires and then form the

triangles on the surface of the wire. They could also form separately but to presume latter agglomeration and growth would not be a reliable conclusion. Another reasonable experiment would be the synthesis of the Ag in the persistence of the template. This could highlight the role of the template and might suggest some formation pathways in order to explain the whole process regardless of the material. A reducing agent was not used in this experiment since the diethyleneglycol (DEG) was chosen as a template which also serves as a reducing agent. Fig.6.6 shows the ESEM images of the Ag formed in the DEG under the RGB light code for 12h.

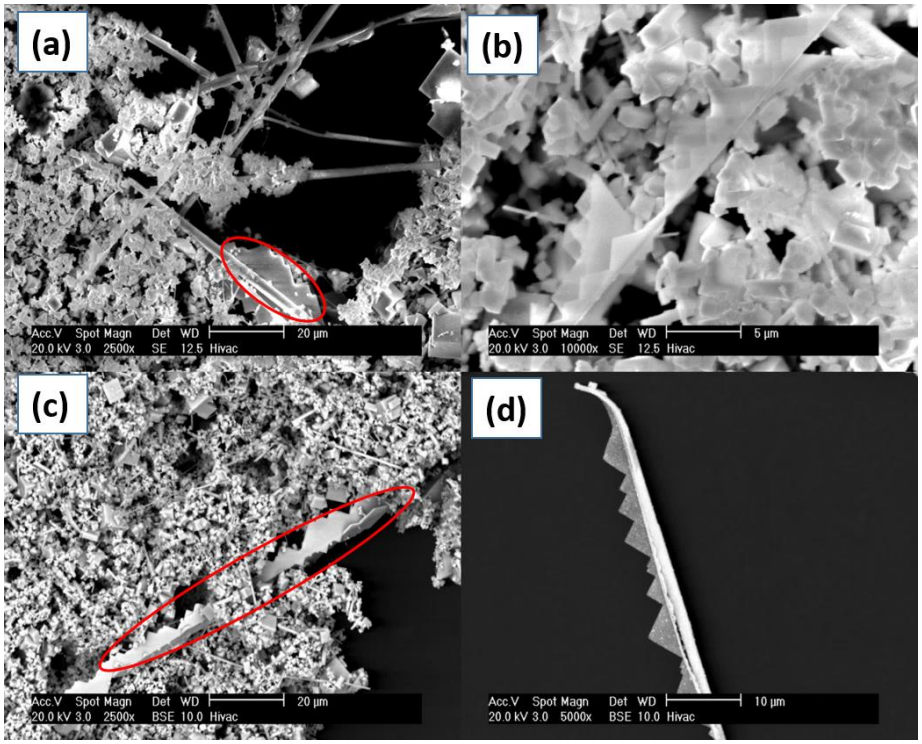

Figure.6.5 The ESEM images of the Ag-Au grown under the Green(10s)-Red(15s) blue(5s) light code for 12h. (a) panoramic view of the structures showing wires, cubes and saws together. (b) zoomed more than 5micrometers "nanosaw". (c) huge "saw" among other types of nanostructures. (d) separately formed "nanosaw" (one sided).

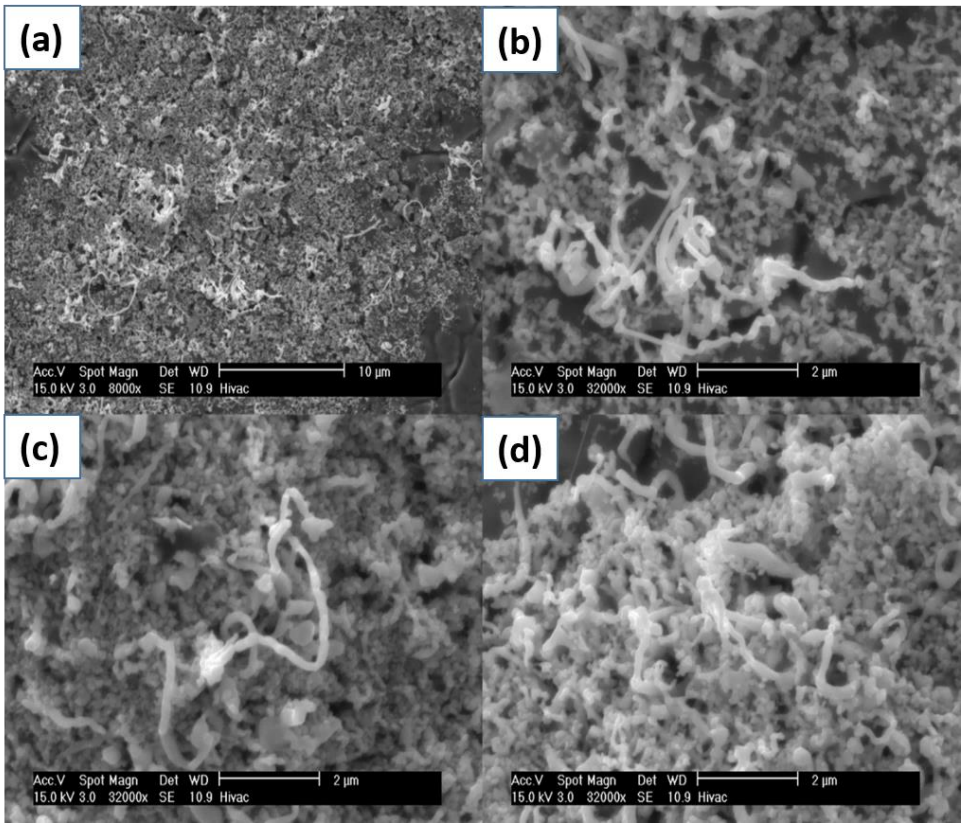

Figure 6.6 the ESEM image of the Ag + DEG used as a template under the RGB for 12h. (a) panoramic view of the Ag "snakes". (b), (c) and (d) zoomed various parts of the sample showing the structures in more detail.

The structures in Fig.6.6 look like “worms” which gives reasonable doubts about the persistence of the Ag inside. These structures could only be formed with the DEG and without the influence of the light. However, Fig.6.7 confirms with EDX the persistence (intensive signal) of the Ag. Other lines are from the background of the sample which was used to deposit the material. The structures are 1D and seem to be flexible (curved) which suggests that the fibers are formed of both the DEG and Ag. If the fibers do not contain the DEG then we can presume that the fibrilar structure was achieved due to the DEG since glycols have been proven to synthesize the Ag fibers. And the distorted orientation was achieved due to the RGB light code.

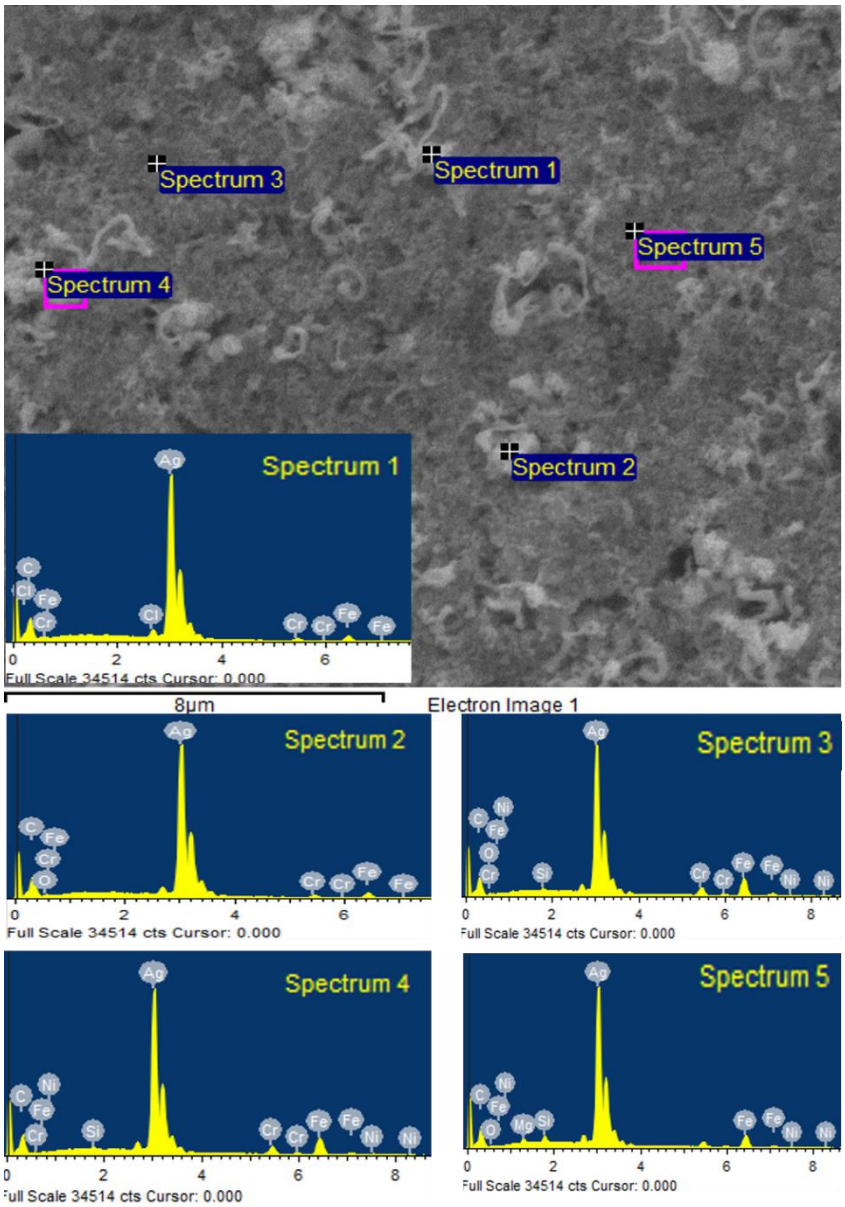

Figure 6.7 the ESEM image of Ag + DEG under the RBG for 12h and EDX spectras. 5 different areas of the sample including the background of the sample.

However, beyond this result we must look at the broader concepts of the effect of light on these structures. The role of the blue light must be investigated alone. Since the blue light contains the highest energy and the UV light was already investigated it is crucial to check the role of the blue light. If the concept is right and every wavelength corresponds to the different growth of the structures, then the influence of the concentration can be neglected or becomes a minor. The concentration was increased twice for the Ag-blue light experiment. And as was predicted before the formations were spherical with some morphology on the surface Fig.6.8. This result fits very nicely into the model puzzle.

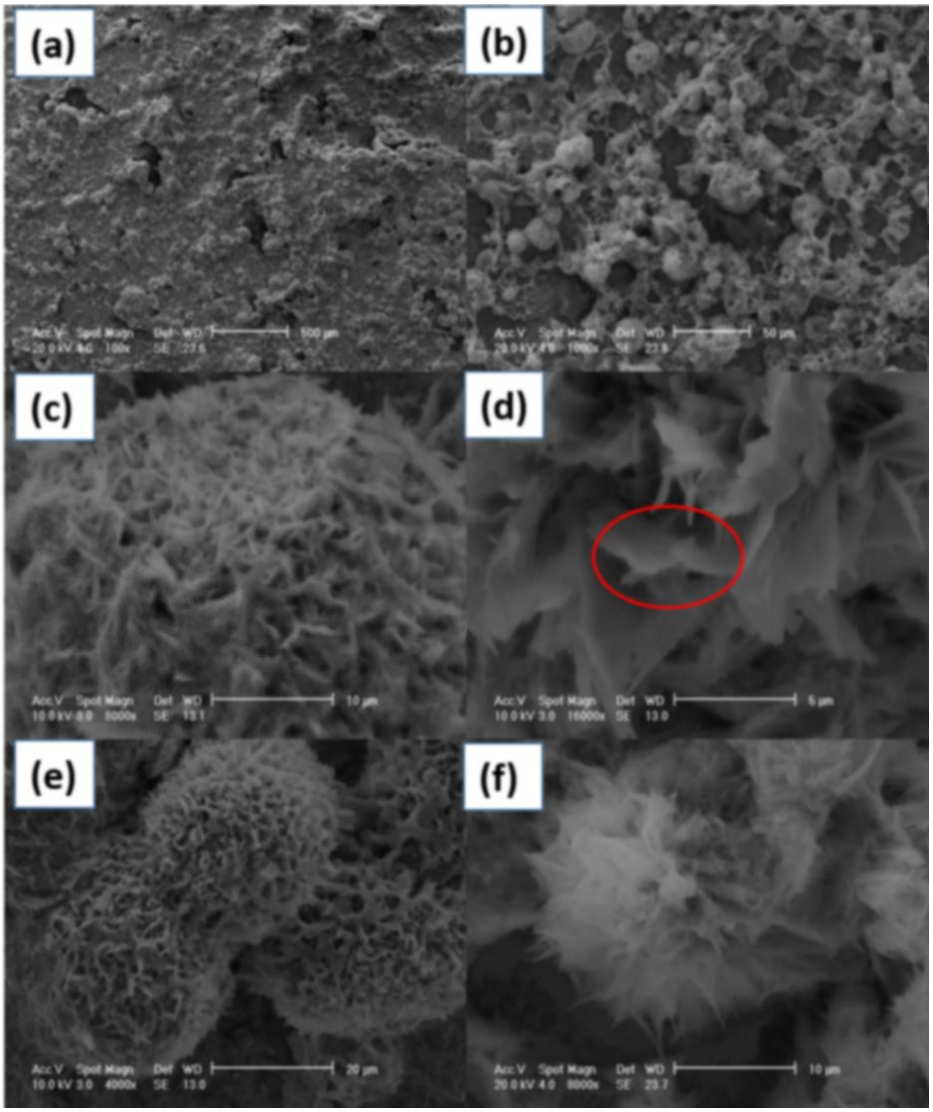

Figure 6.8 the ESEM images of the Ag grown in blue light for 12h. (a) and (b) panoramic views of the sample. (c) zoomed "rafaello" indicates various deposition of the leave-like structures. (d) 1600x magnification of the elements on the Ag structure surface. (e) and (f) other ESEM images of the objects from different areas of the sample.

The shape of the structure clearly depends on the wavelength. Chapter 7 discusses the growth control of the nanostructures via light. Fig.6.9 shows the ESEM elemental mapping analysis image of the Ag sample grown under blue light.

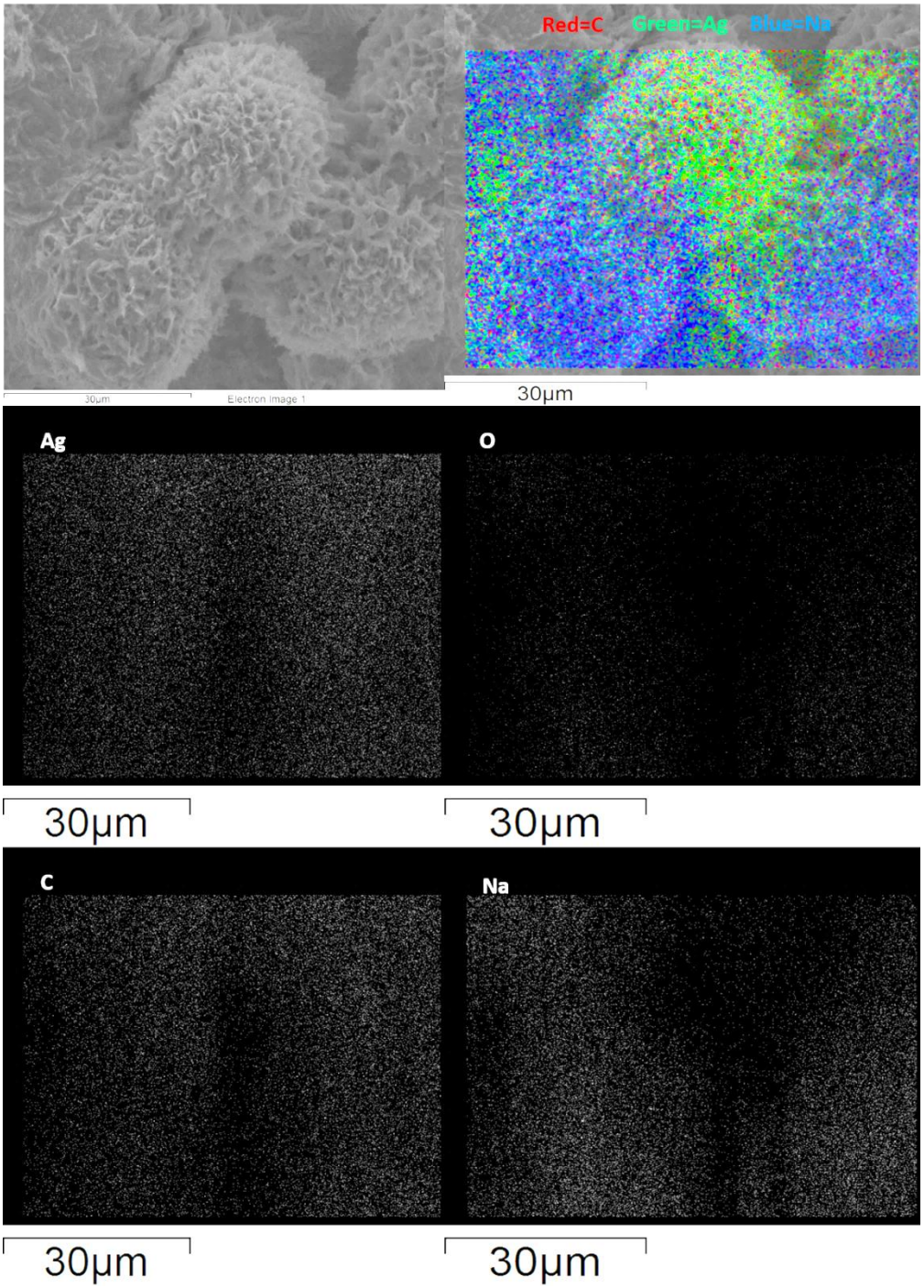

Figure 6.9 the ESEM image of the Ag grown microstructures and the elemental mapping analysis. Silver, Oxygen, Carbon and Sodium.

While Elemental mapping in Fig.6.9 did not show high oxygen content quantitative EDX confirmed oxygen to be nearly 60% Fig.6.10. Regardless of the concentration these systems were shown to form spherical particles with blue light but these were larger than the UV and not like the red light. Other wavelengths that stand between the blue and red are responsible for the shape features. Such wavelengths are the green light (545 nm for instance) which is responsible for the formation of the triangular particles [131]. The combination of the different wavelengths gives different morphologies and this also explains the distorted formation of the dendrite-like Ag structures in Fig.6.1. The elemental mapping was performed for the sample in Fig.6.8 and is depicted in Fig.6.9. Fig.6.9 shows the elements that are persistent in the "rafaello" or micro-sphere. The term "rafaello" describes the structure better since it also has a specific morphology on the surface Fig.6.8 (d). In Fig.6.9 the large amount of oxygen is persistent. This might give new insight into the idea of the formation of the structures. Other samples either contain no oxygen or the signal is very low. Fig.6.10 shows quantitative EDX results of the sample from Fig.6.9. As we can see the amount of oxygen is greatest among all the elements. Other elements are due to the substrate that was used. To make the investigation more precise and profound another experiment the same as that in Fig.6.8 was conducted again but with a small addition of $HAuCl_3$ and also exposed to the blue light for 12h. The ESEM results are depicted in Fig.6.11. The formations were rose-like and were all over the sample in tens of micron sizes Fig.6.11 (a). Fig.6.11 (b) shows the "rose" consisting of cubes and various plates with similar sizes and shapes arranged in a rose-like manner.

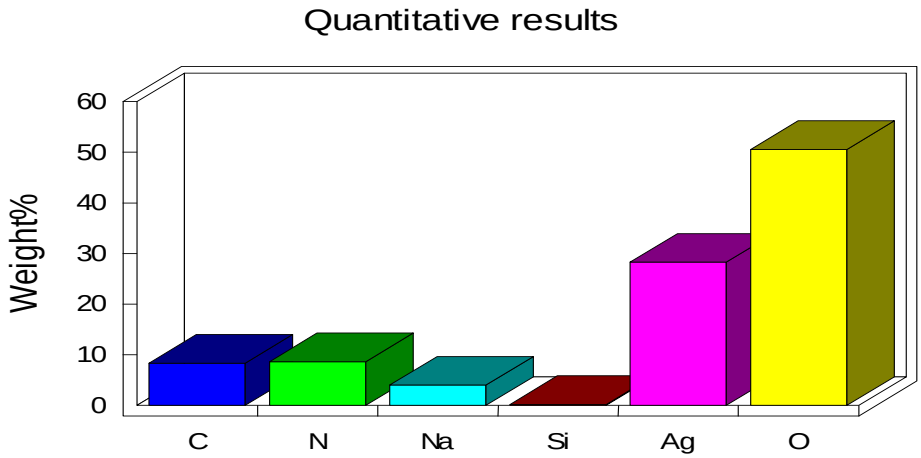

Figure.6.10 quantitative EDX results of the Ag sample from Fig.6.1.9. The result indicates elements in percentage. Oxygen content is highest.

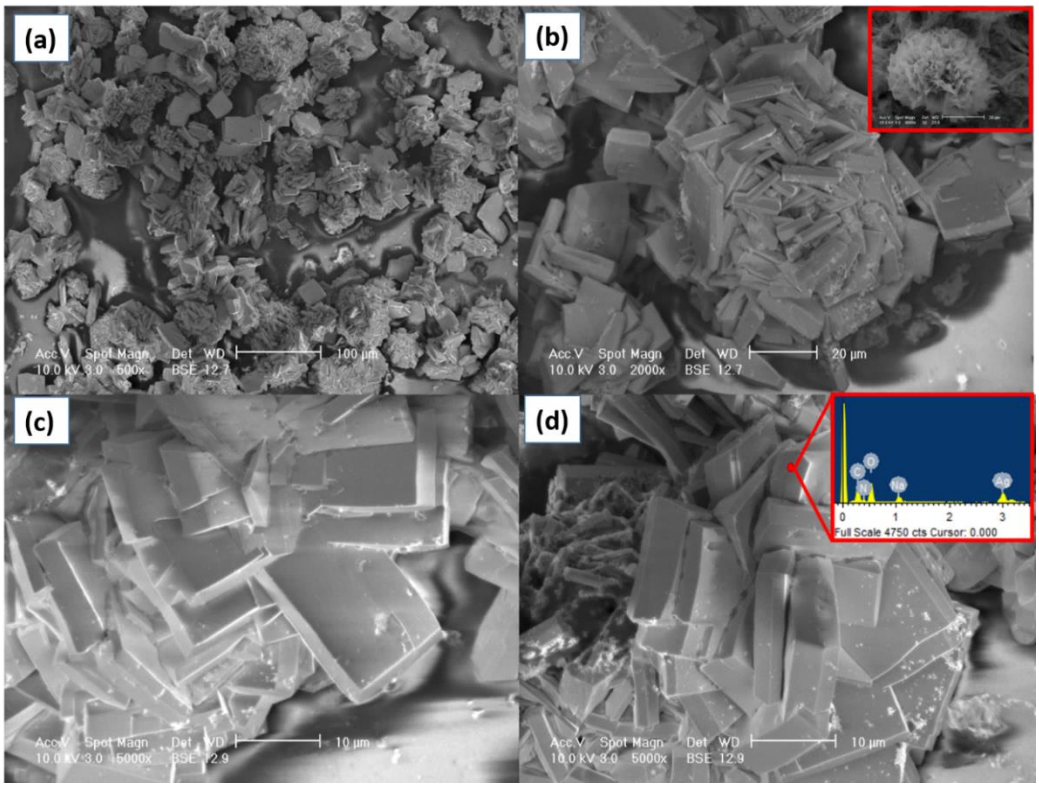

Figure 6.11 the ESEM images of the Ag-Au sample exposed to the blue light for 12h. (a) Panoramic view of the material on the sample. (b) closer zoom of the "rose". (c) and (d) shows squares and microstructures the "rose" made of. EDX in (d) confirms the persistence of oxygen and does not detect Au.

The inset in Fig.6.11(b) is the "rafaello" structure used in the comparison. The result suggests that even a small amount of Au ions leads to the formation of cubes and angle-containing structures while the blue light is responsible for the overall shape of the microstructure. Fig.6.11(c) and (d) shows the zoomed surface of the "rose" which shows cubes and rectangles. Fig.6.12 shows more detailed EDX spectra from the same sample. Three different areas were scanned in order to make a more precise analysis of the sample. As indicated by the EDX in Fig.6.12 the silver contains oxygen which is likely came from the water creating Ag_2O instead of Ag. Surprisingly the EDX did not detect the Au signal at all. This could be due to the small amount of gold added. Also it could be that the Au and Ag form cores at the initial stages of the growth. And later stages would only lead to the attachment of Au atoms on the surface of the Au-Ag crystals. So we would have thick Ag shell. This also explains why we cannot see the Au signal because the EDX beam cannot penetrate deep enough into the structure. Na lines are due to the sodium tricitrate that was used for the slow reduction and the rest of the lines like Cl are coming from the $HAuCl_3$.

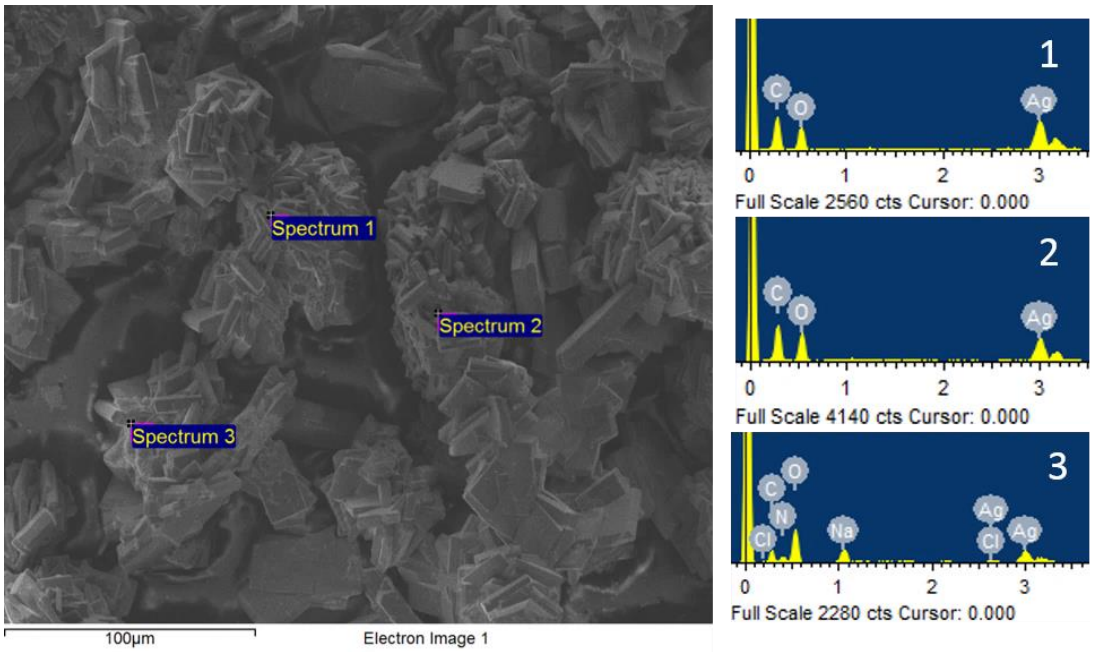

Figure 6.12 the ESEM image of structures on the Au-Ag sample with EDX accordingly. The EDX spectrum 3 detects Cl that is in the Au precursor ($HAuCl_3$) however no detection of Au. The numbers in the EDX spectra correspond to the number of the spectra in the ESEM image accordingly.

As has been demonstrated the Ag nano and micro structures can be grown via light assisted synthesis. The Ag nanostructures were synthesized using a combination of wavelengths. Every wavelength of light gives a different influence on the formation of the structures. The addition and amount of chemicals and polymers is also significant. The experimental results showed silver structures with angles which means that the structure is twinned. The twinning effect cannot be explained by only assuming the concentration factor. All the structures synthesized using light contained angles (except when the polymers were used). Another important factor is oxygen. It is known that oxygen can oxidize Ag and cause specific growth directions. Oxygen could be provided from water or from the citrate molecules. The light was not always at the same wavelength (experiment with nanosaws). When oxygen anchored to the silver the growth direction would change but when the blue light was switched on the direction changed again. As a consequence of this process the structures became "zig-zag" or saw-like. Other structures formed because of the difference in concentration inside the vial.

6.2 Synthesis of the ZnO via Light-Induced and Hydrothermal Methods

In this subchapter experimental results of light-induced synthesis and hydrothermal synthesis of ZnO reviewed. To achieve better conclusions and conduct more precise experiment the concentrations are varied during the experiment. In order to create a model, it is important to find out which factor is actually dominant during the synthesis process: the irradiating wavelength or the concentration of the chemicals. Other factors like entropy or thermodynamics will not be considered since it is beyond the scope of this work.

6.2.1 Specifics of the Methods

In order to make a comparison ZnO was synthesized in the most popular way for this material i.e. hydrothermal. The comparison between the hydrothermal method and light-induced is crucial. The light is an energy portion but the heat is also an energy. For the comparison of "what's going on?" and following the logic of the experiments with silver (section 6.1) we must find out what can distort the ZnO structures. It might be that the answer and model of both the ZnO and the Ag have the same source. To achieve the distorted structures of the ZnO the dendrimer PPI-G4 with amino groups was used. The ZnO hydrothermal synthesis includes the PPI polymer which makes this synthesis both template-assisted and hydrothermal. This is the reason why this synthesis was not included in the template-assisted synthesis part (Chapter 5.0) of the present work. Using dendrimers which have a negative charge NH_2^- but the Zn^+ ion is positive. So here we can expect that the dendrimer will influence the growth of the ZnO structures. Also it is possible that the NH groups will block one or another facet (growth direction). If there is no change and we get the same structures as in the previous experiments then the influence cannot be made by a synthesis method and the molecules. But this is unlikely since by adding other molecules we are actually changing the electrostatic interaction [214].

6.2.2 Hydrothermal Synthesis of the ZnO Nanostructures

Fig.6.13 below depicts the high resolution transmission electron microscope (HRTEM) micrograph of the ZnO nanostructures. It reveals nice and uniformly synthesized nanorods over the sample.

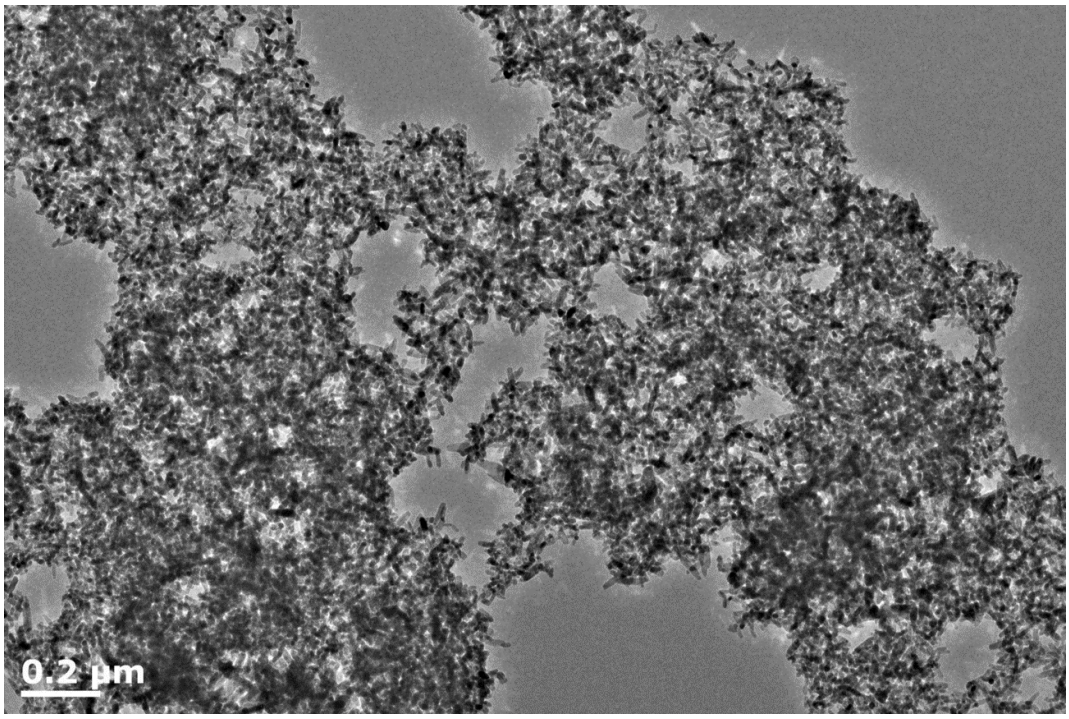

Figure 6.13 the High resolution transmission electron microscope (HRTEM) image Zinc oxide nanostructures. We can see that all the synthesized material creates bush-like agglomerate, however we can perfectly see some single structures.

Since the ZnO structures were synthesized following the traditional hydrothermal procedure the obtained nanorods were transparent for the HRTEM beam and could be characterized very well. The HRTEM micrographs Fig.6.14 reveals that the ZnO nanorods are on top of each other but do not stick together and have widths ranging from around 7 to 15 nanometers while the lengths are ranging from 20-60 nm. Fig.6.15 depicts the atomic force micrograph with the ZnO nanorods. It shows that no other organic or inorganic material is in the sample after centrifuging the solution. Later for the characterization of the ZnO the material was not centrifuged because the characterization was mainly carried out using the ESEM. As indicated by the AFM in Fig.6.15 the centrifuging is crucial for the samples for AFM and might influence the results for TEM. However, this is correct if the experiment is using organic materials such as dendrimers but in the case of ESEM it becomes less important. The hydrothermal method creates rice-like structures under 80^0 C for 30 mins. It is

important to mention that the chemical glassware which was used for the synthesis was not in total darkness as this was impractical to achieve.

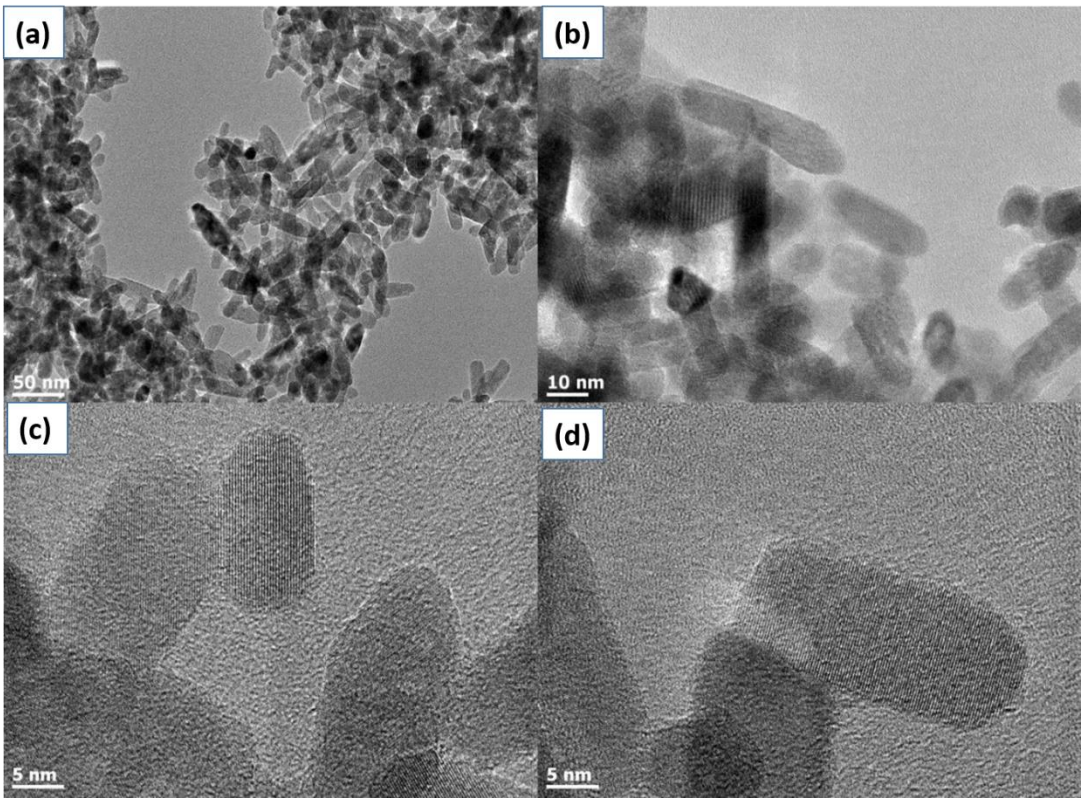

Figure 6.14 the HRTEM images of the ZnO nanostructures synthesized without dendrimer. (a) rice-looking nanostructures scale 50nm, (b), (c) and (d) confirms that structures contain the crystal structure.

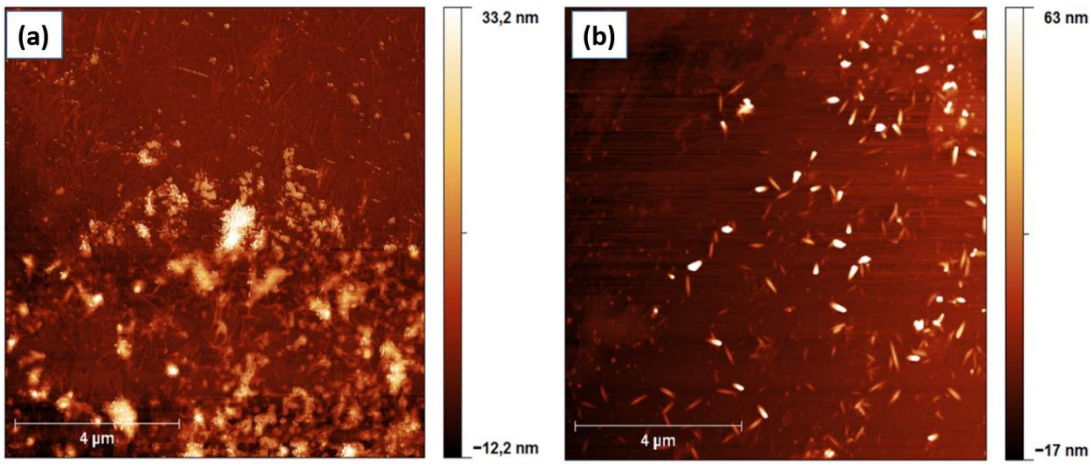

Figure 6.15 the AFM images of the zinc oxide nanostructures. (a) the ZnO before the centrifuging and (b) after the centrifuging.

6.2.3 PPIG4 Dendrimer use in Hydrothermal ZnO Synthesis

The Scanning Transmission Electron Microscopy HAADF Tomography revealed metal structures in the sample and confirmed the formation of zinc oxide by the EDX Fig.6.16. The EDX in Fig.6.16 confirms the purity of the material and the copper energy lines shows the background of the TEM grid. But the most unexpected result was from the experiment with the use of the dendrimer. Fig.6.17 represents "strange" formations which have web-like structure and are made of ZnO. However crystal structures cannot be clearly seen or are not there at all. It seems that atoms have a random configuration within this "web". So far it remains a challenge to understand the formation process in this synthesis which could be promising. And yet it is not well known if the amino groups help to achieve nanostructures with a higher aspect ratio or whether it is just randomly caused effect by the dendrimer for instance. The Fig.6.16 HAADF shows where the metallic structures are (white). But the sample in Fig.6.16 as was mentioned before basically confuses everything.

6.2.4 Metallic Structures in the HAADF

The HAADF confirms the metallic structure persistence but the HRTEM does not show any crystal structure. This result could be due to the dendrimer which is difficult to presume since it is not expected that the dendrimer will interact with the crystal structure of the ZnO. It also might be that the ZnO formed correctly and the dendrimer or its monomers "stacked" around the ZnO structure which made it difficult to see the crystal structure. However, if so it is impossible to wash or centrifuge the ZnO from these organic impurities. On the other hand, the distortion of the ZnO structures was achieved. Before the experiment with the PPI with amino groups another experiment was conducted. The experiment was the synthesis of the ZnO but with the addition of ethylenediamine which also contains amino groups but is not a polymer and has linear structure. Unfortunately, the experiment was not successful and the formations were not observed at all (so the results are not presented in this work). Fig.6.17 (c) also shows a gel-like material which is probably the dendrimer and the red circled part suggests the possible reasons for sharp and longer rods of the ZnO. The dendrimer might provide a narrow path for the growth of the ZnO which would explain the growth.

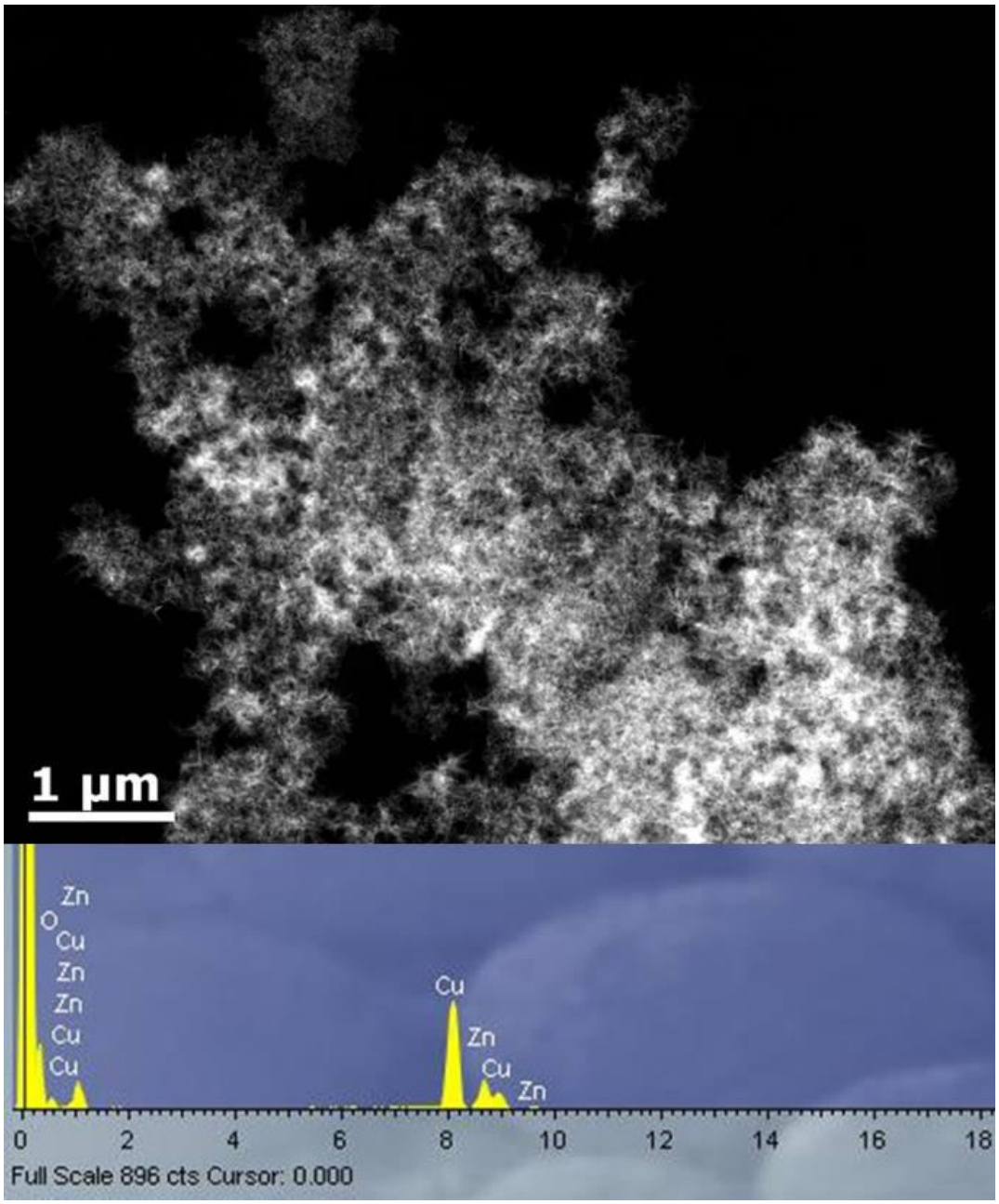

Figure 6.16 the STEM-HAADF tomography of the ZnO nanorods. The copper signals are due to the TEM grids (copper grids). EDX confirms absence of any impurities. The bright areas are the highest concentration of the ZnO.

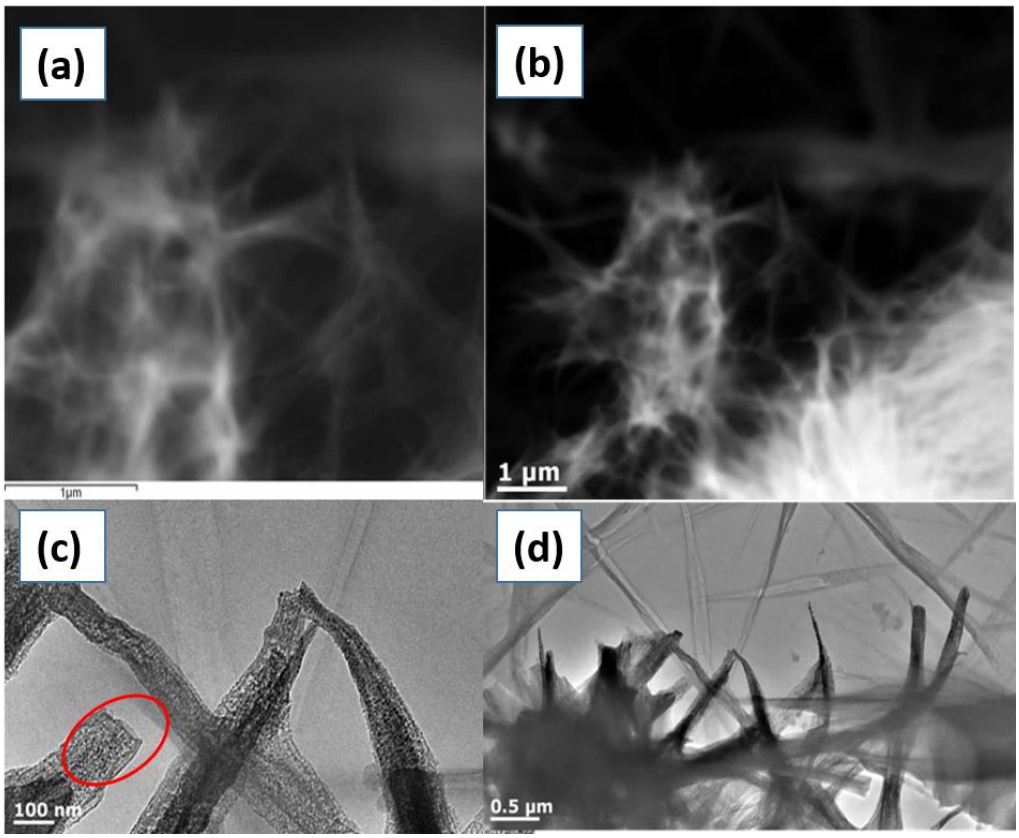

Figure 6.17 (a), (b) the STEM-HAADF image of the ZnO structures grown with the use of the dendrimer PPI-G4. (c) and (d) the HRTEM images of the same material. This is clearly non-transparent for the electron beam which indicates that the structure is high density metal material.

The "empty" parts in Fig.6.17 (d) are the polymer (PPI-G4) without the ZnO. The width of the nanostructures was around 5-10nm and 70-100nm (thickest) with the length from around 60nm to a few micrometers Fig.6.17. The experiment with the dendrimers showed that the nanorods tend to increase in aspect ratio Fig.6.17 and Fig.6.18. As mentioned before the experiment with the EDA was not working but the dendrimer was used for the increase of the aspect ratio of the ZnO nanorods. After adding the dendrimer, the aspect ratio of the ZnO increased from 5 to 10(with smallest nanostructures). This showed the effect of the dendrimer molecules. The exact reason of such behaviour is still not completely clear. But the fact is that the amino groups play an important role in the formation of the nanorods with a higher aspect ratio. Fig.6.18 depicts the HRTEM of the same sample as in Fig.6.17 with zoomed areas of interest. The structures are film or plate-like. Also the structures are transparent for the electron beam which means that they are either made of polymer which is not likely since the polymer cannot take shapes like this under these conditions or they are ZnO structures but with a very low thickness which is more likely. The structures differ from those synthesized without the PPI-G4 in Fig.6.14.

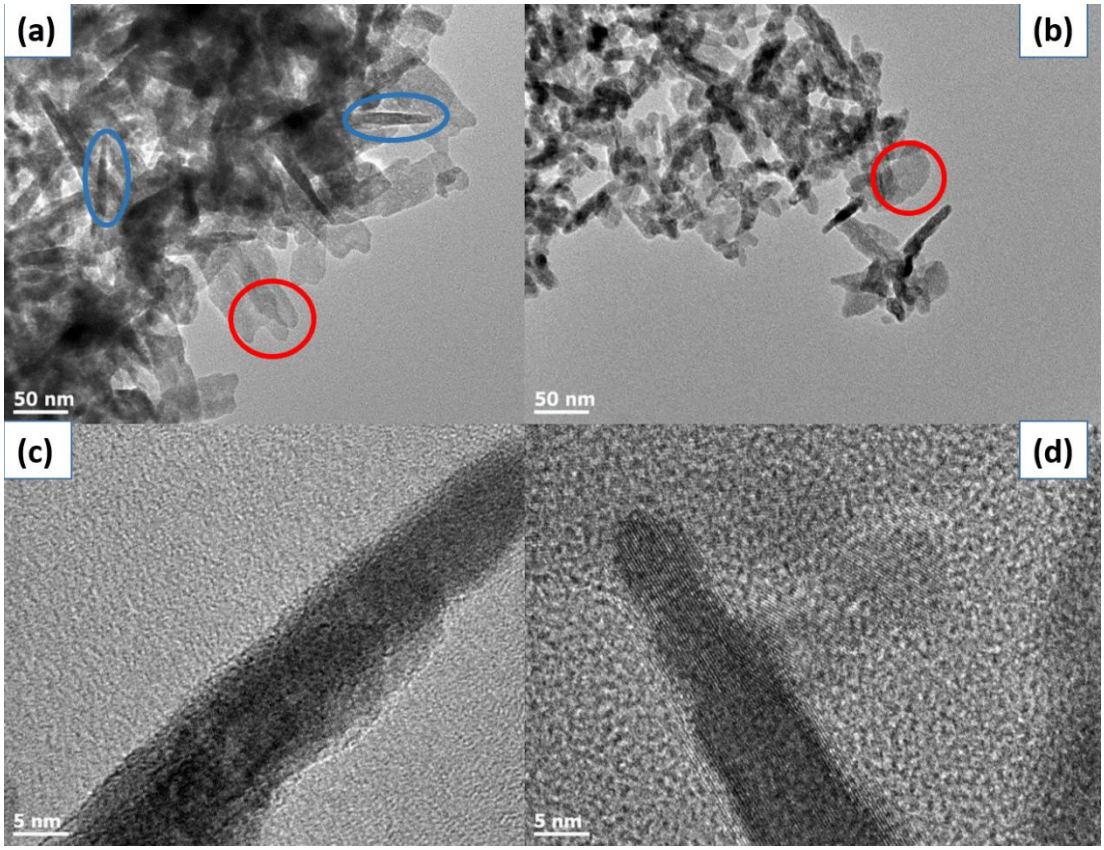

Figure 6.18 the HRTEM of the ZnO nanostructures using the PPI-G4 NH_2 dendrimer of high concentration. (a)structures look similar to previous ones but with slightly different shapes, (b) the ZnO structures are pretty uniform on the whole grid, (c) and (d) demonstrates that they are not accidentally formed structures but ordered with a higher aspect ratio ZnO nanocrystals.

In Fig.6.18 (a) blue circled shows sharp ZnO rods which are twice as long compared to those in Fig.6.14. It can be speculated that the highest influence comes from the dendritic shape of the polymer while the EDA has a linear structure and other atoms might interact in the process. Analyzing each "needle" we can see that the edges of the nanostructures are not smooth (Fig.6.17 (c), (d). This suggests that the dendrimer structure with the amino group forms "needles" and "plates" while the EDA with its linear structure cannot achieve even similar results. The HAADF-STEM scan was performed for this sample and the results are shown in Fig.6.19. Also the EDX was performed for the areas marked on the image. Both the EDX scans showed the persistence of Zn and the background of the grid shows only a Cu signal (copper grids). This investigation showed that ZnO nanorods or rice-like structures can be synthesized via the hydrothermal method and the structures can be distorted via a chemical route with the addition of the dendrimer with amino groups. Web-like structures that are depicted in Fig.6.17 should be investigated further which could lead to potentially interesting results.

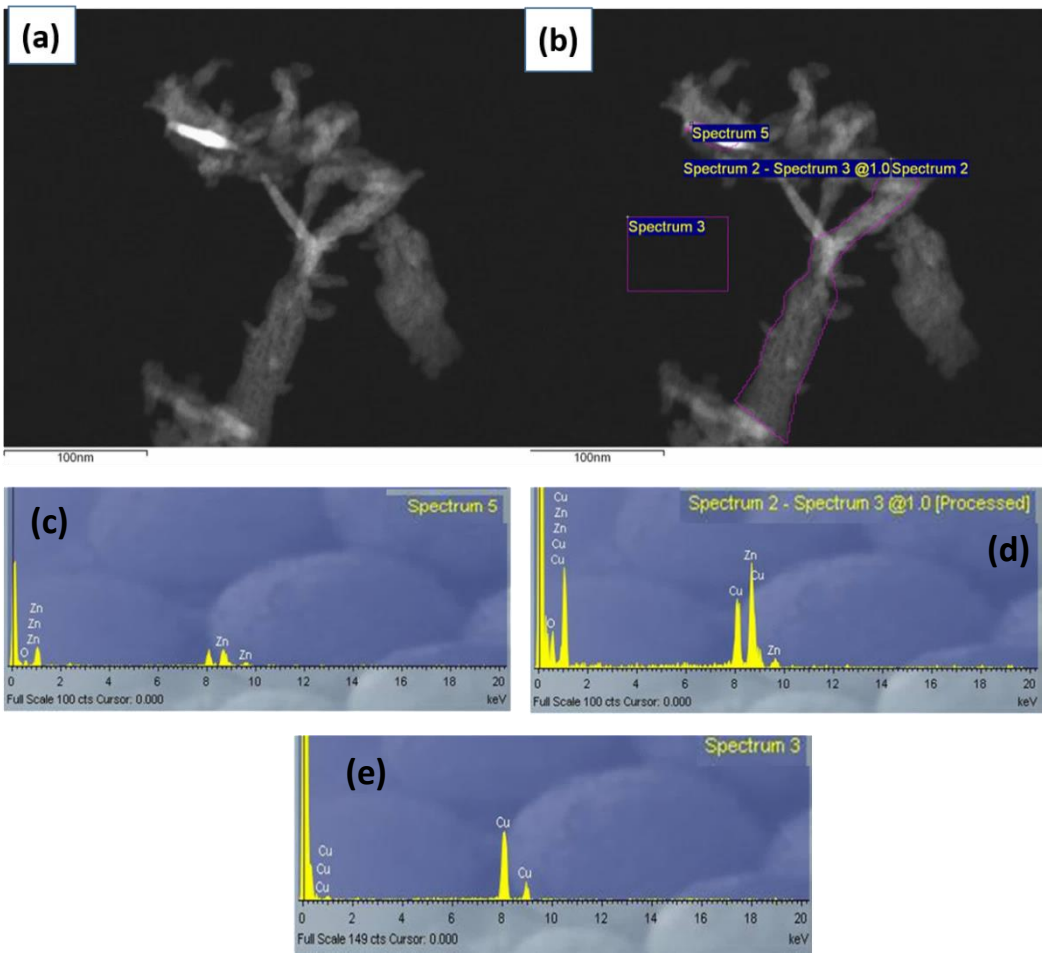

Figure 6.19 the HAADF-STEM image of the ZnO nanostructure synthesized with the PPI-G4 (a) and (b) the same structure but with marked parts for the EDX. (c), (d) and (e) confirm the prediction of the ZnO nanostructure without any impurities. Image (e) is of the background of the sample which was copper grid.

All these analyses strongly suggest that ZnO nanostructures could have a very small thickness of a few atoms or so. Certainly this experiment needs to be repeated multiple times changing the conditions before the final conclusions could be made. The hydrothermal synthesis (subsection 6.6) and the dendrimer involved hydrothermal (section 6.7) synthesis of the ZnO was demonstrated. It is proven that organic molecules such as PPIG4 with amino groups can affect the shapes of ZnO. While the hydrothermal method provides rice-like structures with an ordered arrangement of atoms (Fig.6.14) the PPIG4 involved synthesis showed distorted ZnO without a clear arrangement of atoms (Fig.6.17).

6.3 Light-Induced Synthesis of ZnO

Next we will demonstrate the synthesis of the ZnO structures but using the photochemical method with particular light codes that are present in Tab.3.1. First light code used was the RGB for 12h. Fig.6.20 depicts the ESEM results of the ZnO synthesized using the RGB code. As it can be seen the structures look very similar to the ZnO structures synthesized via the hydrothermal method Fig.6.14. The main difference is the size. In Fig.6.20 the structures are micro sized and have rod shapes.

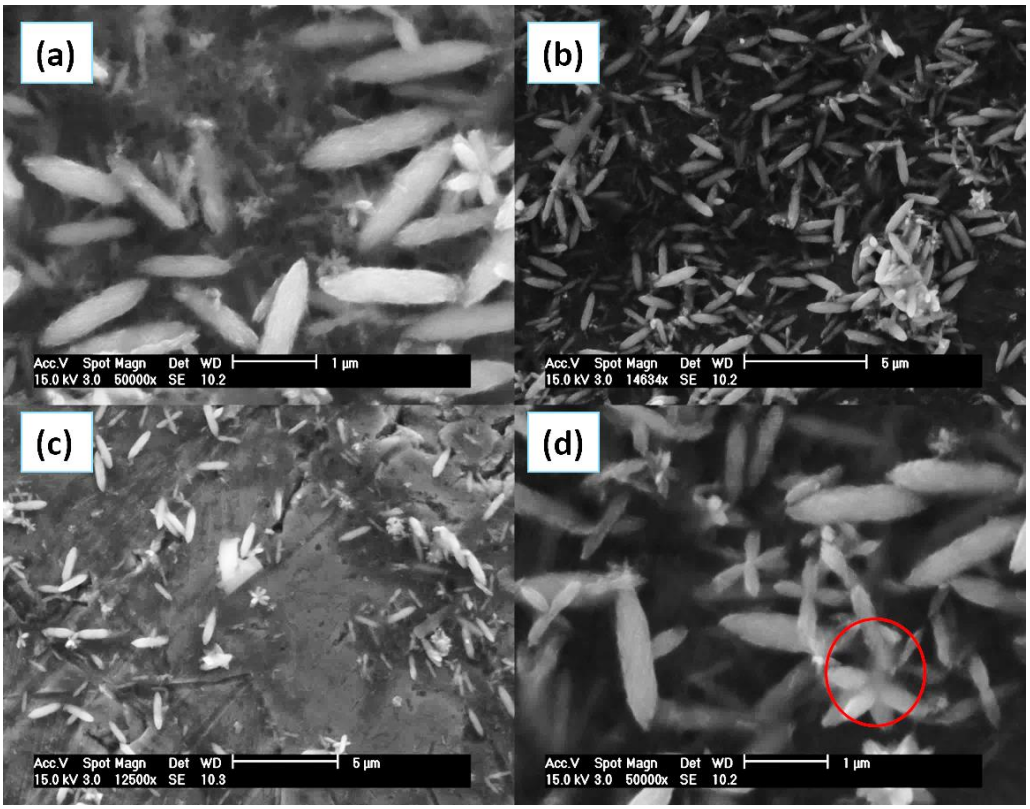

Figure. 6.20 the ESEM images of the ZnO nanostructures synthesized using the RGB LED sequence. (a) clearly seen ZnO of micron size also smaller structures can be seen. (b) the image with less magnification shows roughly the size distribution over the particular area of the sample. Big rods of 1-1.5 micrometer size and canoe shaped are obvious. (c) and (d) focuses on smaller structures (red circled in the image). Smaller structures are branching out and some of them form 3D structures.

It is difficult to explain such results using literature references since there are none that describe light-induced synthesis of ZnO. However, as will be described later, this can be explained considering a few theoretical reports. Other results will shed light on the importance of the wavelength and the light codes. Fig.6.21 shows the ESEM images of the ZnO structures synthesized using the same concentration as in Fig.6.20 but using different light codes Tab.3.1. In Fig. 6.21 (b) we can see the rods as in Fig.6.20 but the difference is that they are branching out forming 2D structures while (c) synthesized

using code3 looks quite different from the other samples. In Fig.6.21 (c) and (d) visibly shows the mixture of the different shapes 2D and 3D but most importantly the size of the structures is different. Roughly 50% are 1 micron or smaller and the other half are bigger than 1 micrometer. While structures in Fig.6.21 (a) was synthesized using code1 and looks difficult to define. It is actually a mixture of nano and micro "rice" which is 1D in most cases.

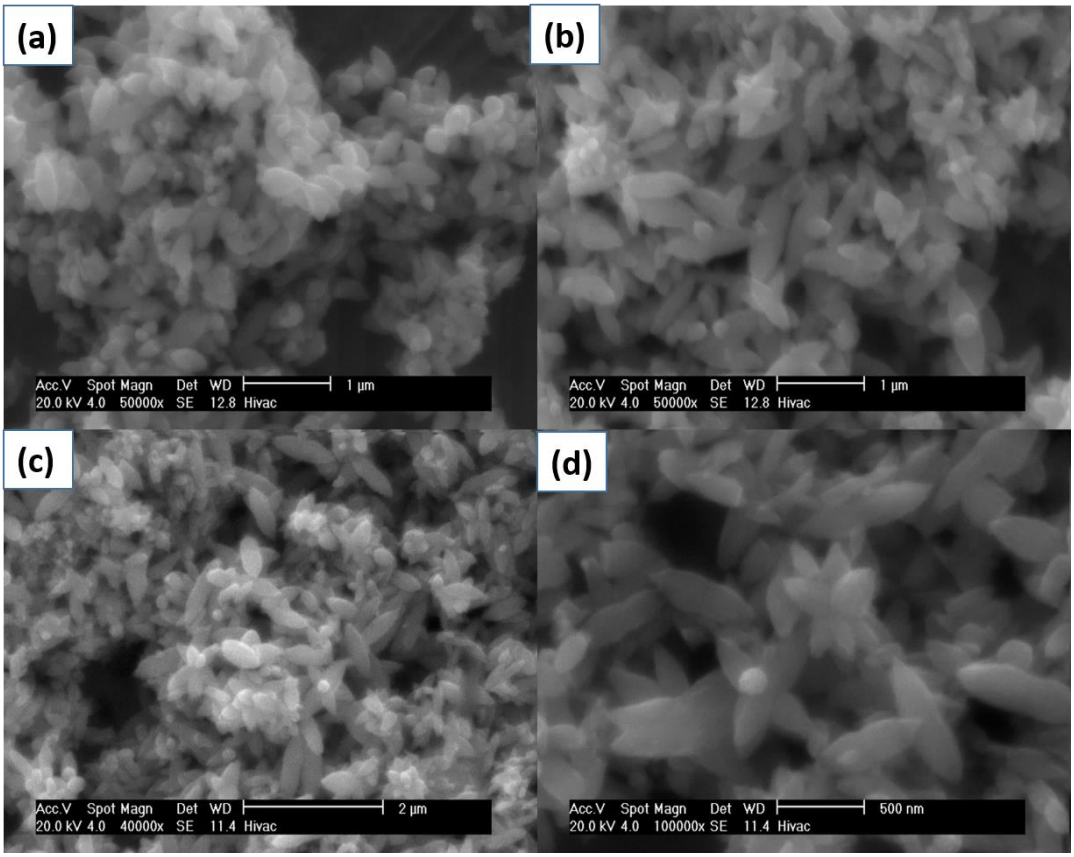

Figure 6.21 the ESEM images of the ZnO nanostructures. (a) was synthesized using Code1 LED sequence for 12 hours. (b) was synthesized using Code2 LED sequence also for 12 hours. (c) and (d) Code3 LED sequence for 12 as well.

The most surprising result was the ZnO synthesized using code4 Fig.6.22. In Fig.6.22 very uniform 3D structures are formed. The "rice" or rod structures evolve into more triangle-like shapes and sharper edges can be observed. While code4 gives stricter structures with less variety code1 gives more distorted formations. The time factor will not be investigated in this study. However, the time factor is one of the most important factors in the formation and control of nano and microstructures. It seems that the ZnO has rod formation habit and other structures like "flowers" as in Fig.6.22 are just the upgrade and assembly of already existing ZnO habit.

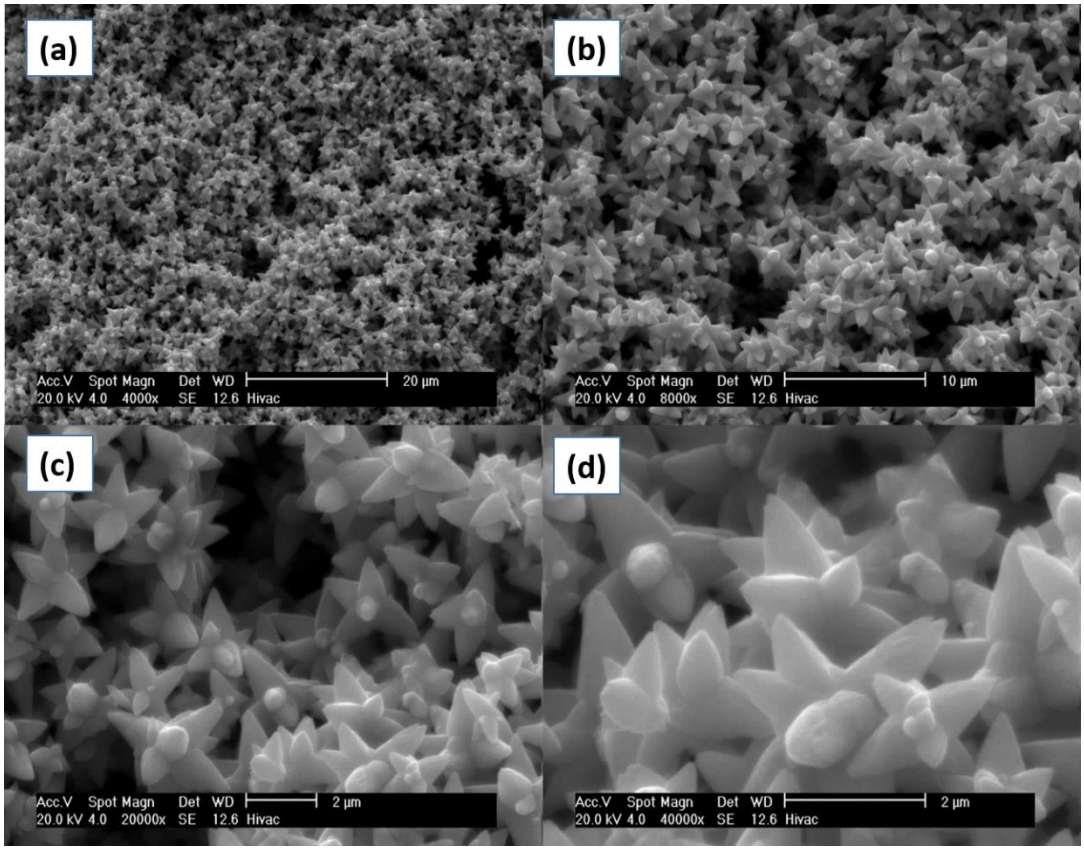

Figure.6.22 the ESEM images of the ZnO microstructures using Code4 LED sequence. (a) shows the distribution of the structures on the sample. (b), (c) and (d) the same sample showing more detailed images indicating that no agglomeration occurred.

To see if the growth has a dependence on the wavelength another synthesis of the ZnO was performed using UV light Fig.6.23. In Fig.6.23 structures look more flower-like than in Fig.6.22 and the sizes are greater than 1micron. Also in order to confirm the thickness of the structures the TEM was conducted Fig.6.24. The importance of this TEM scan is to show that these structures are not made of NaOH that was used during the synthesis. Sometimes centrifuging even at a very high speed cannot remove all the salts and/or impurities so the TEM check is desirable. In this study it is clear that these structures are made of ZnO and are without any salts or impurities. This is because the NaOH was not used in high concentrations and the material was washed several times (and centrifuged) which led to an almost total purity of the structures. The synthesis of ZnO via the photochemical method is attractive and exciting but it is quite difficult to control. To get a step closer to controling the influence of the wavelengths and the concentration were investigated separately. The next step was to synthesize the ZnO using the RGB light code for 12h but increasing the concentration twice. Fig.6.25

shows a twice as high concentration of Zn(ac) with the RGB light code. The formations are very similar to those in Fig.6.22 and Fig.6.23.

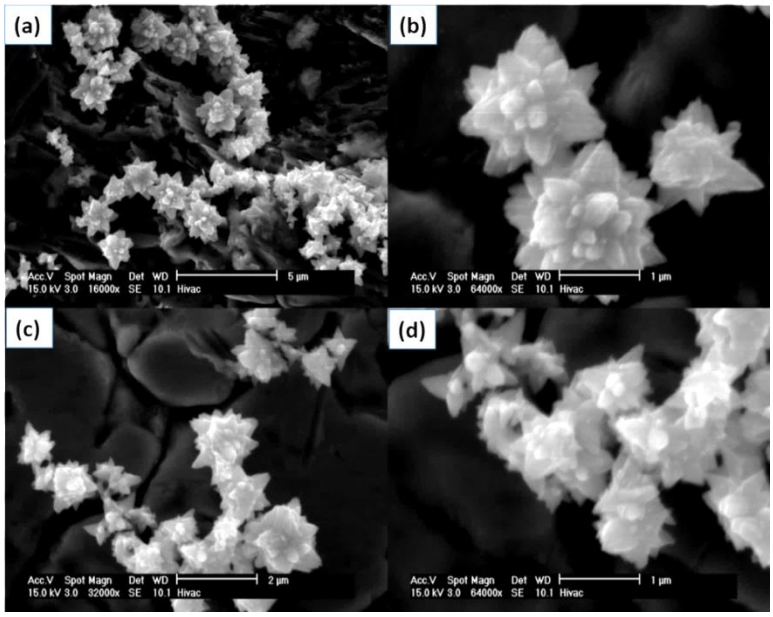

Figure.6.23 the ESEM images of the ZnO 'flowers' formed under the UV irradiation for 12 hours. (a) the ZnO structures with magnification 16000x on steel substrate. (b) the same sample with 64000x magnification. (c) and (d) shows other area of the sample confirming the formations are similar flower-like.

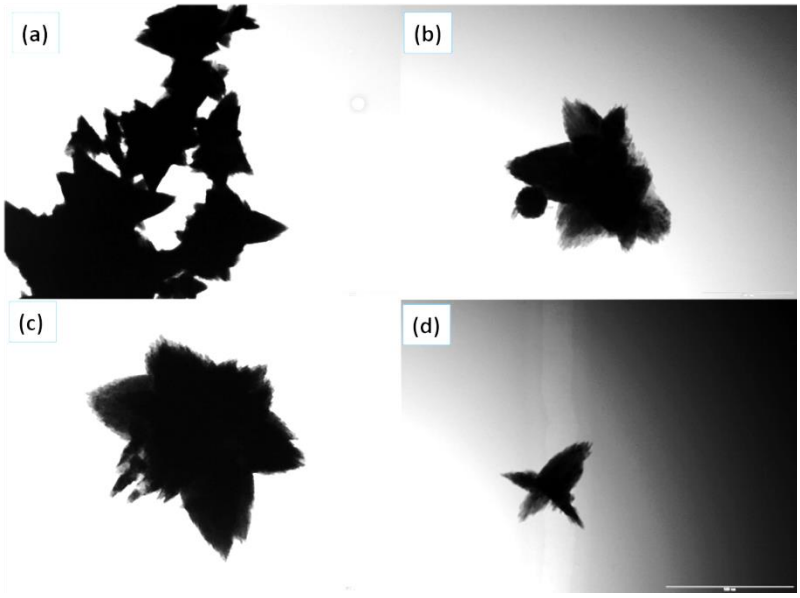

Figure.6.24 the TEM micrographs of the ZnO 'flowers' formed under the UV irradiation for 12 hours. (a) shows clumps and the other images (b), (c) and (d) taken from different areas of the sample. As we can see in all the images the ZnO structures are too thick for the electron beam and are not transparent.

However, some differences still persist. The minor difference is the arrangement of the "flowers" and the formation of micro needless. The "flowers" seem to have self-assembly or packing as depicted in Fig.6.25 (a). Changing the concentration or the light codes seems to affect the ZnO structures only mildly. However, in some cases (like code1 and code4) changes are very obvious. The concentration experiment will be conducted again in further experiments that are below. Now let's come back to the previous concentration of 1mmol/ml of Zn(ac). Some researchers have synthesized the ZnO also at room temperature but not photochemically or using the light-induced approach [215-217].

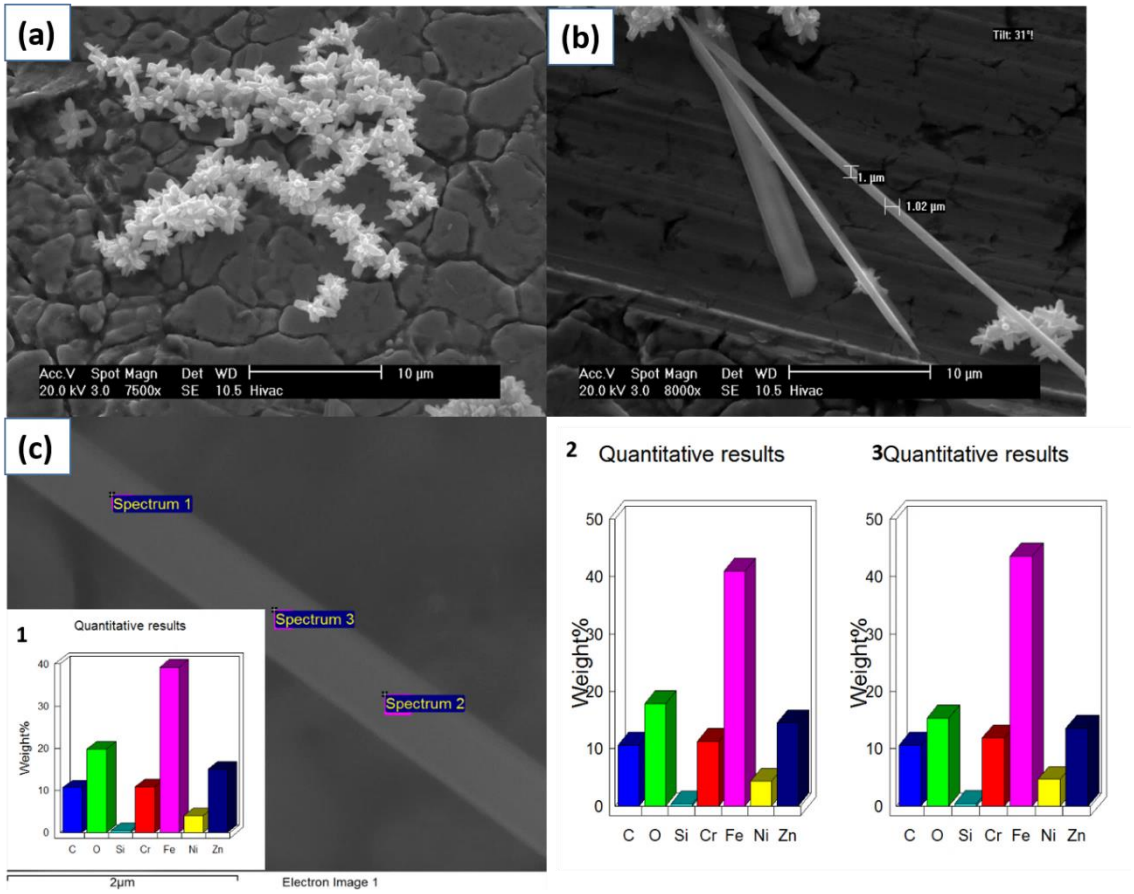

Figure.6.25 the ESEM images of the ZnO with increased concentration of 2mmol/ml (Zn(ac)) grown under RGB for 12h and EDX quantitative spectra. (a) Assembly of ZnO "flowers" in a row. As the ESEM image shows the "flowers" are assembled in a particular way like they are attached to something. (b) shows micro wires and the "flowers" attached to them. (c) EDX analysis. Quantitative results represented in separate numbered graphs. The numbers correspond to the EDX spectrum numbers.

However, those methods report precipitation and pH control during the synthesis which does not mean that they have performed the synthesis in the dark. The sonochemical method also was used [217] which potentially includes the exposure to the daylight or the light in the laboratory. Daylight has all the wavelengths in one with an even higher intensity than is provided by the LEDs. The comparison could not be made without changing the wavelength and changing the concentration. Another experiment with a different LED was performed Fig.6.26. The green light was used for the synthesis with a twice decreased concentration as initially started. In Fig.6.26 the ESEM images depicts the formed structures which look more or less like "flowers" with some slight changes from the previous ones (Fig.6.21, Fig.6.22, Fig.6.23). All the structures have a centre and branch out to form leaves. An important feature is that Fig.6.26 shows "flowers" that are actually on the nanoscale and are few times smaller from previously mentioned figures. This result helps interpret on the role of the energies and concentrations. If the ZnO still has a tendency to grow in a flower-like manner the parameters can still be influenced by concentration. A decrease in the concentration leads to a decrease in the size which is logical.

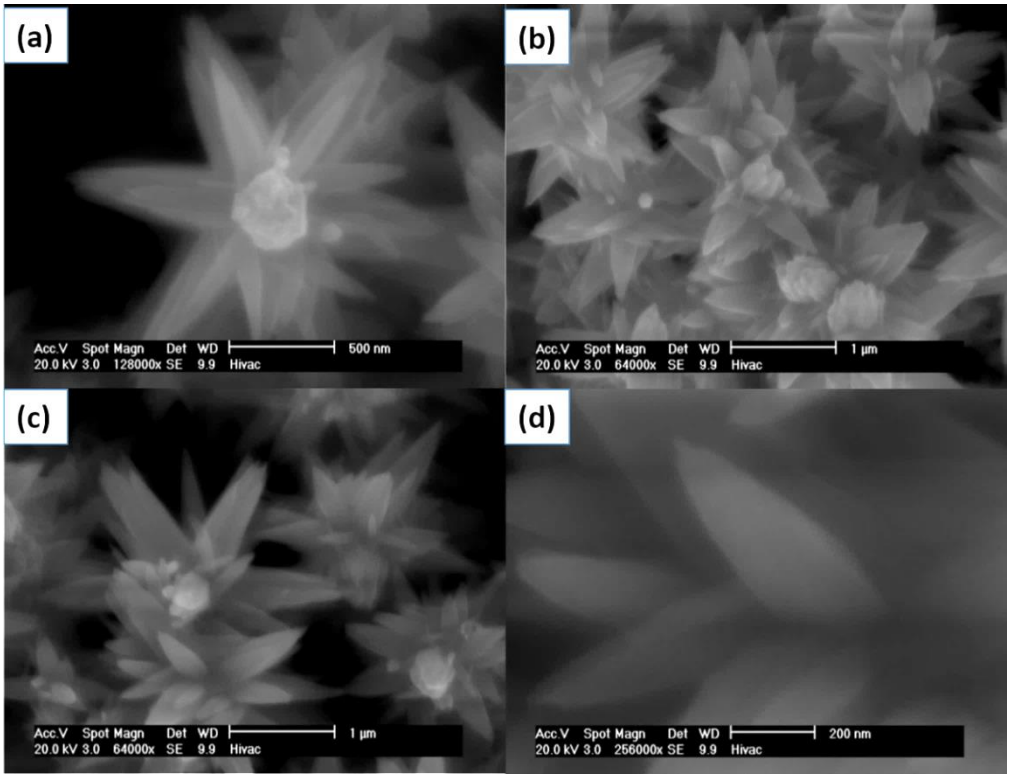

Figure.6.26 the ESEM images of the ZnO nanostructures grown using green light (518nm) for 12 hours. (a) flower-like structure showing in detail 128000x magnification. (b) and (c) image indicates the uniformity of the structures showing their three dimensional fragment details. (d) 256000x magnification on 'leave' of the structure confirming their nanodimensions.

Surprisingly the shape remains the same with small changes like the diameter and shape of the leaves Fig.6.26 (d). In a follow on experiment the same concentration as in Fig.6.26 were used and a different light code. Let's say RGB should fit nicely since it also has green light. For comparison the results are depicted in Fig.6.27. In Fig.6.27 (a) and (c) ZnO synthesized using green light and (b) and (d) synthesized using RGB for 12h. The difference between these structures is not very significant but obvious. "flowers" synthesized using green light are more uniform and look strictly arranged in groups Fig.6.27 (c). While the RGB sample is similar to the one in (a) and (c) it still has some major differences. The RGB structures look more like they are agglomerated or have grown into each other. In the RGB sample we cannot see the separate structures because most of them are in mush-like assembly with each other. It is difficult to say whether the structures are just assembled in this way or if they have grown into each other.

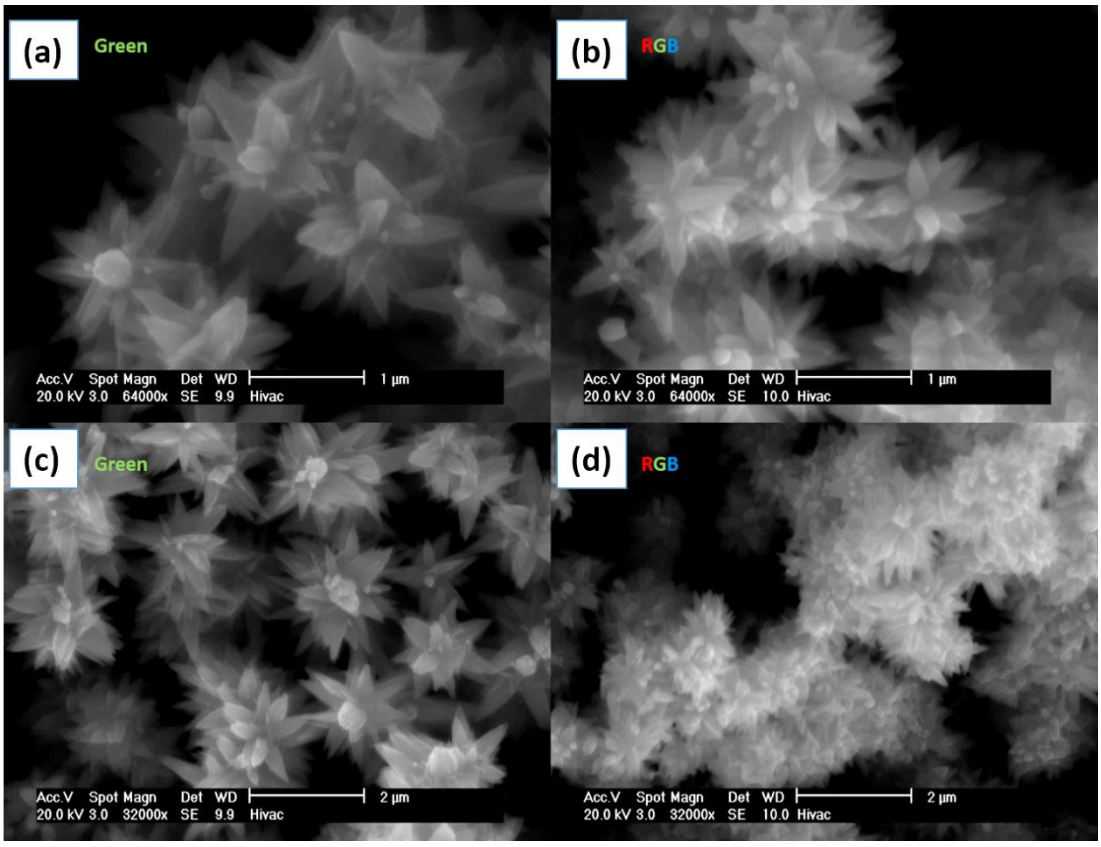

Figure.6.27 the ESEM images of the ZnO synthesized using the Green wavelength (518nm) and the RGB to make a comparison and establish main differences between the samples. (a) and (b) although looks similar the 'RGB' sample structures are more 'packed' and look denser than 'Green'. (c) and (d) have a lower magnification in order to see a more 'panoramic view' of the distribution of the material over the sample (32000x).

It would be logical to presume that the structures are actually grown into each other forming a mush-like assembly because of the RGB energy code. If the green wavelength forms “flowers” then another code which has a green wavelength should also form “flowers”. But if another code has more than just a green wavelength then it is logical to think that it will drag the formation of the structures in a different way. If there is **a** wavelength1 that forms the structure a then wavelength2 will form structure **b**. Now let’s assume that the same material was irradiated with both wavelengths. This process should give the structure between the **a** and **b** or let’s call it **ab**. This new structure should be the hybrid of both the **a** and **b**. A time is also an important influence. If we use both wavelengths at the same time, then the formation of both of the structures might occur at the same time. However, this should give more difficult picture since we are dealing with two different frequencies at the same time. The structure might be very distorted and similar to both **a** and **b**. Now let’s imagine we will use wavelength1 for let’s say 5 seconds and then wavelength2 for 5 seconds. These two energies will have an opportunity to interact or influence the chemicals and the whole formation process separately without being interrupted by another energy portion (wavelength). If we change the exposure time the chemical would get different amounts of energy from different sources.

6.3.1 Time and Energy Influence on ZnO Growth

Exposing the ions and pre-formed structures to light would lead to the influence of the energy on the growth and formation (inside the liquid). Now let’s come back to our RGB sample. RGB- means Red-1second then Green-1second and finally Blue-1second. Here we have three different energies. While the green wavelength gives uniform “flowers” other wavelength should normally give a distorting effect. And in our case we even have three different energies which eventually lead to the structures depicted in Fig.6.27. More wavelengths and investigations on this effect could give a high control degree which actually would be very useful in nanochemistry since it can lead to the controlled growth of desired metal or ZnO shapes or sizes. The concentration must also be taken into account and investigated separately. An important question is: what will happen to those structures if we age them under daylight? And: if there are any structures formed in the dark? Both of these questions is answered and depicted in Fig.6.28. As we can see aging forms microsized hexagons and wires. While synthesizing the ZnO in the dark does not form anything at all.

Fig.6.29 shows the EDX of the marked area in Fig.6.28 (d). The EDX result confirms the persistence of Zn which comes from the Zn(ac) salt used in synthesis and the oxygen line comes from NaOH which was used as an oxygen donor. It was shown that both different wavelengths and concentrations influence the growth of ZnO.

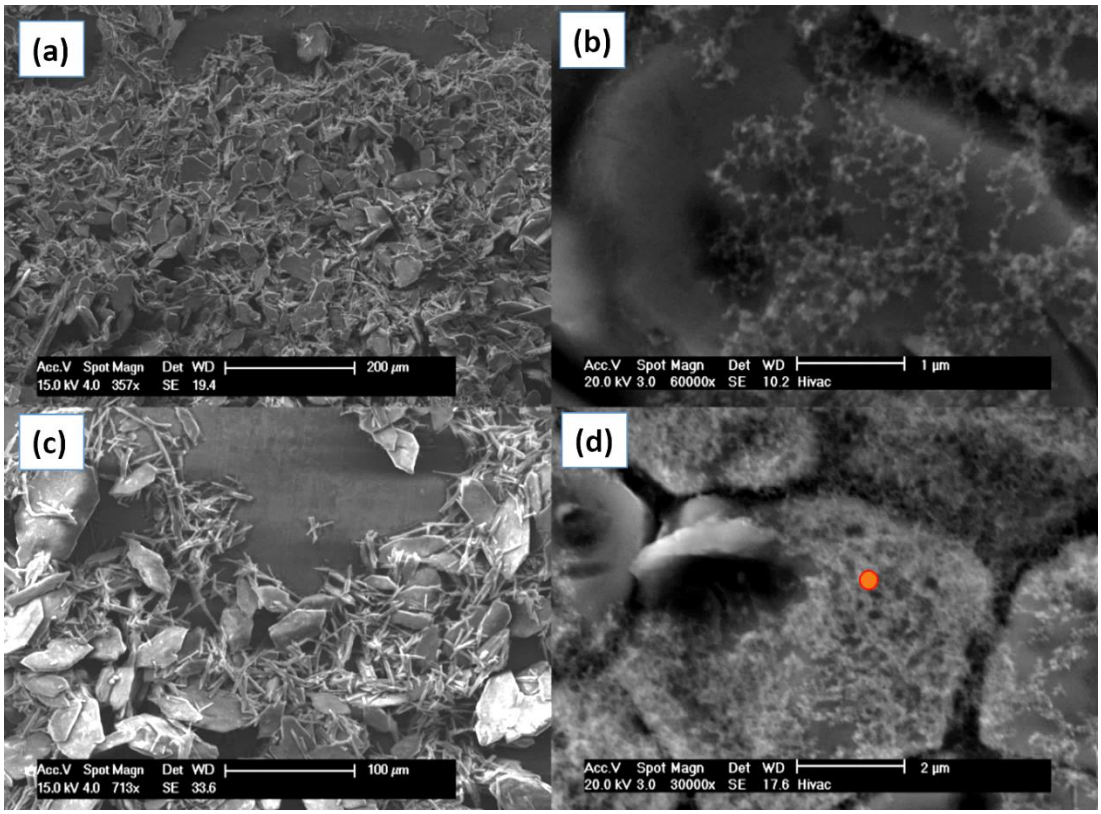

Figure.6.28 the ESEM images of the ZnO for better comparison. (a) and (c) the ZnO solution that was aging for 1 month in the vial under daylight exposure. (b) and (d) the same concentration having solution that was kept in the dark for 1 month. The EDX analysis was performed in (d) marked.

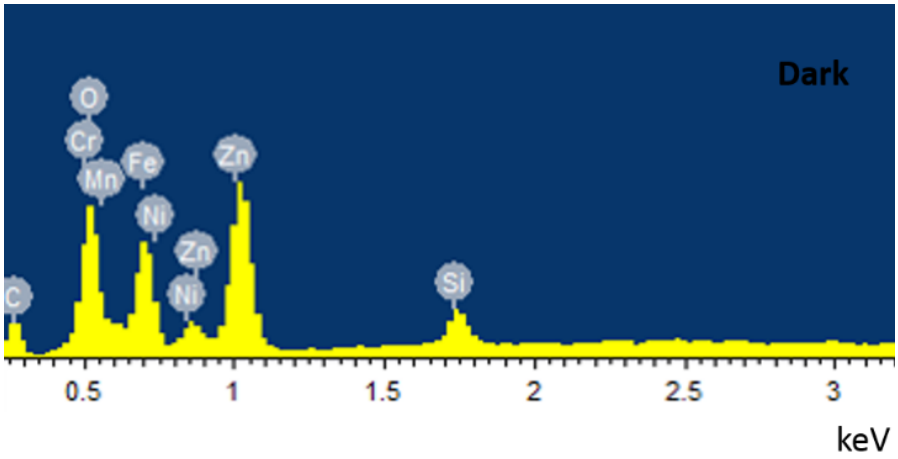

Figure.6.29 the EDX analysis of the ZnO sample that was kept in the dark. The EDX results indicating persistence of the Zn and O atoms confirming that the sample contains salts of zinc acetate that were used initially for the synthesis. This result also confirms a very important hypothesis that for this type of synthesis light plays a great role.

3mmol/ml of Zn(ac) and NaOH and the ethanol as in previous samples (but with a different concentration) was irradiated with the green LED laser (532 nm) for 3hours.The structures obtained were spherical and microsized and looked like "hedgehogs". The branching out needles or wires were a few tens of nm and more. To confirm this result and actually check the presumptions and speculations made above another experiment with the same concentration was conducted. The wavelength was changed to the red which is energetically close to the green but actually has less energy. Fig.6.30 depicts ESEM images of the ZnO structures synthesized using the red laser for 3 hours (650 nm). The structures in Fig.6.30 look very similar to the ones in Fig.6.31. The important characteristic is that they do not have "needles" branching out. As was mentioned before the red light has less energy than the green one which suggests that the green laser gives more energy to the structures and allows them to build more complicated shapes. This explanation sounds very logical and also fits the explanations proposed before. However, to give the precise explanation more investigations both in the experimental part and theoretical simulations should be conducted. In Fig.6.30 (d) shows the 'exploded' structure which reveals what it is made of.

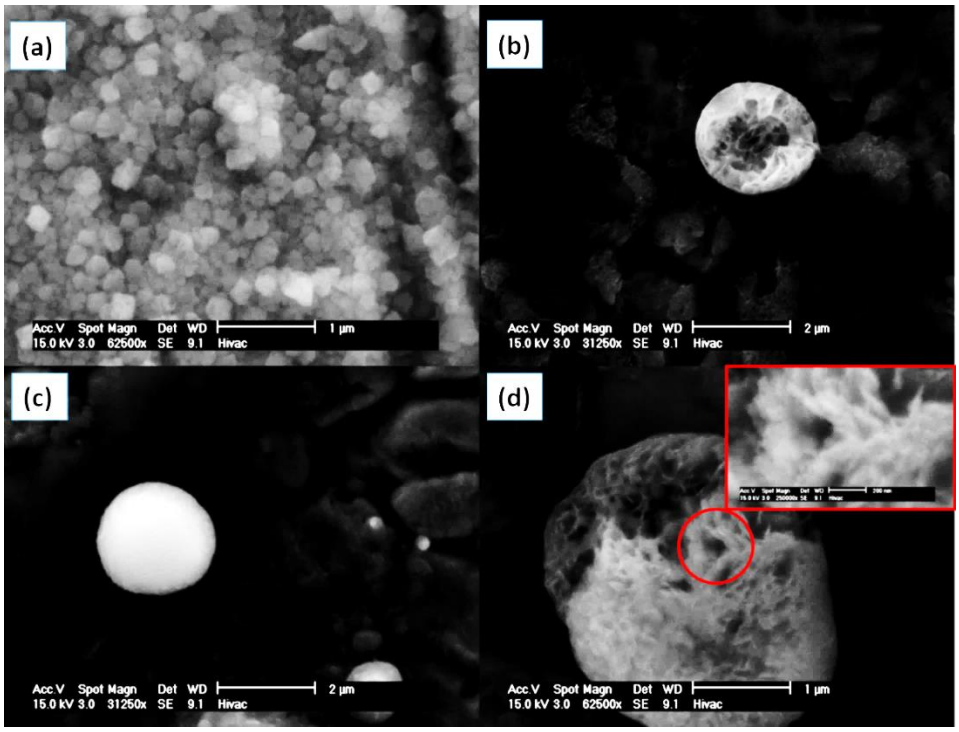

Figure. 6.30 the ESEM images of the ZnO microstructures obtained irradiating the sample with the red laser. (a) sample area with multiple round shaped structures looking more like agglomerates. (b) 'exloded' microsized 'bulb' indicating complicated structure inside. (c) closed 'bulb' not (d) the image of the 'exploded' 'bulb' showing the fragments the structure is made of.

The small structures (circled in red) look like mashed grass (it's difficult to give any other comparison) and have assembled into a microsized sphere. Another question arises now: what is the difference between the laser light from the other sources of light? The answer is: the laser light is coherent. Is it possible that this coherency gives such an effect on the structures? It is difficult to answer. More experiments should be conducted using the laser light in order to find out the role of lasers in the synthesis of ZnO. Normally it is difficult to imagine a system which is so sensitive to light sources. For now, let's speculate that the reason for such formations is due to the fact that the laser did not enlighten the whole vial where the synthesis was performed. The laser beam was going in the y axis in the vial enlightening only the middle part of the vial and leaving the rest poorly enlightened. During the whole ZnO photochemical synthesis process other types of the structures were found and are depicted in Fig.6.32. These structures were found in very low numbers and always different like chemical synthesis side product.

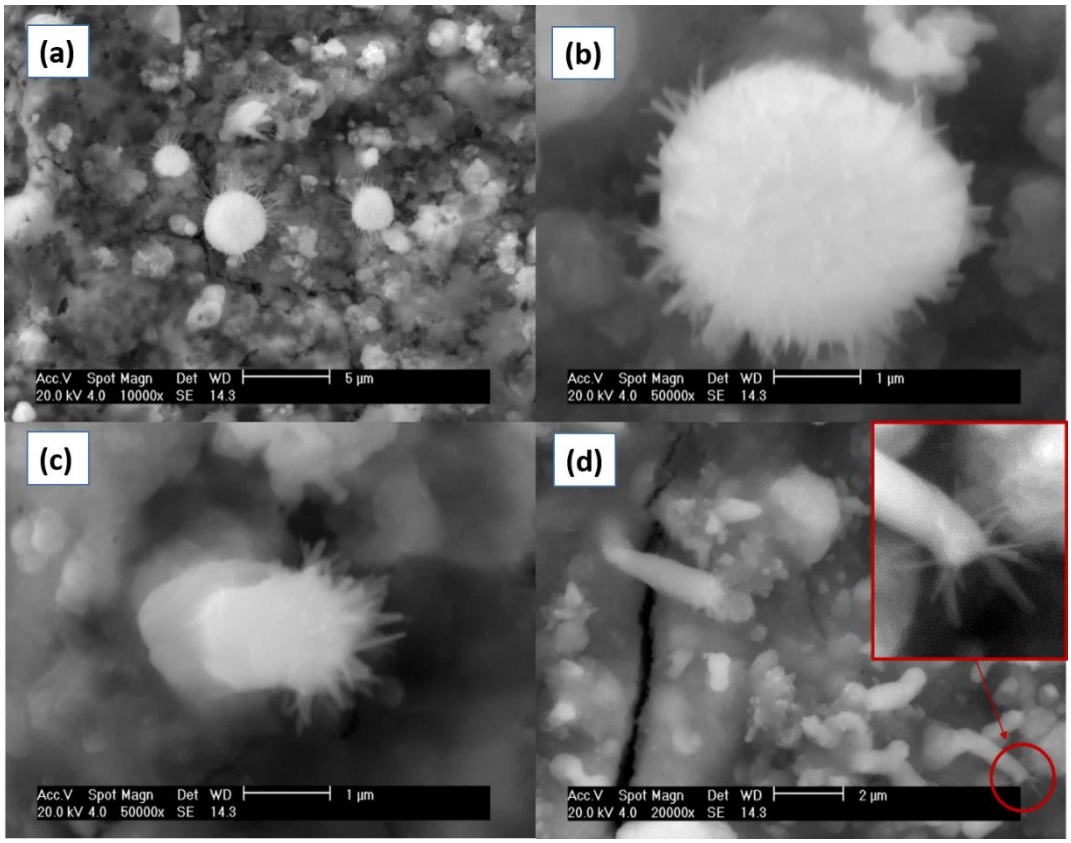

Figure.6.31 the ESEM images of the ZnO structures irradiated with the green laser of 532 nm and changing the concentration and irradiation time (3hours) from 'Green' sample. (a) shows the formation of microsized 'bulbs' with branching out nanowires. (b) Higher magnification 50000x zooming one random 'bulb' on the sample. (c) Microstructure with nanorods branching out. (d) Indicating the 'trend' of branching out structures. Also suggesting the growth process occurred in this way.

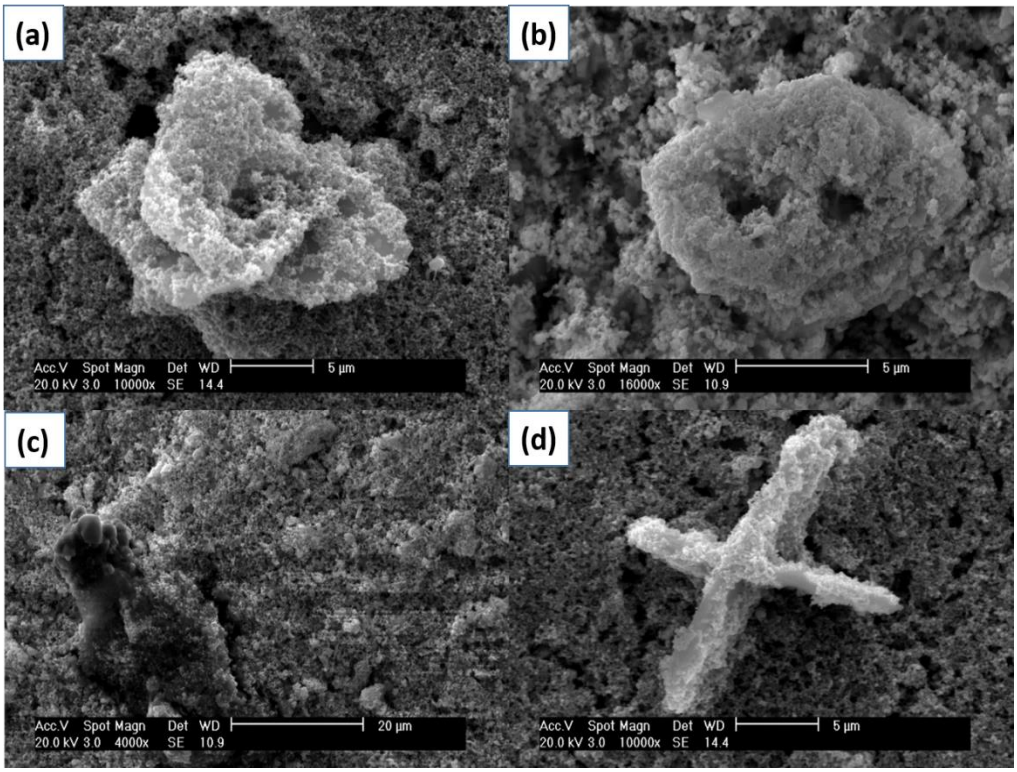

Figure.6.32 the SEM images of the ZnO 'artefacts' obtained during the photochemical synthesis of the ZnO structures. (a) and(d) ZnO 'flower' and 'cross' obtained applying the green LED synthesis approach (b) a 'face' was obtained during the RGB synthesis process and (c) 'feet' was synthesized using the green laser synthesis approach.

6.3.2 Synthesis of ZnO under LED Varying the Precursor Concentration

So far we have seen the light-induced synthesis of the ZnO, Ag, Ag-Au and the nanostructuration of polymers. However, in this list Ag is known for being photosensitive [218] and was used in photography years ago [219]. Polymers also absorb visible light which means that there is a light-matter interaction. The case with the ZnO is very different since it does not absorb visible light but only ultraviolet (UV). The main question here is what happens if the light-matter interaction is not possible? To answer that first we need to synthesize the ZnO structures under the same conditions but using different concentrations. Then we need to repeat the experiment in the dark. The zinc acetate and sodium hydroxide do not absorb visible light which means that no light-matter interaction occurs.

6.3.3 Changing the Concentration of Precursors in the ZnO Synthesis

However, if the results are different by varying the concentration there is a process related to light-matter interaction. On the other hand the ZnO is a white powder which also indicates that it reflects all visible light. On the other hand when the Zn(ac) and the NaOH solutions are mixed the ZnO powder does not form immediately which

means that in theory the light can actually influence the growth of the ZnO structures. In the following experiments the RGB light code was used. The RGB stands for Red-1 second then Green-1 second and finally Blue-1 second and then repeating again. The influence of time is also an important factor that should be checked. If the RGB growth over a longer period of time gives different results from those over a shorter time interval then it could be speculated that the light-matter interaction has greater influence due to the time interval. If time has no influence then the results would be the same.

Concentration 1:10. The concentration was chosen to be 1:10 or 0.5mol/l of Zn(ac) and 5mol/l of NaOH. In order to distinguish the influence of one particular wavelength on a ZnO synthesis it is logical to use only one wavelength of light. Let's choose red LED. Red LED has the lowest energy and can help by showing the difference in synthesis with the RGB and fixed lowest energy light. If there is a difference between them or the red LED gives significantly different results then we can claim that every wavelength of light has its own role in the light-induced synthesis of ZnO. Fig.6.33 shows the ZnO structures synthesized under the red LED for 12h. The structure seems to be like previous the ZnO structures of a round or bubble shape. However, there are specific differences.

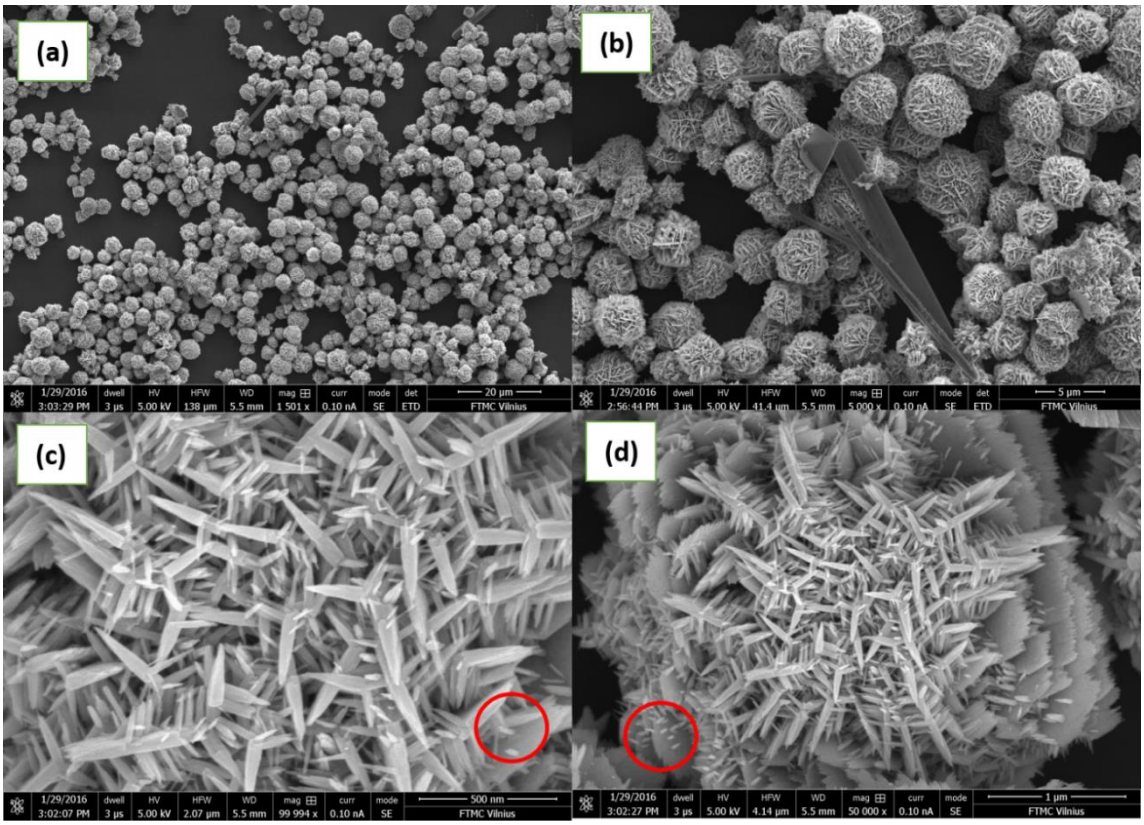

Figure.6.33 shows the ZnO synthesized at room temperature using only the red LED for 12h. (a) bubble-like structures scale bar 20µm (b) zoom of ZnO bubbles with elongated "artifact" scale bar 5 µm (c) zoom of ZnO bubble. Spikes can be easily indicated on the surface of the structure (red circled). scale bar 500nm (d) the structure shown from the larger perspective indicating leaves resembling flower-like structure. Scale bar 1 µm.

Most of the structures are bubble-shaped and have a specific surface texture Fig.6.33(c) and (d). The structures have ordered spikes on the surface which actually look more like tetrapods. The spikes are surrounded with leave-like ZnO structures which resemble a flower. For more simplicity let's call these structures flower-like in the future.

6.4 Self-Assembly or Hierarchical Growth?

In the case of flower-like structures it is important to know whether they were synthesized separately in a solution and only then assembled into one structure or they grew from a core into a more complicated formation. To do so we could use a high frequency ultrasound. If the structures are self-assembled then they can be disassembled also. But on the other hand if the ultrasound would disassemble the structure we will see only fragments without knowing what is inside the structure. To see inside the ZnO structure and make sure it is a self-assembly of ZnO nanofragments

we need to “surgically” cut through the structure. The FIB is capable of doing so. The FIB can cut the structure without destroying or damaging the inside formations.

6.5 Hollow or Full Inside?

Fig.6.34 shows bubbles cross-section indicating no emptiness inside. Fig.6.34(a), (b) and (c) shows different bubbles from the different areas of the sample. Fig.6.34(d) is a zoom of one of the bubbles which actually suggests that there are small branched formations. The structure gives a hint that there might be branched formations at the beginning of the growth of the ZnO. This speculation can be based on the fact that in Fig.6.34(d) there is indication (spacs or holes) of some elongated branches that look like something was growing there in one and the other direction and not completely filling the space.

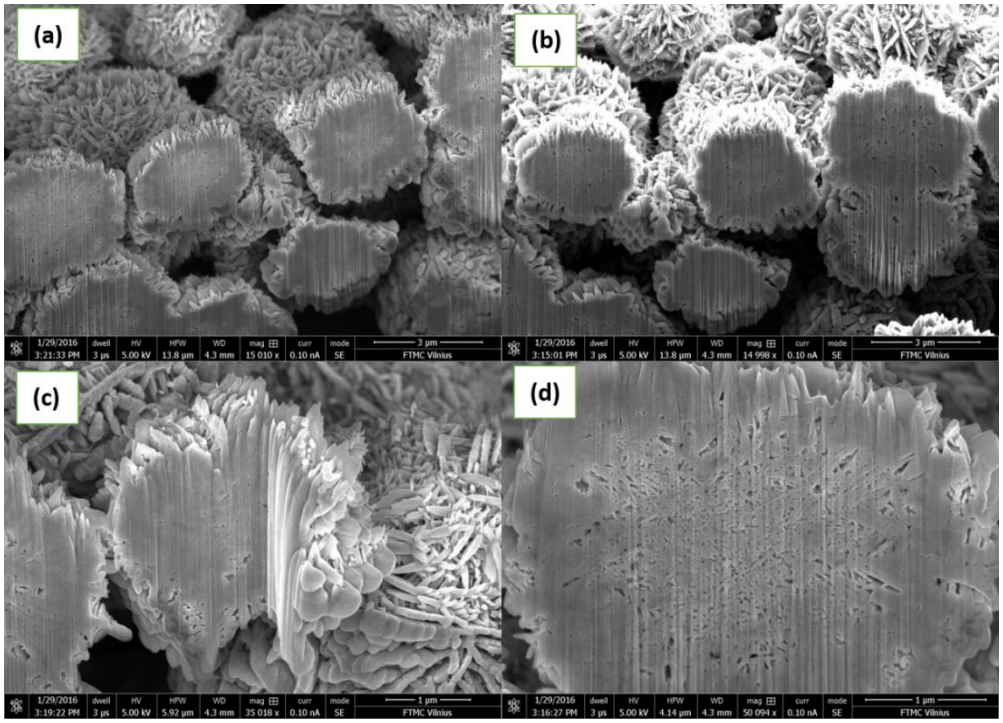

Figure 6.34 shows the ZnO bubbles cut into half using the FIB. (a) few bubbles are selected in order to have more precise results. (b) shows “flat” surface of the ZnO structures in the other area of the sample. (c) angle cut FIB also confirming non-hollow structure hypothesis. (d) zoom of the ZnO cross-section. This image indicates some branched structures inside.

Although in Fig.6.34(d) we can recognize the “signature” of a branched or elongated growth the structure becomes “full” at some point of the growth. This can be seen on the image Fig.6.34(d) the “tracks” or “signature” occurs mostly in the middle of the bubble. This means that there might be something like self-assembly which would evolve into a “full” formation over time. However, to disassemble such a structure using ultrasound would also be quite difficult. Since the edges of the structure are “full” and not showing any cracks or holes. But let’s have a more detailed analysis of the Fig.6.34

6.5.1 Analyzing the ZnO Bubble

In order to understand what is going on during the growth it is necessary to analyze one or a few images. From Fig.6.34 it is clear that the structures are not hollow inside and have a filled morphology. Let’s analyze Fig.6.34 closer. We will take Fig.6.34(d) and divide it into one main image where the bubble can be seen and then divide it into fragments with the surface cut by the FIB. Fig.6.35 shows such an example. Now let’s manually mark all the areas that have holes or voids in with red Fig.6.35(b). If we mark enough of the voids or darker areas we might have a picture of an initial formation of the ZnO bubble. Now let’s take a few areas of the same ZnO bubble and mark the formations that look like fibers or wires with blue. After doing so we can see that there are actually fiber-like paths and they also overlap Fig.6.35(c) and (d). The overlap actually explains why we lose the branching later. When overlapping occurs they grow together assembling ions and lose spaces between the fibers or branches of the ZnO. This is the main reason why in the later stages we do not have branched structures anymore.

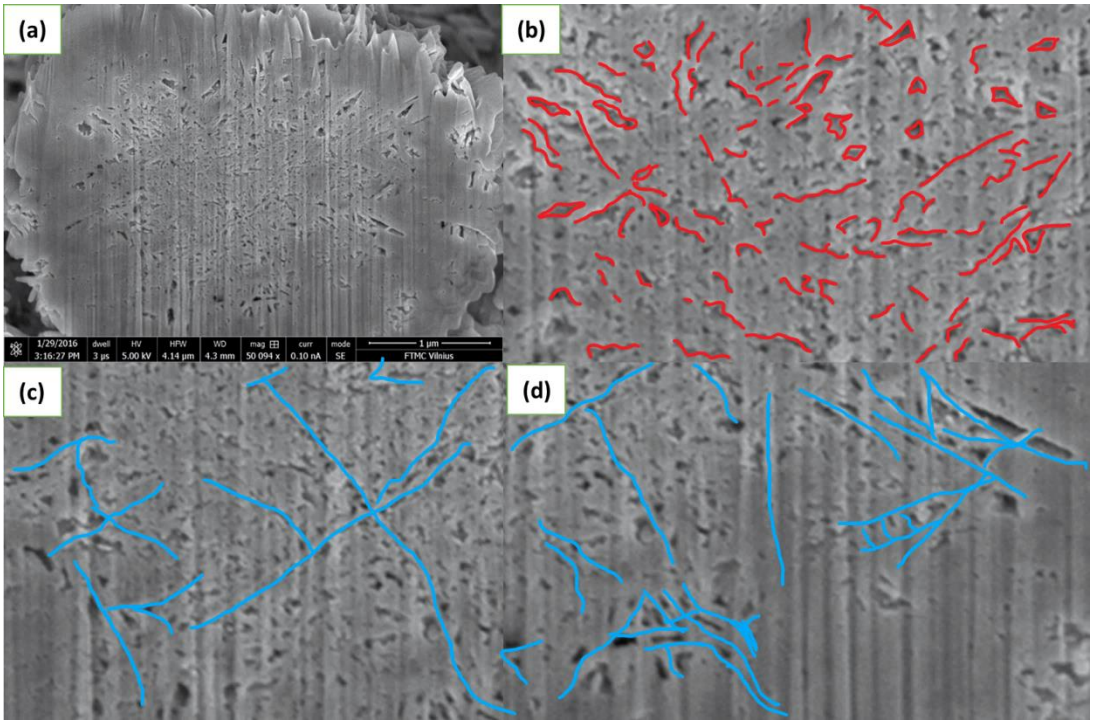

Figure.6.35 shows the ZnO bubble cut using the FIB. (a) general view of the ZnO bubble. (b) red marked darker areas of the sample creating possible growth paths. (c) and (d) are two different areas of the same sample with blue marked areas that resemble fiber like structures which could help understand the growth paths.

6.5.2 Analyzing via Software

Previously we discussed the ZnO bubbles and possible growth paths. The growth paths and fiber-like areas of the sample were marked manually. Unfortunately sometimes it is not enough to use your own guess work and make precise models. To create a model that is trustworthy we could use automatic marking chosen by software. For this purpose we are going to use an open source software called Gwyddion 2.3.1. The software can automatically mark different areas and highlight hidden structures. Fig.6.36 shows the ZnO bubble cut using the FIB. Fig.6.36(a) depicts the analyzed image and Fig.6.36(b) shows a purple marked area (circled) showing the growth of the ZnO at the initial stages of the synthesis. Red arrows indicate cut direction of the FIB in order not to be confused with the fiber structures. Fig.6.36(c) shows the area analyzed by the software of the same ZnO bubble.

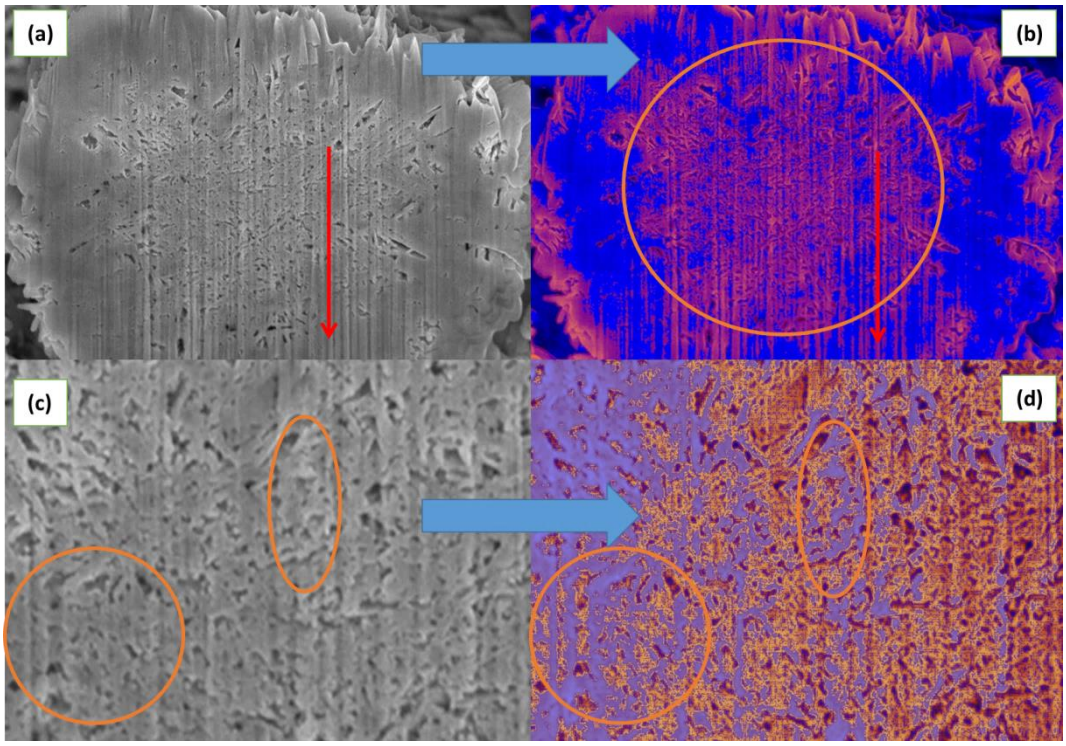

Figure.6.36 depicts the ZnO bubble cut with the FIB and analyzed using Gwyddion. (a) is an original image and (b) the same image analyzed using Gwyddion. The circled area highlighted by software shows branched formation paths at the beginning of the synthesis red arrows show the FIB cutting direction (c) is area from (a) circled areas represent circled areas in (d) highlighted by the software.

In Fig.6.36(c) we see fractalic formations that do not really resemble anything. However, after the software analysis Fig.6.36 (d) we can actually see the formations that look like fractals or bunches of branches. The software analysis highlights the features of the bubble cross-section and confirms the supposition about the small fibrillar formation within the bubbles at the initial stages of the synthesis of the ZnO.

6.6 What About Darkness?

We demonstrated the influence of light on the growth of the ZnO and also the cross-section of the structure. If the ZnO structures form due to the influence of light then without the light either nothing should be happening or the results should differ from the ZnO bubbles. Fig.6.37 shows the ZnO synthesized in the dark at room temperature. We see in Fig.6.37 two types of structures: flowers and elongated planks. The elongated structures do not resemble tubes or wires they actually have wide edges and are stacked or grown attached to each other. This result gives a hint regarding the influence of light on the growth of the ZnO and confirms the hypothesis that the LED light plays a major role in the growth of the ZnO structures.

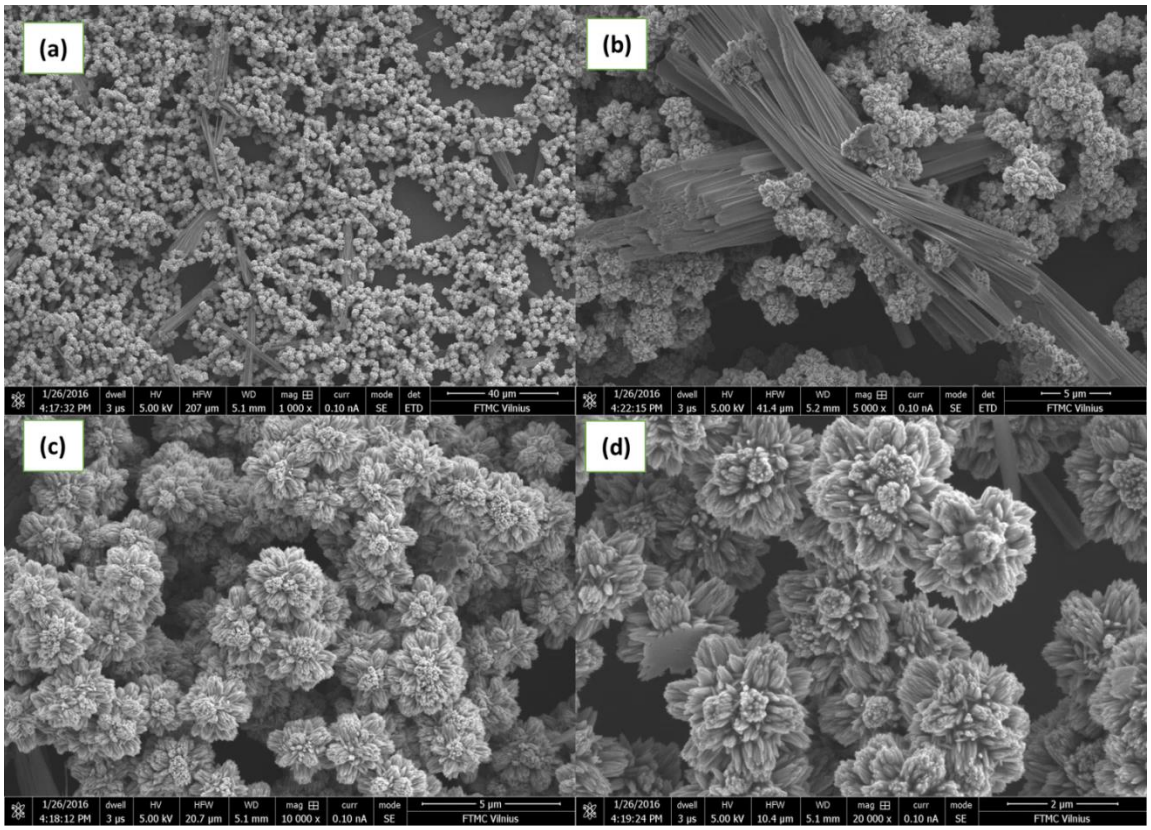

Figure.6.37 the ZnO structures synthesized in the dark using the same concentration 1:10 Zn(ac) and NaOH. (a) view with 1000x magnification (b) more detailed view of the ZnO flowers and elongated structures. (c) and (d) packing and more detailed view of ZnO flowers.

We also saw that concentration plays an important role. Previously using different concentrations the ZnO did not grow in the dark at all and now it has been demonstrated that using a higher concentration there are actually ZnO formations. The question is what will happen if we change the concentration again and grow the same ZnO in the dark? Fig.6.38 shows the SEM images of the ZnO synthesized in the dark but with a different molar ratio: 1:5.5 Zn(ac) and NaOH respectively. The structures seem to be different but let's take a more detailed investigation. In Fig.6.38 the ZnO does not look like bubbles, wires, tubes or flowers. The structures are rather distributed randomly and do not really resemble any hierarchical ZnO formation. The structures look like leaves or sheets that did not form into more complicated structures. Few "artifacts" are constructed from the ZnO sheets and no complicated structures like in previous figures can be observed. This sample strictly contains one type of ZnO morphology.

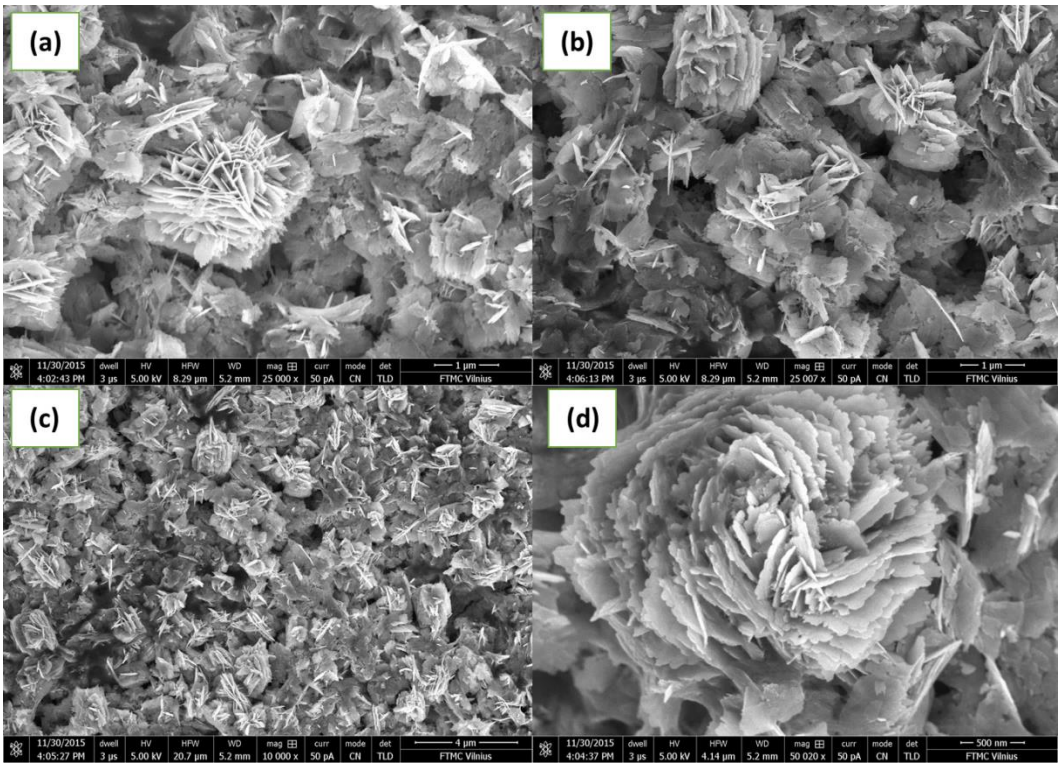

Figure.6.38 depicts the SEM images of the ZnO synthesized at room temperature in the dark using 1:5.5 concentration for the Zn(ac) and the NaOH respectively. (a) sheets of the ZnO assembled into "artifact". (b) and (c) more detailed view of sheets showing no bubbles or flowers. (d) another assembled ZnO sheet "artifact".

This one type of morphology can be related to the concentration "barrier" of ZnO. No hierarchical ZnO structures can be grown in the dark in both cases. In the first case (Fig.6.37) only flowers and planks were observed and flowers cannot be called hierarchical either. The ZnO flowers in Fig.6.37 are rather microstructures with micro features on the surface and cannot be compared to those in Fig.6.33 where tetrapod-like formations have a 20-30nm thickness. This result gives new insight in to the growth and formation of the ZnO. All the samples went through the 12 hours synthesis process at room temperature. As demonstrated the above concentration and light plays an important role in the synthesis of the ZnO. But what about time? In the next subchapter the time as a factor in ZnO synthesis is considered and discussed.

6.7 Time as a Parameter Influencing Light-Induced Synthesis

It is known that time plays a great role in chemistry when we talk about synthesis [198]. Time is important in every chemical process. The longer the time for the synthesis the more different the outcome this could be positive (right reaction time) or negative depending on the type of synthesis and the reactions involved. However, in our case we have a light and matter interaction which makes the experiment more specific and complicated. Fig.6.39 shows the SEM images of the ZnO synthesized under the RGB code for 18 hours. The concentration was 1:10 Zn(ac) and NaOH respectively.

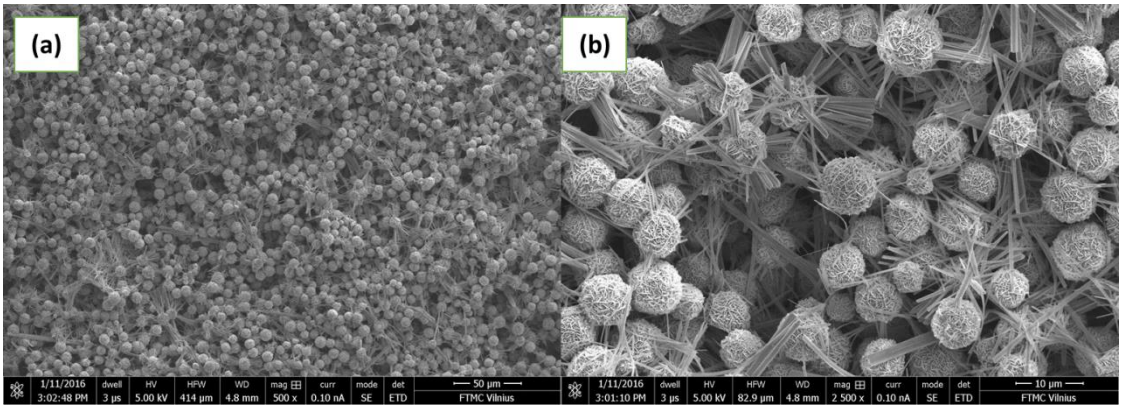

Figure.6.39 depicts SEM images of ZnO bubles with wires growing out. Synthesis at room temperature for 18 hours under RGB code. (a) panoramic view of ZnO bubbles with wires growing out. Scale bar 50µm (b) shows ZnO structures having wires sticking out. Scale bar 10µm.

The structures are really specific. They looked like bubbles before (Fig.6.33) but with wires growing out of them. The images before of the ZnO bubbles showed the samples of the ZnO grown for 12 hours under room temperature. These bubbles are the same in shape as the previous ones but with one different detail: they have wires growing out. The only one factor that was different here was time. Instead of 12 hours it was 18 hours at room temperature using the same LED. One interesting detail would be the surface morphology of the ZnO bubble. Fig.6.40 shows the ZnO zoomed bubble with wires. The wires look “soft” curved and the surface morphology is different from the samples before. There are no “trees” as in Fig.6.33 or flowers or sheets. It has the surface of leaves that do not resemble anything. The whole structure resembles the disordered structure of a flower. Now we have seen the effects of one wavelength, the effect of the RGB code and also the synthesis in the dark and the results when the time interval is changed.

Next it would be logical to try to decrease the time by a few times and increase it under the same conditions (concentration and LED).

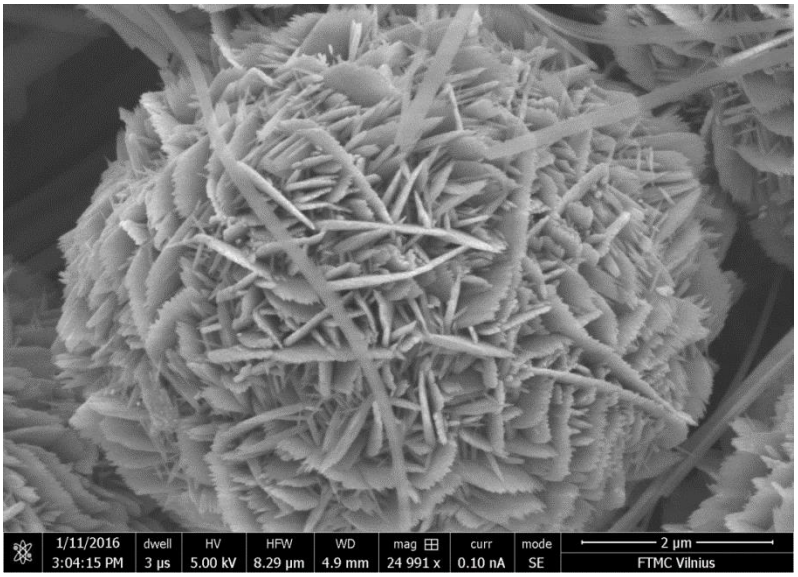

Figure.6.40 shows a more detailed SEM image of the ZnO with wires growing out.

Now let's decrease the time of the synthesis and see what happens if we decrease it 4 times from 12 hours to 3 hours? Also at the same time let's conduct the synthesis by increasing the time 2 times from 12 hours to 48 hours. In both experiments the same type of LEDs were used. Fig.6.41 shows the SEM images of the experiment. The results are very similar but with one different detail. In the ZnO sample that was synthesized for 48 hours we can see long wires sticking out from the bubbles. While for 3 hours the ZnO sample showed the same results as in the 12 hours synthesis experiment. After 3 hours and in 12 hours the ZnO LED synthesis is the same which indicates that bubbles are formed at the initial stages of the synthesis. However, after 48 hours time proves to be a very important factor. Increasing the time did not break the bubble structure but rather "upgraded" it. This result gives a very important insight into the growth and formation of the ZnO structures that has not been reported before.

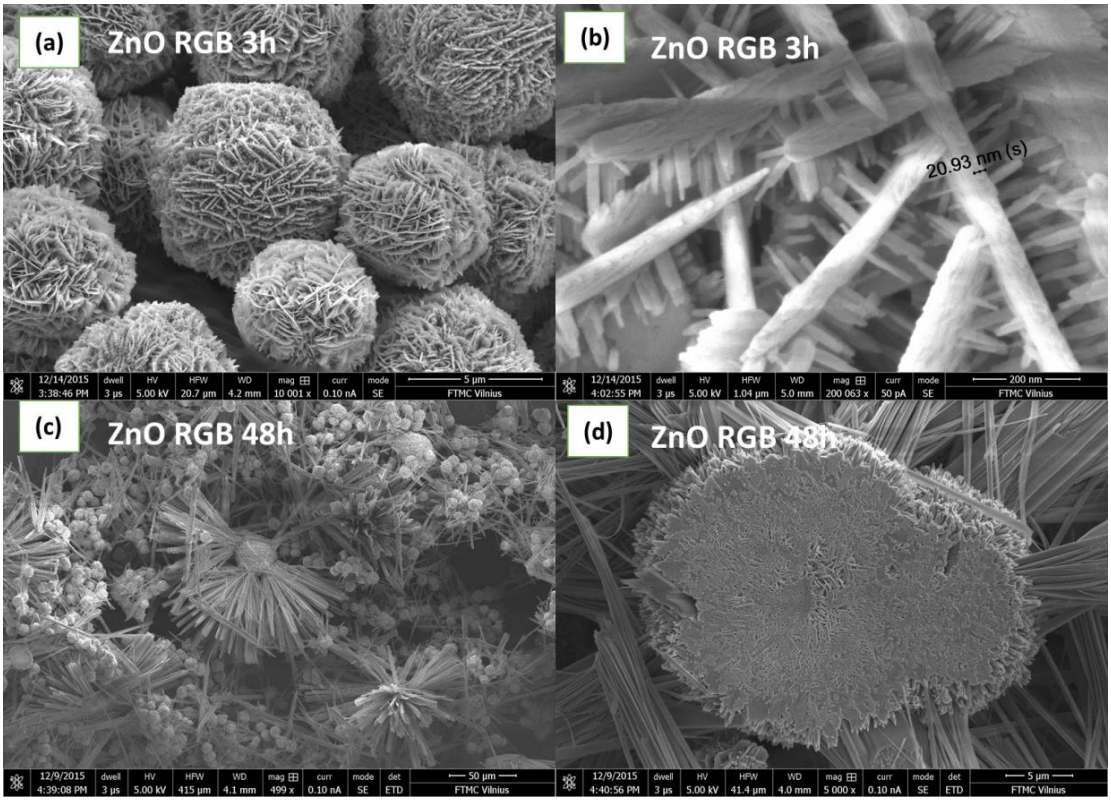

Figure.6.41 shows the ZnO synthesized at room temperature for different time intervals using the RGB code. (a) the ZnO synthesized for 3 hours at room temperature. (b) zoom or the surface of the ZnO bubble. Walls are as thin as 20nm. (c) the ZnO synthesized for 48 hours at room temperature. The structures contain long wires. (d) a zoom of the "broken" bubble indicating that wires grow from inside of the structure.

This result also gives us information about the growth path of light-induced ZnO synthesis. At first the ZnO nanometer range wires are formed then due to the large surface energy they form into microscopic bubbles. After the micro bubbles are formed the structures start growing from the stage they are in to more complicated hierarchical structures until the zinc ions are consumed. But in the case when we extend the synthesis time it appears that the ZnO are partially destroyed and released ions form wires. The solution in the synthesis of the ZnO (in the present experiments) was basic. But the pH in this experiment is not really important since we are trying to figure out the light and morphology connection. Measuring the pH would only give us the value of the acidity which would also change before and after the reaction so the pH in the current case does not play a major role.

6.8 Hydrothermal vs Light-Induced Synthesis Under the Same Concentration

Now let's make the ZnO synthesis hydrothermally but keep the same concentration as before. Let's keep the same time for 12 hours and the same concentration of 1:10 Zn(ac) and NaOH respectively. Fig.6.42 shows the SEM image of the ZnO synthesized hydrothermaly and under the LED light. For better visual analysis let's have a transparent blue scale bar and size distribution graphs. The SEM results reveal that room temperature gives more uniform bubbles. While the hydrothermal synthesis of the ZnO gives a rise of different sizes ranging from 1 to 4 micrometers. From this result it seems that the light-induced synthesis provides an advantage in the synthesis of ZnO.

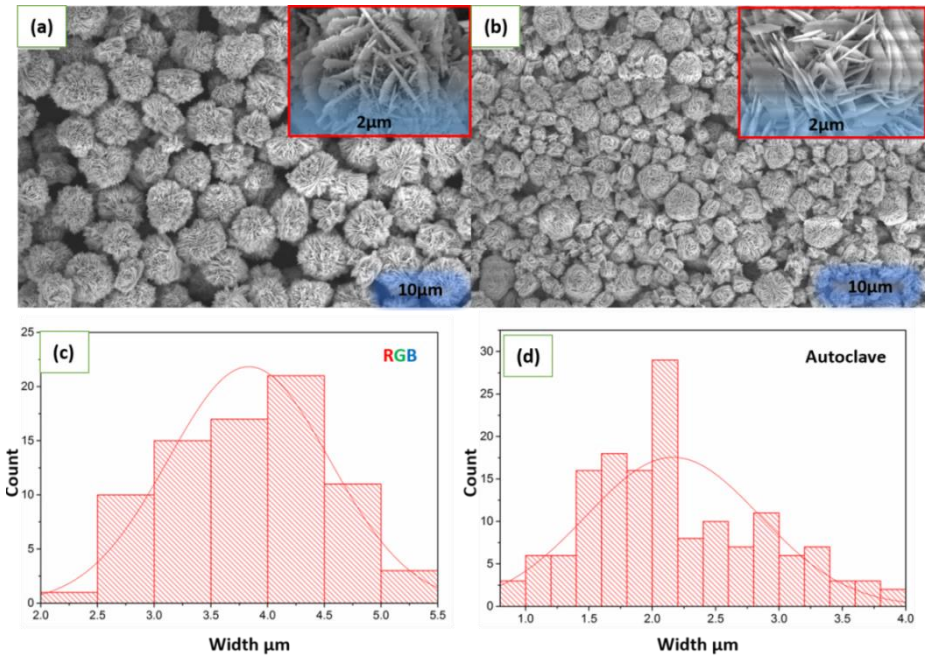

Figure.6.42 depicts the SEM images of the ZnO. (a) synthesized via light-induced synthesis RGB for 12 hours. The inset shows a detailed view of the surface of the bubble. (b) the ZnO synthesized for 12 hours via the hydrothermal method. The inset shows the surface of the bubble. (c) is the size distribution of ZnO light-induced synthesis. (d) the size distribution of the ZnO hydrothermal synthesis.

However, the ZnO bubbles synthesized via LED are larger but have a more complicated surface texture Fig.6.42 inset. And the ZnO synthesized hydrothermally have a smoother wall on the surface (no teeth). The hydrothermal synthesis of the ZnO gives a greater size distribution and a less complicated surface morphology which in this case means that the structures also exhibit a smaller surface area. It has been demonstrated that the light actually has an influence on the synthesis of the ZnO structures and also other factors like the synthesis time and the precursor concentration

play an important role. The question is why when using the same concentration of ZnO do the bubbles differ in size and surface morphology? To answer this we have to imagine what is going on in the solution during the synthesis. In the water ions are floating around and there is a Brownian motion. The higher the temperature of the solution the greater the motion of the ions. Let's not forget that we did not use any stirrer and the synthesis was carried out in the vial which was not stirred or moved in any way. Then conducting the same synthesis with the stirring should produce smaller bubbles of the ZnO. If this statement is true then at room temperature and conducting the RGB for a 12 hours synthesis should give us either distorted bubbles or smaller or both.

6.8.1 Influence of the Movement of the Ions in the Solution

During the hydrothermal synthesis ions in the solution see no light and under the 180^0C temperature the water is boiling and the whole solution are "moving". When water is boiling it is evaporating from the inside. Because of that we have bubbles when the water is boiling. Now this is an important moment in the synthesis of the ZnO. We have a steel autoclave which is Teflon lined and has a lid. When the water is boiling it condensates on the lid and then falls back in to the solution. The solution is boiling and producing bubbles from the bottom of the autoclave. Bubbles (not to be confused with ZnO bubbles) are rising up and exploding. The process takes 12 hours non-stop. The Brownian motion at 180^0C is of course much greater than at room temperature. However, the important factor is the movement of the bubbles while the solution is boiling. For a moment let's forget about the Brownian motion and think only about the mechanical movements. Now let's travel with only one object of the synthesis the "bubble" while the solution is boiling. When the bubble is going up from the bottom of the autoclave it is moving/disturbing all the ions inside the solution. And now let's imagine hundreds of bubbles with different sizes disturbing the solution. What would happen with the final product? The answer is the final product will not have a chance to form properly. The pre-formed small nanometer sized ZnO structures will try to assemble together but they would face a powerful mechanical force. Regardless of the force, nanoparticles or nanostructures will assemble anyway but the assembled structure would be different from that of the ZnO synthesized without disturbances.

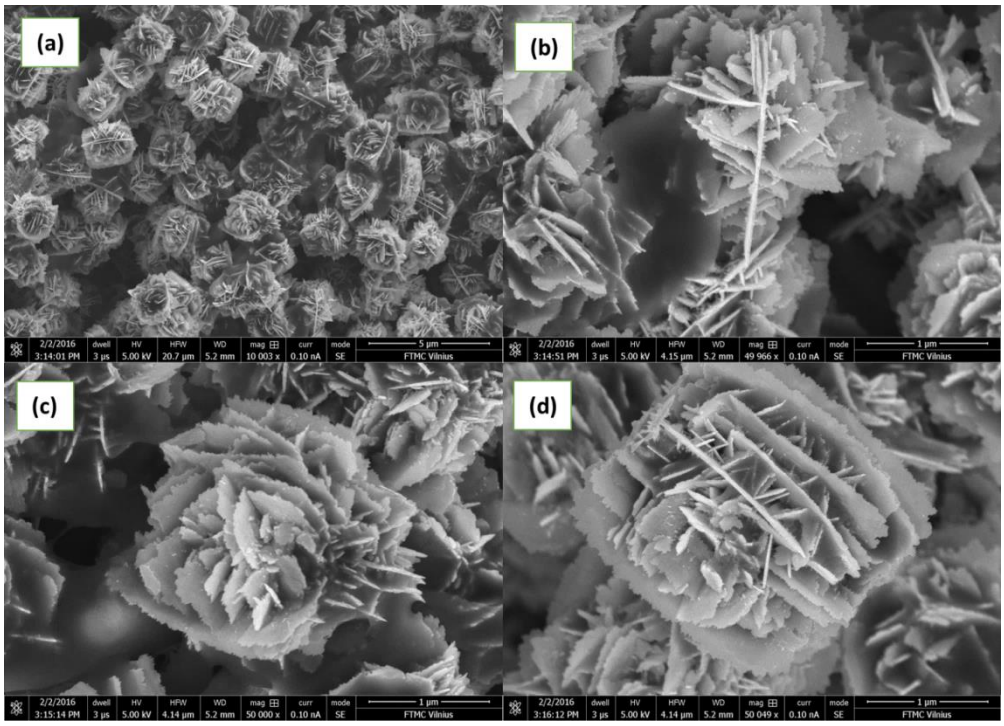

Figure.6.43 the ZnO structures synthesized at room temperature under the RGB light code while mixing with a magnetic stirrer at a speed of 200rpm. (a) the ZnO still maintain a round shape but slightly distorted (b) a zoom of the ZnO structure. (c) and (d) zoom of the round shaped ZnO structures.

If these thoughts are close to the truth then stirring during the synthesis of the ZnO would give different result from that without stirring. Fig.6.43 shows SEM images of the ZnO synthesized at room temperature and at a stirring speed of 200rpm for 12 hours (also RGB code). This result actually gives a hint for future experiments and shows the importance of mechanical movements in the synthesis of nanoobjects. And now let's remember the Brownian motion and combine it with the bubbles during the synthesis. The combination could give a variation in the size distribution of the ZnO final products as shown in Fig.6.43 (b) and (d).

6.8.2 Heat as Light

The previous results demonstrated the importance of mechanical movements in the synthesis of the ZnO but still it did not answer all the questions. In the hydrothermal synthesis there was no light but the structures were similar to that of those synthesized by the light-induced process. The ZnO structures were a bit distorted but were similar in shape and morphology to those synthesized using the LEDs. Why didn't the hydrothermal synthesis give similar structures to those synthesized at room temperature but in the dark? The answer is very simple: because there was actually a

light in the autoclave. When we heat up objects they emit infrared photons which are not visible to the naked eye. The influence of light intensity was not investigated in the present work (it is beyond the scope of this thesis) but we can still make a mental simulation of the hydrothermal growth of ZnO. The greater the temperature the higher the IR intensity which can affect the growth of the ZnO. The reason why the structures have a greater size distribution is because to heat them up to 180^0C was programmed at a rate of 10^0C per minute. This means that to heat up the autoclave to the target temperature we would need like 18-20 minutes (roughly). And also cooling those down took around 30 minutes. Although this does not sound significantly important it also has an influence on the size distribution of the ZnO bubbles.

6.9 Summary

It was demonstrated the synthesis of the ZnO at room temperature using the LED light. The ZnO is not visible-light active material and in theory should not be influenced by light sources during the growth. However, the interaction between light and the ZnO do not happen it happens between water-light. The presumption was checked stirring the solution at room temperature. The result gave smaller structures which demonstrate that the mechanical "disturbance" during the synthesis has a great influence over the entire ZnO morphology. Also an important question rose regarding the hydrothermal syntheses of the ZnO. What role the heat is actually playing during the ZnO synthesis? In order to create a strong crystal formation model important questions regarding the growth and the formation of the crystals should be answered which will be done in the next chapter.

Chapter 7 Growth Model and Formation of the Structures under LED Light

In this chapter the growth process and possible scenarios introducing the defects in the lattice will be discussed. Some models are also proposed and discussed. The growth habit is a crystal habit to grow in one or another way. Some nanoparticles can be grown in a particular shape like triangles for instance. The silver nanoparticles can be grown with a few main shapes: wires or rods, triangles and spheres. Spheres are the most common shapes in nanosynthesis. Since the spherical nanoparticles contain the lowest energy this shape is the most prevalent. All the objects and structures in Nature are trying to occupy the lowest energies because they are the most stable. Usually when templates are added to the synthesis of the nanostructures the nanoobjects take the shapes according to the templates used. For instance, if we are going to synthesize nanowires we will need to use either a polymer which can provide one dimensional growth or we can use a solid template with nanoholes and synthesize nanowires inside the template then remove the template and use the structures as has been described in the Literature review in the Template assisted synthesis in 2.7. But what if we do not have any template and the nanoparticles are still triangular or cube shaped? The answer can be found in a property of the crystals that is called the "growth habit". The growth habit is something that a crystal is used to. It means that crystals can grow in a particular way with specific shapes and then into bigger nano or micro particles.

7.1 Crystal Growth and Characteristics

The crystals can be grown on a various surfaces or in colloids. If the particle is grown on a surface, then the kind of surface and shape of the surface becomes important. However, if the growth occurs in colloid suspension then the story is a bit different. Nanoparticles can change their growth path if they are distorted at the initial stages of growth. Also they can change the shape because of the applied conditions like templates for instance. It has been reported that the process starts with nucleation [220]. Then the secondary growth steps occur. The surface attachment energy plays a great role in the growth process. And the crystal growth rates along different crystallographic orientations differ. One of the main theories describing the growth habits is called the Bravais-Friedel-Donnay-Harker or (BFDH) law [221]. According to this law the crystal morphology is dominated by the slow-growing faces. And the

fast growing faces may grow out too fast and will not be represented at the final crystal growth habit (at the end of the growth). Curie and Wulff suggested that the equilibrium shape of a crystal is the shape that minimizes its surface energy[222]. Another very important theory is the Hartman-Perdok theory describing the relation between the crystal structure and the crystal morphology [223-225]. The Periodic Bond Chains or the PBC is a strong bond between crystalizing units (molecules, atoms, clusters, ions). Crystals also have faces which can be classified into F(flat), K(kinked) and S(stepped). F faces grow very slowly and are most important in the formation of the crystal and contain at least two PBC's. K faces grow fastest and do not contain any PBC. And S faces are between F and K. The crystals may have the same growth faces but different habits. Also different combinations of faces may occur in one crystal. In Fig.7.1a depicted the 2D crystal where the *a* bond is stronger than the *b* bond. The crystal in Fig.1a will be elongated in the direction of *a*. Fig.7.1b shows the F, S and K faces on the crystal.

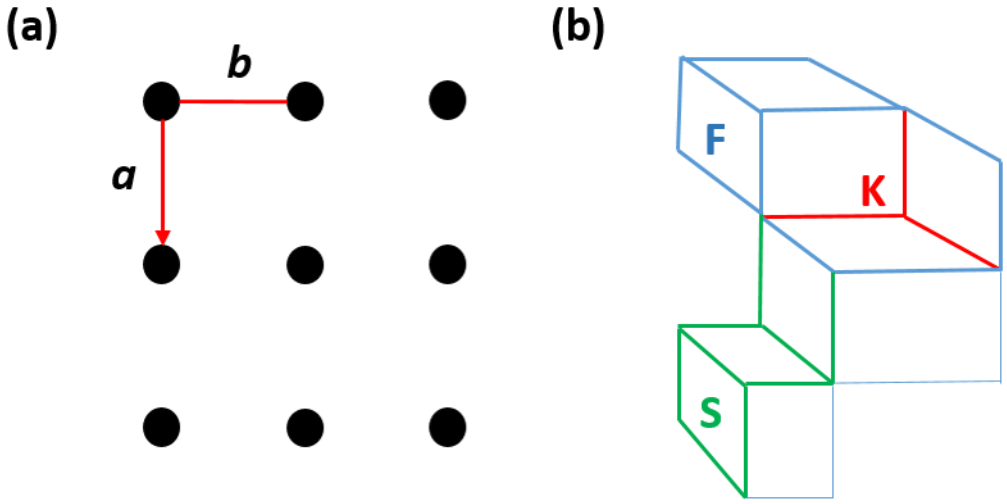

Figure.7.1 depicts the (a) crystal in which the *a* bond is stronger than the *b* bond. (b) depicts the F, S and K faces in the crystal.

The atoms form lattices and then we have growth faces and finally crystals which can be shaped in a variety of ways. The role of light here was poorly investigated. Such research would require both experimental and theoretical investigation. Theoretical investigation of the crystal growth is beyond this work and the aim of the present work is to show the importance and the influence of the light in the synthesis of Ag, Ag-Au

and ZnO materials. According to the results of light-induced synthesis of ZnO and Ag it seems that light influences the chemicals or clusters (clusters of the ZnO or the Ag) while they are in an "embryo" stage. However, this statement needs more discussion.

7.1.1 Nanoparticle Formation

During the nanoparticle formation process, we have chemicals dissolved in liquid (in our case) and then we have atoms "gathering" into lattices. Firstly, they make chemical bonds and then we have a particular type of growth into bigger crystals and nanoparticles with spherical, triangular or other shapes. Light can create or break the chemical bonds and interact with the matter in a particular way as some works suggest [226]. As has been demonstrated with silver it is possible to control the shape and size by varying the wavelengths of light [227]. There are no restrictions prescribed for the ZnO and some other materials. We cannot presume that light somehow "captures" the atom and forces it to go in a particular place in the lattice as it is possible to do with the bricks when building a house. On the other hand, if the light creates a defect then the growth might be different during the rest of the process. This is possible since most of the materials in this work had a reducing agent. In the case of the Ag it was sodium tricitrate which interacted with light and produced a slow reduction for the Ag atoms. In the case of the ZnO we also had NaOH and ethanol. These chemicals might form a new zinc containing compound and then release it under the light. Or the light might modify the surface energy of the atoms on the lattice thus changing the further growth direction and shape of the crystals. Furthermore, both of the mentioned schemes might be involved and greatly influence the process. However, we do not have proof for any of these growth scenarios and the interruption of the computational chemistry is greatly desired here. For the synthesis of the Au in oleic acid the growth could be influenced simply by the oleic acid and also the combination of the nitric acid which could trigger the isomerization of the oleic acid thus creating the distribution of the angle-containing molecules and the straight molecules. This mixture of angles could lead to the growth of the Au triangles and smaller particles which were in greater contact with the angle-containing molecules of oleic acid.

7.1.2 External Factors

A very important part of the synthesis is the influence of external factors such as temperature or light. Hot objects (like the steel autoclave) emit heat or in other words infrared light which is invisible low energy photon. When the ZnO or the Ag is

synthesized the increase in temperature guarantees to speed up the process or sometimes the reaction does not even occur without temperature. But as was demonstrated in this work, temperature can be replaced with light and room temperature is enough to manipulate the experiment. Using light is better than the temperature since we can switch it on and off rapidly so the reaction can be greatly improved. The defects are usually **screw dislocations, grain boundaries** and **crystal twinning.** As was mentioned before the investigation of what exactly is going on in the system requires quantum mechanics and chemical simulations which are beyond this work. In the next subchapter we will introduce a model of the ZnO growth and the discussion of Ag formation will be given. Also a light-induced change of the polymer film morphology will be analysed and main questions will be answered.

7.2 The Formation of ZnO Structures

Now let's forget about the crystal growth for the moment and imagine the growth from the nanosize to the hierarchical structures of ZnO. Let's analyse only ZnO now. As mentioned before zinc oxide is a white material that only absorbs ultraviolet light. The ZnO does not absorb visible light. If light is not absorbed then we cannot analyse the system from the point of light-matter interaction. As we saw before in Fig.6.36 and 6.41 ZnO bubbles are made of nanosized wires inside. Nanowires form solid structures and then grow into bubbles with a complicated surface texture. What happens before the nanowires are assembling into one structure will not be investigated here since it does not influence the latter synthesis path and the final product is still the ZnO bubble. In Fig.7.2 the model of light-induced synthesis of ZnO hierarchical structure is depicted. First step 1 is the assembly of the ZnO wires into a "bush" and the growth of a pre-bubble structure (bush-like). Step 2 is the growth of the ZnO around the pre-formed bubble. At this stage the ZnO fills the gaps between the branched-assembled wires (bushes). Then something like bubbles forms. The bubble does not contain a complicated surface texture yet. After 12 hours (from step 2 to step 3) the ZnO bubble is formed with a complicated-hierarchical surface structure (step 3). After the hierarchical ZnO bubble is formed (after 12 hours) or if the process continues we have ZnO bubbles with elongated wires growing step 4. After 48 hours of growth ZnO structures like in Fig.6.39 are obtained. During the initial stages of the growth the ZnO nanowires initial structures (let's call them embryo ZnO) could assemble from the nanoclusters of the ZnO and form something more complicated.

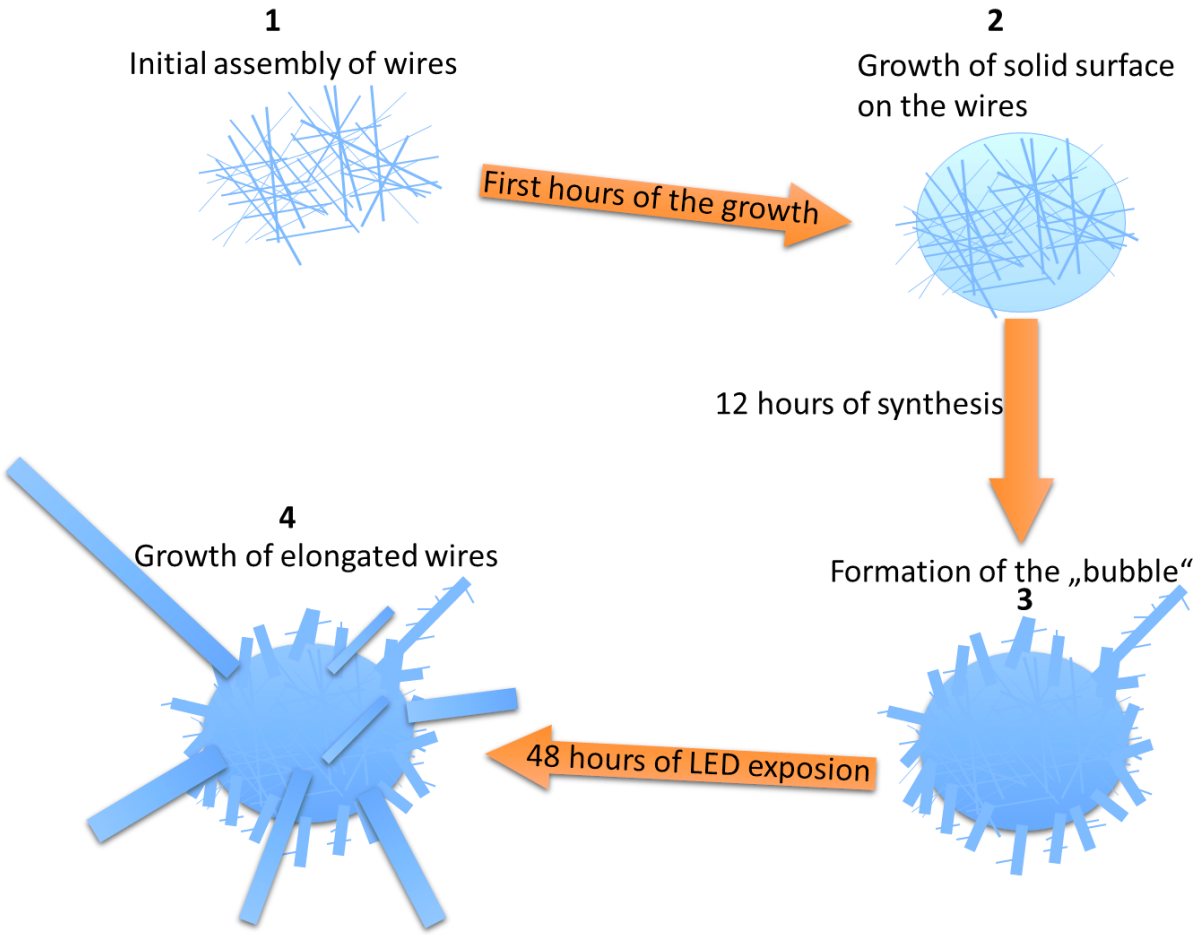

7.2 Figure shows a model of the formation of the ZnO under the LED light. First stage (1) initial assembly of nanowires into one clump. Step (2) growth and filling of the ZnO inside and around the wires. (3) The formation of the ZnO bubble on the surface of the pre-formed clump. Stage (4) is the continuous growth of the ZnO long wires out of the bubble after 48 hours of synthesis under the LED light.

And later those pre-formed ZnO embryo nanoclusters form structures as we saw following the path shown in Fig.7.2. Also another scenario of pre-formation is possible. The ZnO nanoclusters could grow into tetrapods and only then assemble. Or not assemble at all. The pre-formed embryo ZnO tetrapods could grow into a more complicated bush-like structure and only then follow the path model in Fig.7.2. Regardless of the initial starting embryo structures, we will have the same outcome. The model shows how the structures grow into hierarchical ZnO structures but it does

not explain the Ag and polymer structurations. The ZnO does not absorb visible light so it cannot be called photosynthesis.

7.3 Influence of the Light on Electrons

In the case of the Ag there is a visible light related process with sodium tricitrate. But for the consistency and precision let's consider all the light-induced syntheses processes here. So as mentioned the Ag can absorb visible light. When visible light is absorbed it is absorbed by an electron of the material. When it is reflected or scattered it is also because of the electron. But what happens when the light is reflected? What happens with the electron? According to some works there is a pressure of light [228, 229]. But that pressure of light is very weak and cannot influence usual objects. But in our case we do not have usual objects either. We have ions which are floating in the water. This system could be compared to something like space where there is no gravity. Of course ions and other molecules are affected by the force of gravity but they "fly" in the liquid freely and are not bonded to anything (until crystal growth). So here we can say that the pressure of light only has minor effect on the synthesis process. The experiment with the ZnO and also with the polymers demonstrated that there is "something" going on while the light is on and also when it is off. As a matter of fact this mystical "something" is required to explain the process. That "something" could be anything from the affected electron to the electron-electron interaction. Let's not forget that light is not causing the reaction to happen it is influencing the reaction or driving it into one or another way. Experiments without light have also proven to give the results (in the dark) but different from those under the LED light. So we are not really looking for light-matter interaction but searching for the ways light could influence the whole synthesis process. Light can actually not only influence but even modify electron-electron interaction with its electric field [230]. The reason why this concept cannot be applied here is because light modifies electron-electron interactions when it is very strong which is different from our case. When light is weak it is only capable of influencing electrons but not interactions. Also the time factor plays an important role here. Increasing the time of the LED exposure we modify the structures too.

7.4 Magnetic Component of Light

Let's imagine ions freely floating in the liquid at room temperature. If we increase the temperature due to the Brownian motion ions will move faster. So let's consider room temperature only since the experiments were carried out under that condition. Floating ions are not moving too fast and the solution is not mixed. The conditions are simplified as much as possible. Now all the ions have a charge which is either positive or negative. What would possibly affect the ions now? The answer is a magnet. On the other hand we do not apply a magnetic field to the synthesis. Let's speculate that a very weak magnetic field from the light is capable of making a small influence on the system. After 12 hours of synthesis that influence would be greater than after an hour and after 48 hours even greater. For such a brave statement-speculation we need proof that would confirm this at least 50% otherwise it cannot be considered. Fisher and Rand reported light affecting transparent dielectric and showed that static dipole moments can be produced [231]. The important factor is that the intensity of light does not have to be huge to affect the system. This fact in turn could explain that after exposure to the LED light the ZnO changes the growth from a normal direction to a slightly different one which in the end forms hierarchical structures.

7.5 Absorbance of Light by Water

Distilled water is a transparent substance and it is considered that it does not absorb visible light. And it doesn't. However, it absorbs mostly on the infrared region and has its highest peaks there. But as was shown elsewhere the water absorbance spectra has few little peaks in the visible region [232]. Researchers used highly pure water and two peaks at around 600nm and 650nm were observed. What happens when water absorbs light? Depending on the wavelengths of light water molecules can rotate or vibrate in different directions. Since we have very small peaks in the visible range they cannot greatly influence the reaction and it will require more time to do so. As was demonstrated before in Fig.6.43 even a magnetic stirrer can cause changes to the growth while mixing. When there is mechanical mixing it is mixing only in one direction-spinning. Now let's imagine slightly vibrating or bending water molecules due to the LED light. All the water molecules vibrating at once would cause a great influence on the synthesis of the ZnO. And the longer the vibration the greater the influence will be.

7.6 The Most Likely Scenario to Happen

While speculating on the possible scenarios and influences of the external factors brought by the LED light we cannot isolate the most efficient one. It is likely that all the factors influence the growth at once. Water molecules vibrating even slightly would cause a change and increasing the LED light exposure time will only increase that effect. The light creating effect of a magnet is also possible. Not by Heiseberg's uncertainty principle but by the interaction light-transparent dielectric. In our experiment the transparent dielectric is a glass vial. The light pressure is also an important factor. Knowing that the system is sensitive to external factors (even to weak ones) we can say that there is a high chance that it could be influenced by even such a weak factor as the pressure of light. Combining all these possibilities we can say that the whole system is basically slightly influenced by very tiny mechanical vibrations which are caused by light. And since they are extremely small they need more time to cause changes on the morphology of the ZnO. Let's also not forget that the objects that are being affected are also very tiny like ions.

7.7 Summary

It was shown that light can affect the system and influence the formation or the growth of the ZnO at room temperature. The existing models of crystallization and crystal growth were discussed. It would be difficult to link the light-induced synthesis of the ZnO to any of the models. On the other hand such factors as molecular and mechanical vibrations can greatly affect the entire synthesis process. This is an interesting effect which has not been used before and has potentially great influence on nanoscience in the near future.

Chapter 8 Conclusions

As it was demonstrated in this work synthesis and self-assembly can be made at room temperature. Synthesis of nanosized objects has been reviewed and most popular synthesis strategies were discussed in detail and analyzed. Advantages and disadvantages of every method were highlighted and analyzed. Novel method of Light-induced synthesis was introduced in the present work. It was demonstrated that light-induced synthesis can be as efficient as any other well-known synthesis method. Room-temperature is enough for the light-induced synthesis of hierarchical nanostructures. ZnO, Ag nanostructures can be synthesized at room temperature using simple low power LED. This fact makes method very unique and highly efficient since it is very cheap and does not require any specific equipment or dangerous chemicals. ZnO is neither light-sensitive nor even absorbing the visible wavelengths. The effect is attributed to the vibrations of the water molecules. This fact makes any water-based synthesis very specific because nanoparticle precursors (chemicals) can be used to synthesize hierarchical nanostructures in water. Light-induced synthesis of ZnO was compared to the hydrothermal synthesis of ZnO. Results demonstrated that light-induced synthesis has an advantage over the well-known hydrothermal method. Light-induced synthesis gives lower size distribution of ZnO bubbles and greater surface area. Synthesis of Ag nanoparticles was known before but not very well investigated. Synthesis of Ag nanoparticles using light usually linked with the surface plasmon polaritons that appear on the noble metal nanoparticles and that can influence the growth of the crystals. Now the growth process can also be attributed also to the vibration of the water molecules. Also using LED light it was possible to change the polymer film morphology in the solution of chloroform. The effect is investigated using P3HT and PTB7 and shown to have dependence over the wavelength of light. The film morphology was crater-like and using a red LED decreased the diameter of the voids while the blue LED increased the diameter. This effect requires more investigation with more solvents and polymers. Present work proved that light-induced synthesis is as efficient as other popular and well-known methods. This work puts light-induced synthesis on the same level with most popular synthesis methods and raises the question about light-matter interaction. This is cheap and efficient synthesis method to many liquid chemistry based materials and a variety of structures.

8.1 Highlight of the Most Important Aspects of the Thesis

1. Typical nano-synthesis methods were reviewed and discussed in detail, including VLS, sol-method, hydrothermal, photochemical and template-assisted methods.

2. The morphology control of semiconducting polymers via a mixed-solvent approach was demonstrated. Changing solvents and amounts of the solvents can tailor the topography of the polymer films.

3. It was also confirmed that the morphology of semiconducting polymers could be controlled via a light-induced approach: P3HT/$PC_{[70]}BM$ in the chloroform and PTB7/$PC_{[70]}BM$ in the chloroform at room temperature. Using low power LED light, the morphology of the polymer films was successfully changed.

4. The template-assisted synthesis of Au, Ag and CdS nanostructures was demonstrated using PPI type dendrimer, e.g. Au nanoparticles using oleic acid at room temperature. One step synthesis was proven to be simple and efficient for the Au nanoparticles. Ag nanoparticles were synthesized using PPI-G4 dendrimer at room temperature, with narrow particle size distributions. CdS quantum dots were also synthesized using PPI-G4 dendrimer, and self-assembly of CdS quantum dots into nanofibers with 9μm length was demonstrated.

5. The light-induced synthesis was carried out with Ag and ZnO nanostructures at room temperature: Ag nanoparticles were grown in aqueous solution without the use of any template. Light-induced synthesis allowed synthesizing Ag nano-saws and nano-wires, while the synthesis of ZnO was proven to be efficient and formed different morphologies with narrow size distributions. This experiment demonstrated that light-induced method has a potential for the growth of ZnO at room temperature. This is a cheap and efficient method to grow hierarchical nanostructures at room temperature.

6. The advantage of Light-induced synthesis and control over the hydrothermal method was demonstrated. LED light can be switched on and off at any moment during the synthesis which is possible to tailor the growth of nanostructures if required.

7. The synthesis model of the ZnO was proposed based on the experimental results and detailed investigation of the formed nanostructures.

8.2 Important Remarks

The synthesis of nanostructures demonstrated promising results along with key aspects of synthesis itself. Important aspect of the synthesis is the precision. Also impurities play an important role. Small amount of dust in the solution or any impurity from the chemicals (important purity grade) can lead from slightly different to significantly different outcome. If let's say CdS nanoparticles are synthesized then the chemicals should be chosen to provide as less as possible of residues after the reaction. Ions that do not react with the main chemicals still can influence the final product due to the electrostatic interaction in the solution. In the synthesis of Au nanostructures the importance should also be given to the template material. It is not necessarily that oleic acid or dendrimers can be used. Almost any polymer can be used for the template-assisted synthesis of nanoparticles. Any polymer that can be dissolved in the solution with Au salt can be used for the synthesis. However, every molecule will have different interaction with the crystals of Au and this fact should be taken into consideration. During the growth of the crystal (CdS or any other nanoparticle) organic molecules can block the growth of a specific facecets of the crystal. This results in forming specific size and shape of the final nanoparticles. In order to understand the process in detail and be able to predict the future outcome of the nanoparticle synthesis measurements of the product should be taken at some time interval. Initial nanoparticle formation happens fast at the start of the synthesis. But it will take some time before the final result. If the structure is hierarchical then before the final structure is formed there will be at least few steps of the growth. So nanoparticles can be "catched" and characterized during every step of the synthesis. This strategy can help in creating growth model of nanoparticles.

8.3 Morphology of the Polymer Films

Another important aspect in the nanostructuration is the control of the morphology or the topography of the polymer films. As it was demonstrated previously in this work change of the polymer film morphology can be achieved while the polymer is in the solution. This can be done by using different solvents and solvent mixtures or by light. In the case of solvent-approach the polymer is dissolved and has certain arrangement of the molecules in the solution due to the solvent. When solvent dissolves the polymer its molecules float freely in the solution and have certain distance. This distance is defined by a solvent. When we have let's sat 2 solvents with different dissolving

properties (50/50 for instance) then both of the will influence the polymer molecule but in a different way. And if we deposit thin polymer film from the solution of 2 solvents polymer molecules will “settle down” on the substrate and will have different arrangement. The final result will be the change of the whole film morphology. Mixing more solvents together may lead to improvement of the thin film physical properties or to more negative results too depending on the solvents and solvent amounts chosen. In the case with light-induced polymer morphology change the important factor is that there is a light absorbance of the material [233]. If there is no light absorbance then light-matter interaction cannot happen and the system of molecules cannot be influenced by light.

Chapter 9 Suggestions for Future Work

As demonstrated in the present work light-induced synthesis and nanostructuring are unusual for the ZnO and polymers. The proper detailed answer to what is actually going on at an atomic or molecular scale is tricky. The designed set of experimental works in the area of photochemical synthesis of the ZnO and the Ag might give a proper answer and help to build a more precise growth model. In the future more materials should be involved in these experiments. Oxides combined with noble metals in alloy nanoparticles and polymers might give an interesting picture of the future of nanotechnology. The important experiment would be trying more different concentrations of the same material and for the same wavelength of light and then concluding the results. The greatest achievement in this light-induced synthesis and nanostructuring would be obtained increasing the number of possible combinations of light wavelengths i.e. light codes. At some point in the experiment it should be possible to predict the next shape and design. Also changing the time interval of light codes and going from seconds to microseconds would be of great importance and interest. Also changing the intensity and polarity of the light sources during the experiment could give unexpected results. Using templates (polymers) could improve the synthesis and give more uniform particles or structures. The light- induced nanostructuring of the polymers should be more careful and precise since the great importance is also within the solvent parameters (such as capability to dissolve the polymer or the sensitivity to light). In this case it would not be possible to interpret the results without theoretical simulations in computational chemistry. This work showed that there is still a window for the new works in the area of light-induced nanosynthesis and nanostructuring and it awaits new works in this field.

9.1 Sound-Related Synthesis

Sound-related synthesis is of course only a suggested name for the sonochemical synthesis but there is an actual key difference. Sonochemical synthesis is a type of synthesis where ultrasound is used. Humans are not capable of hearing ultrasound as well as seeing infrared or UV light. As we used visible light in the experiments in the present work it would be logical to use sound waves between 30Hz and 20000Hz. As was demonstrated before Fig.6.43 the system is very sensitive to the changing external factors like mechanical stirring. Performing the same type of synthesis but using sound

waves instead of light would be very interesting. In order to conduct a proper experiment we need to eliminate as many factors as possible. If we are using light for the synthesis do not use any other sources of "disturbance" because it will be difficult or impossible to interpret the final results. So having a sound wave in the dark should be interesting since it would also vibrate the water (in the case of ZnO). Use sound codes in the way it was done with the light. Also change the intensity of the sound waves and the frequency and this would shed light on the influence of mechanical vibration related processes during the synthesis. To have stronger effect sound-induced synthesis could be performed in the petri dish. The Petri dish can be placed on a speaker and left for dome time in the lab. One sound wave can be used in order to see the difference and the effects during the first stages. Sonochemical synthesis has proven that it is possible to use sound for the synthesis of nanomaterials [234–236]. But ultrasound is still a sound and there are no rules that say music is not causing any effect on the synthesis of the nanostructures. Sound waves can make water vibrate which is visible when it causes waviness on the surface of a cup or any other dish. Sound-induced synthesis should be used in future experiments related to nanosynthesis.

9.2 Magnetic and Electric Field-Induced Synthesis

Among the mentioned synthesis methods the external field method should also be applied to the synthesis of the nanoobjects. The magnetic field can affect electrons of the materials and thus influence the synthesis process on a nanoscale. The magnetic field would probably be able to influence most if not all the nanomaterial synthesis processes. Every material has electron clouds and magnetic fields that can be great or very low. Every material would probably react in a different way. In the synthesis of magnetite nanoparticles the magnetic field would play a greater role than in the synthesis of gold nanoparticles for instance. Magnetic fields can be varied during the synthesis and do not really require any specific conditions to be applied. Copper coil can be simply used to put the vial inside during the synthesis process. Regarding the electric field it will be difficult to avoid it with giant electromagnets. For the electric field-induced synthesis tesla coil can be used as a source of electric field. Tesla coil is capable of transmitting an electric field on short distances and even lighting fluorescent bulbs. Placing the vial in the tesla coil would surround it with an electric field. It is

also possible to create an electric field by placing two electrodes in the liquid. But that is a more complicated process which would involve electrodes in a chemical reaction.

9.3 Combinational Synthesis Method

By combining one or other mentioned synthesis methods could bring an entirely new and cheap nanomaterial synthesis method. Let's say by using light we can get ZnO nanowires or nanoflowers. And by using a magnetic field we can get nanocrosses. Now combining these two methods by placing a light source into the electromagnet we may get a combination of these two morphologies. Something like elongated nanocrosses or naocrosses growing out of the ZnO nanoflowers. Also using more wavelengths of light would also help to understand the processes and answer the question "what is actually going on there?" IR and UV light sources shining at once and separately would give us information on how the crystals are changing their growth direction. In that case an investigation using X-ray diffraction could be used in order to see if the crystal facet is actually changing. Field assisted distortion or perturbation is very interesting and can be used not only to get the most efficient synthesis results and a "fancy" morphology of the nano or micro particle. This method will also open up a slightly new understanding of what's going on down there. This would also create new topics for PhD students and future research papers.

References

[1] A. S. Aricò, P. Bruce, B. Scrosati, J.-M. Tarascon, and W. van Schalkwijk, "Nanostructured materials for advanced energy conversion and storage devices," *Nature Materials*, vol. 4, no. 5, pp. 366–377, 2005.

[2] Q. Zhang, X. Jiang, D. Tong, S. J. Davis, H. Zhao, G. Geng, T. Feng, B. Zheng, Z. Lu, D. G. Streets, R. Ni, M. Brauer, A. van Donkelaar, R. V. Martin, H. Huo, Z. Liu, D. Pan, H. Kan, Y. Yan, J. Lin, K. He, D. Guan, "Transboundary health impacts of transported global air pollution and international trade," *Nature*, vol. 543, no. 7647, pp. 705–709, 2017.

[3] W.-W. Li, H.-Q. Yu, and B. E. Rittmann, "Reuse water pollutants," *Nature*, vol. 528, no. 7580, pp. 29–31, 2015.

[4] T. Hillie and M. Hlophe, "Nanotechnology and the challenge of clean water," *Nature Nanotechnology*, vol. 2, no. 11, pp. 663–664, 2007.

[5] Y. Min, J. M. Caster, M. J. Eblan, and A. Z. Wang, "Clinical Translation of Nanomedicine," *Chemical Reviews*, vol. 115, no. 19, pp. 11147–11190, 2015.

[6] A. Z. Mirza and F. A. Siddiqui, "Nanomedicine and drug delivery: a mini review," *International Nano Letters*, vol. 4, no. 1, p. 94, 2014.

[7] R. Bogue, "Microrobots and nanorobots: a review of recent developments," *Industrial Robot: An International Journal*, vol. 37, no. 4, pp. 341–346, 2010.

[8] P. Khulbe, "Nanorobots: A review," *International Journal of Pharmateutical Sciences and Research*, vol. 5, no. 6, pp. 2164–2173, 2014.

[9] H. Savin, Repo, G. von Gastrow, P. Ortega, E. Calle, M. Garín, , and R. Alcubilla, "Black silicon solar cells with interdigitated back-contacts achieve 22.1% efficiency," *Nature Nanotechnology*, vol. 10, no. 7, pp. 624–628, 2015.

[10] A. Chen and C. Ostrom, "Palladium-Based Nanomaterials: Synthesis and Electrochemical Applications," *Chemical Reviews*, vol. 115, no. 21. pp. 11999–12044, 2015.

[11] X. Liu, Z. Zhong, Y. Tang, and B. Liang, "Review on the synthesis and applications of Fe_3O_4 nanomaterials," *Journal of Nanomaterials*, vol. 2013, Article ID 902538, 2013.

[12] H. Duan, D. Wang, and Y. Li, "Green chemistry for nanoparticle synthesis," *Chem. Soc. Rev.*, vol. 44, no. 16, pp. 5778–5792, 2015.

[13] X. Xue, Z. Zhou, B. Peng, M. M. Zhu, Y. J. Zhang, W., Ye, Z. G. Ren, X. Chen, and

M. Liu, “Review on nanomaterials synthesized by vapor transport method: growth and their related applications,” *RSC Advances*, vol. 5, no. 97, pp. 79249–79263, 2015.

[14] K. Watanabe, D. Menzel, N. Nilius, and H. J. Freund, “Photochemistry on metal nanoparticles,” *Chemical Reviews*, vol. 106, no. 10, pp. 4301–4320, 2006.

[15] R. T. Vang, J. V. Lauritsen, E. Lægsgaard, and F. Besenbacher, “Scanning tunneling microscopy as a tool to study catalytically relevant model systems,” *Chemical Society Reviews*, vol. 37, no. 10, pp. 2191-2203, 2008.

[16] E. Roduner, “Size matters: why nanomaterials are different,” *Chemical Society Reviews*, vol. 35, no. 7, pp. 583-592, 2006.

[17] G. Guisbiers, S. Mejía-Rosales, and F. Leonard Deepak, “Nanomaterial properties: Size and shape dependencies,” *Journal of Nanomaterials*, vol. 2012, Article ID 180976, 2012.

[18] V. H. Grassian, “When Size Really Matters: Size-Dependent Properties and Surface Chemistry of Metal and Metal Oxide Nanoparticles in Gas and Liquid Phase Environments,” *The Journal of Physical Chemistry C*, vol. 112, no. 47, pp. 18303–18313, 2008.

[19] X. He, X. Song, W. Qiao, Z. Li, X. Zhang, S. Yan, W. Zhong, and Y. Du, “Phase-And size-dependent optical and magnetic properties of CoO nanoparticles,” *Journal of Physical Chemistry C*, vol. 119, no. 17, pp. 9550–9559, 2015.

[20] S. Neeleshwar, C. L. C. Chen, C. B. Tsai, Y. Y. Chen, S. G. Shyu, M. S. Seehra, “Size-dependent properties of CdSe quantum dots,” *Physical Review B - Condensed Matter and Materials Physics*, vol. 71, no. 20, pp. 6–9, 2005.

[21] Z. Wang, L. Tang, L. H. Tan, J. Li, and Y. Lu, “Discovery of the DNA ‘genetic code’ for abiological gold nanoparticle morphologies,” *Angewandte Chemie - International Edition*, vol. 51, no. 36, pp. 9078–9082, 2012.

[22] S. Rackauskas, O. Klimova, H. Jiang, A. Nikitenko, K. A. Chernenko, S. D. Shandakov, E. I. Kauppinen, O. V. Tolochko, and A. G. Nasibulin, “A novel method for continuous synthesis of ZnO tetrapods,” *Journal of Physical Chemistry C*, vol. 119, no. 28, pp. 16366–16373, 2015.

[23] Y. Qiu, M. Yang, H. Fan, S. Lan, Y. Shao, Y. Xu, X. Yang, and S. Yang, “Synthesis and characterization of hollow gold tetrapods,” *Materials Letters*, vol. 65, no. 13, pp. 2022–2024, 2011.

[24] J. Lim, W. K. Bae, K. U. Park, L. Zur Borg, R. Zentel, S. Lee, and K. Char, “Controlled synthesis of CdSe tetrapods with high morphological uniformity by the

persistent kinetic growth and the halide-mediated phase transformation," *Chemistry of Materials*, vol. 25, no. 8, pp. 1443–1449, 2013.

[25] X. Bai, L. Li, H. Liu, L. Tan, T. Liu, and X. Meng, "Solvothermal synthesis of ZnO nanoparticles and anti-infection application in vivo," *ACS Applied Materials and Interfaces*, vol. 7, no. 2, pp. 1308–1317, 2015.

[26] G. N. Abdelrasoul, R. Cingolani, A. Diaspro, A. Athanassiou, and F. Pignatelli, "Photochemical synthesis: Effect of UV irradiation on gold nanorods morphology," *Journal of Photochemistry and Photobiology A: Chemistry*, vol. 275, no. 1 pp. 7–11, 2014.

[27] H. H. Park, H. H. Park, X. Zhang, Y. J. Choi, and R. H. Hill, "Synthesis of Ag nanostructures by photochemical reduction using citrate-capped pt seeds," *Journal of Nanomaterials*, vol. 2011, Article ID 265287, 2011.

[28] S. Iravani, H. Korbekandi, S. V. Mirmohammadi, and B. Zolfaghari, "Synthesis of silver nanoparticles: Chemical, physical and biological methods," *Research in Pharmaceutical Sciences*, vol. 9, no. 6. pp. 385–406, 2014.

[29] M. Zaarour, M. El Roz, B. Dong, R. Retoux, R. Aad, J. Cardin, C. Dufour, F. Gourbilleau, J. P. Gilson, and S. Mintova, "Photochemical preparation of silver nanoparticles supported on zeolite crystals," *Langmuir*, vol. 30, no. 21, pp. 6250–6256, 2014.

[30] A. K. Yetisen, H. Qu, A. Manbachi, H. Butt, M. R. Dokmeci, J. P. Hinestroza, M. Skorobogatiy, A. Khademhosseini, and S. H. Yun, "Nanotechnology in Textiles," *ACS Nano*, vol. 10, no. 3, pp. 3042–3068, 2016.

[31] H. Yang, C. R. Lightner, and L. Dong, "Light-emitting coaxial nanofibers," ACS Nano, vol. 6, no. 1, pp. 622–628, 2012.

[32] H. Lv. M. Liu, B. Deng, J. Li, M. Yu, Q. Huang, and C. Fan, "Laundering durable antibacterial cotton fabrics grafted with pomegranate-shaped polymer wrapped in silver nanoparticle aggregations," *Scientific Reports*, vol. 4, no. 1, p. 5920, 2015.

[33] A. G. Avila and J. P. Hinestroza, "Smart textiles: tough cotton.," *Nature nanotechnology*, vol. 3, no. 8. pp. 458–459, 2008.

[34] T. G. Myers, M. M. MacDevette, F. Font, and V. Cregan, "Continuum mathematics at the nanoscale," *Journal of Mathematics in Industry*, vol. 4, no. 1, p. 11, 2014.

[35] E. Gonzalez, J. Arbiol, and V. F. Puntes, "Carving at the Nanoscale: Sequential Galvanic Exchange and Kirkendall Growth at Room Temperature," *Science*, vol. 334, no. 6061, pp. 1377–1380, 2011.

[36] S. Bhanja, D. K. Karunaratne, R. Panchumarthy, S. Rajaram, and S. Sarkar, "Non-Boolean computing with nanomagnets for computer vision applications.," *Nature nanotechnology*, vol. 11, no. 2, pp. 177–83, 2016.

[37] O. Salata, "Applications of nanoparticles in biology and medicine.," *Journal of nanobiotechnology*, vol. 2, no. 1, p. 3, 2004.

[38] I. Y. Wong, S. N. Bhatia, and M. Toner, "Nanotechnology: Emerging tools for biology and medicine," *Genes and Development*, vol. 27, no. 22. pp. 2397–2408, 2013.

[39] V. Morigi, A. Tocchio, C. Bellavite Pellegrini, J. H. Sakamoto, M. Arnone, and E. Tasciotti, "Nanotechnology in Medicine: From Inception to Market Domination," *Journal of Drug Delivery*, vol. 2012, pp. 1–7, 2012.

[40] T. S. . Satyanarayana and R. Rai, "Nanotechnology: The future," *Journal of Interdisciplinary Dentistry*, vol. 1, no. 2, p. 93, 2011.

[41] S. Liu, G. Chen, P. N. Prasad, and M. T. Swihart, "Synthesis of monodisperse Au, Ag, and Au-Ag alloy nanoparticles with tunable size and surface plasmon resonance frequency," *Chemistry of Materials*, vol. 23, no. 18, pp. 4098–4101, 2011.

[42] R. Schreiber, J. Do, E. -M. Roller, T. Zhang, V. J. Schüller, P. C. Nickels, J. Feldmann, T. Liedl, "Hierarchical assembly of metal nanoparticles, quantum dots and organic dyes using DNA origami scaffolds.," *Nature nanotechnology*, vol. 9, no. 1, pp. 74–8, 2014.

[43] Z. Ren, Y. Guo, C.-H. Liu, and P.-X. Gao, "Hierarchically nanostructured materials for sustainable environmental applications," *Frontiers in Chemistry*, vol. 1, 2013.

[44] R. S. Wagner and W. C. Ellis, "Vapor-liquid-solid mechanism of single crystal growth," *Applied Physics Letters*, vol. 4, no. 5, pp. 89–90, 1964.

[45] J. Hu, T. W. Odom, and C. M. Lieber, "Chemistry and Physics in One Dimensions: Syntesis and Properties of Nanowires and Nanotubes," *Acc. Chem. Res.*, vol. 32, no. 5, pp. 435–445, 1999.

[46] C. M. Lieber, "One-dimensional nanostructures: Chemistry, physics & applications," *Solid State Communications*, vol. 107, no. I, pp. 607–616, 1998.

[47] X. Duan and C. M. Lieber, "General synthesis of compound semiconductor nanowires," *Advanced Materials*, vol. 12, no. 4, pp. 298–302, 2000.

[48] R. Agarwal and C. M. Lieber, "Semiconductor nanowires: Optics and optoelectronics," *Applied Physics A: Materials Science and Processing*, vol. 85, no. 3, pp. 209–215, 2006.

[49] D. Wang, F. Qian, C. Yang, Z. Zhong, and C. M. Lieber, "Rational growth of branched

and hyperbranched nanowire structures," *Nano Letters*, vol. 4, no. 5, pp. 871–874, 2004.

[50] P.-C. Chang, Z. Fan, W.-Y. Tseng, J. Hong, W.-A. Chiou, and G. J. Lu, "Characterization ZnO Nanowires Synthesized by Vapor Trapping CVD Method," *Microscopy and Microanalysis*, vol. 10, no. S02, pp. 390–391, 2004.

[51] V. Schmidt, J. V. Wittemann, S. Senz, and U. Gósele, "Silicon nanowires: A review on aspects of their growth and their electrical properties," *Advanced Materials*, vol. 21, no. 25–26. pp. 2681–2702, 2009.

[52] V. A. Nebol'sin, A. A. Shchetinin, A. A. Dolgachev, and V. V. Korneeva, "Effect of the nature of the metal solvent on the vapor-liquid-solid growth rate of silicon whiskers," *Inorganic Materials*, vol. 41, no. 12, pp. 1256–1259, 2005.

[53] Y. Wang, V. Schmidt, S. Senz, and U. Gösele, "Epitaxial growth of silicon nanowires using an aluminium catalyst.," *Nature nanotechnology*, vol. 1, no. 3, pp. 186–9, 2006.

[54] H. Wang, Y. C. Lan, J. M. Zhang, M. A. Crimp, and Z. F. Ren, "Growth Mechanism and Elemental Distribution of beta-Ga_2O_3 Crystalline Nanowires Synthesized by Cobalt-Assisted Chemical Vapor Deposition," *Journal of Nanoscience and Nanotechnology*, vol. 12, no. 4, pp. 3101–3107, 2012.

[55] V. Mody, R. Siwale, A. Singh, and H. Mody, "Introduction to metallic nanoparticles," *Journal of Pharmacy and Bioallied Sciences*, vol. 2, no. 4, p. 282-289, 2010.

[56] C. Li, C. Gu, Z. Liu, J. Mi, and Y. Yang, "Iron-catalytic growth of prism-shaped single-crystal silicon nanowires by chemical vapor deposition of silane," *Chemical Physics Letters*, vol. 411, no. 1–3, pp. 198–202, 2005.

[57] Z. W. Pan, Z. R. Dai, C. Ma, and Z. L. Wang, "Molten gallium as a catalyst for the large-scale growth of highly aligned silica nanowires," *Journal of the American Chemical Society*, vol. 124, no. 8, pp. 1817–1822, 2002.

[58] M. H. Kim, I. S. Kim, Y. H. Park, T. E. Park, J. H. Shin, and H. J. Choi, "Platinum assisted vapor-liquid-solid growth of er-si nanowires and their optical properties," *Nanoscale Research Letters*, vol. 5, no. 2, pp. 286–290, 2010.

[59] E. Park, S. Shim, R. Ha, E. Oh, B. W. Lee, and H. J. Choi, "Reassembling of Ni and Pt catalyst in the vapor-liquid-solid growth of GaN nanowires," *Materials Letters*, vol. 65, no. 15–16, pp. 2458–2461, 2011.

[60] Z. Zhang, S. J. Wang, T. Yu, and T. Wu, "Controlling the growth mechanism of ZnO nanowires by selecting catalysts," *Journal of Physical Chemistry C*, vol. 111, no. 47, pp. 17500–17505, 2007.

[61] K. W. Kolasinski, "Catalytic growth of nanowires: Vapor-liquid-solid, vapor-solid-solid, solution-liquid-solid and solid-liquid-solid growth," *Current Opinion in Solid State and Materials Science*, vol. 10, no. 3–4, pp. 182–191, 2006.

[62] Y. Ke, X. Weng, J. M. Redwing, C. M. Eichfeld, T. R. Swisher, S. E. Mohney, and Y. M. Habib, "Fabrication and electrical properties of si nanowires synthesized by Al catalyzed vapor-liquid-solid growth," *Nano Letters*, vol. 9, no. 12, pp. 4494–4499, 2009.

[63] B. Mandl "Growth mechanism of self-catalyzed group III-V nanowires," *Nano Letters*, vol. 10, no. 11, pp. 4443–4449, 2010.

[64] H. D. Park and S. M. Prokes, "Study of the initial nucleation and growth of catalyst-free InAs and Ge nanowires," *Applied Physics Letters*, vol. 90, no. 20, pp. 1-3 2007.

[65] H. K. Yu and J.-L. Lee, "Growth mechanism of metal-oxide nanowires synthesized by electron beam evaporation: A self-catalytic vapor-liquid-solid process," *Scientific Reports*, vol. 4, no. 1, pp. 1-8, 2015.

[66] A. I. Hochbaum, R. Fan, R. He, and P. Yang, "Controlled growth of Si nanowire arrays for device integration," *Nano Letters*, vol. 5, no. 3, pp. 457–460, 2005.

[67] T. W. Ho and F. C. N. Hong, "A novel method to grow vertically aligned silicon nanowires on SI (111) and their optical absorption," *Journal of Nanomaterials*, vol. 2012, Article ID 274618, 2012.

[68] M. O. Orlandi, E. R. Leite, R. Aguiar, J. Bettini, and E. Longo, "Growth of SnO nanobelts and dendrites by a self-catalytic VLS process," *Journal of Physical Chemistry B*, vol. 110, no. 13, pp. 6621–6625, 2006.

[69] M. Niederberger and N. Pinna, *Metal Oxide Nanoparticles in Organic Solvents*. Published in 2009 in Dordrecht by Springer. 217 p.

[70] R. Stanley and A. Samson Nesaraj, "Effect of Surfactants on the Wet Chemical Synthesis of Silica Nanoparticles," *International Journal of Applied Science and Engineering Int. J. Appl. Sci. Eng*, vol. 12, no. 12, pp. 9–21, 2014.

[71] B. Jeong, S. W. Kim, and Y. H. Bae, "Thermosensitive sol-gel reversible hydrogels," *Advanced Drug Delivery Reviews*, vol. 64, no. SUPPL. pp. 154–162, 2012.

[72] C.-C. Wang and J. Y. Ying, "Sol–Gel Synthesis and Hydrothermal Processing of Anatase and Rutile Titania Nanocrystals," *Chemistry of Materials*, vol. 11, no. 11, pp. 3113–3120, 1999.

[73] K. Sinkó, "Influence of chemical conditions on the nanoporous structure of silicate aerogels," *Materials*, vol. 3, no. 1. pp. 704–740, 2010.

[74] L. Yu, D. Cai, H. Wang, and M.-M. Titirici, "Hydrothermal synthesis of SnO_2 and SnO_2@C nanorods and their application as anode materials in lithium-ion batteries," *RSC Adv.*, vol. 3, no. 38, pp. 17281–17286, 2013.

[75] B. Baruwati, D. K. Kumar, and S. V. Manorama, "Hydrothermal synthesis of highly crystalline ZnO nanoparticles: A competitive sensor for LPG and EtOH," *Sensors and Actuators, B: Chemical*, vol. 119, no. 2, pp. 676–682, 2006.

[76] H. Uchiyama, Y. Shirai, and H. Kozuka, "Formation of spherical SnO_2 particles consisting of nanocrystals from aqueous solution of $SnCl_4$ containing citric acid via hydrothermal process," *Journal of Crystal Growth*, vol. 319, no. 1, pp. 70–78, 2011.

[77] A. Kolodziejczak-Radzimska and T. Jesionowski, "Zinc oxide-from synthesis to application: A review," *Materials*, vol. 7, no. 4. pp. 2833–2881, 2014.

[78] Y. He, Y. Li, J. Yu, and Y. Qian, "Chemical control synthesis of nanocrystalline SnO_2 by hydrothermal reaction," *Materials Letters*, vol. 40, no. 1, pp. 23–26, 1999.

[79] J. L. Mi, C. Clausen, M. Bremholm, N. Lock, K. M. A. Jensen, M. Christensen, and B. B. Iversen, "Rapid hydrothermal preparation of rutile TiO_2 nanoparticles by simultaneous transformation of primary brookite and anatase: An in situ synchrotron PXRD study," *Crystal Growth and Design*, vol. 12, no. 12, pp. 6092–6097, 2012.

[80] P. W. Dunne, C. L. Starkey, M. Gimeno-Fabra, and E. H. Lester, "The rapid size- and shape-controlled continuous hydrothermal synthesis of metal sulphide nanomaterials.," *Nanoscale*, vol. 6, no. 4, pp. 2406–2418, 2014.

[81] K. Byrappa and M. Yoshimura, *Handbook of Hydrothermal Technology*, Noyes publications; Andrew, 870 pages, 2001.

[82] H. Hayashi and Y. Hakuta, "Hydrothermal Synthesis of metal oxide nanoparticles in supercritical water," *Materials*, vol. 3, no. 7. pp. 3794–3817, 2010.

[83] T. J. Daou, G. Pourroy, S. Begin-Colin, J. M. Greneche, C. Ulhaq-Bouillet, P. Legare, P. Bernhardt, C. Leuvrey, G. Rogez, "Hydrothermal Synthesis of Monodisperse Magnetite Nanoparticles," *Chem. Mater.*, vol. 18, no. 18, pp. 4399–4404, 2006.

[84] S. Baruah and J. Dutta, "Hydrothermal growth of ZnO nanostructures," *Science and Technology of Advanced Materials*, vol. 10, no. 1, pp. 1-18, 2009.

[85] S. Ge, X. Shi, K. Sun, C. Li, J. R. Baker, M. M. Banaszak Holl, B. G. Orr, "A Facile Hydrothermal Synthesis of Iron Oxide Nanoparticles with Tunable Magnetic Properties.," *The journal of physical chemistry. C, Nanomaterials and interfaces*, vol. 113, no. 31, pp. 13593–13599, 2009.

[86] O. Lupan, L. Chow, G. Chai, A. Schulte, S. Park, and H. Heinrich, "A rapid

hydrothermal synthesis of rutile SnO_2 nanowires," *Materials Science and Engineering B: Solid-State Materials for Advanced Technology*, vol. 157, no. 1–3, pp. 101–104, 2009.

[87] G. E. Patil, D. D. Kajale, V. B. Gaikwad, and G. H. Jain, "Preparation and characterization of SnO_2 nanoparticles by hydrothermal route," *PInternational Nano Letters*, p. 2:17, 2012.

[88] T. Adschiri, Y. Hakuta, K. Sue, and K. Arai, "Hydrothermal synthesis of metal oxide nanoparticles at supercritical conditions," *Journal of Nanoparticle Research*, vol. 3, no. 2–3, pp. 227–235, 2001.

[89] X. Cao, Y. C. Shu, Y. N. Hu, G. P. Li, and C. Liu, "Integrated process of large-scale and size-controlled SnO_2 nanoparticles by hydrothermal method," *Transactions of Nonferrous Metals Society of China (English Edition)*, vol. 23, no. 3, pp. 725–730, 2013.

[90] Y. Wang, M. Guo, M. Zhang, and X. Wang, "Hydrothermal synthesis of SnO_2 nanoflower arrays and their optical properties," *Scripta Materialia*, vol. 61, no. 3, pp. 234–236, 2009.

[91] F. Du, Z. Guo, and G. Li, "Hydrothermal synthesis of SnO_2 hollow microspheres," *Materials Letters*, vol. 59, no. 19–20, pp. 2563–2565, 2005.

[92] W. Chen, H. Gan, W. Zhang, and Z. Mao, "Hydrothermal Synthesis and Hydrogen Sensing Properties of Nanostructured SnO_2 with Different Morphologies," *Journal of Nanomaterials*, vol. 2014, Article ID 291273, 2014.

[93] J. Livage, "Hydrothermal synthesis of nanostructured vanadium oxides," *Materials*, vol. 3, no. 8, pp. 4175–4195, 2010.

[94] G. Amin, M. H. Asif, A. Zainelabdin, S. Zaman, O. Nur, and M. Willander, "Influence of pH, precursor concentration, growth time, and temperature on the morphology of ZnO nanostructures grown by the hydrothermal method," *Journal of Nanomaterials*, vol. 2011, Article ID 269692, 2011.

[95] A. Sugunan, H. C. Warad, M. Boman, and J. Dutta, "Zinc oxide nanowires in chemical bath on seeded substrates: Role of hexamine," *Journal of Sol-Gel Science and Technology*, vol. 39, no. 1, pp. 49–56, 2006.

[96] S. Bhat, B. V Shrisha, and K. G. Naik, "Synthesis of ZnO nanostructures by solvothermal method," vol. 4, no. 2, pp. 61–70, 2013.

[97] D. Chen, X. Jiao, and G. Cheng, "Hydrothermal synthesis of zinc oxide powders with different morphologies," *Solid State Communications*, vol. 113, no. 6, pp. 363–366,

1999.

[98] Z. Zhang and J. Mu, “Hydrothermal synthesis of ZnO nanobundles controlled by PEO-PPO-PEO block copolymers,” *Journal of Colloid and Interface Science*, vol. 307, no. 1, pp. 79–82, 2007.

[99] C. H. Lu and C. H. Yeh, “Influence of hydrothermal conditions on the morphology and particle size of zinc oxide powder,” *Ceramics International*, vol. 26, no. 4, pp. 351–357, 2000.

[100] S. Music, S. Popovic, M. Maljkovic, and E. Dragcevic, “Influence of synthesis procedure on the formation and properties of zinc oxide,” *Journal of Alloys and Compounds*, vol. 347, no. 1–2, pp. 324–332, 2002.

[101] D. M. Cunha and F. L. Souza, “Facile synthetic route for producing one-dimensional zinc oxide nanoflowers and characterization of their optical properties,” *Journal of Alloys and Compounds*, vol. 577, no. 15, pp. 158–164, 2013.

[102] R. Viswanathan and R. B. Gupta, “Formation of zinc oxide nanoparticles in supercritical water,” *Journal of Supercritical Fluids*, vol. 27, no. 2, pp. 187–193, 2003.

[103] Z. Li, X. Huang, J. Liu, Y. Li, X. Ji, and G. Li, “Growth and comparison of different morphologic ZnO nanorod arrays by a simple aqueous solution route,” *Materials Letters*, vol. 61, no. 22, pp. 4362–4365, 2007.

[104] S. Shao, P. Jia, S. Liu, and W. Bai, “Stable field emission from rose-like zinc oxide nanostructures synthesized through a hydrothermal route,” *Materials Letters*, vol. 62, no. 8–9, pp. 1200–1203, 2008.

[105] R. Wahab, S. G. Ansari, Y. S. Kim, H. K. Seo, G. S. Kim, G. Khang, H. S. Shin, “Low temperature solution synthesis and characterization of ZnO nano-flowers,” *Materials Research Bulletin*, vol. 42, no. 9, pp. 1640–1648, 2007.

[106] J. Zhang, L. Sun, J. Yin, H. Su, C. Liao, and C. Yan, “Control of ZnO morphology via a simple solution route,” *Chemistry of Materials*, vol. 14, no. 10, pp. 4172–4177, 2002.

[107] Y. Zou, B. Xu, D. Hou, Wu, Y. Sun, “Controlled growth of silver nanoparticles in a hydrothermal process,” *China Particuology*, vol. 5, no. 3, pp. 206–212, 2007.

[108] G. Aksomaityte, M. Poliakoff, and E. Lester, “The production and formulation of silver nanoparticles using continuous hydrothermal synthesis,” *Chemical Engineering Science*, vol. 85, no. 14, pp. 2–10, 2013.

[109] J. Yang and J. Pan, “Hydrothermal synthesis of silver nanoparticles by sodium alginate and their applications in surface-enhanced Raman scattering and catalysis,” *Acta Materialia*, vol. 60, no. 12, pp. 4753–4758, 2012.

[110] N. Kometani and T. Teranishi, “Preparation of size-controlled silver nanoparticles by the hydrothermal method,” *Physica Status Solidi (C)*, vol. 7, no. 11–12, pp. 2644–2647, 2010.

[111] Z. Liu, Y. Zu, Y. Fu, R. Meng, S. Guo, Z. Xing, S. Tan, “Hydrothermal synthesis of histidine-functionalized single-crystalline gold nanoparticles and their pH-dependent UV absorption characteristic,” *Colloids and Surfaces B: Biointerfaces*, vol. 76, no. 1, pp. 311–316, 2010.

[112] H. Liu, Y. Xu, S. Wen, J. Zhu, L. Zheng, M. Shen, J. Zhao, G. Zhang, X. Shi, “Facile hydrothermal synthesis of low generation dendrimer-stabilized gold nanoparticles for in vivo computed tomography imaging applications,” *Polymer Chemistry*, vol. 4, no. 6, pp. 1788-1795, 2013.

[113] Q. Xiang, B. Cheng, and J. Yu, “Hierarchical porous CdS nanosheet-assembled flowers with enhanced visible-light photocatalytic H_2-production performance,” *Applied Catalysis B: Environmental*, vol. 138–139, no. 17, pp. 299–303, 2013.

[114] Y. Lu, L. Li, Y. Ding, F. Zhang, Y. Wang, and W. Yu, “Hydrothermal synthesis of functionalized CdS nanoparticles and their application as fluorescence probes in the determination of uracil and thymine,” *Journal of Luminescence*, vol. 132, no. 1, pp. 244–249, 2012.

[115] E. Caponetti, D. C. Martino, M. Leone, L. Pedone, M. L. Saladino, and V. Vetri, “Microwave-assisted synthesis of anhydrous CdS nanoparticles in a water-oil microemulsion,” *Journal of Colloid and Interface Science*, vol. 304, no. 2, pp. 413–418, 2006.

[116] J. Jiang, G. Oberdörster, and P. Biswas, “Characterization of size, surface charge, and agglomeration state of nanoparticle dispersions for toxicological studies,” *Journal of Nanoparticle Research*, vol. 11, no. 1, pp. 77–89, 2009.

[117] A. P. Lagrow, B. Ingham, M. F. Toney, and R. D. Tilley, “Effect of surfactant concentration and aggregation on the growth kinetics of nickel nanoparticles,” *Journal of Physical Chemistry C*, vol. 117, no. 32, pp. 16709–16718, 2013.

[118] M. Esmaili and A. Habibi-Yangjeh, “Microwave-assisted preparation of CdS nanoparticles in a halide-free ionic liquid and their photocatalytic activities,” *Cuihua Xuebao/Chinese Journal of Catalysis*, vol. 32, no. 6, pp. 933–938, 2011.

[119] M.-G. Ma, Y.-J. Zhu, G.-F. Cheng, and Y.-H. Huang, “Microwave synthesis and characterization of ZnO with various morphologies,” *Materials Letters*, vol. 62, no. 3, pp. 507–510, 2008.

[120] S. C. Motshekga, S. K. Pillai, S. Sinha Ray, K. Jalama, and R. W. M. Krause, "Recent trends in the microwave-assisted synthesis of metal oxide nanoparticles supported on carbon nanotubes and their applications," *Journal of Nanomaterials*, vol. 2012, Article ID 691503, 2012.

[121] Y. J. Zhu, W. W. Wang, R. J. Qi, and X. L. Hu, "Microwave-assisted synthesis of single-crystalline tellurium nanorods and nanowires in ionic liquids," *Angewandte Chemie - International Edition*, vol. 43, no. 11, pp. 1410–1414, 2004.

[122] M. Tsuji, M. Hashimoto, Y. Nishizawa, M. Kubokawa, and T. Tsuji, "Microwave-assisted synthesis of metallic nanostructures in solution," *Chemistry - A European Journal*, vol. 11, no. 2. pp. 440–452, 2005.

[123] Y. J. Zhu and F. Chen, "Microwave-assisted preparation of inorganic nanostructures in liquid phase," *Chemical Reviews*, vol. 114, no. 12. pp. 6462–6555, 2014.

[124] J. Zhang, M. R. Langille, and C. A. Mirkin, "Synthesis of silver nanorods by low energy excitation of spherical plasmonic seeds," *Nano Letters*, vol. 11, no. 6, pp. 2495–2498, 2011.

[125] L. Maretti, P. S. Billone, Y. Liu, and J. C. Scaiano, "Facile photochemical synthesis and characterization of highly fluorescent silver nanoparticles," *Journal of the American Chemical Society*, vol. 131, no. 39, pp. 13972–13980, 2009.

[126] P. L. Redmond, X. Wu, and L. Brus, "Photovoltage and photocatalyzed growth in citrate-stabilized colloidal silver nanocrystals," *Journal of Physical Chemistry C*, vol. 111, no. 25, pp. 8942–8947, 2007.

[127] B. Pietrobon and V. Kitaev, "Photochemical synthesis of monodisperse size-controlled silver decahedral nanoparticles and their remarkable optical properties," *Chemistry of Materials*, vol. 20, no. 16, pp. 5186–5190, 2008.

[128] J. Zhang, S. Li, J. Wu, G. C. Schatz, and C. A. Mirkin, "Plasmon-mediated synthesis of silver triangular bipyramids," *Angewandte Chemie - International Edition*, vol. 48, no. 42, pp. 7787–7791, 2009.

[129] R. Jin, Y. Cao, C. A. Mirkin, K. L. Kelly, G. C. Schatz, J. G. Zheng, A. P. Alivisatos, C. M. Lieber, R. Elghanian, J. J. Storhoff, R. C. Mucic, R. L. Letsinger, C. A. Mirkin, T. A. Taton, C. A., Chan, W. C. W., Nie, S. M., Cui, Y., Wei, Q., Park, H., V. L. Colvin, M. C. Schlamp, V. I. Klimov, T. W. Hu, Z. W. Odom, Z. R. Pan, Z. L. Dai, C. L. Wang, R. P. Haynes, R. P. Duyne, N. R. Jana Van, L. Gearheart, C. J. Murphy, Y. Y. Yu, S. S. Chang, C. L. Lee, C. R. C. Wang, B. Nikoobakht, Z. L. Wang, M. A. El-Sayed, C. A. Foss, G. L. Hornyak, J. A. Stockert, C. R. Martin, T. S. Ahmadi, Z. L

Wang, T. C. Green, A. Henglein, J. H. Fendler, F. C. Meldrum, N. Pinna, K. Weiss, J. Urban, M. -P. Pileni, J. S. Bradley, B. Tesche, W. Busser, M. Maase, M. T. Reetz, A. I. Kirkland, T. Klasu, R. Joerger, E. Olsson, C. -G. Granqvist, M. Li, H. Schnablegger, S. Mann, X. Peng, V. F. Puntes, K. M. Krishnan, L. Manna, E. C. Scher, P. V. Kamat, M. Flumiani, G. V. Hartland, A. Henglein, M. Prochazka, P. Mojzes, J. Stepanek, B. Vlcková, P. -Y. Turpin, D. Cherns, D. A. Jefferson, D. G. Duff, P. P. Edwards, G. Mie, W. H. Yang, R.P. Van, Duyne, S. Schultz, D. R. Smith, J. J. Mock, D. A. Schultz, L. Gang, "Photoinduced conversion of silver nanospheres to nanoprisms.," *Science*, vol. 294, no. 5548, pp. 1901–3, 2001.

[130] R. Jin, Y. Charles Cao, E. Hao, G. S. Métraux, G. C. Schatz, and C. A. Mirkin, "Controlling anisotropic nanoparticle growth through plasmon excitation," *Nature*, vol. 425, no. 6957, pp. 487–490, 2003.

[131] V. Bastys, I. Pastoriza-Santos, B. Rodíguez-González, R. Vaisnoras, and L. M. Liz-Marzán, "Formation of silver nanoprisms with surface plasmons at communication wavelengths," *Advanced Functional Materials*, vol. 16, no. 6, pp. 766–773, 2006.

[132] S.-A. Dong and S.-P. Zhou, "Photochemical synthesis of colloidal gold nanoparticles," *Materials Science and Engineering: B*, vol. 140, no. 3, pp. 153–159, 2007.

[133] K. Esumi, K. Matsuhisa, and K. Torigoe, "Preparation of Rodlike Gold Particles by UV Irradiation Using Cationic Micelles as a Template," *Langmuir*, vol. 11, no. 9, pp. 3285–3287, 1995.

[134] S. M. Siddiqui, M. Mehmood, and T. Yasin, "Low temperature template assisted synthesis of carbon nanowires having different functionality," *Journal of Polymer Research*, vol. 19, no. 10, pp. 1-8, 2012.

[135] Z. Chen, Y. Li, J. Jiang, C. Cao, T. Xu, Q. Chen, X. Xu, H. Zhu, "Template-assisted synthesis of ordered single crystal InN nanowires," *RSC Advances*, vol. 2, no. 17, pp. 6806-6809, 2012.

[136] K. M. Alam, A. P. Singh, R. Starko-Bowes, S. C. Bodepudi, and S. Pramanik, "Template-assisted synthesis of π-conjugated molecular organic nanowires in the sub-100 nm regime and device implications," *Advanced Functional Materials*, vol. 22, no. 15, pp. 3298–3306, 2012.

[137] N. Preda, M. Enculescu, F. Gherendi, E. Matei, M. E. Toimil-Molares, and I. Enculescu, "Synthesis of CdS nanostructures using template-assisted ammonia-free chemical bath deposition," *Journal of Physics and Chemistry of Solids*, vol. 73, no. 9, pp. 1082–1089, 2012.

[138] Y. Sun, Y. Yin, B. T. Mayers, T. Herricks, and Y. Xia, "Uniform silver nanowires synthesis by reducing $AgNO_3$ with ethylene glycol in the presence of seeds and poly(vinyl pyrrolidone)," *Chemistry of Materials*, vol. 14, no. 11, pp. 4736–4745, 2002.

[139] D. A. Tomalia and J. M. J. Fréchet, "Discovery of dendrimers and dendritic polymers: A brief historical perspective," *Journal of Polymer Science, Part A: Polymer Chemistry*, vol. 40, no. 16, pp. 2719–2728, 2002.

[140] R. M. Crooks, M. Zhao, L. Sun, V. Chechik, and L. K. Yeung, "Dendrimer-Encapsulated Metal Nanoparticles: Synthesis, Characterization, and Applications to Catalysis," *Accounts of Chemical Research*, vol. 34, no. 3, pp. 181–190, 2001.

[141] H. Liu, H. Wang, R. Guo, X. Cao, J. Zhao, Y. Luo, M. Shen, G. Zhang, X. Shi, "Size-controlled synthesis of dendrimer-stabilized silver nanoparticles for X-ray computed tomography imaging applications," *Polymer Chemistry*, vol. 1, no. 10, pp. 1677-1683, 2010.

[142] M. Behbahani, T. Gorji, M. Mahyari, M. Salarian, A. Bagheri, and A. Shaabani, "Application of Polypropylene Amine Dendrimers (POPAM)-Grafted MWCNTs Hybrid Materials as a New Sorbent for Solid-Phase Extraction and Trace Determination of Gold(III) and Palladium(II) in Food and Environmental Samples," *Food Analytical Methods*, vol. 7, no. 5, pp. 957–966, 2014.

[143] S. Fuchs, T. Kapp, H. Otto, T. Schöneberg, P. Franke, R. Gust, A. D. Schüter, "A Surface-Modified Dendrimer Set for Potential Application as Drug Delivery Vehicles: Synthesis, In Vitro Toxicity, and Intracellular Localization," *Chemistry - A European Journal*, vol. 10, no. 5, pp. 1167–1192, 2004.

[144] Y. G. Kim, S. K. Oh, and R. M. Crooks, "Preparation and Characterization of 1-2 nm Dendrimer-Encapsulated Gold Nanoparticles Having Very Narrow Size Distributions," *Chemistry of Materials*, vol. 16, no. 1, pp. 167–172, 2004.

[145] K. Esumi, A. Suzuki, A. Yamahira, and K. Torigoe, "Role of Poly(amidoamine) Dendrimers for Preparing Nanoparticles of Gold, Platinum, and Silver," *Langmuir*, vol. 16, no. 6, pp. 2604–2608, 2000.

[146] J. Dupont and J. D. Scholten, "On the structural and surface properties of transition-metal nanoparticles in ionic liquids," *Chemical Society Reviews*, vol. 39, no. 5, pp. 1780-1804, 2010.

[147] V. S. Myers, M. G. Weir, E. V. Carino, D. F. Yancey, S. Pande, and R. M. Crooks, "Dendrimer-encapsulated nanoparticles: New synthetic and characterization methods

and catalytic applications," *Chemical Science*, vol. 2, no. 9, pp. 1632-1646, 2011.

[148] J. Huang, S. Y. Chiam, H. H. Tan, S. Wang, and W. K. Chim, "Fabrication of silicon nanowires with precise diameter control using metal nanodot arrays as a hard mask blocking material in chemical etching," *Chemistry of Materials*, vol. 22, no. 13, pp. 4111–4116, 2010.

[149] W. Lee and S.-J. Park, "Porous anodic aluminum oxide: Anodization and templated synthesis of functional nanostructures," *Chemical Reviews*, vol. 114, no. 15, pp. 7487–7556, 2014.

[150] R. Yang, C. Sui, J. Gong, and L. Qu, "Silver nanowires prepared by modified AAO template method," *Materials Letters*, vol. 61, no. 3, pp. 900–903, 2007.

[151] K. Kim, M. Kim, and S. M. Cho, "Pulsed electrodeposition of palladium nanowire arrays using AAO template," *Materials Chemistry and Physics*, vol. 96, no. 2–3, pp. 278–282, 2006.

[152] L. Yuan, S. Meng, Y. Zhou, and Z. Yue, "Controlled synthesis of anatase TiO2 nanotube and nanowire arrays via AAO template-based hydrolysis," *Journal of Materials Chemistry A*, vol. 1, no. 7, p. 2552, 2013.

[153] J.-K. Wang, J.-M. Char, and P.-J. Lien, "Optimization Study on Supercritical Electrodeposition of Nickel Nanowire Arrays Using AAO Template," *ISRN Chemical Engineering*, vol. 2012, Article ID 610510, 2012.

[154] J. Y. Miao, Y. Cai, Y. F. Chan, P. Sheng, and N. Wang, "A novel carbon nanotube structure formed in ultra-long nanochannels of anodic aluminum oxide templates," *Journal of Physical Chemistry B*, vol. 110, no. 5, pp. 2080–2083, 2006.

[155] N. U. Saidin, K. Y. Kok, I. K. Ng, and S. H. Ilias, "Fabrication of Au/Ni Multilayered Nanowires by Electrochemical Deposition," *Journal of Physics: Conference Series*, vol. 431, p. 12006, 2013.

[156] R. Bales, "Handbook of Conducting Polymers," *Notes*, vol. 8, no. 2. p. 361, 1951.

[157] A. O. Patil, A. J. Heeger, and F. Wudl, "Optical properties of conducting polymers," *Chemical Reviews*, vol. 88, no. 1, pp. 183–200, 1988.

[158] T. K. Das and S. Prusty, "Review on Conducting Polymers and Their Applications," *Polymer-Plastics Technology and Engineering*, vol. 51, no. 14, pp. 1487–1500, 2012.

[159] B. M. W. Langeveld-Voss, R. A. J. Janssen, A. J. H. Spiering, J. L. J. van Dongen, E. C. Vonk, and H. A. Claessens, "End-group modification of regioregular poly(3-alkylthiophene)s," *Chemical Communications*, vol. 0, no. 1, pp. 81–82, 2000.

[160] E. Bundgaard and F. C. Krebs, "Low band gap polymers for organic photovoltaics,"

Solar Energy Materials and Solar Cells, vol. 91, no. 11. pp. 954–985, 2007.

[161] H. Bai and G. Shi, "Gas Sensors Based on Conducting Polymers," *Sensors*, vol. 7, no. 3, pp. 267–307, 2007.

[162] W. M. Kochemba, S. M. Kilbey, and D. L. Pickel, "End-group composition of poly(3-hexylthiophene)s prepared by in situ quenching of the grignard metathesis polymerization: Influence of additives and reaction conditions," *Journal of Polymer Science, Part A: Polymer Chemistry*, vol. 50, no. 14, pp. 2762–2769, 2012.

[163] R. H. Lohwasser and M. Thelakkat, "Toward perfect control of end groups and polydispersity in poly(3-hexylthiophene) via catalyst transfer polymerization," *Macromolecules*, vol. 44, no. 9, pp. 3388–3397, 2011.

[164] V. Senkovskyy, M. Sommer, R. Tkachov, H. Komber, W. T. S. Huck, and A. Kiriy, "Convenient route to initiate kumada catalyst-Transfer polycondensation using Ni(dppe)Cl_2 or Ni(dppp)Cl_2 and sterically hindered grignard compounds," *Macromolecules*, vol. 43, no. 23, pp. 10157–10161, 2010.

[165] A. Smeets, K. Van Den Bergh, J. De Winter, P. Gerbaux, T. Verbiest, and G. Koeckelberghs, "Incorporation of different end groups in conjugated polymers using functional nickel initiators," *Macromolecules*, vol. 42, no. 20, pp. 7638–7641, 2009.

[166] N. V. Handa, A. V. Serrano, M. J. Robb, and C. J. Hawker, "Exploring the synthesis and impact of end-functional poly(3-hexylthiophene)," *Journal of Polymer Science, Part A: Polymer Chemistry*, vol. 53, no. 7, pp. 831–841, 2015.

[167] M. Jeffries-El, G. Sauvé, and R. D. McCullough, "Facile synthesis of end-functionalized regioregular poly(3-alkylthiophene)s via modified Grignard metathesis reaction," *Macromolecules*, vol. 38, no. 25, pp. 10346–10352, 2005.

[168] R. H. Lohwasser, J. Bandara, and M. Thelakkat, "Tailor-made synthesis of poly(3-hexylthiophene) with carboxylic end groups and its application as a polymer sensitizer in solid-state dye-sensitized solar cells," *Journal of Materials Chemistry*, vol. 19, no. 24, pp. 4126-4130, 2009.

[169] F. Monnaie, W. Brullot, T. Verbiest, J. De Winter, P. Gerbaux, A. Smeets, G. Koeckelberghs, "Synthesis of end-group functionalized P3HT: General protocol for P3HT/nanoparticle hybrids," *Macromolecules*, vol. 46, no. 21, pp. 8500–8508, 2013.

[170] C. N. R. Rao, S. R. C. Vivekchand, K. Biswas, and A. Govindaraj, "Synthesis of inorganic nanomaterials," *Dalton Transactions*, vol. 0, no. 34, pp. 3728-3749, 2007.

[171] A. Huczko, "Template-based synthesis of nanomaterials," *Applied Physics A: Materials Science and Processing*, vol. 70, no. 4, pp. 365–376, 2000.

[172] D. Chen, A. Nakahara, D. Wei, D. Nordlund, and T. P. Russell, "P3HT/PCBM bulk heterojunction organic photovoltaics: Correlating efficiency and morphology," *Nano Letters*, vol. 11, no. 2, pp. 561–567, 2011.

[173] H. Yoon, "Current Trends in Sensors Based on Conducting Polymer Nanomaterials," *Nanomaterials*, vol. 3, no. 3, pp. 524–549, 2013.

[174] S. Islam, E. Islam, A. B. Ismail, H. Baerwolff, and E. T. Al, "Influence of Thickness and Annealing Temperature on the Optical Properties of Spin-Coated Photoactive P3HT : PCBM Blend," *Optics and Photonics Journal*, vol. 2013, no. December, pp. 28–32, 2013.

[175] J. Shi, L. Lv, W. Zhou, and L. Zhang, "Improvement of the photovoltaic properties for P3HT:PCBM system annealed at the temperature in liquid crystalline regions induced by liquid crystal molecules," *Polymer Bulletin*, vol. 71, no. 11, pp. 2963–2979, 2014.

[176] S. Grigorian, S. Joshi, and U. Pietsch, "Temperature-dependent structural properties of P3HT films," *IOP Conference Series: Materials Science and Engineering*, vol. 14, no. 1, p. 12007, 2010.

[177] M. E. Nicho, C. H. García-Escobar, M. C. Arenas, P. Altuzar-Coello, R. Cruz-Silva, and M. Güizado-Rodríguez, "Influence of P3HT concentration on morphological, optical and electrical properties of P3HT/PS and P3HT/PMMA binary blends," in *Materials Science and Engineering B: Solid-State Materials for Advanced Technology*, vol. 176, no. 17, pp. 1393–1400, 2011.

[178] H. Yan, B. A. Collins, E. Gann, C. Wang, H. Ade, and C. R. McNeill, "Correlating the efficiency and nanomorphology of polymer blend solar cells utilizing resonant soft X-ray scattering," *ACS Nano*, vol. 6, no. 1, pp. 677–688, 2012.

[179] M. T. Dang, L. Hirsch, and G. Wantz, "P3HT:PCBM, best seller in polymer photovoltaic research," *Advanced Materials*, vol. 23, no. 31, pp. 3597–3602, 2011.

[180] Y. Lu, Y. Wang, Z. Feng, Y. Ning, X. Liu, Y. Lü, Y. Hou, "Temperature-dependent morphology evolution of P3HT:PCBM blend solar cells during annealing processes," *Synthetic Metals*, vol. 162, no. 23, pp. 2039–2046, 2012.

[181] L. Chang, H. W. A. Lademann, J. B. Bonekamp, K. Meerholz, and A. J. Moulé, "Effect of trace solvent on the morphology of P3HT:PCBM bulk heterojunction solar cells," *Advanced Functional Materials*, vol. 21, no. 10, pp. 1779–1787, 2011.

[182] H. -C. Liao, C. -S. Tsao, Y. -C. Huang, M. -H. Jao, K. -Y. Tien, C. -M. Chuang, C. -Y. Chen, C. -J. Su, U. -S. Jeng, Y. -F. Chen, W. -F. Su, "Insights into solvent vapor annealing on the performance of bulk heterojunction solar cells by a quantitative

nanomorphology study," *RSC Advances*, vol. 4, no. 12, pp. 6246-6253, 2014.

[183] E. Verploegen, C. E. Miller, K. Schmidt, Z. Bao, and M. F. Toney, "Manipulating the morphology of P3HT-PCBM bulk heterojunction blends with solvent vapor annealing," *Chemistry of Materials*, vol. 24, no. 20, pp. 3923–3931, 2012.

[184] M. Wright and A. Uddin, "Organic-inorganic hybrid solar cells: A comparative review," *Solar Energy Materials and Solar Cells*, vol. 107. pp. 87–111, 2012.

[185] M. Al-Ibrahim, O. Ambacher, S. Sensfuss, and G. Gobsch, "Effects of solvent and annealing on the improved performance of solar cells based on poly(3-hexylthiophene): Fullerene," *Applied Physics Letters*, vol. 86, no. 20, pp. 1–3, 2005.

[186] B. T. De Villers, C. J. Tassone, S. H. Tolbert, and B. J. Schwartz, "Improving the reproducibility of P3HT:PCBM solar cells by controlling the PCBM/ cathode interface," *Journal of Physical Chemistry C*, vol. 113, no. 44, pp. 18978–18982, 2009.

[187] A. Keawprajak, P. Piyakulawat, A. Klamchuen, P. Iamraksa, and U. Asawapirom, "Influence of crystallizable solvent on the morphology and performance of P3HT:PCBM bulk-heterojunction solar cells," *Solar Energy Materials and Solar Cells*, vol. 94, no. 3, pp. 531–536, 2010.

[188] D. Chirvase, J. Parisi, J. C. Hummelen, and V. Dyakonov, "Influence of nanomorphology on the photovoltaic action of polymer–fullerene composites," *Nanotechnology*, vol. 15, no. 9, pp. 1317–1323, 2004.

[189] L. Ye, S. Zhang, D. Qian, Q. Wang, and J. Hou, "Application of bis-PCBM in polymer solar cells with improved voltage," *Journal of Physical Chemistry C*, vol. 117, no. 48, pp. 25360–25366, 2013.

[190] V. Saini, Z. Li, S. Bourdo, E. Dervishi, Y. Xu, X. Ma, V. P. Kunets, G. J. Salamo, T. Viswanathan, A. R. Biris, D. Saini, A. S. Biris, "Electrical, Optical, and Morphological Properties of P3HT-MWNT Nanocomposites Prepared by in Situ Polymerization," *The Journal of Physical Chemistry C*, vol. 113, no. 19, pp. 8023–8029, 2009.

[191] S. Guo, E. M. Herzig, A. Naumann, G. Tainter, J. Perlich, and P. Müller-Buschbaum, "Influence of solvent and solvent additive on the morphology of PTB7 films probed via X-ray scattering," *Journal of Physical Chemistry B*, vol. 118, no. 1, pp. 344–350, 2014.

[192] Z. He, C. Zhong, S. Su, M. Xu, H. Wu, Y. Cao, A. K. K. A. Kyaw, D. D. H. Wang, V. Gupta, J. Zhang, S. Chand, G. C. Bazan, A. J. Heeger, "Enhanced power-conversion efficiency in polymer solar cells using an inverted device structure," *Nature Photonics*, vol. 25, no. 17, pp. 593–597, 2013.

[193] T. Yanagidate, S. Fujii, M. Ohzeki, Y. Yanagi, Y. Arai, T. Okukawa, A. Yoshida, H. Kataura, Y. Nishioka, "Flexible PTB7:PC71BM bulk heterojunction solar cells with a LiF buffer layer," *Japanese Journal of Applied Physics*, vol. 53, no. 2 PART 2, pp. 1-5, 2014.

[194] D. D. Laws, H.-M. L. Bitter, and A. Jerschow, "Solid-State NMR Spectroscopic Methods in Chemistry," *Angewandte Chemie International Edition*, vol. 41, no. 17, pp. 3096–3129, 2002.

[195] M. E. Smith and J. H. Strange, "NMR techniques in materials physics: A review," *Measurement Science and Technology*, vol. 7, no. 4, pp. 449–475, 1996.

[196] D. Alberga, A. Perrier, I. Ciofini, G. F. Mangiatordi, G. Lattanzi, and C. Adamo, "Morphological and charge transport properties of amorphous and crystalline P3HT and PBTTT: insights from theory," *Phys. Chem. Chem. Phys.*, vol. 17, no. 28, pp. 18742–18750, 2015.

[197] F. Liu, D. Chen, C. Wang, K. Luo, W. Gu, A. L. Briseno, J. W. P. Hsu, T. P. Russell, "Molecular weight dependence of the morphology in P3HT:PCBM solar cells," *ACS Applied Materials and Interfaces*, vol. 6, no. 22, pp. 19876–19887, 2014.

[198] J. K. Patra and K. H. Baek, "Green Nanobiotechnology: Factors Affecting Synthesis and Characterization Techniques," *Journal of Nanomaterials*, vol. 2014, Article ID 417305, 2014.

[199] D. A. Tomalia and J. M. Fréchet, "Introduction to 'dendrimers and Dendritic Polymers,'" *Progress in Polymer Science (Oxford)*, vol. 30, no. 3–4, pp. 217–219, 2005.

[200] A. Fahmi, D. Appelhans, N. Cheval, T. Pietsch, C. Bellmann, N. Gindy, B. Voit, "Hybrid nanoalloy: Nanofibers fabricated by self-assembling dendrimers mediate in situ CdSe quantum dots and their metallization with discrete gold nanoparticles," *Advanced Materials*, vol. 23, no. 29, pp. 3289–3293, 2011.

[201] M. Garzoni, N. Cheval, A. Fahmi, A. Danani, and G. M. Pavan, "Ion-selective controlled assembly of dendrimer-based functional nanofibers and their ionic-competitive disassembly," *Journal of the American Chemical Society*, vol. 134, no. 7, pp. 3349–3357, 2012.

[202] H. Weller, A. Fojtik, and A. Henglein, "Photochemistry of semiconductor colloids: Properties of extremely small particles of Cd_3P_2 and Zn_3P_2," *Chemical Physics Letters*, vol. 117, no. 5, pp. 485–488, 1985.

[203] A. Henglein, "Small-Particle Research: Physicochemical Properties of Extremely

Small Colloidal Metal and Semiconductor Particles," *Chemical Reviews*, vol. 89, no. 8, pp. 1861–1873, 1989.

[204] A. Eychmüller, "Structure and Photophysics of Semiconductor Nanocrystals," *The Journal of Physical Chemistry B*, vol. 104, no. 28, pp. 6514–6528, 2000.

[205] M. Thambidurai, N. Murugan, N. Muthukumarasamy, S. Vasantha, R. Balasundaraprabhu, and S. Agilan, "Preparation and characterization of nanocrystalline cds thin films," *Chalcogenide Letters*, vol. 6, no. 4, pp. 171–179, 2009.

[206] D. C. R. L. S. Pedrotti, "Change in Structure of Blue and Green Fluorescence in Cadmium Sulfide at Low Temperatures," *Physical Review*, vol. 119, no. 6, pp. 1897-189, 1960.

[207] L. S. Pedrotti and D. C. Reynolds, "Energy model for edge emission in cadmium sulfide," *Physical Review*, vol. 120, no. 5, pp. 1664–1669, 1960.

[208] B. A. Kulp and R. H. Kelley, "Displacement of the sulfur atom in CdS by electron bombardment," *Journal of Applied Physics*, vol. 31, no. 6, pp. 1057–1061, 1960.

[209] P. R. Sajanlal, T. S. Sreeprasad, A. K. Samal, and T. Pradeep, "Anisotropic nanomaterials: structure, growth, assembly, and functions," *Nano Reviews*, vol. 2, no. 1, p. 5883, 2011.

[210] T. Edwards, *Elements of Chemistry, Including the Recent Discoveries and Doctrines of the Science*. London: 1840. Reprint. London: Forgotten Books, 2013.

[211] T. H. Ha, H. J. Koo, and B. H. Chung, "Shape-controlled syntheses of gold nanoprisms and nanorods influenced by specific adsorption of halide ions," *Journal of Physical Chemistry C*, vol. 111, no. 3, pp. 1123–1130, 2007.

[212] C. Zhu, H.-C. Peng, J. Zeng, J. Liu, Z. Gu, and Y. Xia, "Supporting Information for Facile Synthesis of Gold Wavy Nanowires and Investigation of Their Growth Mechanism," *Journal of the American Chemical Society*, vol. 134, no. 50, pp. 1–15, 2012.

[213] B. Khodashenas and H. R. Ghorbani, "Synthesis of silver nanoparticles with different shapes," *Arabian Journal of Chemistry*, pp. 1-18, 2015. In press.

[214] K. M. Koczkur, S. Mourdikoudis, L. Polavarapu, and S. E. Skrabalak, "Polyvinylpyrrolidone (PVP) in nanoparticle synthesis," *Dalton Trans.*, vol. 44, no. 41, pp. 17883–17905, 2015.

[215] S. Chakraborty, a. K. Kole, and P. Kumbhakar, "Room temperature chemical synthesis of flower-like ZnO nanostructures," *Materials Letters*, vol. 67, no. 1, pp. 362–364, 2012.

[216] E. J. A. Campo, M. Peiteado, A. C. Caballero, M. Villegas, and J. E. Rodriguez-Paez, "Room temperature synthesis of high purity 2D ZnO nanoneedles," *Journal of Ceramic Processing Research*, vol. 10, no. 4, pp. 477–481, 2009.

[217] R. Wahab, S. G. Ansari, Y.-S. Kim, H.-K. Seo, and H.-S. Shin, "Room temperature synthesis of needle-shaped ZnO nanorods via sonochemical method," *Applied Surface Science*, vol. 253, no. 18, pp. 7622–7626, 2007.

[218] K. O. Hill, Y. Fujii, D. C. Johnson, and B. S. Kawasaki, "Photosensitivity in optical fiber waveguides: Application to reflection filter fabrication," *Applied Physics Letters*, vol. 32, no. 10, pp. 647–649, 1978.

[219] F. Classical and D. Technologies, *The Chemistry of Photography*, vol. 41, no. 1057. 1890.

[220] W. Zhou, "Reversed crystal growth: Implications for crystal engineering," *Advanced Materials*, vol. 22, no. 28, pp. 3086–3092, 2010.

[221] R. Docherty, G. Clydesdale, K. J. Roberts, and P. Bennema, "Application of Bravais-Friedel-Donnay-Harker, attachment energy and Ising models to predicting and understanding the morphology of molecular crystals," *Journal of Physics D: Applied Physics*, vol. 24, no. 2, pp. 89–99, 2000.

[222] P. Curie, "On the Formation of Crystals and on the capillary constants of their different faces," Journal of Chemical Education, vol. 47, no. 9, pp. 636–637, 1970.

[223] P. Hartman, *Ch.14 in Crystal Growth: An Introduction*. Amsterdam: North-Holland Publishing Cy, Volume 78, no. 11, November, Pages 1276, 1974.

[224] C. F. Woensdregt, "Computation of Surface Energies in an Electrostatic Point Charge Model : I . Theory," *Group*, pp. 52–58, 1992.

[225] I. Sunagawa, "Growth and Morphology of Crystals," *Forma*, vol. 14, no. 358, pp. 147–166, 1999.

[226] T. E. Glover, D. M. Fritz, M. Cammarata, T. K. Allison, S. Coh, J. M. Feldkamp, H. Lemke, D. Zhu, Y. Feng, R. N. Coffee, M. Fuchs, S. Ghimire, J. Chen, S. Shwartz, D. A. Reis, S. E. Harris, J. B. Hastings, "X-ray and optical wave mixing," *Nature*, vol. 488, no. 7413, pp. 603–608, 2012.

[227] A. Callegari, D. Tonti, and M. Chergui, "Photochemically Grown Silver Nanoparticles with Wavelength-Controlled Size and Shape," *Nano Letters*, vol. 3, no. 11, pp. 1565–1568, 2003.

[228] P. N. Lebedev, "Experimental Examination of Light Pressure," *Annalen der Physik*, vol. 6, no. 433, pp. 1–26, 1901.

[229] L. Zhang, W. She, N. Peng, and U. Leonhardt, “Experimental evidence for Abraham pressure of light,” *New Journal of Physics*, vol. 17, no. 5, pp. 1-13, 2015.

[230] Y. Hinschberger and P. A. Hervieux, “How light modifies the electron-electron interaction under extreme conditions,” *Physics Letters, Section A: General, Atomic and Solid State Physics*, vol. 379, no. 37, pp. 2261–2266, 2015.

[231] W. M. Fisher and S. C. Rand, “Optically-induced charge separation and terahertz emission in unbiased dielectrics,” *Journal of Applied Physics*, vol. 109, no. 6, 2011.

[232] V. S. Langford, A. J. McKinley, and T. I. Quickenden, “Temperature dependence of the visible-near-infrared absorption spectrum of liquid water,” *Journal of Physical Chemistry A*, vol. 105, no. 39, pp. 8916–8921, 2001.

[233] M. Manceau, S. Chambon, A. Rivaton, J. L. Gardette, S. Guillerez, and N. Lematre, “Effects of long-term UV visible light irradiation in the absence of oxygen on P3HT and P3HT: PCBM blend,” *Solar Energy Materials and Solar Cells*, vol. 94, no. 10, pp. 1572–1577, 2010.

[234] N. Wongpisutpaisan, P. Charoonsuk, N. Vittayakorn, and W. Pecharapa, “Sonochemical synthesis and characterization of copper oxide nanoparticles,” in *Energy Procedia*, vol. 9, pp. 404–409, 2011.

[235] R. A. Salkar, P. Jeevanandam, S. T. Aruna, Y. Koltypin, and A. Gedanken, “The sonochemical preparation of amorphous silver nanoparticles,” *Journal of Materials Chemistry*, vol. 9, no. 6, pp. 1333–1335, 1999.

[236] B. M. Teo, S. K. Suh, T. A. Hatton, M. Ashokkumar, and F. Grieser, “Sonochemical synthesis of magnetic Janus nanoparticles,” *Langmuir*, vol. 27, no. 1. pp. 30–33, 2011.

Publication

2016 – **V. Astachov**, M. Garzoni, A. Danani, K-L. Choy, G.M Pavan, A. Fahmi; "In situ functionalization of self-assembled dendrimer nanofibers with cadmium sulfide quantum dots through simple ionic-substitution," *New Journal of Chemistry*, vol. 40, no. 7, pp. 6325-6331, 2016.

2013 - S. Sekowski, N. Cheval, O. Liszka, **V. Astachov**, C. Fowkes, A. Fahmi; "Synthesis and characterisation of hybrid materials based on gold nanoparticles and HBP hyperbranched polyesters: Preparation of "volcano-rings" nanostructures," *Colloids and Surfaces A: Physicochem. Eng. Aspects* vol. 417, no. 20, pp. 170-178. 2013.

2012- B. Mahltig, N. Cheval, **V. Astachov**, M. Malkoch, M. I. Montañez, H. Haase, A. Fahmi; "Hydroxyl functional polyester dendrimers as stabilizing agent for preparation of colloidal silver particles - a study in respect to antimicrobial properties and toxicity against human cells," *Colloid and Polymer Science* vol. 290, no. 14 pp. 1413–1421, 2012.

Conferences:

2-5 September 2013, Riva del Garda, Italy. International Conference of Diamonds and Carbon Materials. Poster presentation.